

Advances in the Physicochemical Characterization of Dissolved Organic Matter: Impact on Natural and Engineered Systems

ACS SYMPOSIUM SERIES 1160

Advances in the Physicochemical Characterization of Dissolved Organic Matter: Impact on Natural and Engineered Systems

Fernando Rosario-Ortiz, Editor

*University of Colorado
Boulder, Colorado*

**Sponsored by the
ACS Division of Environmental Chemistry, Inc.**



American Chemical Society, Washington, DC

Distributed in print by Oxford University Press



Library of Congress Cataloging-in-Publication Data

Advances in the physicochemical characterization of dissolved organic matter : impact on natural and engineered systems / Fernando Rosario-Ortiz, editor, University of Colorado, Boulder, Colorado ; sponsored by the ACS Division of Environmental Chemistry, Inc. pages cm. -- (ACS symposium series ; 1160) Includes bibliographical references and index.

ISBN 978-0-8412-2951-8 (acid-free paper) 1. Water--Organic compound content--Congresses. I. Rosario-Ortiz, Fernando L., editor. II. American Chemical Society. Division of Environmental Chemistry, sponsoring body.

TD427.O7A385 2014

628.1'61--dc23

2014018641

The paper used in this publication meets the minimum requirements of American National Standard for Information Sciences—Permanence of Paper for Printed Library Materials, ANSI Z39.48n1984.

Copyright © 2014 American Chemical Society

Distributed in print by Oxford University Press

All Rights Reserved. Reprographic copying beyond that permitted by Sections 107 or 108 of the U.S. Copyright Act is allowed for internal use only, provided that a per-chapter fee of \$40.25 plus \$0.75 per page is paid to the Copyright Clearance Center, Inc., 222 Rosewood Drive, Danvers, MA 01923, USA. Republication or reproduction for sale of pages in this book is permitted only under license from ACS. Direct these and other permission requests to ACS Copyright Office, Publications Division, 1155 16th Street, N.W., Washington, DC 20036.

The citation of trade names and/or names of manufacturers in this publication is not to be construed as an endorsement or as approval by ACS of the commercial products or services referenced herein; nor should the mere reference herein to any drawing, specification, chemical process, or other data be regarded as a license or as a conveyance of any right or permission to the holder, reader, or any other person or corporation, to manufacture, reproduce, use, or sell any patented invention or copyrighted work that may in any way be related thereto. Registered names, trademarks, etc., used in this publication, even without specific indication thereof, are not to be considered unprotected by law.

PRINTED IN THE UNITED STATES OF AMERICA

Foreword

The ACS Symposium Series was first published in 1974 to provide a mechanism for publishing symposia quickly in book form. The purpose of the series is to publish timely, comprehensive books developed from the ACS sponsored symposia based on current scientific research. Occasionally, books are developed from symposia sponsored by other organizations when the topic is of keen interest to the chemistry audience.

Before agreeing to publish a book, the proposed table of contents is reviewed for appropriate and comprehensive coverage and for interest to the audience. Some papers may be excluded to better focus the book; others may be added to provide comprehensiveness. When appropriate, overview or introductory chapters are added. Drafts of chapters are peer-reviewed prior to final acceptance or rejection, and manuscripts are prepared in camera-ready format.

As a rule, only original research papers and original review papers are included in the volumes. Verbatim reproductions of previous published papers are not accepted.

ACS Books Department

Preface

The study of dissolved organic matter (DOM) has fascinated scientists and engineers for at least 60 years — from the initial efforts focused on measuring the concentrations of carbon in marine and aquatic systems, to the discovery of the role of DOM in the formation of disinfection byproducts, all the way to the new emphasis on the detailed understanding of the different functional groups and basic structural features which are the basis for the physicochemical properties of the material. After 50 years of work in the area, there are still many questions regarding DOM.

The idea to develop this book came after the conclusion of a symposium that E. M. Thurman and I had organized for the 245th meeting of the American Chemical Society, which was held on April 7-11, 2013 in New Orleans, Louisiana, U.S.A. The main goal of this symposium was to bring different experts to discuss the progress on DOM characterization and also celebrate the 30th anniversary of the collection of the first organic matter standard offered by the International Humics Substances Society (IHSS). The session was developed following five major themes, including impact of DOM on engineered and natural systems, general characterization, and photochemical and redox properties. The session was a success. We had over 40 oral presentations and posters. Afterward, the idea of collecting the information presented in this symposium — and combining it with other topics — resulted in the motivation for the development of this book.

I would like to acknowledge all of the participants of the original symposium, in addition to the presenters and those who contributed chapters to this book. The work presented in this book represents just a small cross section of the research being conducted on the physicochemical characterization of DOM, but it offers an overview on some key aspects that are important to both scientists and engineers. I also graciously thank E. M. Thurman for his help and mentoring during the development of this book. In addition, I express my gratitude to the reviewers who took time out of their busy schedules to make sure that the content of the book was up to par. I would also like to acknowledge financial support for the original ACS symposium from the IHSS and the Water Research Foundation. I'd like to thank the Division of Environmental Chemistry of ACS along with the editorial personnel who made the process of putting this book together very pleasant. Lastly I'd like to acknowledge Caitlin Glover for helping with the editorial process, James Saunders for providing the picture for the cover, and Veronika and Isabel Rosario for helping with the additional design of the cover.

Fernando L. Rosario-Ortiz

Department of Civil, Environmental, and Architectural Engineering
University of Colorado
428 UCB
Boulder, CO 80309, U.S.A.

Editor's Biography

Dr. Fernando Rosario-Ortiz

Dr. Fernando Rosario-Ortiz is currently an assistant professor at the University of Colorado in Boulder. He received his B.S. and M.S. in Chemistry from the University of Puerto Rico and the California Institute of Technology. He received his doctoral degree from UCLA in Environmental Science and Engineering in 2006 (Major Professor: I. H. Suffet). He was a post-doctoral researcher at the Southern Nevada Water Authority before joining Boulder in 2008. His current research focuses on environmental photochemistry, impact of watershed perturbations on water quality, and characterization of organic matter in different environments.

Chapter 1

Introduction

Fernando L. Rosario-Ortiz*

**Department of Civil, Environmental, and Architectural Engineering,
University of Colorado, Boulder, Colorado 80309**

***E-mail: Fernando.Rosario@colorado.edu.**

The study of dissolved organic matter (DOM) has fascinated researchers in different fields of science and engineering for many decades. The impact that DOM has on a wide array of environmental processes has resulted in the development of a multidisciplinary community of researchers all focusing on using different analytical techniques and experimental design to better understand DOM. This book offers select case studies focusing on the advanced characterization of DOM in different environments and with respect to different processes.

Organic Matter

The study of the physicochemical properties of dissolved organic matter (DOM) focuses on answering one key question: *How do we accurately predict (and potentially minimize) the effect that DOM has on a wide array of processes?* These processes include metal binding, fate and transport of organic compounds, formation of disinfection byproducts, light penetration in ecosystems, etc. Given the broad scientific impact of these processes, the study of DOM extends over many different disciplines ranging from ecology, environmental engineering, organic geochemistry, marine and atmospheric sciences, and analytical chemistry. As a result, the study of DOM may represent one of the most interdisciplinary topics in basic and applied sciences and engineering.

Perhaps the key to the multidisciplinary nature of the study of DOM is the lack of a fundamental understanding of the chemical structure of this material. The concentration and physicochemical properties of DOM are a function of the source of the material (e.g., terrestrial vegetation and biological processes within the water column) and the different processing mechanisms that occur in the environment (e.g., photolysis, settling, and microbial degradation). In spite of the chemical

complexity of DOM, there have been advances in understanding its effects on specific processes. For example, it is well known that the degree of aromaticity (as measured by NMR and characterized as the specific UV absorbance or SUVA) is a good predictor of the relative DOM source and of the formation of disinfection byproducts during water chlorination. Although there have been great advances in understanding, the development of a chemical model that could be used in *a priori* predictions of DOM physicochemical properties remains a distant goal.

While historically the focus has been on the characterization of DOM from either terrestrial or aquatic origins, there has been a shift to include other sources of organic matter that are important for understanding different environmental processes. For example, the contribution of algae-derived organic matter to the DOM pool in source waters for potable water production has gained attention over the past decade. This source of organic matter, termed algogenic organic matter (AOM), includes both intracellular and extracellular organic matter (IOM and EOM), and is characterized by differences in molecular weight and composition. In addition, the characterization of wastewater-derived organic matter, known as effluent organic matter (EfOM), has also gained attention, especially as the field of water reuse has gained importance. EfOM includes background DOM plus contributions from biological processes within wastewater treatment and as such is described as closer to aquatic-derived DOM in terms of aromaticity and fluorescence properties. Another interesting extension of DOM research is the characterization of organic mixtures in aerosols and fog. When the organic carbon in aerosol samples is extracted in water and characterized using typical DOM analytical tools, the results indicate the presence of what has been termed HUMic-LIKE Substances, known as HULIS, or in more general terms water-soluble organic carbon. HULIS, which is formed in part by the chemical reactions involving secondary aerosol formation, is a relatively new field and has important implications for the understanding of carbon transport in the atmosphere. These are just a number of examples where the study of DOM is being redefined to characterize other material, which shares some of the same complexity and importance that first motivated the study of DOM.

Book Organization

The development of any book focusing on DOM faces the immense challenge of defining a scope that is somewhat representative of the larger universe with regards to DOM research. In addition, there are other volumes being published that focus on specific aspects of DOM, including fluorescence characterization and physicochemical properties. The objective of this volume is to give the reader an overview of a select number of case studies where advanced understanding of DOM has resulted in a better understanding of a specific process.

Following this introductory chapter, the book includes three main sections. The first section of this volume, titled “Characterization of Dissolved Organic Matter,” deals with the topic of DOM characterization in general. The first chapter offers a detailed examination of the most impactful publications with regards to DOM characterization over time. The authors offer their interpretation

of the importance of different publications through the analysis of the number of citations and the Hirsch-index. The authors also provide what they term “classical papers” over the past five decades. The second chapter is an excellent review of the application of fluorescence for the characterization of DOM. The authors review the use of PARAFAC models for DOM characterization in surface and ocean waters. The third chapter explores the acid/base properties of DOM. The last chapter in the first section of the book offers a detailed review of water soluble organic carbon in aerosols, an emerging field within atmospheric research.

The second section is titled “Impact of Dissolved Organic Matter on Environmental Processes.” This section offers the reader a glimpse into the impact that DOM has on environmental processes, including interactions with contaminants, oxidants, and photochemical processes in wastewater-derived EfOM. The first chapter in this section is a review of the role organic matter plays as a natural xenobiotic. This work summarizes different aspects of DOM that are important for biological processes in the water column. The second chapter describes recent work on the sorption of hydrophobic organic contaminants to DOM, specifically focusing on DOM impacted by storm runoff. This chapter is followed by recent work on the study of the interactions between DOM and hydroxyl radicals using polymers to evaluate the role of molecular weight on the reaction rate constant. The next chapter focuses on the characterization of organic phosphorous in the Everglades region. The last chapter in this section describes the study of DOM and EfOM photochemical and photophysical properties as a function of molecular weight. This work focuses on measuring quantum yields for the formation of different reactive intermediates, including hydroxyl radical and fluorescence.

The last section of the book is titled “Impact of Dissolved Organic Matter on Water Treatment.” The first chapter describes new work on the role of molecular weight on the formation of DBPs. This is an interesting topic as there are potential differences in the chemical composition of the different molecular weight components. The second chapter investigates the sources and sinks of DBPs in DOM during treatment, focusing on coagulation. The third chapter examines changes in DOM and reactivity towards DBPs for samples collected during extreme weather events. Lastly, an evaluation of fluorescence for DOM removal by coagulation compares different data analysis methods and their resulting interpretations.

Concluding Remarks

As we move into the next decade of work in DOM characterization, we will continue to uncover different aspects of this mixture’s complex chemistry. The advent of ever more powerful analytical techniques and the vast amount of knowledge already amassed will continue to allow scientists and engineers to investigate different processes. Even though we may never be able to offer a complete chemical model representative of all DOM properties, continuing advances will allow researchers and engineers to fine tune our understanding of DOM and its impact on the numerous processes which are of interest to us.

Chapter 2

“Classic Papers” on Aquatic Humic Substances: Use of the Hirsch Index

E. Michael Thurman* and Imma Ferrer

Department of Civil, Environmental, and Architectural Engineering,
University of Colorado, Boulder, Colorado 80309, United States

*E-mail: mthurman@ono.com.

Citation impact data from the journals, *Science* and *Nature*, are used as a benchmark for defining a classic paper with a new application of the journal Hirsch-index, h_j . The h_j -index was first published eight years ago as a citation metric of journal impact. Here we use the h_j -index, to measure not only the impact of a journal, but also to measure the impact of papers within a journal. Next the h_j -index is applied to the field of environmental science with an example of “citation classics” dealing with aquatic humic substances from a 50-year record and a field of >20,000 journal articles. We hypothesize that the h_j -index may be readily calculated for any scientific paper, regardless of its age or field of activity, to gauge its past, present, or future citation-impact and that of its author.

Introduction

Recently (2005), Hirsch developed the h -index (1) to measure the citation impact of an individual research scientist. The index is equal to h if one has published h papers, each of which has h citations. Thus, if one has published, let us say 30 papers or more, and if 20 of those papers have 20 citations or more then the h -index would be the minimum value of 20. An h -index of 20 is an average value for a full professor in academia (1). The h -index has been rapidly accepted by the scientific community as a measure of a scientist’s impact in their field of endeavor.

However, there has been criticism of the h -index for individual scientists (2), which include the following. Firstly, age plays a factor, i.e. older scientists

have had more time to accrue citations than younger scientists. However, this criticism will be shown to be less important later in this chapter, since the number of scientists citing papers has increased, thus, giving more recent papers an advantage over older papers. This conclusion also implies that there is a bias toward citing recent papers to show relevancy and impact. Secondly, comparisons of h -indices for people from various fields will vary because of differences in citation statistics. This is readily seen if one compares say mathematics to human biology, where the number of scientists working in these two fields differs by several orders of magnitude. Thirdly, there is no discrimination among the various authors on a paper, so that all receive equal credit for citations no matter what their contribution was. Fourthly, review papers receive a large number of citations, which do not reflect scientific accomplishment of the individual, and some authors may write numerous reviews (2). In this chapter, we address these issues, as will be discussed later in this chapter.

The concept of the h -index has also been applied to journals by Braun et al. (3). The journal h -index is equal to h_j if a journal has published h_j papers, each of which has received h_j citations for a given year. Braun et al. (3) show that the h_j -index is another measure of the impact of a journal. Our work here further explores the bibliometric usefulness of the h_j -index in new ways. The first aim of this chapter is to show that the h_j -index evaluates a paper's prestige and popularity. The second aim is to evaluate h_j -indices among journals and to establish a rating of a "classic impact paper" based on the most prestigious journals, *Science* and *Nature*. The third and final aim is to show the value of these metrics in environmental science, and by way of example, to all fields of the physical sciences, with special reference to "aquatic humic substances". The significance of this chapter is that important papers may be rapidly culled from the literature using the h_j -index and that this index is a valuable tool for the working scientist to stay current in the rapidly expanding literature of today, especially with regard to environmental chemistry and "aquatic humic substances".

The Journal Hirsch Index (h_j)

The h_j -index is easily determined using the Institute for Scientific Information (ISI) database called the "ISI Web of KnowledgeSM". One simply goes to the search page and lists a journal in the field labeled "publication name" and a year of publication in the "timespan" field (i.e. 1980 to 1980), and pushes the "Search" button, which then calls up all papers within that year. Next the research articles are culled from the entire list by marking the "Article" box and pushing the "Refine" button. The citation report is calculated from this subset of journal articles using the "Create Citation Report" button, in the upper right-hand portion of the computer screen. The database then reports the total number of papers published within the year, the total number of times cited, the average citations per item, and the journal Hirsch index, h_j . Finally, the entire list of papers is given ranked from the highest to lowest citations by the ISI database. For example, using this exact procedure for *Science* in 1980 gives an h_j -index of 176 and for *Environmental Science and Technology* an h_j -index of 51.

Table 1. List of Environmental Journals Examined in This Study of h_j -Indices and Classic Papers for 1995 Compared to *Science* and *Nature* (Data from 11 November 2013)

<i>Journal</i>	<i>h_j-Index (1995)</i>	<i>Journal Impact Factor 2010</i>	<i>Total Annual Citations (1995)</i>	<i>Number of Classic Papers (1995) $\geq h_j$-index_{science/nature}</i>
Environmental Science & Technology	95	5.3	29075	7
Journal of Chromatography A	74	4.6	30936	0
J. Agricultural and Food Chemistry	66	2.9	19712	6
Water Research	60	5.4	13222	1
Science of the Total Environment	50	3.8	11017	0
Environmental Toxicology & Chemistry	48	2.6	8030	0
Chemosphere	46	3.6	8681	0
J. Environmental Quality	45	3.5	6909	3
Marine Chemistry	42	2.8	6195	3
J. Hydrology	38	3.7	5258	0
Archives Environmental Contaminant & Toxicology	33	2.0	3254	0
Organic Geochemistry	29	2.8	3205	0
Groundwater	26	1.4	2361	0
J. Environmental Engineering ASCE	26	1.2	2197	0
Marine Environmental Research	26	1.9	1959	0

Continued on next page.

Table 1. (Continued). List of Environmental Journals Examined in This Study of h_j -Indices and Classic Papers for 1995 Compared to *Science* and *Nature* (Data from 11 November 2013)

<i>Journal</i>	<i>h_j-Index (1995)</i>	<i>Journal Impact Factor 2010</i>	<i>Total Annual Citations (1995)</i>	<i>Number of Classic Papers (1995) $\geq h_j$-index_{science/nature}</i>
International J. Environmental Analytical Chemistry	20	1.8	1713	0
Applied Geochemistry	21	1.7	1549	1
Science	310	31	343842	310
Nature	318	38	315901	318

Using this procedure we indexed two of the most popular and prestigious journals in science, that is *Science* and *Nature*. Both journals have a more than 50-year citation history as major scientific journals and have current impact factors of 26 and 29, respectively, for 2007. These impact factors are some of the highest for major journals that publish papers inclusive of all fields of science. We also indexed the environmental journal with the highest impact factor, *Environmental Science & Technology* (*ES&T*) with an impact factor of 4.4 for 2007. *ES&T* was chosen from a list of 17 environmental journals (Table 1) that have published in this field since 1995.

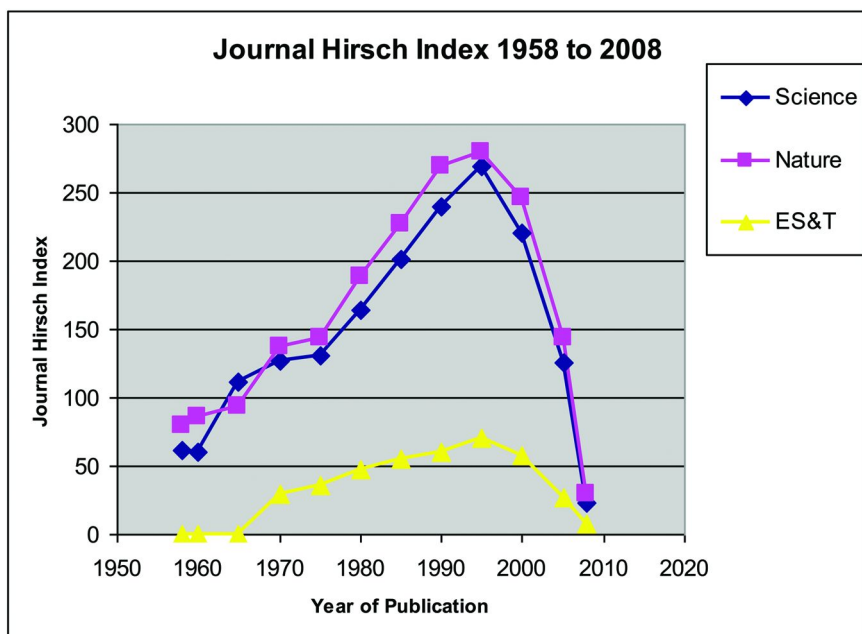


Figure 1. The increase in Journal Hirsch Index, h_j , from 1958 to 1995 and then decrease to the present for *Science* and *Nature* and for *Environmental Science and Technology*.

Figure 1 shows the increase and recent decrease in the h_j -index for *Science*, *Nature*, and *ES&T* for the last 50 years from 1958 to 2008 (40 years for *ES&T*, 1969-2008). The h_j -indices peak at between 250 and 280 for *Science* and *Nature*. At the peak of the h_j -index in 1995, the papers exceeding the h_j -index account for 70% of the citations in *Science* and 68% in *Nature*. Because both journals published ~1000 journal articles per year between 1990 and 1995, the $\geq h_j$ papers represent 25-30% of the papers accounting for ~70% of the citations, which is

a Pareto distribution (sometimes called the 80/20 rule). The Pareto distribution (4), an example of a hyperbolic distribution, is applicable here in that the majority of the citation impact of the journals is derived from these $\geq h_j$ papers. Because *Science* and *Nature* represent the “crème-de la crème” of scientific papers condensed from the key fields of the physical sciences, we argue that this boundary of h_j papers may be considered a definition of a “classic impact paper” as discussed below.

(Author’s Note) We chose the term h_j -index to prevent confusion with the original definition of h -index by Hirsch (1). Impact factor for 2007 is equal to the number of citations that a journal receives in 2007 for articles published in the same journal during 2005 and 2006 divided by the number of papers indexed for those two years.

Defining Classic Papers

Status, as defined by Bollen et al. (5), states that it is comprised of both popularity and prestige. For example, the popularity of an actor is one who is widely known and appreciated by everyone, both experts and non-experts alike. While prestige is popularity derived only from experts. For example, the difference between an actor receiving a People’s Choice Award (a popular award to actors/actresses chosen by the general public) and an Oscar (prestigious award chosen by the Academy of Motion Pictures) is a good example of the difference between popularity and prestige. Both *Science* and *Nature* match the definition of prestige in that they are journals based in both Europe and in the United States with the highest impact factor for journals accepting all papers in the physical sciences. They have the highest standards of acceptance in the reviewing process as determined by leading-world experts.

They are also popular, in that they are continually indexed by newspapers, radio, and television from around the world for the latest discoveries in the physical sciences. Furthermore, it is known by nearly all publishing scientists that only true discovery papers or papers of the broadest scientific interest (a measure of impact) are published in *Science* and *Nature*. Many scientists read or subscribe to these journals to stay current with the latest breakthroughs in the physical sciences. For these reasons, we conclude that papers from *any journal* with annual citations that exceed the h_j -index of *Science* and *Nature* could be considered “classic impact papers” in their respective fields for they exceed the requirements of popularity, prestige, and citation impact.

Several definitions of “classic papers” were given by Garfield in series of essays (1977-1989) appearing in *Current Contents* (6-8). Garfield (8) concludes in his final essay on this topic with an example of Nobel Prize winners. Their Nobel papers receive at least 300 citations, which meets the definition of a classic paper because their work is obviously of classic proportions. Garfield has acknowledged, however, the difficulty of deciding classics that are non-Nobel in all of his essays dealing with this subject (6-8). Garfield’s Nobel-Prize definition of a classic paper compares closely in citations with our definition (within $\pm 10\%$) for 1995 citations.

The h_j -index over Time

Figure 1 shows that the h_j -index for *Science* and *Nature* has increased over the last 50 years from 75 to 250 over a 40-year time period before decreasing to ~25 in 2008. The number of annual citations has increased from 50,000 in 1960 to 250,000 in 1995. The peak in citations occurred in 1994-1995 after 15 years or ~2 half-lives of an average journal article (9), which is equal to 75% of the total citations received. Figure 2 shows the correlation of the h_j -index with the number of annual citations of *Science* and *Nature*. The trend line is a power plot that shows a correlation of 0.97 and follows the hyperbolic laws of bibliometrics (4). This plot is important in that it shows that the number of citations that these journals receive goes up exponentially while the number of h_j “classic impact papers” increases linearly.

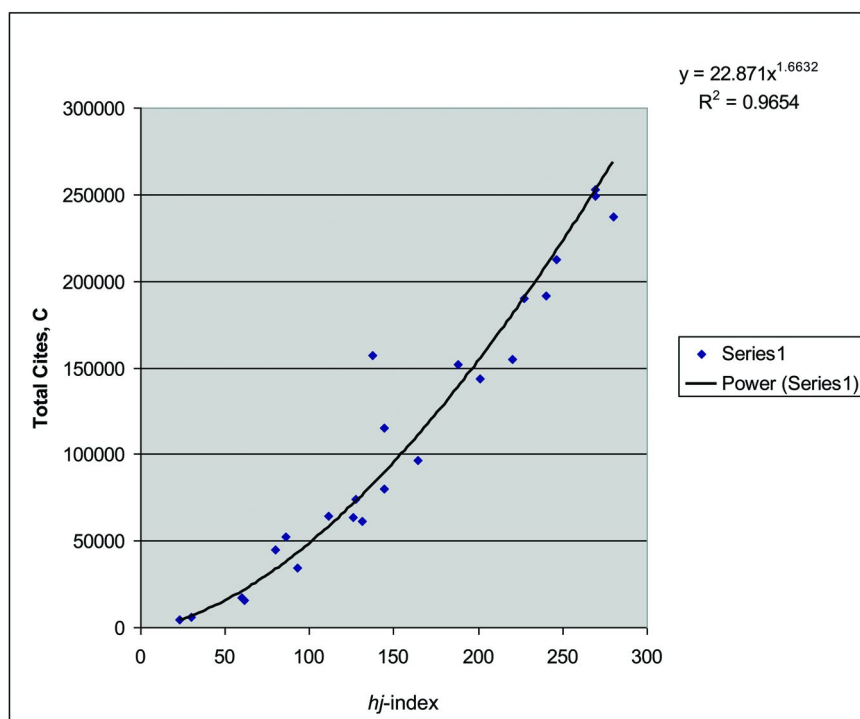


Figure 2. The power-series relationship of h_j -index to total cites, C, over a 50-year period for *Science* and *Nature* combined.

We found, while plotting the data in Figure 2, that the older papers (i.e. >30 years) and younger papers (i.e. <5 years) have low total citations and thus a lower h_j but they are still classic impact papers by the h_j definition. This result of low total citations seems reasonable for younger papers since their citation life-history lies

ahead of them, but is counter intuitive for older papers! It would seem that older papers would have had more time to accumulate the highest number of citations, but this is not the case. At least two reasons are involved. First the number of scientists that were citing older papers is much less during the critical two half-lives of the paper's publication. Secondly, newer papers have replaced older "citation classics". The fact that papers in the 1990s have the highest h_j -index makes sense too because of the increasing number of journals (and citations) that can give rise to higher citations for classic impact papers. Thus, it seems valid to accept a sliding scale for the h_j -index for both the older papers and, more importantly, for the younger papers. By a sliding scale for classic papers, we mean the following. Looking at the data in Figure 1, papers published in 1970 have an h_j -index of greater than 150, in 1998 the h_j -index is greater than 280, and in 2008 the h_j -index is greater than 150 again. Thus, papers are considered to be classics if they exceed these sliding scale values. The value of this sliding scale is that it addresses one of the major criticisms of the h -index for individual scientists. In that a classic paper may be defined in the first three years by comparing it to the h_j -index of the journal for that same year! This is a valuable tool then for the working scientist to evaluate his or her work and that of others.

We hypothesize for these reasons that younger papers will continue their classic status ($\geq h_j$ -index of *Science* and *Nature*) over one to two half-lives and these papers should be recognized as classic papers at the present time rather than waiting for time to pass and >300 citations or more to accumulate (7). Thus, the h_j -index is a tool to evaluate younger papers for their popularity, prestige, and impact. The corollary to this statement is that young or recent new authors in a field may be evaluated by the cited impact of their recent h_j papers. Recent h_j papers also show the continued performance (as measured by citation impact) of older more established scientists (i.e. tenured).

Classic Papers in Environmental Science

Figure 1 shows the relationship of time to h_j values from 1969 to the present and represents the 40 years of record for *ES&T*. The h_j -indices for *ES&T* are considerably less than *Science* and *Nature* as would be expected given that *ES&T* has a much lower impact factor, 4.4 versus 26-29. The shape of the h_j curve though is similar with the peak h_j -index occurring in 1994-1995. The number of annual citations is also considerably less, about 10-15 times, but a similar power relationship exists for the h_j -index and total citations in *ES&T* (Figure 3). The exponent of the power curves are different though for Figures 2 and 3. *Science* and *Nature* have an exponent of 1.66 while *ES&T* is 1.95. These values mean that to double the h_j -index of *Science* and *Nature* a factor of ~3 times more citations are needed while for *ES&T* a doubling of the h_j -index requires ~4 times more total journal citations. We consider this exponent to be a measure of the significance factor of the journal within a field (i.e. the smaller the exponent the greater the significance of a journal in the field because less citations are needed per paper to reach h_j status).

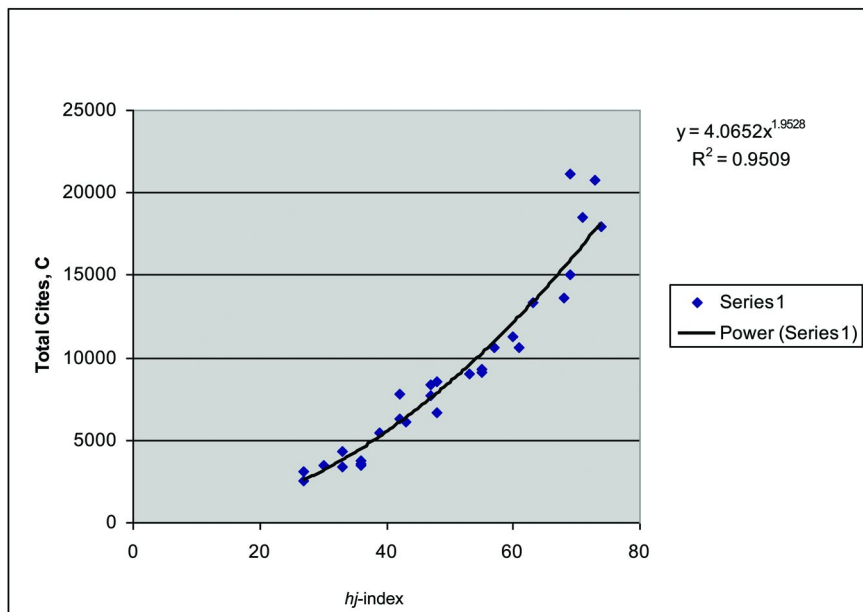


Figure 3. The h_j -index for *ES&T* versus to total citations from 1969 to 2008 Also showing a power-series relationship.

The x coefficient of this power plot (Figures 2 and 3) is ~23 for *Nature* and *Science* and is ~4 for *ES&T*. The x coefficient is a measure of the readership-impact of the journal or impact factor of the journal over its lifetime. The larger this x-coefficient is, the more citations that a journal is receiving per h_j paper that is published. In fact, these values of the x coefficient are quite close to the journal impact factors of *Science* and *Nature* (26-29) and *ES&T* (4.4) for 2007. The difference being that the x-coefficient rates the journal over its lifetime while the impact factor rates the journal for a two-year period (2005-2006 for values in Table 1).

“Citation Classics” on Aquatic Humic Substances.

We begin the compilation of classic-citation papers on aquatic humic substances with the decade of the 1960s, which is just prior to the beginning of the journal *Environmental Science and Technology* (1968). In the future, we will refer to the citation classics and simply classic papers. This time line represents the beginning of an important mark as the importance of environmental science to the

scientific community at large. The decade of the 1960s began with several highly cited papers that dealt with organic matter in the ocean and were the preamble of studies dealing with dissolved organic matter and aquatic humic substances. The citation classics are culled from the literature using a series of keywords including: aquatic humus, aquatic humic, fulvic, humic, dissolved organic matter, and natural organic matter. We then ordered these papers by citation numbers and checked each one manually to be sure they dealt with aquatic humic substances and dissolved organic matter rather than soil organic matter. If the number of citations for these papers exceeded the h_i for *Science* and *Nature* for that year (Figure 1), it was chosen as a citation classic for our list. For example, using the terms above we found that the 1960s only papers on dissolved organic carbon or dissolved organic matter gave citations greater than the *Science* and *Nature* scale of 100-150 citations (see data in Figure 1 for those years). Authors' note: The senior author of this chapter (Thurman) was an active researcher in aquatic humic substances during the decades of 1960s-1990s and thus, this knowledge was brought to bear on term selection and searching the literature during these decades.

Decade of the 1960s

The 1960s were the beginning of the study of dissolved organic carbon in seawater and freshwater. It began with the invention of the carbon analyzer and the subsequent paper by Menzel and Vaccaro (1964) that has been cited more than 700 times. The original work resulted in the Oceanographic carbon analyzer, which was one of the original, commercial total organic carbon analyzers. The “original carbon analyzer” that began this revolution in studies of dissolved organic matter resides at Wood Hole Oceanographic Institute (viewed by Thurman, 1985). After the invention of the total organic carbon (TOC) analyzer it was applied to seawater samples and the paradigm shifted to “what is the organic matter in the ocean”? This led to oceanographers showing the way with studies of organic matter and humic substances. The two papers that were cited as classics illustrate this important first step in the study of aquatic humic substances in water. There were no classic papers found that deal with aquatic humic substances in literature searches of the 1960s. However, the paper by Ghassemi and Christman (1968) has been cited 94 times and is as close to classic that appeared in the freshwater literature of humic substances. The title of this 1968 paper is “Properties of yellow organic acids in natural waters”. This paper was one of the initial papers that pointed out the importance of humic substances in freshwater chemistry. It was published in Limnol. Oceanogr. 1968, 13, 583-592., as were the papers below that are classics from the 1960s. There were no papers that dealt directly with aquatic humic substances, i.e. using these terms as a search criteria. However, it is instructive to search the marine chemistry literature for classics that paved the way, so to speak, for the work to come in the following decade.

Classic Papers on Dissolved Organic Matter 1960s

1. (350 Cites) *Dissolved organic matter in seawater as a source of particulate food*; Baylor, E. R.; Sutcliffe, W. H. *Limnol. Oceanogr.* **1963**, *8*, 369–371.
2. (750 Cites) *The measurement of dissolved organic and particulate carbon in seawater*; Menzel, D. W.; Vaccaro, R. F. *Limnol. Oceanogr.* **1964**, *9*, 138–142.

Decade of the 1970s

The decade of the 1970s saw the studies of marine organic matter become important especially with the development of XAD resins in the mid-1970s with the paper by Mantoura on removing humic substances from seawater. This work was followed up by the work of Aiken et al. on XAD isolation so that it was possible to remove and study humic substances at trace levels from all types of natural waters. The book by Egil Gjessing in 1976 on characterization of aquatic humus was the first detailed study of aquatic humic substances and is one of the first titles using the term, “aquatic humus”.

The removal of humic substances (organic matter and iron) by flocculation was a classic paper by Sholkovitz and represented the marine/freshwater boundary. The paper by Reuter and Perdue emphasized the importance of heavy metal-organic interactions—a theme that re-appears in papers by Buffle et al., as well as papers dealing with metal complexation in natural waters by humic substances. But perhaps one of the papers of the 1970s that started a revolution in the study of aquatic humic substances, which is still important today, is the paper by Rook in 1977 on the chlorination of fulvic acid and the effect that it has on formation of chlorination by-products such as chloroform and its related products. The following 10 papers are the citation classics of the 1970s that paved the way for the detailed studies of aquatic humic substances of the 1980s.

Classic Papers on Aquatic Humic Substances 1970s

1. (284 Cites) *Chemical and isotopic evidence for the in situ origin of marine humic substances*; Nissenbaum, A.; Kaplan, I. R. *Limnol. Oceanogr.* **1972**, *17*, 570–582.
2. (210 Cites) Analytical concentration of humic substances from natural waters; Mantoura, R. F. C.; Riley, J. P. *Anal. Chim. Acta* **1975**, *76*, 97–106.
3. (Unknown) *Physical and Chemical Characteristics of Aquatic Humus*; Gjessing, E. CRC Press: Boca Raton, **1976**; 120 p. (Citations number Unknown).

Publication Date (Web): June 19, 2014 | doi: 10.1021/bk-2014-1160.ch002

4. (569 Cites) *Flocculation of dissolved organic and inorganic matter during mixing of river water and seawater*; Sholkovitz, E. R. *Geochim. Cosmochim. Acta* **1976**, *40*, 831–845.
5. (273 Cites) *Importance of heavy metal-organic interactions in natural waters*; Reuter, J. H.; Perdue, E. M. *Geochim. Cosmochim. Acta* **1977**, *41*, 325–334.
6. (198 Cites) *Measurement of complexation properties of humic and fulvic acids in natural waters with lead and copper ion selective electrodes*; Buffle, J.; Greter, F. L.; Haerdi, W. *Anal. Chem.* **1977**, *49*, 216–222.
7. (364 Cites) *Chlorination reactions of fulvic acids in natural waters*; Rook, J. J. *Environ. Sci. Technol.* **1977**, *11*, 478–482.
8. (271 Cites) *Removal of dissolved humic acids and iron during estuarine mixing*; Sholkovitz, E. R.; Boyle, E. A.; Price N. B. *Earth Planet Sc. Lett.* **1978**, *40*, 130–136.
9. (522 Cites) *Complexation of metals with humic materials in natural waters*; Mantoura, R. F. C.; Dickson, A.; Riley, J. P. *Estuarine Coastal Mar. Sci.* **1978**, *6*, 387–408.
10. (205 Cites) *Comparison of XAD macroporous resins for the concentration of fulvic acid from aqueous solution*; Aiken, G. R.; Thurman, E. M.; Malcolm, R. L. *Anal. Chem.* **1979**, *51*, 1799–1803.

Decade of the 1980s

The decade of the 1980s saw a major shift from marine science to freshwater aquatic humic substances and the establishment of the International Humic Substances Society (IHHS) in 1981 by Ron Malcolm and Pat McCarthy. The first paper to lead the way was a method's paper on the isolation of aquatic humic substances from water by Thurman and Malcolm (1981). This paper was the culmination of five years of effort by the U.S. Geological Survey's research team in Denver, Colorado, on the isolation of aquatic humic substances. The paper has become of the foundation of isolation of aquatic humic substances and was adopted by the International Humic Substances Society (IHHS). A second paper that was closely related to the IHHS was the importance of humic standards. The paper by Malcolm and McCarthy on the limitations in the use of commercial humic acids in water and soil research is a classic and a fundamental reason for the establishment of a reference collection of “real” humic substances from many environments, such as soil and water. The paper by Malcolm and McCarthy points out that Aldrich Humic acid is in fact not humic acid but an oxidized coal and does not represent aquatic or soil humic substances. Thus, one of the original goals of the International Humic Substances Society (IHHS) was the establishment of a reference collection of humic substances. The website (<http://www.humicsubstances.org/index.html>) states all the goals of the IHHS:

“This website provides information on the International Humic Substance Society, its products and services. IHSS was founded in Denver, Colorado, USA, on September 11, 1981 to bring together scientists in the coal, soil, and water sciences with interests in humic substances. IHSS has a membership of nearly 900 scientists. The Society is recognized as a world leader in fostering scientific education and research, and promoting public understanding of humic substances.”

There were 60 papers published in the decade of the 1980s with aquatic humic substances in the title, the most papers from any decade, and of those there are two classics by Thurman and Malcolm (1981) and Tipping (1981). There are a thousand papers on dissolved organic matter from the same time period and 24 classic papers are listed below. Two classic books also appeared during this decade on aquatic humic substances and natural organic matter. They are included with the classic papers of this decade.

What is most obvious in the transition from the decade of the 1970s to the 1980s is, firstly, the number of papers that appeared on aquatic humic substances and dissolved organic matter. This represents a doubling of classic papers that deal with many topics of the interactions of aquatic humic substances (AHS) with metals and organic pollutants. Isolation and characterization of aquatic humic substances (AHS) transport of AHS, photochemical reactions of AHS, biodegradability and origin of AHS. It is important to realize that when the classic papers double the amount of papers published on this topic has increased by a logarithmic amount. Thus, the 1980s were the blossoming of the study of aquatic humic substances. Although the paper by Frimmel in 1980 was not a classic in citations, it was the first use of the term, “aquatic humic substances” in a journal article that was found in searched literature. In fact, Frimmel authored a number of papers during the 1980s using the term “aquatic humic substances” and was a leader in this field, in spite of papers not reaching the classic status in citations. Perhaps this shows the weakness of using a citation index as the only definition of classic papers. Surely, the first use of the term in a journal article qualifies as a classic.

Metal-ion complexation by aquatic humus. 1. A bog lake as a source of humic substances, Frimmel, F.H., Niedermann, H. Zeitschrift fur wasser und abwasser forschung **1980**, (Journal for Water and Wastewater Research), *13*, 119-124.

The term aquatic humus was used in the 1970s and 1980s by Norwegian researchers, in particular, the classic work of Egil Gjessing, which was discussed in the preceding section of the 1970s. The reader is encouraged to browse through and read these papers as they represent the classic works of the 1980s, and to some degree, at least in the view of the authors, the coming of age of aquatic humic substances in the scientific literature.

An interesting aside in the study of aquatic humic substances and dissolved organic carbon is the paper by Sugimura and Suzuki (1987) in Marine Science. They describe a “new” organic carbon analyzer that uses high temperature combustion and a platinum catalyst. Firstly, this is hardly new since the first author (Thurman) used a similar instrument for his PhD thesis in the 1970s, ten years earlier. Secondly, and more importantly, this paper sparked a heated

controversy concerning the nature and amount of DOC in the oceans. Sugimura and Suzuki suggested that it was under-estimated by previous methods and that an unknown amount of DOC, humic-like, was responsible. This controversy eventually dissolved as it was shown that the persulfate method had given good values for seawater DOC and there was no “unknown” humic-like DOC in seawater. Nonetheless, this paper became a classic.

The following 25 papers are the citation classics of the 1980s, which in some way, were the golden years for the initial studies of aquatic humic substances in the environment. This will be seen more clearly as we move to the decade of the 1990s. The reader is encouraged to read over these two classic books as primers of their time on dissolved organic matter and the role of aquatic humic substances.

Classic Books on Aquatic Humic Substances

1. **(2000 Cites)** *Organic Geochemistry of Natural Waters*; Thurman, E. M.; Martinus Nijhoff Publishers: The Netherlands, **1985**; 497 p.
2. **(750 Cites)** *Humic Substances in Soil, Sediment, and Water: Geochemistry, Isolation, and Characterization*; Aiken, G. R., McKnight, D. M., Wershaw, R. L., McCarthy, P., Eds.; Wiley & Sons, Inc.: New York, **1985**; 692 p.

Classic Papers on Aquatic Humic Substances 1980s

3. **(931 Cites)** *Preparative isolation of aquatic humic substances*; Thurman, E. M.; Malcolm, R. L. *Environ. Sci. Technol.* **1981**, *15*, 463–466.
4. **(552 Cites)** *The adsorption of aquatic humic substances by iron oxides*; Tipping, E. *Geochim. Cosmochim. Acta* **1981**, *45*, 191–199.
5. **(626 Cites)** *Comprehensive approach to preparative isolation and fractionation of dissolved organic carbon from natural waters and wastewaters*; Leenheer, J. A. *Environ. Sci. Technol.* **1981**, *15*, 578–587.
6. **(749 Cites)** *Adsorption by dissolved organic matter of the sea (yellow substance) in the UV and visible domains*; Bricaud, A.; Morel, A.; Prieur, L. *Limnol. Oceanogr.* **1981**, *26*, 43–53.
7. **(220 Cites)** *The effects of adsorbed humic substances on the surface charge of goethite (alpha FeOOH) in fresh waters*; Tipping, E.; Cooke, D. *Geochim. Cosmochim. Acta* **1982**, *46*, 75–80.
8. **(479 Cites)** *Binding of DDT to dissolved humic material*; Carter, C. W.; Suffet, I. H. *Environ. Sci. Technol.* **1982**, *16*, 735–740.
9. **(417 Cites)** *Adsorption of natural dissolved organic matter at the oxide water interface*; Davis, J. A. *Geochim. Cosmochim. Acta* **1982**, *46*, 2381–2393.

10. (374 Cites) *The contribution of humic substances to the acidity of colored natural waters*; Oliver, B. G.; Thurman, E. M.; Malcolm, R. L. *Geochim. Cosmochim. Acta* **1983**, *47*, 2013–2035.
11. (243 Cites) *Conservative behavior of riverine dissolved organic carbon in the Severn estuary-chemical and geochemical implications*; Mantoura, R. F. C.; Woodward, E. M. S. *Geochim. Cosmochim. Acta* **1983**, *47*, 1293–1309.
12. (374 Cites) *Reverse-phase separation method for determining pollutant binding to Aldrich humic acid and dissolved organic carbon of natural waters*; Landrum, P. F.; Nihart, S. R.; Eadie, B. J. *Environ. Sci. Technol.* **1984**, *18*, 187–192.
13. (275 Cites) *The chemistry and transport of soluble humic substances in forested watersheds of the Adirondack Park: New York*; Cronan, C. S.; Aiken, G. R. *Geochim. Cosmochim. Acta* **1985**, *49*, 1697–1705.
14. (271 Cites) *Photosensitized transformations of involving electronic energy transfer in natural waters-The role of humic substances*; Zepp, R. G.; Schlotzhauer, P. F.; Sink, R. M. *Environ. Sci. Technol.* **1985**, *19*, 74–81.
15. (299 Cites) *Interaction between polycyclic aromatic hydrocarbons and dissolved humic material-binding and dissociation*; McCarthy, J. F.; Jimenez, B. D. *Environ. Sci. Technol.* **1985**, *19*, 1072–1076.
16. (286 Cites) *Limitations in the use of commercial humic acids in water and soil research*; Malcolm, R. L.; McCarthy, P. *Environ. Sci. Technol.* **1986**, *20*, 904–911.
17. (776 Cites) *Water solubility enhancement of some organic pollutants and pesticides by dissolved humic and fulvic acids*; Chiou, C. T.; Malcolm, R. L.; Brinton, T. I. *Environ. Sci. Technol.* **1986**, *20*, 502–508.
18. (219 Cites) *Dissolved humic substances in the Amazon River system*; Ertel, J. R.; Hedges, J. I.; Devol, A. H. *Limnol. Oceanogr.* **1986**, *31*, 739–754.
19. (319 Cites) *Fluorescence quenching method for determining equilibrium constants for polycyclic aromatic hydrocarbons binding to dissolved humic material*; Gauthier, T. D.; Shane, E. C.; Guerin, E. F. *Environ. Sci. Technol.* **1986**, *20*, 1162–1166.
20. (296 Cites) *A comparison of water solubility enhancements of organic solutes by aquatic humic materials and commercial humic acids*; Chiou, C. T.; Kile, D. E.; Brinton, T. I. *Environ. Sci. Technol.* **1987**, *21*, 1231–1234.
21. (414 Cites) *Effects of structural and compositional variations of dissolved humic materials on pyrene Koc values*; Gauthier, T. D.; Seitz, W. R.; Grant, C. L. *Environ. Sci. Technol.* **1987**, *21*, 243–248.
22. (239 Cites) *Determination of the biodegradable fraction of dissolved organic matter in waters*; Servais, P.; Billen, G.; Hascoet, M. C. *Water Res.* **1987**, *21*, 445–450.
23. (300 Cites) *Availability of dissolved organic carbon for planktonic bacteria in oligotrophic lakes of differing humic content*; Tranvik, L. J. *Microbial Ecol.* **1988**, *16*, 311–322.

24. (495 Cites) *A high-temperature catalytic-oxidation method for the determination of non-volatile dissolved organic carbon in seawater by direct injection of a liquid sample*; Sugimura, Y.; Suzuki, Y. *Mar. Chem.* **1988**, *24*, 105–131.

25. (406 Cites) *Origin, composition, and flux of dissolved organic carbon in the Hubbard Brook Valley*; McDowell, W. H.; Likens, G. E. *Ecol. Monogr.* **1988**, *58*, 177–195.

Decade of the 1990s

The decade of the 1990s saw a different trend with aquatic humic substances being used less in the titles of papers and a much more diverse nature of papers which used humic substances as a keyword. The papers dealt with many aspects of how humic chemistry affects water quality and reactions. The field of environmental engineering became involved with AHS and their influence shaped the studies of the 1990s. For example, the importance of chlorine on AHS became a dominant issue. The engineering community was interested in the entire spectrum of organic matter in water and we saw the rise of a new term, natural organic matter or NOM, which was introduced to the literature in the mid-90s. Dissolved organic matter became the focus and less work occurred with characterization of aquatic humic substances and their isolation, at least as far as the classic papers are concerned. The citation classics of the 1990s dealt with water treatment, membrane fouling, UV oxidation, carbon cycle, photoreactions, sorption, and fluorescence as a tool to understand the nature of dissolved organic matter. This decade has 13 papers that have humic substances in the title and deal with aquatic samples, which is approximately half as many as in the previous decade. The reader is encouraged to read over these classics as we see a transition to classic papers of the 2000s that deal with the applied aspects of aquatic humic substances.

Classic Papers on Aquatic Humic Substances 1990s

1. (333 Cites) *Chlorination of humic materials-by-product formation and chemical interpretations*; Reckhow, D. A.; Singer, P. C.; Malcolm, R. L. *Environ. Sci. Technol.* **1990**, *24*, 1655–1664.
2. (342 Cites) *Formation of carbonyl compounds from UV-induced photodegradation of humic substances in natural waters-fate of riverine carbon in the sea*; Kieber, R. J.; Zhou, X. L.; Mopper, K. *Limnol. Oceanogr.* **1990**, *35*, 1503–1515.
3. (351 Cites) *Fluxes of dissolved organic nutrients and humic substances in a deciduous forest*; Qualls, R. G.; Haines, B. L. *Ecology* **1991**, *72*, 254–266.

4. (405 Cites) *A unifying model of cation binding by humic substances*; Tipping E.; Hurley, M. A. *Geochim. Cosmochim. Acta* **1992**, *56*, 3627–3641.
5. (297 Cites) *Effects of aqueous chemistry on the binding of polycyclic aromatic hydrocarbons by dissolved humic materials*; Schlautman, M. A.; Morgan J. J. *Environ. Sci. Technol.* **1993**, *27*, 961–969.
6. (249 Cites) *Adsorption of aquatic humic substances on hydrophobic ultrafiltration membranes*; Jucker, C.; Clark, M. M. *J. Membrane Sci.* **1994**, *97*, 37–52.
7. (927 Cites) *Molecular-weight, polydispersity, and spectroscopic properties of aquatic humic substances*; Chin, Y. P.; Aiken, G.; Oloughlin, E. *Environ. Sci. Technol.* **1994**, *28*, 1853–1858.
8. (659 Cites) *Humic substances as electron acceptors for microbial respiration*; Lovley, D. R.; Coates, J. D.; Blunt-Harris, E. L. *Nature*, **1996**, *382*, 445–448.
9. (223 Cites) *Fluorescence characterization of IHSS humic substances: Total luminescence spectra with absorbance correction*; Mobed, J. J.; Hemmingsen, S. L.; Autry, J. L. *Environ. Sci. Technol.* **1996**, *30*, 3061–3065.
10. (356 Cites) *Binding of pyrene to aquatic and commercial humic substances: The role of molecular weight and aromaticity*; Chin, Y. P.; Aiken, G. R.; Danielsen, K. M. *Environ. Sci. Technol.* **1997**, *31*, 1630–1635.
11. (310 Cites) *Molecular size distribution and spectroscopic properties of aquatic humic substances*; Peuravuori, J.; Pihlaja, K. *Anal. Chim. Acta* **1997**, *337*, 133–149.
12. (472 Cites) *Humic ion-binding model VI: An improved description of the interactions of protons and metal ions with humic substances*; Tipping, E. *Aquat. Geochem.* **1998**, *4*, 3–48.
13. (309 Cites) *Quinone moieties act as electron acceptors in the reduction of humic substances by humics-reducing microorganisms*; Scott, D. T.; McKnight, D. M.; Blunt-Harris, E. L. *Environ. Sci. Technol.* **1998**, *32*, 2984–2989.

Decade of the 2000s

There were only two papers considered as classic status with the key words of aquatic humic substance(s), as explained in the keyword search for the decade of the 2000s. These two papers dealt with proton binding and the Donnan model for proton binding in aquatic humic substances. When the terms dissolved organic matter was searched there are approximately 20 classic papers, most of which, do not deal directly with humic substances, but rather are applied to various environmental issues revolving around the dissolved organic matter pool and what is now called natural organic matter. The reader may think that it is not important the terms we use for dissolved organic matter, but we would argue that the terms are important in that they direct the focus of our research.

1. (263 Cites) *Generic NICA Donnan model parameters for proton binding by humic substances*; Milne, C. J.; Kinniburgh, D. G.; Tipping, E. *Environ. Sci. Technol.* **2001**, 35, 2049–2059.
2. (236 Cites) *Proton binding study of standard and reference fulvic acids, humic acids, and natural organic matter*; Ritchie, J. D.; Perdue, E. M. *Geochim. Cosmochim. Acta* **2003**, 67, 85–96.

Basically, there has been a keen interest in natural organic matter, not so much as what it is, but what role it may have in environmental chemistry. It is at this point that we, the authors, leave the reader to ponder the future of aquatic humic substances. It is, in effect, that the people who worked on aquatic humus, have slowly left the field and it has been replaced by a vast number of scientists and engineers with totally different interests. The role of the IHHS, perhaps it is as the original organizers envisioned an organization that serves as a source of soil and aquatic humic substances and dissolved organic matter (i.e. total collection of NOM via reverse osmosis) for scientific study. We would like to end the chapter with some of the wisdom of the founders of IHHS, in particular, Pat MacCarthy, who said, and we paraphrase, “When we determine the structure(s) of humic substances, they will cease to exist!” The point being that humic substances are a general term for natural organic matter for which we do not know the structures or names. But at some time in the future, when we should learn their structures, the term aquatic humic substances will no longer be necessary and will be forgotten. However, given the complexity of dissolved organic matter, with literally thousands of different compounds, it is not likely that the structure will be easily known, although classes of compounds will continue to be determined. Thus, the term “humic substances” is safe, at least at the moment.

Conclusions

We conclude that the h_j -index is a valuable research tool for the working scientist or journalist to stay current in the rapidly expanding literature of today, especially in the field of aquatic humic substances and dissolved organic matter. We realize that this chapter using the h_j -index is only one approach to evaluate research papers and their effect on a scientific field. The most obvious weakness to this approach is in the evaluation of the most recent literature, where citations have not yet accrued, and citation classics have not yet occurred. This weakness is most important for the literature of the past 5–8 years, which is the first half life of a paper’s total citations. However, this limitation was addressed by comparisons of any selected paper with the h_j -index papers from that same year and the idea of a sliding h_j -index. With this caveat, we offer the h_j -index as a measure of the scientific impact of journal articles within a journal and between journals within a field. Finally, the h_j -index may be readily calculated for any scientific paper within a specific journal, regardless of its age or field of activity, to gauge its past, present, or future citation impact and that of its authors.

References

1. Hirsch, J. E. An index to quantify an individual's scientific research output. *Proc. Natl. Acad. Sci. U.S.A.* **2005**, *102*, 16569–16572.
2. Ciriminna, R.; Pagliaro, M. On the use of the h-index to evaluate chemical research. *Chem. Cent. J.* **2013**, *7*, 132–137.
3. Braun, T.; Glänzel, W.; Schubert, A. A Hirsch type index for journals. *Scientometrics* **2005**, *69*, 169–173.
4. Fairthorne, R. A. Progress in documentation-Empirical hyperbolic distributions (Bradford-Zipf-Mandelbrot) for bibliometric description and prediction. *J. Doc.* **1969**, *25*, 319–343.
5. Bollen, J.; Rodriguez, M. A.; Van de Sompel, H. Journal Status. *Scientometrics* **2006**, *69*, 669–687.
6. Garfield, E. The 100 most cited papers ever and how we select them. *Curr. Contents* **1984**, *23*, 175–181.
7. Garfield, E. Introducing citation classics: The human side of scientific reports. *Curr. Contents* **1977**, *1*, 5–7.
8. Garfield, E. Do Nobel prize winners write citation classics? *Curr. Contents* **1986**, *23*, 3–8.
9. Tsay, M. Y. Library journal use and citation half-life in medical science. *J. Am. Soc. Inform. Sci.* **1998**, *4*, 1283–1292.

Chapter 3

Applications of Excitation Emission Matrix Fluorescence with Parallel Factor Analysis (EEM-PARAFAC) in Assessing Environmental Dynamics of Natural Dissolved Organic Matter (DOM) in Aquatic Environments: A Review

Rudolf Jaffé,^{*,1} Kaelin M. Cawley,² and Youhei Yamashita³

¹Southeast Environmental Research Center and Department of Chemistry and Biochemistry, Florida International University, Miami, Florida 33199, U.S.A.

²Institute of Arctic and Alpine Research and Department of Civil and Environmental Engineering, University of Colorado at Boulder, Boulder, Colorado, 80309, U.S.A.

³Faculty of Environmental Earth Sciences, Hokkaido University, Sapporo, Hokkaido 060-0810 Japan

*E-mail: Jaffér@fiu.edu.

Excitation emission matrix fluorescence combined with parallel factor analysis (EEM-PARAFAC) has emerged over the past ten years as a powerful and popular technique applied in the characterization of natural dissolved organic matter (DOM) in aquatic ecosystems. The exponential production of peer reviewed manuscripts including EEM-PARAFAC in recent years merits a review, intended to assist researchers interested in applying this methodology in ecosystem studies of aquatic environments. In this paper the authors list most of the existing EEM-PARAFAC applications in studies related to DOM dynamics in headwater streams, rivers, lakes, wetlands, estuaries, coastal areas and the open ocean, and provide specific examples of such applications as illustrative case studies. While the inclusions of technical details of the technique are beyond the scope of this paper, pros and cons are briefly discussed and general approaches to its applicability are suggested.

Introduction

Dissolved organic matter (DOM) is ubiquitous in the environment and represents the largest pool of reduced carbon in aquatic ecosystems. As such, it plays important roles in ecosystem functions and biogeochemical processes (1). Among other functions, DOM serves as a light attenuator in aquatic systems (2), as a metabolic substrate for heterotrophic bacteria (3), and as a medium to transport trace metals (4). In fluvial systems DOM is derived from allochthonous and autochthonous sources, such as terrestrial landscape derived organic matter and in-stream primary productivity, respectively. Riverine transport of dissolved organic carbon (DOC; *ca.* 0.25 Gt C/yr (5, 6)) is an important process in the global C-cycle as it integrates sources and processes within watersheds. Within fluvial systems, and on watershed scales, DOM quantity and quality has been shown to vary (e.g. (7)) and its photochemical, microbial and physical processing was reported to be affected on landscape scales (6). While the fluvial discharge of DOM represents a direct link between the terrestrial system and the marine environment, the traditional view that rivers represent simple conduits of refractory carbon to the oceans has been proven wrong. In fact, rivers serve as active reactors of DOM processing (8) and a significant portion of DOM is lost during transport (3). Similarly, through complex interactions of physical, chemical and biological processes, receiving water bodies such as lakes, wetlands and estuaries can process large amounts of DOM exported by rivers (9, 10) ultimately affecting the quantity, quality, transport and fate of DOM. Carbon cycling in aquatic environments is controlled by a variety of physical and biological drivers such as watershed land-use, morphology, microbial activity, hydrology and climate. As such, human activities such as agricultural development, urbanization (and associated pollution), and natural resources management can modify the quantity and quality on DOM on spatial and temporal scales (e.g. (11–14)).

However, despite the importance of DOM as a critical component of the global carbon cycle, the number of studies focused on large spatial scales and long term temporal resolutions are limited due to a lack of adequate analytical techniques that feature large sample throughput and both sensitivity and selectivity (15). In this respect, the application of optical properties as a proxy for DOM composition and reactivity has been largely applied (15–22). Excitation emission matrix fluorescence (EEM) and EEM combined with parallel factor analysis modeling (EEM-PARAFAC) have been particularly popular due to the fact that fluorescence methods are not only highly sensitive, but the PARAFAC modeling provides additional benefits regarding the characterization of the compositional features of DOM. It is therefore not surprising that over 50% of publications in this field focus on applications of excitation emission spectrofluorometry in aquatic ecosystems (21). Several recent reviews have reported on the advantages of EEM fluorescence as an ideally suited analytical tool for environmental applications (18–21, 23–25), and describe in detail analytical procedures, technical issues, pros and cons of the technique as compared to other DOM characterization methods, as well as specifics with regards to environmental applications. Analytical and

technical issues regarding fluorescence measurements, and effects of metal complexation, pH, salinity and other environmental conditions are not within the scope of this review and are therefore not discussed.

While EEM studies based on ‘peak picking’ (26) are still widely and successfully used, the higher peak resolution and statistical significance of adding PARAFAC modeling significantly enhances the potential interpretations of the data in ecosystem studies, particularly when applied on large spatial or temporal scales (e.g. (27, 28)). This field was pioneered by the early work featured in publications by Stedmon and collaborators and Cory and McKnight (17, 29–31), and has since taken off exponentially with a large and ever increasing number of published works over the past decade. Therefore, this review is focused only on applications of EEM-PARAFAC in ecosystem studies, and is presented in sections based on specific aquatic environments, such as headwater streams and rivers, lakes, wetlands, estuaries, coasts and open-ocean.

Headwater Streams and Rivers

In recent years, EEM-PARAFAC has been widely applied to the study of DOM in fluvial systems, from headwater streams (13, 14, 32–38) to mid-size and large rivers (28, 39–49). Most of the reported studies focus on assessing allochthonous vs. autochthonous DOM source contributions, associated reactivity, effect of hydrology (e.g. storm events) on DOM quality, and effects of land-use and pollution due to anthropogenic activities in the watershed. The description below follows these specific topics.

Environmental Heterogeneity and Spatial Connectivity in Fluvial Systems

Environmental heterogeneity and spatial connectivity in fluvial systems is critical in understanding DOM dynamics. However, little is still known about the environmental drivers controlling DOM quality in large river systems, where nutrient gradients, changes in lithology and geomorphology, variations in hydrology such as surface vs. groundwater contributions, and shifts in vegetation cover and soil characteristics can have a strong impact on both the quantity and quality of DOM. These are systems where DOM studies can benefit from the application of a high sample throughput characterization method such as EEM-PARAFAC. Indeed, Yamashita et al. (50) reported a DOM source assessment on a large geographical scale, where three large fluvial systems (watersheds) from the Guayana Shield draining into the Orinoco River, Venezuela, were studied using EEM-PARAFAC. The authors used a principal component analysis (PCA) approach to determine that optical properties were strongly related to different geological settings and associated vegetation cover, and to nutrient levels within these watersheds. While the study area was for the most part quite remote and mostly undeveloped, higher levels of protein-like fluorescence were related to localized environmental disturbances, such as gold-mining activities in some of the studied streams. Similarly, but on a smaller geographical scale, Fellman et al. (43) reported a gradient of DOM sources along an Australian

stream discharging into an agro-urban estuary. Here a spatially induced shift from humic-like to protein-like enriched PARAFAC components was observed and related to autochthonous production of DOM associated with changes in nutrient availability (anthropogenic discharges). The authors report three distinct DOM sources, namely (a) riverine DOM derived mainly from vascular plants and their remains in soils, as indicated by the presence of terrestrial humic-like PARAFAC components, (b) recently produced autochthonous DOM, as indicated by the presence of tryptophan-like fluorescence, and (c) autochthonous DOM originating in the estuarine zone of the river, as indicated by the presence of tyrosine-like and marine humic-like fluorescence. The enriched tryptophan-fluorescence signal may also be influenced by agricultural and/or urban pollution sources, since this kind of fluorescence has been reported to be enhanced by discharges of untreated sewage (47) and wastewater effluents (51). As such, the use of protein-like fluorescence as a proxy for autochthonous DOM and potential anthropogenic disturbances has been applied in river systems.

The application of EEM-PARAFAC in the assessment of DOM dynamics in complex fluvial systems was highlighted through studies of the longitudinal and lateral connectivity of water masses in the St. Lawrence River system (44, 49). This river system is a mosaic of heterogeneous hydrogeomorphic zones with a multitude of tributaries draining watersheds with diverse land-use, riparian areas, and floodplain associated wetlands (44). As such, DOM source strengths and the assessment of biogeochemical drivers controlling the cycling of DOC are highly complex. The authors use asymmetric eigenvector map (AEM) modeling in combination with EEM-PARAFAC DOM characterization to produce environmental and spatial models to explain DOM dynamics. Their findings suggest that increases in DOM along the longitudinal axis were controlled by contributions from tributaries, while the reactivity of DOM was driven by source variations. Here, freshly produced, protein-like DOM served as a key substrate for heterotrophic bacterial growth, while the fate of humic-like fluorescent materials was determined by photochemical processing (44). Seasonal trends also suggest that detrital macrophyte derived DOM contributions were significant and correlated with protein-like fluorescence (49). These studies confirm that the combination of EEM-PARAFAC with spatial analysis modeling is an ideal approach to better understand DOM sources and processing in large, heterogeneous, fluvial systems.

Hydrological Flow Paths and DOM Quality

Hydrological flow paths are also critical not only in controlling the DOM loading in streams (2) but also DOM quality (52). As such, storms are important physical events affecting DOC export and carbon budgets in rivers. Considering the effectiveness of EEM-PARAFAC in characterizing DOM, the effects of storm events on DOM quality have been studied through this approach to better understand the influence of hydrological flow paths on carbon export from terrestrial systems (38, 42, 53, 54). While the increase in aromaticity of DOM during a storm event has been reported (52), an enhanced signal in the humic-like fluorescence has been observed during storms (35, 38, 42). Similarly, higher

aromaticity and average molecular weight of DOM during storms have been suggested (53). While it is clear that storm events induce a temporary shift in DOM quality, due to a shift from protein-like fluorescence enriched DOM during base flow to a humic-like enriched DOM during storm surface water runoff (i.e. ground vs. surface waters; (35, 54, 55)), a study on the effects of stormflows on quantity, source characteristics and bioavailable DOM (BDOM) from coastal temperate watersheds showed that these were also strongly related to watershed characteristics. For example, while the protein-like fluorescence decreased as humic-like fluorescence increased during stormflow in upland watersheds, the opposite was observed in streams from watersheds containing wetlands ((38), Figure 1). Higher relative abundances of protein-like fluorescence during base flow and/or drier climatic conditions were reported (35, 42), and suggested to be linked to changes in hydrologic flow paths with decreased contributions of surface flow to groundwater flow. Considering the changes in organic matter sources with variations in flow paths, it is not surprising that seasonal drivers including litterfall and autochthonous primary productivity were also identified as playing a role in DOM dynamics during storm events (35, 42). Taken together, applications of EEM-PARAFAC lead to the conclusions that storms and associated variations in flow paths, can induce significant changes in the fluorescence of DOM, and thus, DOM quality, affecting not only carbon export, but the bioavailability of DOM down streams (38, 56), and the potential for disinfection byproducts formation in associated water treatment facilities (57).

Environmental Processing of DOM in Streams

In headwater streams, EEM-PARAFAC characteristics are commonly dominated by terrestrial humic-like fluorescence (36, 37), but differences in the degree of autochthonous DOM contributions have been identified based on enhanced protein-like fluorescence (34). EEM-PARAFAC humic-like and protein-like fluorescence (particularly tyrosine-like fluorescence) have been suggested as potential proxies of the assessment of photo- and bio-degradation processes in DOM cycling in streams, respectively (7, 9, 37, 38, 44, 56, 58–60). In this respect, EEM-PARAFAC was applied in assessing variations in DOM processing, where in some fluvial systems the preferential loss of humic-like fluorescence was associated with photobleaching processes directly coupled to water residence times (7), or to the heterotrophic bacterial processing preferentially removing the protein-like fluorescence (56). Indeed, bioavailable dom (BDOM) has been directly correlated with protein-like fluorescence in diverse aquatic systems (9, 13, 37, 44, 56, 58, 60).

While the combination of tryptophan-like and tyrosine-like fluorescence, has been found as a proxy for overall BDOM in streams, the contributions of the individual protein-like PARAFAC components to DOM processing remains somewhat controversial. Short term (<2 days) and long term (30 days) lability (STL and LTL respectively) incubation experiments have shown that stream DOM bioavailability was indeed positively correlated with the combined tryptophan-like and tyrosine-like fluorescence, but while tyrosine-like fluorescence correlated with both STL and LTL, tryptophan-like fluorescence correlated with STL but not LTL

(9). This suggests that tyrosine-like fluorescence is consumed over longer periods of time, and that tryptophan-like DOM is consumed preferentially compared to tyrosine-like materials. While this is in agreement with previous reports (31), it seems to conflict with a recent report suggesting that tyrosine-like fluorescence is more sensitive to biodegradation compared to tryptophan-like fluorescence (58). These authors report the distribution of both, tyrosine and tryptophan protein-like fluorescence in stream water DOM, and show that both are present in the labile, semi-labile and refractory DOM pools, with up to 73% of tryptophan being refractory, while 100% of the tyrosine-fluorescence was biodegraded and the majority was present in the labile pool. It is likely that the determining factor of the influence of specific protein-like fluorescence on the respiration of DOM is related to the specific sources of these materials (e.g. plankton vs. terrestrial), and if the protein-like fluorescence is derived from unaltered proteins or from smaller peptides or free amino acids. In this respect, more research is needed to determine the composition of protein-like fluorescence along the DOM molecular size continuum (61) and its effects on BDOM. In addition, the consideration that low molecular weight polyphenols, such as gallic acid, feature protein-like fluorescence characteristics (62) is critical in the resolution of this issue. What is clear is that indeed protein-like fluorescence is a proxy for BDOM in fluvial systems, while terrestrial humic-like fluorescence has been found to be related to water residence times, and thus photobleaching (7) and to long term carbon consumption (9). While riverine sources of protein-like fluorescence range from soil leachates (56, 60), planktonic primary productivity (9), aquatic macrophytes (49), to salmon-derived DOM (63), rivers are considered important sources of protein-like DOM to lakes, wetlands, estuaries and ultimately the oceans.

Effects of Land-Use and Pollution

Changes in land-use have been shown to have significant effects on the composition of DOM. In a recent report on the character (optical properties) for 34 riverine sites along a gradient of watersheds with variations in the amount of wetland to cropland cover (12), wetlands loss and increase cover of croplands was related to an enrichment of microbial components at the expense of terrestrial components. Indeed, several reports applying EEM-PARAFAC to studies related to land-use change have reported enrichments in the protein-like fluorescence in streams with significant human activities in their watersheds (11, 13, 14, 40, 46, 64). Williams et al. (64) reported that, protein-like fluorescence was enhanced in streams with a higher cropland cover in their watershed, while those with higher proportions of forest and wetlands featured enhanced fluorescence from humic-like components. In addition, the watersheds with land-use characterized by agricultural activities and higher bacterial production exported DOM in a more reduced redox state (based on EEM-PARAFAC characteristics; (65)) compared to that from forested watersheds containing wetlands. This suggests that DOM draining from agriculturally impacted watersheds may be more bioavailable and thus more reactive than for non-impacted watersheds. Similar results were reported by Lu et al. (14) who found that anthropogenic activities (cropland, pasture and urban) increased microbial activity and enhanced the relative

abundance of protein-like fluorescence of DOM (Figure 2). The authors applied PCA for relative abundance of PARAFAC components and suggest that PC1 is mostly controlled by the relative contributions of terrestrial vs. microbial sources because it negatively correlates with the relative abundance of two terrestrial fluorescence components, C1 and C2, but positively correlates with the relative abundance of two components related to microbial sources and activities, C3 and C4. PC2 represents the relative contribution of diagenetic DOM because it positively correlates with C4 but negatively correlates with C5; protein-like fluorescence (C4) is often related to freshly produced DOM, and C5 is thought to be a photodegradation product of terrestrial DOM. In addition, these authors (13) determined the effects of such compositional changes in the lability of DOM. Due to the coupling of photoreactivity and the relative abundance of terrestrial humic-like DOM, the loss of wetlands and forest cover to agricultural and urban landscapes results in a reduction in photo-reactivity of DOM. In contrast, the bioreactivity of DOM was found to be similar between forested and human-altered watersheds. Petrone et al. (46) also reported that the relative abundance of the protein-like fluorescence could be applied as a proxy for BDOM in an agro-urban stream setting. In contrast, terrestrial humic-like fluorescence was negatively correlated to BDOM and related to legacy soil carbon from former wetland systems in the watershed.

From the discussion above it is clear that landscape factors such as human-disturbances can have a clear effect on DOM quality on spatial scales. However, little is known on how land-use can impact DOM quality on temporal scales. In a recent report Catalan et al. (33) applied EEM fluorescence spectroscopy to study landscape factors based on seasonal characteristics of DOM in ephemeral washes in a Mediterranean landscape. The authors suggest that for some seasons, changes in DOM composition and source are driven by hydromorphology and landscape features (land-use) in the watershed. Longer term studies of this nature that apply EEM-PARAFAC are needed to increase our understanding of seasonal effects of land-use on DOM in streams.

While the effect on DOM quality as a result of changes in land-use from natural systems to human-impacted watersheds through increases in agricultural and urban landscapes has been clearly demonstrated using EEM-PARAFAC approaches, less is known about effects resulting from forest management. In this respect, Yamashita et al. (36), first reported that forest disturbance, such as clear cutting and re-growth, clear cutting and harvesting, or conversion to different species, resulted in long-term DOM compositional changes, notably as an enhancement in the relative abundances of protein-like fluorescence. The authors suggest changes in soil OM content due to litter accumulation rate differences and litter quality differences, as well as associated modifications in hydromorphology as possible explanations for this observation. Similarly, Burrows et al. (32) applied EEM-PARAFAC to assess differences in DOM character between old-growth and clearfelled headwater streams. While the authors did not detect significant compositional differences or DOM source changes between old growth and clearfelled watersheds, they did report, in agreement with Yamashita et al. (36) that managed forest watersheds were characterized by lower relative abundances in terrestrial humic-like fluorescence

and higher protein-like fluorescence. While DOM compositional differences between undisturbed and impacted forest watersheds were observed, no significant differences between such reference and study sites on temporal scales could be identified (36). Additional research in this area is needed to better constrain environmental drivers affecting DOM quality in managed forest systems.

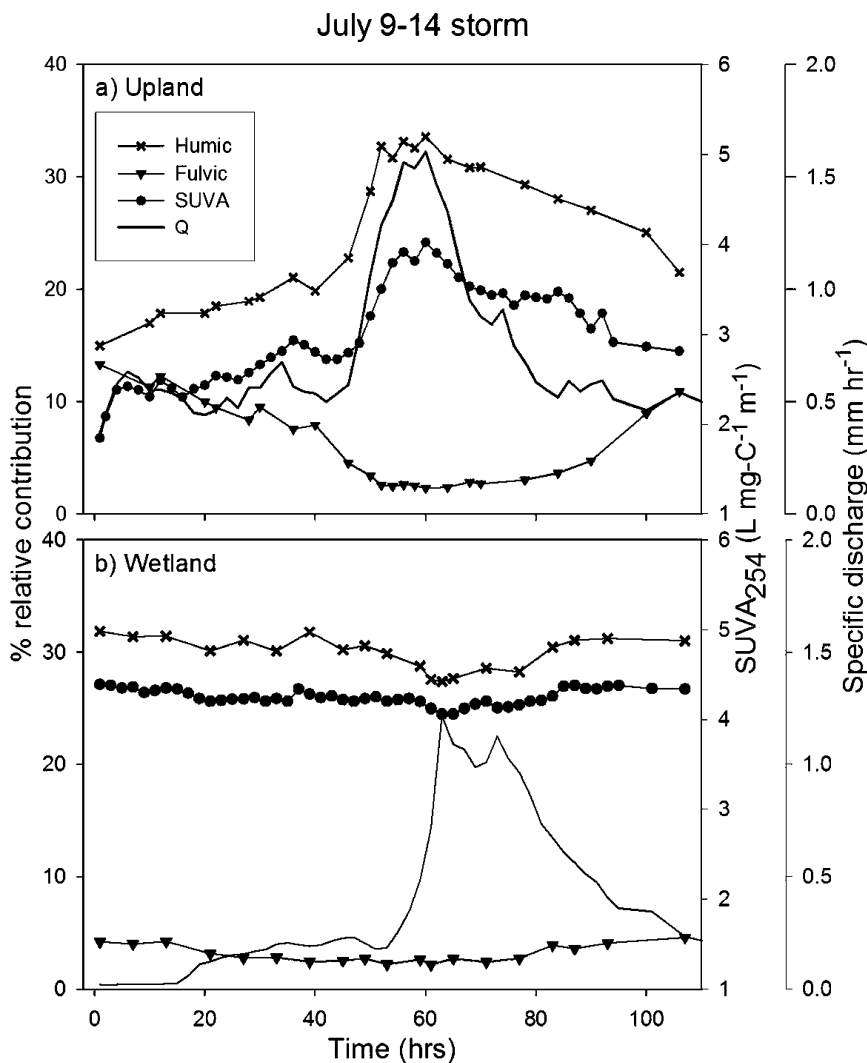


Figure 1. Relationship between specific discharge (Q), SUVA_{254} , and the relative contribution of the humic- and fulvic-like PARAFAC components for a storm event in upland and wetland watersheds in Alaska. (Reproduced from reference (38). Copyright 2009 American Geophysical Union)

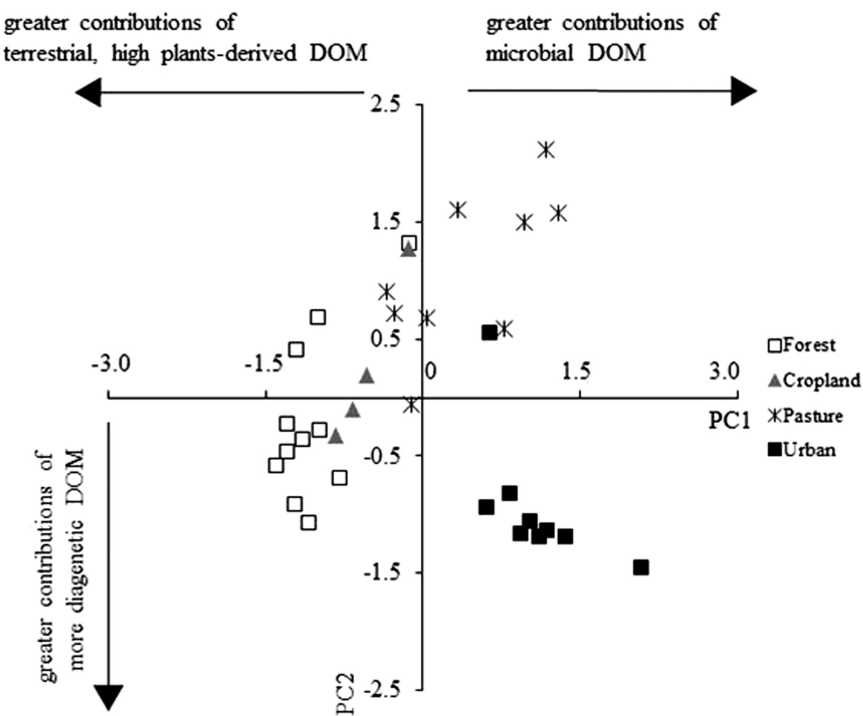


Figure 2. Score plot of principal component analysis of the relative abundance of EEM-PARAFAC components in DOM from headwater streams (eight streams collected in five different months) draining watersheds of different land use types.

Five fluorescence components were identified: C₁ terrestrial, fulvic acid type, C₂ terrestrial, humic acid type, C₃ microbial humic-like, C₄ protein-like, and C₅ humic-like. (Modified from reference (14). Copyright 2014 Springer)

EEM fluorescence spectroscopy has been suggested as a useful technique to monitor sewage-impacted rivers, as high tryptophan and fulvic-like fluorescence features have been identified in such effluents (23, 66). In fact, several recent reports have focused on the application of EEM-PARAFAC in determining effects of urban activities such as sewage or waste water treatment discharges into streams (41, 45, 47, 51). In a study by Yao et al. (51) the sources and fate of DOM in a lake and associated tributaries in China were assessed. Among others, these authors reported the importance of local geology and land-use in driving DOM sources, but also suggest that pollution activities influence DOM composition on spatial scales by incrementing the relative abundance of protein-like fluorescence. As such, the authors suggest that while tyrosine-fluorescence is most likely derived from planktonic primary productivity (possibly associated with anthropogenic nutrient inputs), tryptophan-like fluorescence was more closely associated

with waste water effluents. Mostafa et al. (47) reported on the presence of enhanced protein-like (particularly tryptophan-like) fluorescence in the Nanming River, China, and also related this signature to the presence of waste waters and possibly untreated sewage in the system. Similarly, Borisover et al. (45) reported fluorescent characteristics of DOM usually associated with biological productivity (but not tryptophan-like) in an urban river in Israel with locations characterized by important inputs of industrial effluents.

Lakes

Allochthonous and Autochthonous DOM Dynamics in Lakes

EEM-PARAFAC has been useful for understanding ecological processes taking place within and among lakes. For instance, the relative abundance of humic-like to protein-like PARAFAC components was useful for assessing trophic dynamics and elevation effects. Among high mountain lakes Zhang et al. (67) reported relationships between PARAFAC component relative abundances and trophic state. They found that at higher eutrophication, two humic-like PARAFAC components were more abundant concomitant with an increase in UV absorbance. Land use changes around the eutrophic lakes were suggested to be a potential source of terrestrial humic-like components. A blue-shifted, microbial humic-like component was reported to correlate with chlorophyll *a* concentration and was also more abundant in the eutrophic lakes relative to the mesotrophic or oligotrophic lakes. In contrast, the oligotrophic lakes were dominated by two protein-like components (77.9 % of the total fluorescence) with very little humic-like fluorescence at all. In large lakes, wastewater influence was reported to play a role in DOM characteristics (68). The ratio of C5 to C1 (N/A peak ratio) was used as a tracer for wastewater impacts. The highest autochthonous production of DOM was reported for lakes with the highest nutrient concentrations, and was potentially due to bacterial production rather than primary production. In these large temperate lakes, the ratio of watershed area to lake area and anthropogenic effects were more important drivers of DOM character than seasonal trends.

In addition to terrestrial and wastewater derived allochthonous inputs to lakes, there have been reports of DOM inputs from atmospheric deposition. In clear alpine lakes, Mladenov et al. (69) used EEM-PARAFAC analysis to discriminate between DOM in alpine lakes and polar lakes due to differences in the protein-like component relative abundances, with the alpine lakes have higher protein-like fluorescence. The fluorescence characteristics of the alpine lakes were also reported to be highly similar to the fluorescence characteristics of dry deposition samples, which had similar fluorescence properties as pollen, airborne bacteria, and formaldehyde. Among the alpine lakes, there were latitudinal trends in fluorescence with dust inputs and photo-humification processes contributing to higher humic-like fluorescence at lower latitudes. In addition to natural dry deposition, PARAFAC has been used to discriminate between natural and anthropogenic aerosols (70). The 3-component PARAFAC model identified

a PARAFAC component linked to diesel exhaust in the water soluble organic carbon fraction of the aerosols. However, to date there have been no studies to determine the effect of the anthropogenic aerosols directly on lake ecosystems using PARAFAC analysis. For more information on humic-like substances in aerosols see Duhl et al. chapter in this book.

The relative importance of DOM sources, i.e. allochthonous vs. autochthonous, to lakes are often seasonally variable. Using an existing geographically broad PARAFAC model developed by Cory and McKnight (29) and then applying PCA to the results, Miller and McKnight (71) reported that in alpine lakes in Colorado DOM is dominated by allochthonous inputs mobilized by snowmelt in the spring. However, during the late spring and summer, these same lakes are dominated by algal-derived, autochthonous DOM. In addition to using PARAFAC and PCA, these authors (71) developed a redox index (RI) defined as the ratio of reduced quinone-like to total quinone-like PARAFAC components (Note: ‘quinone-like’ definition was based on spectral similarity of PARAFAC components, not through molecular confirmation). The RI shifted from relatively reduced to more oxidized values concomitant with an increase in the relative abundance of amino acid-like PARAFAC components. The RI was also used by Miller et al. (72) as a forcing function in a model to quantify the inputs of different DOM source pools throughout the summer in an alpine lake. These model results quantitatively support the hypothesis that alpine lakes act more like streams, with shorter water residence times and little change in DOC concentration during snowmelt, while later in the season these lakes act as sources of autochthonous DOM to downstream surface waters with longer residence times (72, 73). This seasonal influx of autochthonous, microbial DOM in alpine lakes is also reactive in surface waters. Miller et al. (74) used the fluorescence index (FI) and the PARAFAC-based RI to better understand the transformations of non-humic autochthonous DOM in alpine lakes. They proposed that photochemically driven condensation reactions transformed non-humic cellular exudates to microbial fulvic acids (Figure 3). In Arctic thaw ponds, photo-exposure of DOM in lakes has also been reported to alter the quality of DOM (75). Following photo-exposure, DOC concentration did not change appreciably, but the humic-like PARAFAC components decreased to a greater extent than the protein-like component and the spectral slope measures indicated a likely decrease in molecular weight (75). These changes are likely to alter DOM quality in such a way that it becomes more bioavailable to micro-organisms, particularly if Arctic summers increase in length with climate change.

In addition to microorganisms producing DOM in lakes, laboratory mesocosm studies have advanced the understanding of the microbial influence on DOM dynamics (e.g. (9, 31, 76)). As reported by Guillemette and del Giorgio (9), PARAFAC components from both river and lake DOM were correlated to long-term (LTL) and short-term lability (STL) of DOM (see also section above). In a laboratory study using samples collected from a eutrophic lake during “bloom” conditions, Zhang et al. (76) reported a significant contribution to the DOM pool from phytoplankton degradation and a link between chlorophyll a concentrations and DOM lability. Phytoplankton degradation resulted in an overall enrichment in two ‘marine’ humic-like PARAFAC components (76). After

an initial increase in the protein-like component, there was ultimately a decrease in protein-like relative abundance concomitant with an increase in relative abundance of the two marine/microbial PARAFAC components. Thus, the PARAFAC results indicate that there is release of microbial humic-like material during phytoplankton degradation followed by some loss of the protein-like PARAFAC components.

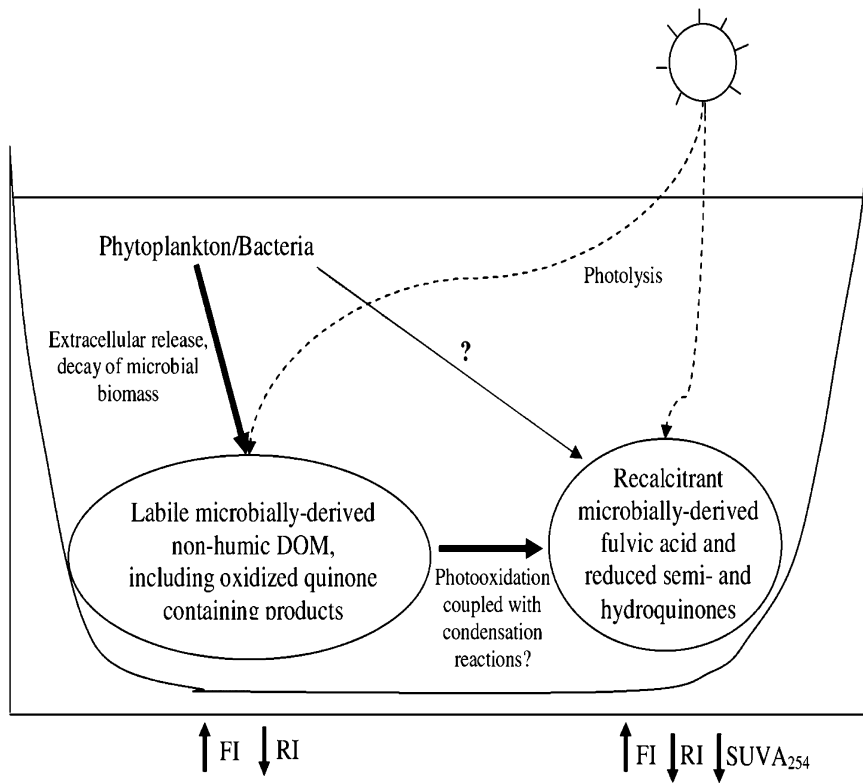


Figure 3. Conceptual model showing that both photolysis and microbial processing influence the fluorescence character of Lake DOM. The abundance of oxidized and reduced quinone-like PARAFAC components contributed to changes in the RI. (Reproduced from reference (72). Copyright 2009 Springer)

Spatial Variation in DOM Sources among Lakes

For lakes in the Canadian Shield, Mueller et al. (77) successfully used EEM-PARAFAC analysis to link watershed composition (i.e., %rock, %vegetation, and %water) to lake DOM quality characteristics. The 4-component PARAFAC model identified two ubiquitous, reduced quinone-like components,

one allochthonous, oxidized quinone-like component and one protein-like component. The relative abundance of the protein-like component was significantly higher, and the allochthonous component was significantly lower, for lakes with lower watershed-to-lake areas. There was also a positive correlation between DOC concentrations and terrestrial DOM quality. Thus, the dominant DOM source was a function of the watershed characteristics surrounding the lakes in the Canadian Shield (77). In urban stormwater ponds, however, DOM quality was reported to depend more on the level of autochthonous production rather than surrounding watershed characteristics (78). Based on PARAFAC models increases in DOC concentration and total suspended solid (TSS) were reported to be due to increased primary productivity driving the DOM characteristics to be more microbial for the higher DOC ponds. The different trends in the DOC quality with increasing DOC concentration between these two types of systems, highlights the value in using EEM-PARAFAC to assess DOM quality in order to understand biogeochemical processes governing organic carbon production, transport, and transformation in lakes and ponds.

In lakes within the Alaskan tundra, water residence time was reported to be an important factor controlling DOM quality (7). Whole water and fulvic acid samples collected from 9 surface water bodies, all had low FI values indicative of terrestrial source material and depleted $\delta^{13}\text{C}$ values (-28‰). Differences were reported for microbial contributions, which increased with increasing water residence time. In addition to looking at DOM source material, photo-degradation was tracked with specific ultraviolet absorbance at 254 nm (SUVA₂₅₄) and the ratio of two PARAFAC components, terrestrial SQ1 and microbial SQ2. A preferential loss of SQ2 and a decrease in SUVA₂₅₄ upon photo-degradation was observed. Overall, similar trends in optical properties were reported for both, fulvic acid samples and whole water samples. While SUVA₂₅₄ was higher for fulvic acid fractions indicating that the CDOM is rich in the fulvic acid fraction in these lake systems, most of the fluorescence was reported to be in fulvic acid fraction as well (7). Some differences between fulvic acid and whole water samples were higher FI for whole water samples and higher relative abundance for amino-acid-like fluorescence, suggesting that autochthonous and amino-acid-like compounds are not retained in the fulvic acid fraction. Overall, these findings indicated that photo-degradation rather than DOM source or microbial processes control DOM quality in Arctic surface waters (see also rivers section above).

Lake Stratification and Spatial Variation in DOM Source within Lakes

In stratified lakes, DOM source and quality can vary with depth due to changes in biogeochemical processes dominant at different regions within the lake. In Lake Kinneret (a major water resource in Israel) DOC concentration did not vary with depth, but the distribution of PARAFAC components for water samples was variable during seasons when the lake was thermally stratified (79). Using a 3-component PARAFAC model, the authors were able to determine that sediments were contributing substantially to the DOM pool in the hypolimnion due to greater abundance of humic-like fluorescence. The authors also hypothesized that photo-

degradation could play a role, with photo-bleaching processes leading to the lower scores for humic-like PARAFAC components in the epilimnion. In contrast, the protein-like component did not show any trends comparable to the two humic-like components and were higher near the water surface during January-April when the lake was not stratified, indicating that protein-like fluorescence was derived from seasonal biological activity at the surface of the lake.

In a stratified lake used as a drinking water source, Pifer et al. (80) reported an increase in total fluorescence at mid-depth (10m below the surface) compared to 3 m or 18 m depths. The deepest sample had the lowest fluorescence intensity. The protein-like component had the highest relative abundance at the surface and based on field flow fractionation data was predominantly present in the larger sized fraction of DOM. These findings suggest that drinking water treatment facilities may be able to use DOM characterization techniques, such as EEM-PARAFAC, to understand their source water characteristics in order to control disinfection byproduct (DBP) formation by choosing a different mixture of source waters or locating their intake at a different depth based on DOM quality. Similarly, Beggs et al. (81) reported that overall fluorescence intensity and quinone-like PARAFAC component abundance were both linearly related to DBP formation and are likely better predictors of DBP formation potential than DOC concentration alone.

Wetlands

DOM Sources in Wetlands

Wetlands are often cited as important sources of DOM to downstream aquatic ecosystems (8, 64, 82). However, most wetlands are dynamic systems that are not only conduits for soluble soil and plant organic matter to enter surface waters, but are also reactors where biological and photochemical activity alter DOM quality. DOM sources within wetlands vary both spatially and temporally as in many other ecosystems, such as estuaries and lakes (discussed in other sections of this chapter). One of the most spatially comprehensive studies of DOM quality in a wetland system was performed in the Everglades, Florida (27). Using EEM-PARAFAC a North-to-South gradient was observed, where the relative abundances of protein-like PARAFAC components increased towards the southern Everglades, likely as a result of primary production and/or degradation or dilution of humic-like DOM derived from soils and agricultural activities in the northern Everglades (adjacent to the Everglades Agricultural Area; EAA) ((27), Figure 4). Regardless of the N-to-S gradient, three of the humic-like components C1, C3, and C4 have sources throughout the Everglades ecosystem, while C2 seemed to be enriched in canals and may thus be primarily sourced in the EAA as a soil organic matter oxidation product (28). The 8-component PARAFAC model developed as part of this spatial study (and others) has been used extensively to characterize organic matter from long-term Everglades datasets (28), from Everglades estuarine and groundwater samples (83, 84), and has also been applied to other wetland systems ((85); see below).

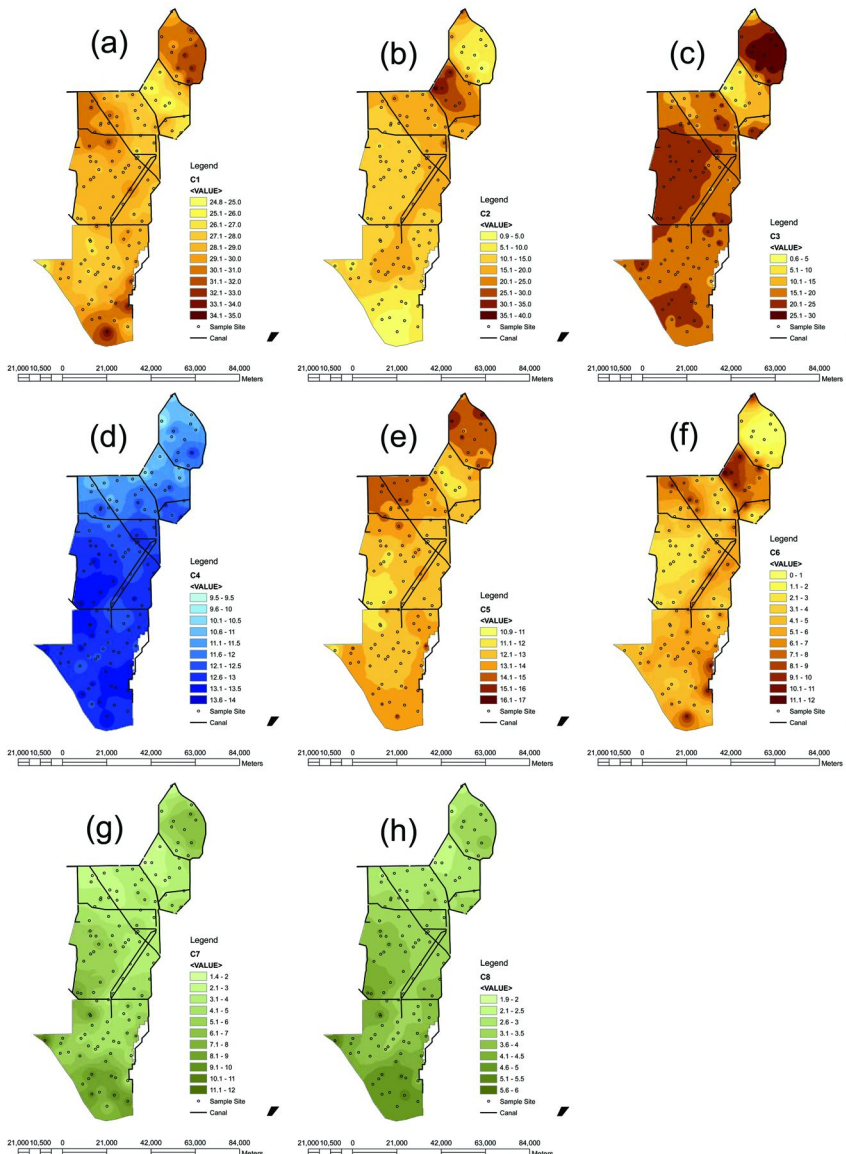


Figure 4. Spatial distribution of PARAFAC components in the Everglades showing a clear trend of greater abundance of humic-like PARAFAC components in the northern areas due to soil oxidation and terrestrial inputs (6a, b, c, e and f) and an enhanced microbial humic-like and protein-like fluorescence in the southern area derived from primary productivity (6d, g, h). (Reproduced from reference (27). Copyright 2010 Springer)

Mladenov et al. (86) used the 13-component PARAFAC model (29), to study surface water DOM isolates in the Okavango Delta for evaluating DOM quality in conjunction with other spectroscopic techniques and stable isotope analysis. The fulvic acids isolated from leached plant material and surface waters were reported to feature similar fluorescence characteristics and PARAFAC component abundances. Thus, the predominant DOM source in the Okavango Delta was determined to be vascular plants. However, the plant leachates did have a higher amount of PARAFAC component C1, which was correlated to anomeric C content (29), and lower relative abundance of the ‘reduced quinone-like’ components relative to the surface water DOM fulvic acids, indicating that microbial and photochemical alteration of plant-derived DOM was taking place within the wetland (86). The transformation of DOM within the wetland is likely hydrologically controlled with constant inputs of fresh plant-derived DOM having an “overprinting” effect on the biogeochemically modified DOM already in the wetland surface water.

Temporal variation in DOM quality has also been extensively studied in the Everglades by Chen et al. (28) who reported consistent seasonal trends in DOM quality. The seasonality of DOM quality in the freshwater region of the Everglades was determined predominantly by the hydrological conditions (e.g. hydroperiod), leading to seasonal changes in the contribution of soil vs. plant derived DOM. In contrast, the DOM quality in the estuarine and coastal sites was also driven by primary productivity and tidal exchange or seawater intrusions during low freshwater head. Cluster analysis of all PARAFAC data (15 sites, monthly for 6 yrs) clearly separated sites by environment type such as freshwater marsh with peat vs. marl soils, fringe mangroves with peat vs. marl soils, and coastal (Figure 5). In addition, PCA of the dataset showed distinct clusters for the different sub-environments and differences between wet and dry season DOM quality (28). Clearly, long-term PARAFAC data lead to a better understanding of Everglades DOM quality on spatial and temporal scales, and aided in the identification of some of the environmental drivers (e.g. hydrology vs. primary productivity) controlling DOM dynamics in this wetland. In contrast to such long temporal scale studies (28), Austnes et al. (82) studied a Welsh peatland catchment and reported changes to DOM quality due to storms on short temporal scales. Three storm events were sampled in addition to baseflow conditions and it was reported that the dominant DOM source changed and was represented by a decrease in the ratio of two PARAFAC components. However, mixing model results indicated that in-stream processing was likely to be the dominant driver of DOM quality rather than a change in DOM source material (82). While the effect of storms on DOM quality in fluvial systems has been discussed in headwater streams and rivers section, it is clear that similar effects are important for wetlands and further research in this area is needed.

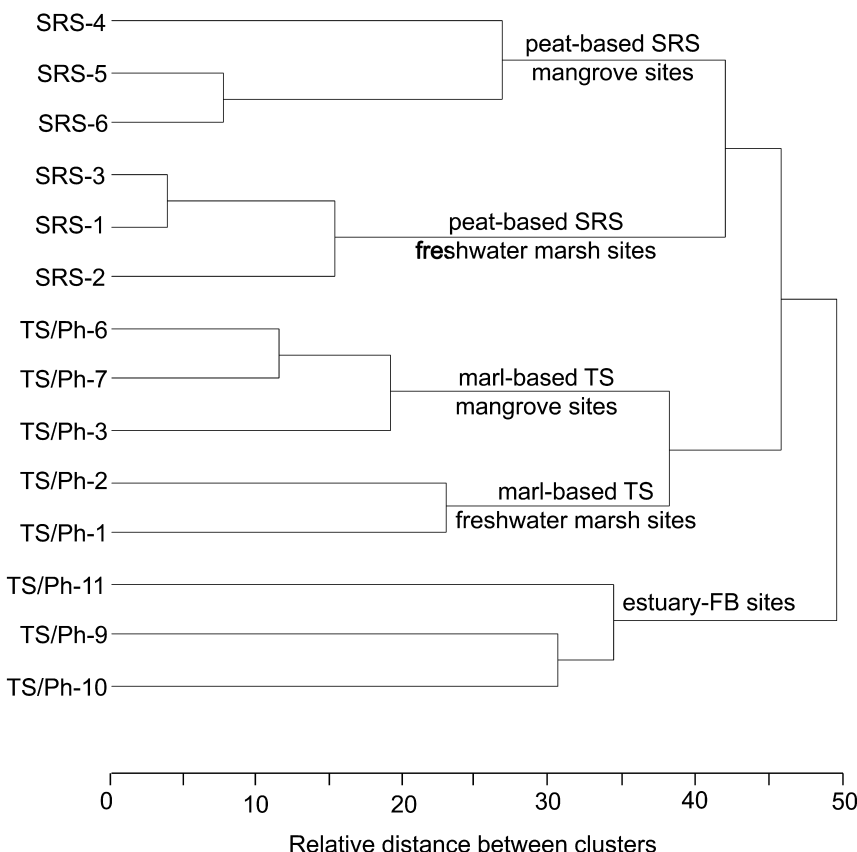


Figure 5. Cluster analysis (Ward method) of normalized EEM-PARAFAC data for Everglades DOM samples collected monthly for four years at fourteen different stations. (Reproduced from reference (28). Copyright 2013 Springer)

Alteration of DOM Quality in Wetlands

Microbial alteration is a mechanism for DOM quality changes reported in wetland systems. Micro-organisms can be both producers or decomposers of DOM by using it as a substrate for heterotrophic activity. In the Okavango Delta, Botswana, Cawley et al. (85) reported that DOM source may account for up to 46% of the variability in the fluorescence character using PARAFAC data (8-component model; (27, 84)) in conjunction with PCA. Microbial production of DOM was greatest, as indicated by a higher relative abundance of protein-like PARAFAC components and a correlation with higher dissolved oxygen concentrations, in the seasonal floodplains where local conditions may facilitate primary production (85). In other studies, however, biodegradation, likely due to bacterial respiration, has been reported to be an important factor controlling DOM quality in wetlands. For example, the work by Guillemette

and del Giorgio (9), which is also discussed in the rivers and lakes sections of this chapter, reported that marshes had significantly higher degradation rates of DOC and % biological DOC consumption (%BDOC) during long-term (1 month) experiments compared to lakes and rivers. This enhanced bio-availability of DOM in wetland systems is likely due to a difference in DOM quality, with the marshes having a higher contribution of DOM freshly-derived from macrophytes (9).

Photo-exposure is another major mechanism for the alteration of DOM quality in wetland ecosystems and has been reported to occur concomitantly with microbial processing and changes in DOM source. Using EEM-PARAFAC, Austnes et al. (82) reported that the diurnal pattern (peak in fluorescence in the morning and decrease throughout the day) due to photo-bleaching was altered by storm events when biological degradation of fresh soil inputs was the dominant factor controlling DOM quality in water draining from a peatland area. In the Everglades, a subtropical wetland, Chen et al. (28) reported a distinct change in DOM quality wherein the photo-refractory component C2 had a higher relative abundance in the dry season that likely reflected greater photo-bleaching of DOM in the freshwater wetland area of the Everglades at that time of year. This may be a hydrologically controlled phenomenon as the freshwater discharge is decreased in the dry season allowing for longer residence times and greater photo-exposure. Similarly, Cawley et al. (85) reported a greater relative abundance of C2 and lower relative abundance of C6 (a photo-labile component; (84)) in the most downstream areas (occasional floodplains) of the Okavango Delta using the same 8-component PARAFAC model as Chen et al. (28). Overall, while DOM derived from wetland systems appears to be photo-reactive and bio-reactive in most wetland ecosystems, the exact photochemically and biologically driven DOM dynamics can be highly variable and are often site-specific.

Redox Processes in Wetlands

Because wetlands often have high hydraulic connectivity to anoxic sediments and/or are anoxic near the sediment surface, redox processes can be important to DOM character. Larsen et al. (87) studied redox processes in the Everglades using a 13-component PARAFAC model (29). Applying the PARAFAC model outputs with PCA and discriminant analysis, these authors were able to deconvolute DOM redox properties, which tended to have a vertical distribution with more oxidized fluorescence at the surface in the ridge and slough landscape of the Everglades. Mladenov et al. (88) also studied redox properties of DOM in a wetland system, the Okavango Delta, Botswana, using the 13-component PARAFAC model (29). This model has been proposed for studying redox properties because of the potential presence of oxidized and reduced ‘quinone-like’ components suggested in the model. Using this model, Mladenov et al. (88) reported a higher redox index, a more reduced fluorescence signature, along a longitudinal gradient from the edge to the center (>100 m from edge) of the islands in the Okavango Delta, and concluded that DOM behaved non-conservatively and may be important for metal complexation and electron shuttling in wetland groundwater.

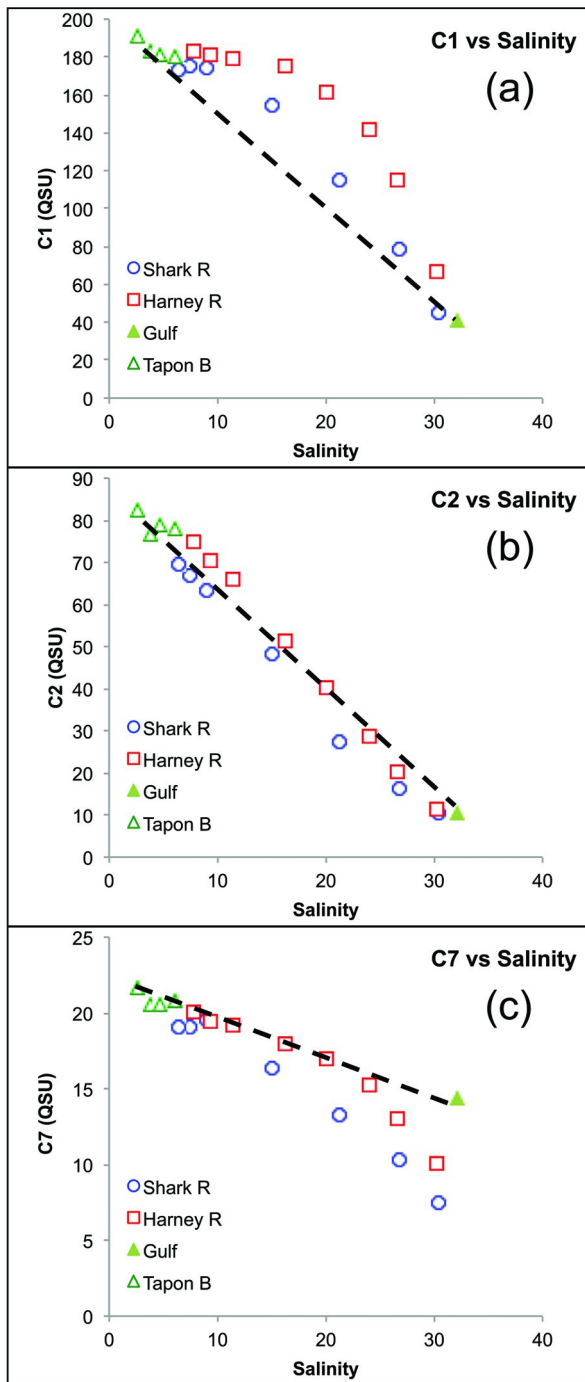


Figure 6. Examples of estuarine PARAFAC component dynamics relative to a conservative mixing line (black dashed line) in the estuarine region of the Everglades' Shark and Harney Rivers. (a) C1, a ubiquitous humic-like component C2 shows Type II behavior with a source within the estuary, (b) C2 shows Type I behavior with conservative mixing, (c) C7 shows Type V behavior with removal in the lower estuary. (Reproduced from reference (89). Copyright 2014 Springer) (see color insert)

Estuaries and Coasts

Spatial Changes in DOM character

Estuaries are aquatic environments, often tidally influenced, that connect rivers, lakes and wetlands to the coastal ocean. Much of the terrestrial organic matter contributed to the ocean carbon pool passes through estuarine environments on its way out to sea. In this section we will discuss sources and sinks of DOM in estuarine and coastal environments along with mixing behavior that has been elucidated using EEM-PARAFAC analysis. Throughout estuaries, a broad range of humic-like, protein-like and unidentified PARAFAC components have been detected that often correspond to those found in freshwater and marine systems (25). Along the estuarine salinity gradient, both conservative and non-conservative behavior have been reported for DOM as measured by PARAFAC component fluorescence intensity and relative abundance ((89); Figure 6).

In estuarine and coastal systems with net DOM flow to the ocean, PARAFAC component intensities, especially terrestrial humic-like components, have been reported to decrease with increasing salinity due to conservative mixing and/or a gradual dilution with marine-derived DOM (17, 48, 89–94). However, sources of PARAFAC components have been identified at both the freshwater and marine end-members of the estuarine environment. These observational results are consistent with experimental data that many humic-like PARAFAC components are produced microbially during mesocosm experiments (31). In addition, it was reported that humic-like components were produced by macroalgae (95) and seagrass (96). As such, conservative mixing of 'terrestrial' humic-like components may not be observed for some coastal environments. For example, in the high salinity zone of the Bohai Bay, China, where river inflow was low during the dry season, decreases in terrestrial PARAFAC components with increasing in salinity were not observed (97). Similarly, increases in humic-like PARAFAC components with increasing salinity observed on the southwest Florida shelf were likely due to a combination of microbial production and extensive evaporation (98).

In general terms, microbial (protein-like) components behave differently than terrestrial components (humic-like) in estuarine and coastal systems (53, 89, 99–102), with higher relative abundances of the former at the marine end-member and higher relative abundances for the latter at the freshwater end-member. Such different behaviors can be clearly seen from their spatial distribution (e.g., Figure

7; (92)). For a study of the coastal zone of the Florida Keys, USA, the levels of humic-like component were highest in the adjacent Florida Bay where terrestrial DOM from the Florida coastal Everglades can contribute, and sharply decreased toward the Atlantic Ocean and Gulf of Mexico, indicative of strong control of terrestrial inputs of humic-like components. On the other hand, the levels of the protein-like component were relatively uniformly distributed throughout the study area, suggesting a primarily autochthonous character of the protein-like component.

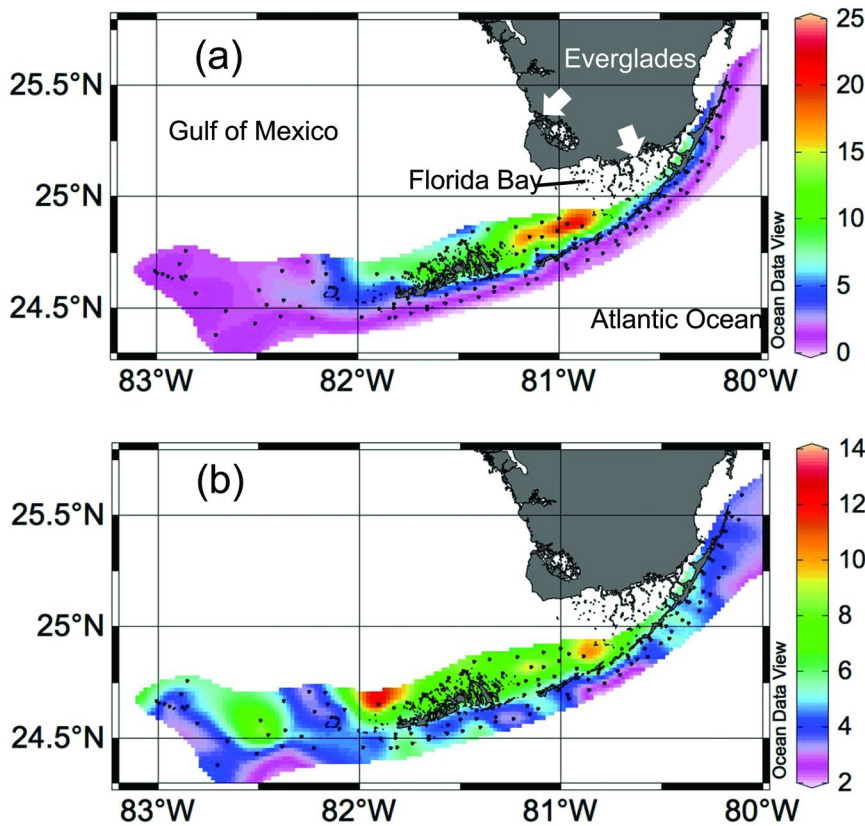


Figure 7. Distributions of fluorescence intensity of humic-like (upper panel) and protein-like (lower panel) components at the coastal region of the Florida Keys. (Reproduced from reference (92). Copyright 2013 Elsevier) (see color insert)

Stedmon and Markager (31) first reported the production of protein-like components during phytoplankton exponential growth, and these components have been observed above the conservative mixing line in the estuarine mid-salinity range, likely due to autochthonous productivity (4, 102). The production of protein-like components by phytoplankton (54, 91, 103), seagrass (83, 96), and coral reef communities (92) have all been suggested for

estuarine/coastal environments. As a result, the relative abundance of protein-like components usually becomes larger with increases in salinity (92, 93). Similar to protein-like fluorescence, the M peak, identified by Coble (26) as a 'marine humic-like' peak, is more abundant in the marine end-member of estuaries. However, recent studies suggest that the M peak may also be produced from microbial activity in soils, and thus may have a terrestrial source in addition to a marine source. Luciani (104) determined the spatial distribution of PARAFAC components in the Sepetiba Bay, Brazil and reported that the relative abundance of a component similar to the M peak did not change significantly from riverine to open ocean, indicative of a terrestrial/riverine contribution of the M component that is of a similar magnitude as the marine environment.

Based on the studies discussed above, the estuarine behavior of EEM-PARAFAC components can be classified into five categories based on their distribution relative to salinity values (91): Type I: Conservative behavior, which indicates that mixing is the dominant control on these components (Figure 6b); Type II: The dominant source is in the freshwater end-member with an additional source within the estuary (105), which is indicated by the component showing abundances above the conservative mixing line, but a decreasing trend from the freshwater end-member (Figure 6a); Type III: Mid-salinity maximum, where the component has a higher intensity at mid-salinity than the freshwater or marine end-member indicating that the dominant production of the fluorescent component is within the estuary rather than at either end-member; Type IV: No relationship with salinity. Type V (not listed in (91)): sources at both end-members with removal within the estuary as shown by abundances below the conservative mixing line (Figure 6c). These trends are summarized in Table 1.

Table 1. List of Behavior Classifications for PARAFAC Components in Estuarine Environments

Behavior	Description	Components
Type I	Conservative	A ¹ ,C ¹ ,C2 ² ,C1-3 ³ , C1-3&C5-6 ⁴
Type II	Source within an estuary	M ¹ , humic-like peaks ² , C4 ³
Type III	Mid-salinity maximum	C4-5 ¹ ,C4 ⁴
Type IV	No relationship with salinity	tyrosine-like ¹
Type V	Sources at both end-members	C7 ²

¹ (91); ² (89); ³ (105); ⁴ (102).

Seasonal Changes in Estuarine/Coastal DOM Character

Seasonal changes in precipitation, storm events, and primary productivity have the potential to alter DOM source material and fate and transport processes. Thus, DOM quality may be variable on seasonal timescales in estuarine and

coastal environments. In an estuary with a distinct monsoon season (Bay of Bengal) the salinity decreased just before and during the monsoons concomitant with an increase in intensity of a terrestrially derived component and a decrease in the tyrosine-like component indicating a seasonal shift from microbial to terrestrial-derived DOM (90). In a sub-tropical environment with distinct “wet” and “dry” seasons (Everglades), the DOC concentration and quality showed a similar trend of increasing terrestrial DOM export during the wet season (89). Maie et al. (83) carried out two-year monitoring of DOM quantity and quality in Florida Bay and reported that contributions of protein-like components were highest during the early wet season when primary productivity of seagrass communities is highest. In contrast, the contributions of humic-like components were greater during the late wet season when water discharge from the adjacent coastal wetlands (Everglades) is at its peak (28). Similarly, clear changes in the composition of PARAFAC components from relatively high protein-like values during the drought to a dominance of humic-like components during high river flow periods were observed for the Cape Fear River plume (93). Interestingly, climate disturbances in the form of hurricanes did not have a significant effect on the distribution of PARAFAC components on both spatial and temporal scales in Florida Bay, with the exception of a few near-shore stations that were most strongly impacted by freshwater discharge associated with the storm events (83).

Other Factors Influencing Estuarine and Coastal DOM Character

In addition to spatial and temporal changes in DOM source material, the transformation of DOM within estuaries is an important process influencing EEM-PARAFAC characteristics of DOM. Aside from physical mixing of the distinct DOM pools in estuaries, there is mixing of saline and fresh water resulting in ionic strength variations within estuaries. Boyd et al. (106) built PARAFAC models for mixtures of DOM at different salinities in a laboratory experiment using ultrafiltered DOM. The model components, identified based on similarities to EEM peaks (26), such as the N and T type peaks (unknown source and protein-like, respectively) generally increased with increasing salinity, while the A and C type peaks (terrestrial humic-like) generally decreased or first increased to then decrease with salinity. Boyd et al. (106) found that the variation in fluorescence behavior of components due exclusively to changes in salinity may be due to variations in metal binding and associated alteration of the 3-D DOM structure. Similarly, Catala et al. (99) attributed changes in DOM fluorescence under hypersaline conditions at least partly to conformational changes in DOM molecules taking place at higher ionic strength in estuarine field samples. Changes in EEM-PARAFAC components relative abundance due to enhanced metal binding have previously been reported (4, 107).

Due to the ability of the fluorescent fraction of DOM to absorb light, its degradation through photo-bleaching or photo-degradation has been suggested as an important sink (108, 109). In addition, photo-alteration of DOM in sunlit waters has been reported to be an important process controlling DOM quality in estuaries and coastal systems (89, 91, 110, 111). Specifically, Stedmon et

al. (111) reported the photo-degradation of several terrestrial and microbial PARAFAC components and the photo-production of one terrestrial PARAFAC component in lab irradiated Baltic Sea water. The difference in the PARAFAC distribution between surface and ground-water DOM in Florida Bay and parts of the Everglades has also been explained in part through higher photo-bleaching of surface waters (84). Additionally, photo-induced dissolution of sediments and suspended particulate organic matter was shown to generate humic- and protein-like components in estuaries (112, 113) suggesting that photo-chemical processes can be assessed using EEM-PARAFAC.

In addition to photochemical modification of terrestrial DOM derived from upstream freshwater sources, microbial processing of DOM can take place in estuarine and coastal ecosystems. Zhang et al. (114) performed laboratory degradation experiments and reported that microbial degradation of phytoplankton and macrophytes produced humic-like peaks (A and C type components) that have traditionally been considered as originating from allochthonous or terrigenous sources. While heterotrophic bacterial processing within an estuary may alter the DOM quality, DOM composition may also affect the bio-reactivity of DOM. The bio-availability of DOM as the %BDOC has been reported to increase with increasing protein-like PARAFAC component abundance ((102); see also rivers section above).

Diverse allochthonous contributions to the DOM pool within estuarine systems have been reported in addition to upstream terrestrial DOM inputs and in-estuary DOM processing, often resulting in non-conservative behavior (Type-II or Type-III; see above Table 1). In an estuary lined with fringe mangrove forests, the above and below ground biomass along with tidal pumping of soil porewaters can be potential sources of fluorescent DOM (FDOM) (89). Maie et al. (115) compared the distributional patterns of DOC, CDOM and PARAFAC components along salinity gradients in the oligo/meso-haline zones for three distinct wetland-influenced rivers and found that distributional patterns of spectrally similar PARAFAC components with salinity were different among three estuaries. The authors report the importance of the local hydrology, geomorphology, and ecosystem functions in determining environmental dynamics of DOM at the oligo/meso-haline zone.

EEM-PARAFAC of fulvic and humic acids extracted from estuarine soils and sediments confirm that these can be a source of humic-like DOM to aquatic systems (99, 116). However, while Yamashita et al. (91) suggested very little input from sediments to estuarine waters in Ise Bay, Japan, sediment porewaters and soil organic matter have been largely accepted as significant sources of DOM to estuarine ecosystems. Once mobilized through resuspension or erosional processes, soil and sediment derived particulate organic matter can further contribute to the FDOM pool through leaching and/or photo-dissolution (38, 50, 112, 113). As such, EEM-PARAFAC has been applied to study the characteristics of particulate organic matter (POM) following extraction to the water phase. Osburn et al. (117) reported seasonal and spatial changes in base extractable organic matter from POC in the water column that were different to the corresponding DOM trends, indicating a decoupling of the dissolved and particulate organic matter fractions.

Anthropogenic activities can also be allochthonous sources of DOM. For instance, Catalá et al. (99) reported an increase in protein-like fluorescent component intensity in the summer tourist season in a Mediterranean estuary and suggested that sewage may be responsible for that change in DOM quality. Similarly, Stedmon and Markager (30) reported a likely wastewater contribution to the FDOM pool in a Danish estuary. While industrial activities such as paper pulp mill discharges may also contribute to the coastal FDOM signature (118), agricultural activities and road construction may increase weathering processes and contribute to the mobilization of organic matter to aquatic systems in anthropogenically impacted watersheds (53). Similar effects of anthropogenic activities on PARAFAC distributions in river systems have been discussed above.

Quantitative Estimates Based on EEM-PARAFAC

Over the past few years, fluorescence and EEM-PARAFAC have been applied not only to understand spatial and temporal variations of DOM quality in estuarine and coastal ecosystems, but also to quantify sources and export of organic carbon to the ocean. For example, Bergamaschi et al. (119) estimated, from in-situ fluorescence probe measurements, that DOC exports from sub-tropical fringe mangrove-rivers in the Everglades, ranged from $1.5 (\pm 0.02) \times 10^9 \text{ mg d}^{-1}$ during the dry season to $9.1 (\pm 0.6) \times 10^9 \text{ mg d}^{-1}$ during the wet season. Building on these findings, Cawley et al. (89) used DOC measurements in combination with EEM-PARAFAC analysis along salinity transects to estimate that of the DOC exported by these coastal rivers, up to ~ 20% of the DOC was derived from the estuary and was likely produced within the mangrove ecotone, while the remainder of the DOC (~ 80%) was transported from the upstream freshwater regions of the Everglades. These authors also observed a significant degree of variability in the distribution of PARAFAC components along the estuary (Figure 6), suggesting contributions of humic-like components to the DOM pool by the fringe mangroves, conservative mixing of one of the freshwater end-member humic-like components, and consumption of tyrosine-like fluorescence at higher salinities. In another study, the export of DOM from Arctic glacial rivers to the Gulf of Alaska has been reported to be ~0.01 Tg of DOC (120). A significant portion of this DOC was found to be highly labile based on EEM-PARAFAC and bioavailability studies, suggesting that changes in terrestrial DOC and nutrients from these rivers may affect long-term ecosystem dynamics in the coastal ocean (102). Using PARAFAC fluorescence and DOC relationships, Osburn and Stedmon (121) were able to estimate the net flux of terrestrial C from the Baltic Sea to the North Sea at 0.8 Tg yr^{-1} , which represents 45% of the calculated net flux (1.7 Tg yr^{-1}). Thus, EEM-PARAFAC has provided a greater understanding of large-scale carbon fluxes by allowing researchers to better constrain the fate and transport of different DOC pools that are not readily discernible based on DOC or CDOM concentration measurements alone.

Open Ocean

In the open ocean, the stable and radiocarbon isotope signature of bulk DOM indicates that a major fraction of DOM is of marine origin and is old compared to the thermohaline circulation (apparent age is 2000~6000 yrs) (122). Chemical characterization of DOM showed that chromatographically identifiable biomolecules such as sugars, lipids and amino acids, can only justify ~10% of DOM, while levels of terrestrial biomarkers, such as lignin phenols, are quite low in oceanic DOM (123–125). These chemical characteristics of oceanic DOM indicate that molecularly uncharacterized components (MUC) in DOM are produced *in situ* and may be bio-recalcitrant. However, the production mechanism of bio-recalcitrant DOM and the fate of terrestrial DOM in ocean environments have not been fully documented (126). Even though remnants of microbial membranes were detected in DOM as recalcitrant biomolecules (e.g., (127–129)), the microbial production of bio-recalcitrant MUC was also experimentally determined (e.g., (130)). These processes have recently been defined as the microbial carbon pump (131).

Fluorescence techniques, such as fluorescence intensity at fixed Ex/Em (e.g., (132, 133)) and EEM (e.g., (26, 134)), have been applied to evaluate the environmental dynamics of DOM in the open ocean. Even though fluorescence techniques provide “semi-quantitative” information (carbon amount cannot be obtained from fluorescence analysis), the unique aspects of fluorescence listed below are useful for evaluating the environmental dynamics of DOM in the open ocean: (a) spectral characteristics of marine humic-like fluorophores (traditionally defined as peak M) are different from terrestrial humic-like fluorophores (traditionally defined as peaks A and C) (26), and thus, fluorescence may allow the tracing of terrestrial DOM in the open ocean; (b) since humic-like fluorophores can be considered as MUC, production mechanisms of MUC may be evaluated using fluorescence; (c) microbial production of bio-recalcitrant (at least 900 yrs) humic-like fluorophores have been determined (135), indicating that fluorescence can be used to evaluate the microbial carbon pump; and (d) linear relationships between concentrations of aromatic amino acids and fluorescence intensity of protein-like components (136, 137) allow for the evaluation of the environmental dynamics of semi-labile DOM as represented by amino acids (138). Although the number of EEM-PARAFAC studies of oceanic DOM is relatively small compared with terrestrial and coastal environments at present, EEM-PARAFAC studies have provided new insights into the environmental dynamics of oceanic FDOM as well as DOM.

Tracing Allochthonous DOM Components in Ocean Systems

The levels of humic-like components in the open ocean are quite low compared with coastal environments. In the Arctic Ocean where contributions of terrestrial DOM are greater than other oceans due to high river discharge, humic-like components can be useful as terrestrial DOM tracers. In the regions most strongly affected by riverine inputs, a decrease in both terrestrial and marine humic-like components with increase in salinity have been reported

(139, 140), whereas decoupling of the behavior between terrestrial and microbial humic-like components at high salinity waters, possibly due to in situ production of microbial humic-like components (139–142) has also been suggested. Walker et al. (143) determined the distribution of FDOM in the Canadian Archipelago and Beaufort Sea surface waters using EEM-PARAFAC and found that four terrestrial components were positively linearly correlated with concentrations of lignin phenols, which can be used as terrestrial biomarkers, whereas marine humic-like (peak M type) and protein-like (peak T type) components were unrelated to river sources. The strong linear correlation between terrestrial humic-like component (peak A type) and lignin phenol concentrations were also found in the Baltic-North Sea transition zone (121).

From the deviation in the relationships between apparent oxygen utilization (AOU, the amount of the oxygen consumed by respiration) and fluorescence intensity at 320 nm excitation and 420 nm emission, Yamashita and Tanoue (135) suggested that, in addition to in-situ production of FDOM, terrestrial FDOM contributes to the DOM pool in the North Pacific Intermediate Water (NPIW) at ~800 m depth. The NPIW is influenced by the Sea of Okhotsk water, to which terrestrial humic substances from the Amur River evidently contribute to the FDOM pool (144). Relatively high concentrations of lignin phenol in the NPIW compared with other water masses were also observed (145). Jørgensen et al. (146) determined relationships between AOu and humic-like PARAFAC components and found relatively high levels of humic-like PARAFAC components in the North Atlantic Deep Water (NADW) compared with other water masses of the global deep ocean. The contributions of terrestrial DOM in the NADW from the Arctic rivers have also been evaluated by the distribution of lignin phenol concentrations (147). These results suggest that some terrestrial humic-like components are transported into the dark ocean where they cannot be subjected to photo-bleaching.

Murphy et al. (148) determined FDOM distributions for surface waters from coastal to open ocean for the Pacific, Atlantic and Mediterranean using EEM-PARAFAC. They evaluated the environmental dynamics of the peak M type component and peak C and A type components using log-log plots of the PARAFAC fluorescence intensity. The study suggests that the sources of peak C and A type components in surface samples were only terrestrial, whereas peak M type component was sourced from both terrestrial and oceanic environments. These results imply that the traditional marine humic-like (peak M type component) is produced not only in marine environments but can also have terrestrial origins. This is consistent with data from other EEM-PARAFAC studies conducted on terrestrial environments (see Lakes, Estuaries and Coasts sections above). In addition, these authors estimated that fluorescence of terrestrial humic material (A and C peak type fluorescence) was detectable in the surface open ocean at levels approximately 1.5% of original freshwater concentrations. However, as pointed out by the authors, this fluorescence cannot be used as a conservative tracer of terrestrial humic materials considering that it can also be produced in the deep ocean ((146, 149); see discussion below). In summary, while terrestrial humic-like materials can be traceable through EEM-PARAFAC in marine environments where contribution of riverine inputs are significant

and/or where DOM photo-bleaching is not severe, further studies are necessary for evaluating the applicability of this technique, especially in surface waters where photo-bleaching and in situ production of humic-like components might be major factors controlling their levels.

Anthropogenic influences are another factor impacting DOM quality in the oceans. The significant differences in the levels of terrestrial humic-like components between coast and open ocean waters have been reported to be useful to trace the source of ballast water (148, 150). Murphy et al. (150) applied EEM-PARAFAC to distinguish between ports and oceanic waters as the source of ballast water. They reported that a humic-like component ($Ex/Em = 370/494$, peak C type) was sufficient for discriminating between port and oceanic waters as a source of most ballast waters. Murphy and coworkers (148, 151) also identified an EEM-PARAFAC component that featured spectral characteristics similar to polycyclic aromatic hydrocarbons (PAH) in oceanic waters. They reported that the distribution of this component was clearly consistent with an anthropogenic source, considering that high concentrations were detected in ports (148). In addition, the fate and transformation processes of oil derived from an unprecedented deep water spill in the Gulf of Mexico were determined using EEM-PARAFAC (152–154). Zhou et al. (154) revealed the presence of three oil-related PARAFAC components corresponding to crude and weathered oil in the water column. Such results imply that EEM-PARAFAC is also a useful technique for assessing the contributions of anthropogenically derived organic matter in the open ocean.

Distribution of PARAFAC Components in the Open Ocean

PARAFAC models developed using oceanic samples identified one to three humic-like components which can basically be categorized as peak M, C, and A type (146, 149, 155–157). The number of such components is smaller than those obtained from PARAFAC models using coastal and terrestrial samples, suggesting that humic-like PARAFAC components in the open ocean are relatively less complex, more homogeneous, irrespective of differences in seasons, depths, and oceanic regions.

Photo-bleaching has been reported to be a major sink for humic-like components in coastal and terrestrial environments (see Lakes, Estuaries and Coasts section). Even though photo-bleaching processes of oceanic DOM have not been evaluated using EEM-PARAFAC, photo-degradation of humic-like fluorophores in oceanic DOM have been well studied using fluorescence intensity at fixed Ex/Em and EEMs (22, 133, 158). As a result of this process, low levels of humic-like fluorescence in surface water have been observed for the Atlantic (e.g., (133)), the Pacific (e.g., (132, 134)), the Indian (e.g., (159)), and the Southern Ocean (e.g., (160)). Similarly, levels of humic-like PARAFAC components, both marine humic-like (peak M type) and terrestrial humic-like component (peaks A and C type), were lowest in surface waters, increased with depth in intermediate waters, and then, remained within a relatively narrow range in deep waters, irrespective of the specific oceanic region ((146, 149); Figure 8). Autochthonous sources of humic-like components, including peak M and peak

C type, have been observed for controlled experiments using both traditional fluorescence techniques (161–164) as well as EEM-PARAFAC (31, 114). For open ocean waters, Yamashita et al. (149) and Jørgensen et al. (146) reported that fluorescence intensities of both marine and terrestrial humic-like components correlated linearly with AOU for water depths greater than 200 m. Interestingly, the vertical gradient of the fluorescence intensity was larger for the terrestrial humic-like component (peak C type) compared with the marine humic-like component (peak M type) (Figure 8; (146)). Similarly, the ratio of fluorescence intensity of a terrestrial humic-like component to a marine humic-like component was lowest in the surface water, increased with depth in the intermediate water, and then, was constant in the deep water of the northwestern North Pacific (149). Such quantitative changes in PARAFAC component distribution with increases in depths were consistent with qualitative differences in EEMs observed between the surface and deep waters (26, 134). These EEM-PARAFAC based experimental and observational findings indicate that both marine and terrestrial humic-like components are produced *in situ* in the open ocean, and thus, *in situ* produced humic-like components are likely responsible for their high levels at intermediate and deep waters.

The quantitative evaluation of EEM-PARAFAC component abundance provided new insights regarding oceanic DOM dynamics. The microbial production of bio-refractory (at least 900 yrs) humic-like fluorescence in the deep ocean water was indicated by the linear relationship between AOU and fluorescence intensity ($Ex/Em = 320/420$ nm; (135)). The similarity in the ratios between the two humic-like components (marine vs. terrestrial) in the deep ocean water (146, 149) where vertical gradients of AOU were evident, suggests that fluorophore composition of *in situ* produced humic-like substances is not changed biotically nor abiotically with the thermohaline circulation in the deep ocean. On the other hand, decreases in the ratio of terrestrial humic-like component to marine humic-like component (Figure 8; (146, 149)) are possibly due to different rates of photo-bleaching between two components, causing a blue shift in the EEMs (e.g., (108)). However, using *in vitro* experiments with EEM analysis, Romera-Castillo et al. (163, 165) recently reported that eukaryotes mainly produce peak M type fluorescence, whereas prokaryotes mainly produce peak C type fluorescence. Such differences in fluorophore composition by different organisms may also contribute to the observed vertical changes in the ratio of humic-like components. Additional *in vitro* experiments with EEM-PARAFAC are necessary to gain further knowledge on the relationship between fluorophore composition and source organisms.

EEM-PARAFAC has also contributed to the evaluation of the interactions between humic-like components and trace metals in the open ocean. From the linear relationships between humic-like fluorescence intensity at $Ex/Em = 320/420$ nm and Fe(III) solubility in the deep ocean water, Fe(III) complexation with humic-like substances was suggested to be critical in controlling iron solubility and its ultimate concentration in the deep ocean (166). As such, Yamashita et al. (149) reported that Fe(III) solubility linearly correlated with levels of terrestrial humic-like components, but not with those of marine humic-like components in the deep water of the northwestern North Pacific, indicative of the dominance of

terrestrial humic-like component acting as ligands for Fe(III) compared to marine humic-like components. In contrast, Heller et al. (156), using EEM-PARAFAC, suggested that although humic-like components were not significantly correlated with Fe(III) solubility, they were weakly correlated with iron solubility in iron-enriched Atlantic surface water.

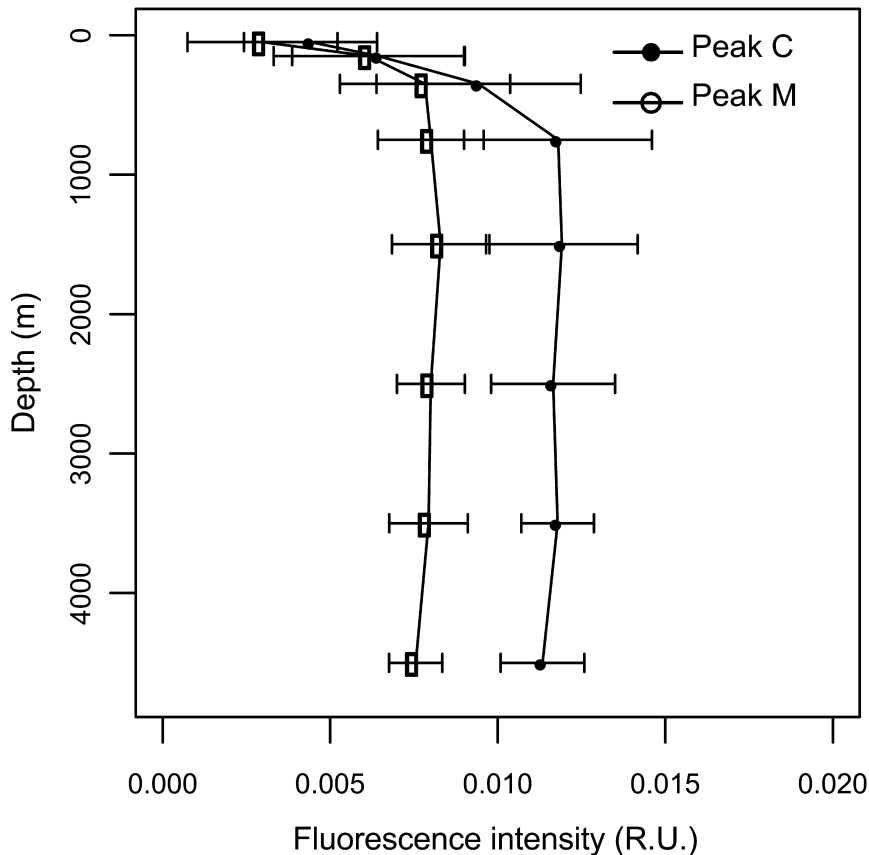


Figure 8. Global mean vertical distribution of humic-like fluorescence components in the open ocean. Mean values are calculated for eight depth intervals (0–100, 100–200, 200–500, 500–1000, 1000–2000, 2000–3000, 3000–4000 and 4000–5000 m) from 170 stations. Error bars represent standard deviations. Data from the top 200 m of the Atlantic (except the Sargasso Sea) and the Eastern South Pacific are omitted. (Reproduced from reference (146). Copyright 2011 Elsevier)

In the ocean surface layer, levels of humic-like components, including M, C, and A types, are lower compared to deeper layers due to photobleaching as discussed above (Figure 8; (146)). However, in surface waters, levels of humic-like components for the Atlantic (except for the Sargasso Sea) were

higher than those at other regions, indicative of terrestrial inputs from Arctic rivers (146). EEM-PARAFAC data for meriodional transects of the Atlantic surface layer showed that levels of marine humic-like component (156) and total humic-like components (157) at the equator and continental regions were higher than those at tropical-subtropical regions, indicating that the distribution of humic-like components in the surface layer of the open ocean is controlled by a combination of photo-bleaching, in situ production, upwelling of the deep water, and terrestrial inputs. Furthermore, Kowalcuk et al. (157) reported that total humic-like components exhibited a significant negative correlation with salinity, and temperature and a positive correlation with AOU and suggested that a net equilibrium between the supply of humic-like substances from the continental margins, in situ production by the microbial activity and photo-degradation in the surface waters was responsible for these trends.

Heller et al. (156) reported that the marine humic-like component (peak M type) showed a well-developed minimum in the southern tropical gyre of the Atlantic Ocean. In contrast, the terrestrial humic-like component (peak A type) was distributed relatively uniformly throughout surface waters of the Atlantic. In addition, Murphy et al. (148) showed that the ratio of C9 (peak A type component) to terrestrial humic-like C3 (peak A and C type) increased with increasing distance from land, indicative of a long-lived product of the photo-degradation of organic matter. Similar components have been suggested to be photo-refractory and/or photo-produced in coastal environments (see Estuaries and Coasts section). Thus, these components (and their ratio to other humic-like components) might be a useful proxy to trace the photo-chemical history of oceanic DOM. Further studies on the photo-reactivity of oceanic DOM using EEM-PARAFAC are necessary to advance this field.

The presence of protein-like EEM-PARAFAC components in oceanic environments is ubiquitous, and one to four protein-like components have been identified (146, 149, 155–157). Although levels of protein-like components were commonly low in the open ocean compared to coastal regions, the relative abundance of protein-like components in total FDOM usually increases from shore to open ocean, indicative of an autochthonous enrichment of protein-like as compared to humic-like components (48, 92, 93, 148). In contrast to terrestrial and coastal PARAFAC models, the numbers of protein-like components using oceanic waters were similar or exceeding those of humic-like components, suggesting a higher spectral variability and compositional complexity of protein-like fluorescence. The vertical patterns of protein-like components in the open ocean were usually quite different from those of humic-like components, where levels were highest in the surface layer, decreased with depth, and were lowest in the intermediate and deep waters (146, 149). Such vertical patterns are similar to the DOC profiles (167), suggesting that production and degradation are dominant process at the surface layer and below the surface layer, respectively. Wedborg et al. (155) showed that levels of protein-like components were correlated with chlorophyll a in the surface waters of the Southern Ocean, and were found to mix down to the core of the Antarctic intermediate water (AAIW). Similarly, Jørgensen et al. (146) reported relatively high levels of phenylalanine- and tyrosine-like PARAFAC components in the NADW at the North, Equatorial,

and South Atlantic compared with other deep water masses and suggested that these components were transported from surface to deep layers and then flow southward along the direction of the NADW. These results imply that a part of protein-like components are at least semi-labile and transported from the surface layer to below the surface layer through ocean circulation.

Kowalcuk et al. (157) reported that the fluorescence intensity of three protein-like components displayed a subsurface maximum at depths between 100-200 m that were deeper than the corresponding subsurface chlorophyll maximum, even though the causes of the subsurface maximum have not been well documented. Heller et al. (156) found that the abundance of the tyrosine-like component reached a maximum in the upper 100 m of the oligotrophic southern tropical gyre, while the tryptophan-like component showed higher and lower values at the South and North Atlantic, respectively. In addition, they found high variability of the tryptophan-like component below the mixed layer and pointed out that “hotspots” of this component might be related to zooplankton grazing. As such, while different protein-like components show different distributional patterns (e.g., tyrosine-like and tryptophan-like), the environmental drivers resulting in these distributional patterns have not been fully elucidated. Since protein-like fluorescence is not only caused by the presence of aromatic amino acids and amino acid-containing molecules in DOM (136, 137), but can have potential contributions from the fluorescence of phenolic compounds (62), further molecular-based evaluations of the protein-like EEM-PARAFAC fluorescence are needed to better evaluate the chemical/physical character, and thus, reactivity of ‘protein-like’ fluorophore-containing DOM.

Characteristics of Fluorescent Components in Sea Ice

Sea ice formation, biological processes in sea ice, and sea ice melt are important biogeochemical processes in surface waters at the Polar Ocean. Although solutes in seawater are mostly excluded from the ice during sea ice formation, about 10–40% of solutes may become entrained in channels within the sea ice (168). In addition, biological activity in sea ice may consume or produce organic matter within the ice. Thus, sea ice melt can supply freshwater-associated DOM to the surface layer of the ocean. Based on sea ice formation experiments, Müller et al. (168) showed that protein-like components were effectively incorporated into sea ice (enrichment factor 1.10-3.94) compared to humic-like components (enrichment factor 1.0-1.39). Stedmon et al. (169) applied EEM-PARAFAC for the characterization of DOM in sea ice and underlying water of the coastal Baltic Sea and reported that humic-components were incorporated during sea ice formation, while protein-like components were produced within the ice. Similarly, Stedmon et al. (170) determined the FDOM composition of Antarctic sea ice brines and found that accumulations of tryptophan-like components in sea ice were accompanied with accumulation of low C/N DOM. Although several studies have been reported regarding EEM-PARAFAC applications for the characterization of DOM in sea ice, further studies combining fluorescence with DOC and DON abundances will provide

a better understanding of the drivers controlling the biogeochemical cycling of carbon within sea ice as well as the impacts of sea ice melt to the biological productivity of surface waters of the Polar Ocean.

Conclusions and Considerations

EEM-PARAFAC has been applied to a great variety of aquatic environments with the main objective to better understand DOM dynamics in diverse ecosystems. The enhanced resolution of EEM-PARAFAC compared to the traditional EEM 'peak picking' technique allows for a better quantification of different FDOM components and provides more detailed information regarding the quality or composition of FDOM. As such, the technique has been used in assessing allochthonous vs. autochthonous source strengths in aquatic systems, effects of storms and hydrological disturbances on DOM composition and source, as a proxy to assess photo- and bio-reactivity, and to determine effects of land-use change, forest management and pollution on DOM dynamics. Although EEM-PARAFAC is limited to only measuring a relatively small fraction of the total DOM (the FDOM), its strength lies in the fact that it is a relatively simple, cheap, sensitive and high throughput technique that allows for the generation of large databases over a relatively short period of time. Sample size (volume) and preparation (filtration) are small and simple respectively, creating an ideal technique for ecosystem studies on large temporal and spatial scales. Although EEM-PARAFAC has also been used to assess detailed compositional features of DOM (e.g. (29)) and has been suggested as a means to determine DOM red-ox conditions, photo-reactivity and bio-availability, such approaches need to be performed with great care, and for well-characterized ecosystems, as little is still known about the links between EEM-PARAFAC components and their actual chemical composition and molecular character. In addition to the chemical composition of individual DOM molecules, EEM-PARAFAC results may also be affected by intermolecular interactions. A recent report by Korak et al. (171) highlights that DOM metrics derived from EEM fluorescence may be influenced by non-ideal interactions within the DOM solution and suggests that care should be taken to evaluate the validity of underlying assumptions of linearity in fluorescence intensity with concentration and shifts in peak locations when calculating indices.

One of the merits of this technique for ecosystem studies is easy handling of large datasets, which allow statistical analyses for the interpretation of data based on the variation in the distribution patterns on spatial and temporal scales. On the other hand, studies with a low number of samples seem to have some limitation in scope due to potentially large variations in the ecological processes driving DOM dynamics in complex ecosystems. However, large datasets do not necessarily generate a larger number of validated PARAFAC components, nor do PARAFAC models featuring a larger numbers of components fit data better than those with a low number of components. Comparisons of PARAFAC components between models developed for different ecosystems are commonly

performed and can be quite useful as an aid in data interpretations. This task is facilitated through the availability of PARAFAC components characteristics in the literature (25, 172). However, care must be exercised using this approach since fluorescence features may appear ‘similar’ between different systems, but may represent quite different DOM compositions. In addition, small differences in the spectral characteristics between models can translate into significant differences in fluorescence maxima ratios between PARAFAC components or relative abundances of PARAFAC components (118, 173). In this regard, much discussion in this field has focused on the potential advantages in developing a robust, ‘global PARAFAC model’ to be used in general, or if regional PARAFAC models provide more accurate site-specific data interpretation (e.g. (55)). A rigorous analysis of the PARAFAC model residuals may be helpful in determining whether a potential global model adequately fits an individual dataset or not (e.g., (118)). However, only one literature report has, to the best of our knowledge, performed a detailed comparison of a variety of different, site-specific PARAFAC models and compared them to a potentially more broad-based PARAFAC model (174). When EEMs are collected from similar environments (174) and with proper instrument correction factors (175), a potentially broad-based PARAFAC model might be adequate for determining variability of DOM character within a system. However, some of the sensitivity to unique, site-specific ecological processes is likely to be lost if regionally-specific models are not used (174). In the absence of a true, globally applicable PARAFAC model, more research in this area is needed.

An additional issue requiring further studies is the use and true identity of the ‘protein-like’ PARAFAC components. While such fluorescence has been clearly linked to the abundance of hydrolysable amino acids in ocean water, and in most instances is likely applied correctly, it has also been shown to be representative of fluorescence features of polyphenols commonly found in the environment (62), such as gallic acid. Such potential differences in DOM composition for the ‘protein’-like fluorescence may lead to misinterpretations if not accounted for. As such, while EEM-PARAFAC has undergone a remarkable growth in its use and development in aquatic biogeochemistry, and will likely continue to grow as a highly popular and user-friendly analytical tool in DOM dynamics studies, one critically underrepresented research aspect in this field is the determination of clear links between PARAFAC components’ fluorescence characteristics and their actual chemical composition and molecular features.

Acknowledgments

The authors thank Dr. Fernando Rosario-Ortiz for the invitation to contribute to this book with a review chapter. The authors are particularly thankful to Dr. N. Mladenov and an anonymous reviewer for their constructive comments which significantly improved this review. Special thanks to Drs. J. Fellman, Y. Lu and C. Stedmon for kindly providing modified versions of Figures 1, 2 and 8 used in this review. R. Jaffé thanks the National Science Foundation through the FCE-LTER

program and the George Barley Endowment, for many years of support, resulting in several EEM-PARAFAC publications presented in this review. Y. Yamashita thanks the Japan Society for the Promotion of Science (JSPS) for research support. This is SERC Contribution number 662.

References

1. Benner, R. In *Aquatic Ecosystems: Interactivity of Dissolved Organic Matter*; Findlay, S., Sinsabaugh, R. L., Eds.; Academic Press: New York, 2003; pp 121–137.
2. Zhang, Y. L.; Zhang, E. L.; Liu, M. L.; Wang, X.; Qin, B. Q. Variation of chromophoric dissolved organic matter and possible attenuation depth of ultraviolet radiation in Yunnan Plateau lakes. *Limnology* **2007**, *8*, 311–319.
3. Kaplan, L. A.; Wiegner, T. N.; Newbold, J. D.; Ostrom, P. H.; Gandhi, H. Untangling the complex issue of dissolved organic carbon uptake: a stable isotope approach. *Freshwater Biol.* **2008**, *53*, 855–864.
4. Yamashita, Y.; Jaffé, R. Characterizing the interactions between trace metals and dissolved organic matter using excitation-emission matrix and parallel factor analysis. *Environ. Sci. Technol.* **2008**, *42*, 7374–7379.
5. Hedges, J. I.; Keil, R. G.; Benner, R. What happens to terrestrial organic matter in the ocean? *Org. Geochem.* **1997**, *27*, 195–212.
6. Battin, T. J.; Kaplan, L. A.; Findlay, S.; Hopkinson, C. S.; Marti, E.; Packman, A. I.; Newbold, J. D.; Sabater, F. Biophysical controls on organic carbon fluxes in fluvial networks. *Nat. Geosci.* **2008**, *1*, 95–100.
7. Cory, R. M.; McKnight, D. M.; Chin, Y. P.; Miller, P.; Jaros, C. L. Chemical characteristics of fulvic acids from Arctic surface waters: Microbial contributions and photochemical transformations. *J. Geophys. Res.: Biogeosci.* **2007**, *112*, G04S51.
8. Cole, J. J.; Prairie, Y. T.; Caraco, N. F.; McDowell, W. H.; Tranvik, L. J.; Striegl, R. G.; Duarte, C. M.; Kortelainen, P.; Downing, J. A.; Middelburg, J. J.; Melack, J. Plumbing the global carbon cycle: Integrating inland waters into the terrestrial carbon budget. *Ecosystems* **2007**, *10*, 171–184.
9. Guillemette, F.; del Giorgio, P. A. Reconstructing the various facets of dissolved organic carbon bioavailability in freshwater ecosystems. *Limnol. Oceanogr.* **2011**, *56*, 734–748.
10. Spencer, R. G. M.; Ahad, J. M. E.; Baker, A.; Cowie, G. L.; Ganeshram, R.; Upstill-Goddard, R. C.; Uher, G. The estuarine mixing behaviour of peatland derived dissolved organic carbon and its relationship to chromophoric dissolved organic matter in two North Sea estuaries (UK). *Estuarine, Coastal Shelf Sci.* **2007**, *74*, 131–144.
11. Holbrook, R. D.; Yen, J. H.; Grizzard, T. J. Characterizing natural organic material from the Occoquan Watershed (Northern Virginia, US) using fluorescence spectroscopy and PARAFAC. *Sci. Total Environ.* **2006**, *361*, 249–266.

12. Wilson, H. F.; Xenopoulos, M. A. Effects of agricultural land use on the composition of fluvial dissolved organic matter. *Nat. Geosci.* **2009**, *2*, 37–41.
13. Lu, Y.; Bauer, J. E.; Canuel, E. A.; Yamashita, Y.; Chambers, R. M.; Jaffé, R. Photochemical and Microbial Alteration of Dissolved Organic Matter in Temperate Headwater Streams Associated with Different Land Use. *J. Geophys. Res.: Biogeosci.* **2013**, *118*, 566–580.
14. Lu, Y.; Bauer, J. E.; Canuel, E. A.; Chambers, R. M.; Yamashita, Y.; Jaffé, R.; Barrett, A. Effects of land use on sources and ages of inorganic and organic carbon in temperate headwater streams. *Biogeochemistry* **2014** DOI:10.1007/s10533-014-9965-2.
15. Jaffé, R.; McKnight, D.; Maie, N.; Cory, R.; McDowell, W. H.; Campbell, J. L. Spatial and temporal variations in DOM composition in ecosystems: The importance of long-term monitoring of optical properties. *J. Geophys. Res.: Biogeosci.* **2008**, *113*, G04032.
16. McKnight, D. M.; Boyer, E. W.; Westerhoff, P. K.; Doran, P. T.; Kulbe, T.; Andersen, D. T. Spectrofluorometric characterization of dissolved organic matter for indication of precursor organic material and aromaticity. *Limnol. Oceanogr.* **2001**, *46*, 38–48.
17. Stedmon, C. A.; Markager, S.; Bro, R. Tracing dissolved organic matter in aquatic environments using a new approach to fluorescence spectroscopy. *Mar. Chem.* **2003**, *82*, 239–254.
18. Coble, P. G. Marine optical biogeochemistry: The chemistry of ocean color. *Chem. Rev.* **2007**, *107* (2), 402–418.
19. Fellman, J. B.; Hood, E.; Spencer, R. G. M. Fluorescence spectroscopy opens new windows into dissolved organic matter dynamics in freshwater ecosystems: A review. *Limnol. Oceanogr.* **2010**, *55*, 2452–2462.
20. Andrade-Eiroa, A.; Canle, M.; Cerdá, V. Environmental Applications of Excitation-Emission Spectrofluorimetry: An In-Depth Review I. *Appl. Spectrosc. Rev.* **2013**, *48*, 1–49.
21. Andrade-Eiroa, A.; Canle, M.; Cerdá, V. Environmental Applications of Excitation-Emission Spectrofluorimetry: An In-Depth Review II. *Appl. Spectrosc. Rev.* **2013**, *48*, 77–141.
22. Helms, J. R.; Stubbins, A.; Perdue, E. M.; Green, N. W.; Chen, H.; Mopper, K. Photochemical bleaching of oceanic dissolved organic matter and its effect on absorption spectral slope and fluorescence. *Mar. Chem.* **2013**, *155*, 81–91.
23. Henderson, R. K.; Baker, A.; Murphy, K. R.; Hamblya, A.; Stuetz, R. M.; Khan, S. J. Fluorescence as a potential monitoring tool for recycled water systems: A review. *Water Res.* **2009**, *43*, 863–881.
24. Mostofa, K. M. G.; Wu, F. C.; Liu, C. Q.; Vione, D.; Yoshioka, T.; Sakugawa, H.; Tanoue, E. Photochemical, microbial and metal complexation behavior of fluorescent dissolved organic matter in the aquatic environments. *Geochem. J.* **2011**, *45*, 235–254.
25. Ishii, S. K. L.; Boyer, T. H. Behavior of Reoccurring PARAFAC Components in Fluorescent Dissolved Organic Matter in Natural and Engineered Systems: A Critical Review. *Environ. Sci. Technol.* **2012**, *46*, 2006–2017.

26. Coble, P. G. Characterization of marine and terrestrial DOM in seawater using excitation emission matrix spectroscopy. *Mar. Chem.* **1996**, *51*, 325–346.
27. Yamashita, Y.; Scinto, L. J.; Maie, N.; Jaffé, R. Dissolved Organic Matter Characteristics Across a Subtropical Wetland's Landscape: Application of Optical Properties in the Assessment of Environmental Dynamics. *Ecosystems* **2010**, *13*, 1006–1019.
28. Chen, M.; Maie, N.; Parish, K.; Jaffé, R. Spatial and temporal variability of dissolved organic matter quantity and composition in an oligotrophic subtropical coastal wetland. *Biogeochemistry* **2013**, *115*, 167–183.
29. Cory, R. M.; McKnight, D. M. Fluorescence spectroscopy reveals ubiquitous presence of oxidized and reduced quinones in dissolved organic matter. *Environ. Sci. Technol.* **2005**, *39*, 8142–8149.
30. Stedmon, C. A.; Markager, S. Resolving the variability in dissolved organic matter fluorescence in a temperate estuary and its catchment using PARAFAC analysis. *Limnol. Oceanogr.* **2005**, *50*, 686–697.
31. Stedmon, C. A.; Markager, S. Tracing the production and degradation of autochthonous fractions of dissolved organic matter by fluorescence analysis. *Limnol. Oceanogr.* **2005**, *50*, 1415–1426.
32. Burrows, R. M.; Fellman, J. B.; Magierowski, R. H.; Barmuta, L. A. Allochthonous dissolved organic matter controls bacterial carbon production in old-growth and clearfelled headwater streams. *Freshwater. Sci.* **2013**, *32*, 821–836.
33. Catalan, N.; Obrador, B.; Alomar, C.; Pretus, J. L. Seasonality and landscape factors drive dissolved organic matter properties in Mediterranean ephemeral washes. *Biogeochemistry* **2013**, *112*, 261–274.
34. Jaffé, R.; Yamashita, Y.; Maie, N.; Cooper, W. T.; Dittmar, T.; Dodds, W. K.; Jones, J. B.; Myoshi, T.; Ortiz-Zayas, J. R.; Podgorski, D. C.; Watanabe, A. Dissolved Organic Matter in Headwater Streams: Compositional Variability across Climatic Regions of North America. *Geochim. Cosmochim. Ac.* **2012**, *94*, 95–108.
35. Inamdar, S.; Finger, N.; Singh, S.; Mitchell, M.; Levia, D.; Bais, H.; Scott, D.; McHale, P. Dissolved organic matter (DOM) concentration and quality in a forested mid-Atlantic watershed, USA. *Biogeochemistry* **2012**, *108*, 55–76.
36. Yamashita, Y.; Kloepfel, B. D.; Knoepp, J.; Zausen, G. L.; Jaffé, R. Effects of Watershed History on Dissolved Organic Matter Characteristics in Headwater Streams. *Ecosystems* **2011**, *14*, 1110–1122.
37. Balcarczyk, K. L.; Jones, J. B. R.; Maie, N. Stream dissolved organic matter bioavailability and composition in watersheds underlain with discontinuous permafrost. *Biogeochemistry* **2009**, *94*, 255–270.
38. Fellman, J. B.; Hood, E.; Edwards, R. T.; D'Amore, D. V. Changes in the concentration, biodegradability, and fluorescent properties of dissolved organic matter during stormflows in coastal temperate watersheds. *J. Geophys. Res.: Biogeosci.* **2009**, *114*, G01021.
39. Chen, H.; Meng, W.; Zheng, B. H.; Wang, C. Y.; An, L. H. Optical signatures of dissolved organic matter in the watershed of a globally large river (Yangtze River, China). *Limnologica* **2013**, *43*, 482–491.

40. Yang, L. Y.; Hong, H. S.; Guo, W. D.; Huang, J. L.; Li, Q. S.; Yu, X. X. Effects of changing land use on dissolved organic matter in a subtropical river watershed, southeast China. *Reg. Environ. Change* **2012**, *12*, 145–151.
41. Hur, J.; Cho, J. Prediction of BOD, COD, and Total Nitrogen Concentrations in a Typical Urban River Using a Fluorescence Excitation-Emission Matrix with PARAFAC and UV Absorption Indices. *Sensors (Basel)* **2012**, *12*, 972–986.
42. Hong, H. S.; Yang, L. Y.; Guo, W. D.; Wang, F. L.; Yu, X. X. Characterization of dissolved organic matter under contrasting hydrologic regimes in a subtropical watershed using PARAFAC model. *Biogeochemistry* **2012**, *109*, 163–174.
43. Fellman, J. B.; Petrone, K. C.; Grierson, P. F. Source, biogeochemical cycling, and fluorescence characteristics of dissolved organic matter in an agro-urban estuary. *Limnol. Oceanogr.* **2011**, *56*, 243–256.
44. Massicotte, P.; Frenette, J. J. Spatial connectivity in a large river system: resolving the sources and fate of dissolved organic matter. *Ecol. Appl.* **2011**, *21*, 2600–2617.
45. Borisover, M.; Laor, Y.; Parparov, A.; Bukhanovsky, N.; Lado, M. Spatial and seasonal patterns of fluorescent organic matter in Lake Kinneret (Sea of Galilee) and its catchment basin. *Water. Res.* **2009**, *43*, 3104–3116.
46. Petrone, K. C.; Fellman, J. B.; Hood, E.; Donn, M. J.; Grierson, P. F. The origin and function of dissolved organic matter in agro-urban coastal streams. *J. Geophys. Res.: Biogeosci.* **2011**, *116*, G01028.
47. Mostofa, K. M. G.; Wu, F. C.; Liu, C. Q.; Fang, W. L.; Yuan, J.; Ying, W. L.; Wen, L.; Yi, M. Characterization of Nanming River (southwestern China) sewerage-impacted pollution using an excitation-emission matrix and PARAFAC. *Limnology* **2010**, *11*, 217–231.
48. Yamashita, Y.; Panton, A.; Mahaffey, C.; Jaffé, R. Assessing the spatial and temporal variability of dissolved organic matter in Liverpool Bay using excitation-emission matrix fluorescence and parallel factor analysis. *Ocean. Dyn.* **2011**, *61*, 569–579.
49. Lapierre, J. F.; Frenette, J. J. Effects of macrophytes and terrestrial inputs on fluorescent dissolved organic matter in a large river system. *Aquat. Sci.* **2009**, *71*, 15–24.
50. Yamashita, Y.; Maie, N.; Briceno, H.; Jaffé, R. Optical characterization of dissolved organic matter in tropical rivers of the Guayana Shield, Venezuela. *J. Geophys. Res.: Biogeosci.* **2010**, *115*, G00F10.
51. Yao, X.; Zhang, Y. L.; Zhu, G. W.; Qin, B. Q.; Feng, L. Q.; Cai, L. L.; Gao, G. A. Resolving the variability of CDOM fluorescence to differentiate the sources and fate of DOM in Lake Taihu and its tributaries. *Chemosphere* **2011**, *82*, 145–155.
52. Hood, E.; Gooseff, M. N.; Johnson, S. L. Changes in the character of stream water dissolved organic carbon during flushing in three small watersheds, Oregon. *J. Geophys. Res.: Biogeosci.* **2006**, *111*, G01007.
53. Yang, L. Y.; Guo, W. D.; Chen, N. W.; Hong, H. S.; Huang, J. L.; Xu, J.; Huang, S. Y. Influence of a summer storm event on the flux and composition

of dissolved organic matter in a subtropical river, China. *Appl. Geochem.* **2013**, *28*, 164–171.

54. Inamdar, S.; Singh, S.; Dutta, S.; Levia, D.; Mitchell, M.; Scott, D.; Bais, H.; McHale, P. Fluorescence characteristics and sources of dissolved organic matter for stream water during storm events in a forested mid-Atlantic watershed. *J. Geophys. Res.: Biogeosci.* **2011**, *116*, G03043.
55. Singh, S.; Inamdar, S.; Scott, D. Comparison of Two PARAFAC Models of Dissolved Organic Matter Fluorescence for a Mid-Atlantic Forested Watershed in the USA. *J. Ecosyst.* **2013**, *16*, 532424.
56. Fellman, J. B.; Hood, E.; D'Amore, D. V.; Edwards, R. T.; White, D. Seasonal changes in the chemical quality and biodegradability of dissolved organic matter exported from soils to streams in coastal temperate rainforest watersheds. *Biogeochemistry* **2009**, *95*, 277–293.
57. Nguyen, H. V. M.; Lee, M. H.; Hur, J.; Schlautman, M. A. Variations in spectroscopic characteristics and disinfection byproduct formation potentials of dissolved organic matter for two contrasting storm events. *J. Hydrol.* **2013**, *481*, 132–142.
58. Cory, R. M.; Kaplan, L. A. Biological lability of streamwater fluorescent dissolved organic matter. *Limnol. Oceanogr.* **2012**, *57*, 1347–1360.
59. Fellman, J. B.; Hood, E.; Edwards, R. T.; Jones, J. B. Uptake of Allochthonous Dissolved Organic Matter from Soil and Salmon in Coastal Temperate Rainforest Streams. *Ecosystems* **2009**, *12*, 747–759.
60. Fellman, J. B.; D'Amore, D. V.; Hood, E.; Boone, R. D. Fluorescence characteristics and biodegradability of dissolved organic matter in forest and wetland soils from coastal temperate watersheds in southeast Alaska. *Biogeochemistry* **2008**, *88*, 169–184.
61. Romera-Castillo, C.; Chen, M.; Yamashita, Y.; Jaffé, R. *Water Res.* **2014**, *55*, 40–51.
62. Maie, N.; Scully, N. M.; Pisani, O.; Jaffé, R. Composition of a protein-like fluorophore of dissolved organic matter in coastal wetland and estuarine ecosystems. *Water Res.* **2007**, *41*, 563–570.
63. Fellman, J. B.; Hood, E.; Edwards, R. T.; D'Amore, D. V. Return of salmon-derived nutrients from the riparian zone to the stream during a storm in southeastern Alaska. *Ecosystems* **2008**, *11*, 537–544.
64. Williams, C. J.; Yamashita, Y.; Wilson, H. F.; Jaffé, R.; Xenopoulos, M. A. Unraveling the role of land use and microbial activity in shaping dissolved organic matter characteristics in stream ecosystems. *Limnol. Oceanogr.* **2010**, *55*, 1159–1171.
65. Miller, M. P.; McKnight, D. M.; Cory, R. M.; Williams, M. W.; Runkel, R. L. Hyporheic exchange and fulvic acid redox reactions in an alpine stream/wetland ecosystem, Colorado front range. *Environ. Sci. Technol.* **2006**, *40*, 5943–5949.
66. Baker, A. Fluorescence excitation–emission matrix characterization of some sewage-impacted rivers. *Environ. Sci. Technol.* **2001**, *35*, 948–953.
67. Zhang, Y. L.; Zhang, E. L.; Yin, Y.; van Dijk, M. A.; Feng, L. Q.; Shi, Z. Q.; Liu, M. L.; Qin, B. Q. Characteristics and sources of chromophoric dissolved

organic matter in lakes of the Yungui Plateau, China, differing in trophic state and altitude. *Limnol. Oceanogr.* **2010**, *55*, 2645–2659.

68. Hiriart-Baer, V. P.; Binding, C.; Howell, T. E. Dissolved organic matter quantity and quality in Lake Simcoe compared to two other large lakes in southern Ontario. *Inland Waters* **2013**, *3*, 139–152.

69. Mladenov, N.; Alados-Arboledas, L.; Olmo, F. J.; Lyamani, H.; Delgado, A.; Molina, A.; Reche, I. Applications of optical spectroscopy and stable isotope analyses to organic aerosol source discrimination in an urban area. *Atmos. Environ.* **2011**, *45*, 1960–1969.

70. Mladenov, N.; Sommaruga, R.; Morales-Baquero, R.; Laurion, I.; Camarero, L.; Dieguez, M. C.; Camacho, A.; Delgado, A.; Torres, O.; Chen, Z.; Felip, M.; Reche, I. Dust inputs and bacteria influence dissolved organic matter in clear alpine lakes. *Nat. Commun.* **2011**, *2*, 405.

71. Miller, M. P.; McKnight, D. M. Comparison of seasonal changes in fluorescent dissolved organic matter among aquatic lake and stream sites in the Green Lakes Valley. *J. Geophys. Res.: Biogeosci.* **2010**, *115*, G00F12.

72. Miller, M. P.; McKnight, D. M.; Chapra, S. C. Production of microbially-derived fulvic acid from photolysis of quinone-containing extracellular products of phytoplankton. *Aquat. Sci.* **2009**, *71*, 170–178.

73. Hood, E.; McKnight, D. M.; Williams, M. W. Sources and chemical character of dissolved organic carbon across an alpine/subalpine ecotone, Green Lakes Valley, Colorado Front Range, United States. *Water Resour. Res.* **2003**, *39*, 1188.

74. Miller, M. P.; McKnight, D. M.; Chapra, S. C.; Williams, M. W. A model of degradation and production of three pools of dissolved organic matter in an alpine lake. *Limnol. Oceanogr.* **2009**, *54*, 2213–2227.

75. Laurion, I.; Mladenov, N. Dissolved organic matter photolysis in Canadian arctic thaw ponds. *Environ. Res. Lett.* **2013**, *8*, 030526.

76. Zhang, Y. L.; van Dijk, M. A.; Liu, M. L.; Zhu, G. W.; Qin, B. Q. The contribution of phytoplankton degradation to chromophoric dissolved organic matter (CDOM) in eutrophic shallow lakes: Field and experimental evidence. *Water Res.* **2009**, *43*, 4685–4697.

77. Mueller, K. K.; Fortin, C.; Campbell, P. G. C. Spatial Variation in the Optical Properties of Dissolved Organic Matter (DOM) in Lakes on the Canadian Precambrian Shield and Links to Watershed Characteristics. *Aquat. Geochem.* **2012**, *18*, 21–44.

78. Williams, C. J.; Frost, P. C.; Xenopoulos, M. A. Beyond best management practices: pelagic biogeochemical dynamics in urban stormwater ponds. *Ecol. Appl.* **2013**, *23*, 1384–1395.

79. Borisover, M.; Laor, Y.; Saadi, I.; Lado, M.; Bukhanovsky, N. Tracing Organic Footprints from Industrial Effluent Discharge in Recalcitrant Riverine Chromophoric Dissolved Organic Matter. *Water Air Soil Pollut.* **2011**, *222*, 255–269.

80. Pifer, A. D.; Miskin, D. R.; Cousins, S. L.; Fairey, J. L. Coupling asymmetric flow-field flow fractionation and fluorescence parallel factor analysis reveals stratification of dissolved organic matter in a drinking water reservoir. *J. Chromatogr. A* **2011**, *1218*, 4167–4178.

81. Beggs, K. M. H.; Summers, R. S.; McKnight, D. M. Characterizing chlorine oxidation of dissolved organic matter and disinfection by-product formation with fluorescence spectroscopy and parallel factor analysis. *J. Geophys. Res.: Biogeosci.* **2009**, *114*, G04001.
82. Austnes, K.; Evans, C. D.; Eliot-Laize, C.; Naden, P. S.; Old, G. H. Effects of storm events on mobilisation and in-stream processing of dissolved organic matter (DOM) in a Welsh peatland catchment. *Biogeochemistry* **2010**, *99*, 157–173.
83. Maie, N.; Yamashita, Y.; Cory, R. M.; Boyer, J. N.; Jaffé, R. Application of excitation emission matrix fluorescence monitoring in the assessment of spatial and seasonal drivers of dissolved organic matter composition: Sources and physical disturbance controls. *Appl. Geochem.* **2012**, *27*, 917–929.
84. Chen, M. L.; Price, R. M.; Yamashita, Y.; Jaffé, R. Comparative study of dissolved organic matter from groundwater and surface water in the Florida coastal Everglades using multi-dimensional spectrofluorometry combined with multivariate statistics. *Appl. Geochem.* **2010**, *25*, 872–880.
85. Cawley, K. M.; Wolski, P.; Mladenov, N.; Jaffé, R. Dissolved Organic Matter Biogeochemistry Along a Transect of the Okavango Delta, Botswana. *Wetlands* **2012**, *32*, 475–486.
86. Mladenov, N.; McKnight, D. M.; Macko, S. A.; Norris, M.; Cory, R. M.; Ramberg, L. Chemical characterization of DOM in channels of a seasonal wetland. *Aquat. Sci.* **2007**, *69*, 456–471.
87. Larsen, L. G.; Aiken, G. R.; Harvey, J. W.; Noe, G. B.; Crimaldi, J. P. Using fluorescence spectroscopy to trace seasonal DOM dynamics, disturbance effects, and hydrologic transport in the Florida Everglades. *J. Geophys. Res.: Biogeosci.* **2010**, *115*, G03001.
88. Mladenov, N.; Huntsman-Mapila, P.; Wolski, P.; Masarnba, W. R. L.; McKnight, D. M. Dissolved organic matter accumulation, reactivity, and redox state in ground water of a recharge wetland. *Wetlands* **2008**, *28*, 747–759.
89. Cawley, K. M.; Yamashita, Y.; Maie, N.; Jaffé, R. Using optical properties to quantify fringe mangrove inputs to the dissolved organic matter (DOM) pool in a subtropical estuary. *Estuaries Coasts* **2014**, *37*, 399–410.
90. Chari, N. V. H. K.; Sarma, N. S.; Pandi, S. R.; Murthy, K. N. Seasonal and spatial constraints of fluorophores in the midwestern Bay of Bengal by PARAFAC analysis of excitation emission matrix spectra. *Estuarine, Coastal Shelf Sci.* **2012**, *100*, 162–171.
91. Yamashita, Y.; Jaffé, R.; Maie, N.; Tanoue, E. Assessing the dynamics of dissolved organic matter (DOM) in coastal environments by excitation emission matrix fluorescence and parallel factor analysis (EEM-PARAFAC). *Limnol. Oceanogr.* **2008**, *53*, 1900–1908.
92. Yamashita, Y.; Boyer, J. N.; Jaffé, R. Evaluating the distribution of terrestrial dissolved organic matter in a complex coastal ecosystem using fluorescence spectroscopy. *Cont. Shelf Res.* **2013**, *66*, 136–144.
93. Kowalcuk, P.; Durako, M. J.; Young, H.; Kahn, A. E.; Cooper, W. J.; Gonsior, M. Characterization of dissolved organic matter fluorescence in the

South Atlantic Bight with use of PARAFAC model: Interannual variability. *Mar. Chem.* **2009**, *113*, 182–196.

94. Kowalcuk, P.; Cooper, W. J.; Durako, M. J.; Kahn, A. E.; Gonsior, M.; Young, H. Characterization of dissolved organic matter fluorescence in the South Atlantic Bight with use of PARAFAC model: Relationships between fluorescence and its components, absorption coefficients and organic carbon concentrations. *Mar. Chem.* **2010**, *118*, 22–36.

95. Wada, S.; Hama, T. The contribution of macroalgae to the coastal dissolved organic matter pool. *Estuarine, Coastal Shelf Sci.* **2013**, *129*, 77–85.

96. Cawley, K. M.; Ding, Y.; Fourqurean, J.; Jaffé, R. Characterising the sources and fate of dissolved organic matter in Shark Bay, Australia: a preliminary study using optical properties and stable carbon isotopes. *Mar. Freshwater Res.* **2012**, *63*, 1098–1107.

97. Chen, H.; Zheng, B. H. Sources of fluorescent dissolved organic matter in high salinity seawater (Bohai Bay, China). *Environ. Sci. Pollut. Res.* **2013**, *20*, 1762–1771.

98. Mendoza, W. G.; Zika, R. G. On the temporal variation of DOM fluorescence on the southwest Florida continental shelf. *Progr. Oceanogr.* **2014**, *120*, 189–204.

99. Catala, T. S.; Mladenov, N.; Echevarria, F.; Reche, I. Positive trends between salinity and chromophoric and fluorescent dissolved organic matter in a seasonally inverse estuary. *Estuarine, Coastal Shelf Sci.* **2013**, *133*, 206–216.

100. Huguet, A.; Vacher, L.; Relexans, S.; Saubusse, S.; Froidefond, J. M.; Parlanti, E. Properties of fluorescent dissolved organic matter in the Gironde Estuary. *Org. Geochem.* **2009**, *40*, 706–719.

101. Singh, S.; D'Sa, E. J.; Swenson, E. M. Chromophoric dissolved organic matter (CDOM) variability in Barataria Basin using excitation-emission matrix (EEM) fluorescence and parallel factor analysis (PARAFAC). *Sci. Total Environ.* **2010**, *408*, 3211–3222.

102. Fellman, J. B.; Spencer, R. G. M.; Hernes, P. J.; Edwards, R. T.; D'Amore, D. V.; Hood, E. The impact of glacier runoff on the biodegradability and biochemical composition of terrigenous dissolved organic matter in near-shore marine ecosystems. *Mar. Chem.* **2010**, *121*, 112–122.

103. Mendoza, W. G.; Kang, Y.; Zika, R. G. Resolving DOM fluorescence fractions during a *Karenia brevis* bloom patch on the Southwest Florida Shelf. *Cont. Shelf Res.* **2012**, *32*, 121–129.

104. Luciani, X.; Mounier, S.; Paraquetti, H. H. M.; Redon, R.; Lucas, Y.; Bois, A.; Lacerda, L. D.; Raynaud, A.; Ripert, A. Tracing of dissolved organic matter from the SEPETIBA Bay (Brazil) by PARAFAC analysis of total luminescence matrices. *Mar. Environ. Res.* **2008**, *65*, 148–157.

105. Guo, W. D.; Yang, L. Y.; Hong, H. S.; Stedmon, C. A.; Wang, F. L.; Xu, J.; Xie, Y. Y. Assessing the dynamics of chromophoric dissolved organic matter in a subtropical estuary using parallel factor analysis. *Mar. Chem.* **2011**, *124*, 125–133.

106. Boyd, T. J.; Barham, B. P.; Hall, G. J.; Osburn, C. L. Variation in ultrafiltered and LMW organic matter fluorescence properties under simulated estuarine

mixing transects: 1. Mixing alone. *J. Geophys. Res.: Biogeosci.* **2010**, *115*, G00F13.

107. McIntyre, A. M.; Gueguen, C. Binding interactions of algal-derived dissolved organic matter with metal ions. *Chemosphere* **2013**, *90*, 620–626.
108. Moran, M. A.; Sheldon, W. M.; Zepp, R. G. Carbon loss and optical property changes during long-term photochemical and biological degradation of estuarine dissolved organic matter. *Limnol. Oceanogr.* **2000**, *45*, 1254–1264.
109. Blough, N. V.; Del Vecchio, R. In *Biogeochemistry of Marine Dissolved Organic Matter*; Hansell, D. A., Carlson, C. A., Eds.; Academic Press: San Diego, CA, 2002; pp 509–446.
110. Boyd, T. J.; Barham, B. P.; Hall, G. J.; Schumann, B. S.; Paerl, R. W.; Osburn, C. L. Variation in ultrafiltered and LMW organic matter fluorescence properties under simulated estuarine mixing transects: 2. Mixing with photoexposure. *J. Geophys. Res.: Biogeosci.* **2010**, *115*, G00F14.
111. Stedmon, C. A.; Markager, S.; Tranvik, L.; Kronberg, L.; Slatis, T.; Martinsen, W. Photochemical production of ammonium and transformation of dissolved organic matter in the Baltic Sea. *Mar. Chem.* **2007**, *104*, 227–240.
112. Shank, G. C.; Evans, A.; Yamashita, Y.; Jaffé, R. Solar radiation-enhanced dissolution of particulate organic matter from coastal marine sediments. *Limnol. Oceanogr.* **2011**, *56*, 577–588.
113. Pisani, O.; Yamashita, Y.; Jaffé, R. Photo-dissolution of flocculent, detrital material in aquatic environments: Contributions to the dissolved organic matter pool. *Water Res.* **2011**, *45*, 3836–3844.
114. Zhang, Y. L.; Liu, X. H.; Wang, M. Z.; Qin, B. Q. Compositional differences of chromophoric dissolved organic matter derived from phytoplankton and macrophytes. *Org. Geochem.* **2013**, *55*, 26–37.
115. Maie, N.; Sekiguchi, S.; Watanabe, A.; Tsutsuki, K.; Yamashita, Y.; Melling, L.; Cawley, K.; Shima, E.; Jaffé, R. Dissolved organic matter dynamics in the oligo/meso-haline zone of wetland-influenced coastal rivers. *J. Sea Res.* **2014** DOI:10.1016/j.seares.2014.02.016.
116. Santin, C.; Yamashita, Y.; Otero, X. L.; Alvarez, M. A.; Jaffé, R. Characterizing humic substances from estuarine soils and sediments by excitation-emission matrix spectroscopy and parallel factor analysis. *Biogeochemistry* **2009**, *96*, 131–147.
117. Osburn, C. L.; Handsel, L. T.; Mikan, M. P.; Paerl, H. W.; Montgomery, M. T. Fluorescence Tracking of Dissolved and Particulate Organic Matter Quality in a River-Dominated Estuary. *Environ. Sci. Technol.* **2012**, *46*, 8628–8636.
118. Cawley, K. M.; Butler, K. D.; Aiken, G. R.; Larsen, L. G.; Huntington, T. G.; McKnight, D. M. Identifying fluorescent pulp mill effluent in the Gulf of Maine and its watershed. *Mar. Pollut. Bull.* **2012**, *64*, 1678–1687.
119. Bergamaschi, B. A.; Krabbenhoft, D. P.; Aiken, G. R.; Patino, E.; Rumbold, D. G.; Orem, W. H. Tidally Driven Export of Dissolved Organic Carbon, Total Mercury, and Methylmercury from a Mangrove-Dominated Estuary. *Environ. Sci. Technol.* **2012**, *46*, 1371–1378.

120. Hood, E.; Fellman, J.; Spencer, R. G. M.; Hernes, P. J.; Edwards, R.; D'Amore, D.; Scott, D. Glaciers as a source of ancient and labile organic matter to the marine environment. *Nature* **2009**, *462*, 1044–1047.
121. Osburn, C. L.; Stedmon, C. A. Linking the chemical and optical properties of dissolved organic matter in the Baltic-North Sea transition zone to differentiate three allochthonous inputs. *Mar. Chem.* **2011**, *126*, 281–294.
122. Bauer, J. E. In *Biogeochemistry of Marine Dissolved Organic Matter*; Hansell, D. A., Carlson, C. A., Eds.; Academic Press: San Diego, CA, 2002; pp 59–90.
123. Ogawa, H.; Tanoue, E. Dissolved organic matter in oceanic waters. *J. Oceanogr.* **2003**, *59*, 129–147.
124. Benner, R. In *Biogeochemistry of Marine Dissolved Organic Matter*; Hansell, D. A., Carlson, C. A., Eds.; Academic Press: San Diego, CA, 2002; pp 405–453.
125. Opsahl, S.; Benner, R. Distribution and cycling of terrigenous dissolved organic matter in the ocean. *Nature* **1997**, *386*, 480–482.
126. Hedges, J. I.; Eglinton, G.; Hatcher, P. G.; Kirchman, D. L.; Arnosti, C.; Derenne, S.; Evershed, R. P.; Kogel-Knabner, I.; de Leeuw, J. W.; Littke, R.; Michaelis, W.; Rullkötter, J. The molecularly-uncharacterized component of nonliving organic matter in natural environments. *Org. Geochem.* **2000**, *31*, 945–958.
127. Tanoue, E.; Nishiyama, S.; Kamo, M.; Tsugita, A. Bacterial-Membranes - Possible Source of a Major Dissolved Protein in Seawater. *Geochim. Cosmochim. Acta* **1995**, *59*, 2643–2648.
128. McCarthy, M. D.; Hedges, J. I.; Benner, R. Major bacterial contribution to marine dissolved organic nitrogen. *Science* **1998**, *281*, 231–234.
129. Yamada, N.; Tanoue, E. The inventory and chemical characterization of dissolved proteins in oceanic waters. *Progr. Oceanogr.* **2006**, *69*, 1–18.
130. Ogawa, H.; Amagai, Y.; Koike, I.; Kaiser, K.; Benner, R. Production of refractory dissolved organic matter by bacteria. *Science* **2001**, *292*, 917–920.
131. Jiao, N.; Herndl, G. J.; Hansell, D. A.; Benner, R.; Kattner, G.; Wilhelm, S. W.; Kirchman, D. L.; Weinbauer, M. G.; Luo, T. W.; Chen, F.; Azam, F. Microbial production of recalcitrant dissolved organic matter: long-term carbon storage in the global ocean. *Nat. Rev. Microbiol.* **2010**, *8*, 593–599.
132. Hayase, K.; Tsubota, H.; Sunada, I.; Goda, S.; Yamazaki, H. Vertical-Distribution of Fluorescent Organic-Matter in the North Pacific. *Mar. Chem.* **1988**, *25*, 373–381.
133. Chen, R. F.; Bada, J. L. The Fluorescence of Dissolved Organic-Matter in Seawater. *Mar. Chem.* **1992**, *37*, 191–221.
134. Mopper, K.; Schultz, C. A. Fluorescence as a Possible Tool for Studying the Nature and Water Column Distribution of Doc Components. *Mar. Chem.* **1993**, *41*, 229–238.
135. Yamashita, Y.; Tanoue, E. Production of bio-refractory fluorescent dissolved organic matter in the ocean interior. *Nat. Geosci.* **2008**, *1*, 579–582.
136. Yamashita, Y.; Tanoue, E. Chemical characterization of protein-like fluorophores in DOM in relation to aromatic amino acids. *Mar. Chem.* **2003**, *82*, 255–271.

137. Yamashita, Y.; Tanoue, E. Chemical characteristics of amino acid-containing dissolved organic matter in seawater. *Org. Geochem.* **2004**, *35*, 679–692.
138. Davis, J.; Benner, R. Quantitative estimates of labile and semi-labile dissolved organic carbon in the western Arctic Ocean: A molecular approach. *Limnol. Oceanogr.* **2007**, *52*, 2434–2444.
139. Gueguen, C.; Granskog, M. A.; McCullough, G.; Barber, D. G. Characterisation of colored dissolved organic matter in Hudson Bay and Hudson Strait using parallel factor analysis. *J. Marine Syst.* **2011**, *88*, 423–433.
140. Para, J.; Charriere, B.; Matsuoka, A.; Miller, W. L.; Rontani, J. F.; Sempere, R. UV/PAR radiation and DOM properties in surface coastal waters of the Canadian shelf of the Beaufort Sea during summer 2009. *Biogeosciences* **2013**, *10*, 2761–2774.
141. Gueguen, C.; McLaughlin, F. A.; Carmack, E. C.; Itoh, M.; Narita, H.; Nishino, S. The nature of colored dissolved organic matter in the southern Canada Basin and East Siberian Sea. *Deep-Sea Res. Pt. II* **2012**, *81-84*, 102–113.
142. Dainard, P. G.; Gueguen, C. Distribution of PARAFAC modeled CDOM components in the North Pacific Ocean, Bering, Chukchi and Beaufort Seas. *Mar. Chem.* **2013**, *157*, 216–223.
143. Walker, S. A.; Amon, R. M. W.; Stedmon, C.; Duan, S. W.; Loucheuarn, P. The use of PARAFAC modeling to trace terrestrial dissolved organic matter and fingerprint water masses in coastal Canadian Arctic surface waters. *J. Geophys. Res.: Biogeosci.* **2009**, *114*, G00F06.
144. Nakatsuka, T.; Toda, M.; Kawamura, K.; Wakatsuchi, M. Dissolved and particulate organic carbon in the Sea of Okhotsk: Transport from continental shelf to ocean interior. *J. Geophys. Res.: Oceans* **2004**, *109*, C09S14.
145. Hernes, P. J.; Benner, R. Transport and diagenesis of dissolved and particulate terrigenous organic matter in the North Pacific Ocean. *Deep Sea Res., Part I* **2002**, *49*, 2119–2132.
146. Jorgensen, L.; Stedmon, C. A.; Kragh, T.; Markager, S.; Middelboe, M.; Sondergaard, M. Global trends in the fluorescence characteristics and distribution of marine dissolved organic matter. *Mar. Chem.* **2011**, *126*, 139–148.
147. Hernes, P. J.; Benner, R. Terrigenous organic matter sources and reactivity in the North Atlantic Ocean and a comparison to the Arctic and Pacific oceans. *Mar. Chem.* **2006**, *100*, 66–79.
148. Murphy, K. R.; Stedmon, C. A.; Waite, T. D.; Ruiz, G. M. Distinguishing between terrestrial and autochthonous organic matter sources in marine environments using fluorescence spectroscopy. *Mar. Chem.* **2008**, *108*, 40–58.
149. Yamashita, Y.; Cory, R. M.; Nishioka, J.; Kuma, K.; Tanoue, E.; Jaffé, R. Fluorescence characteristics of dissolved organic matter in the deep waters of the Okhotsk Sea and the northwestern North Pacific Ocean. *Deep Sea Res., Part II* **2010**, *57*, 1478–1485.
150. Murphy, K. R.; Boehme, J. R.; Brown, C.; Noble, M.; Smith, G.; Sparks, D.; Ruiz, G. M. Exploring the limits of dissolved organic matter fluorescence for

determining seawater sources and ballast water exchange on the U.S. Pacific coast. *J. Mar. Syst.* **2013**, *111*, 157–166.

151. Murphy, K. R.; Ruiz, G. M.; Dunsmuir, W. T. M.; Waite, T. D. Optimized parameters for fluorescence-based verification of ballast water exchange by ships. *Environ. Sci. Technol.* **2006**, *40*, 2357–2362.
152. Zhou, Z. Z.; Guo, L. D. Evolution of the optical properties of seawater influenced by the Deepwater Horizon oil spill in the Gulf of Mexico. *Environ. Res. Lett.* **2012**, *7*, 025301.
153. Mendoza, W. G.; Riemer, D. D.; Zika, R. G. Application of fluorescence and PARAFAC to assess vertical distribution of subsurface hydrocarbons and dispersant during the Deepwater Horizon oil spill. *Environ. Sci.: Processes Impacts* **2013**, *15*, 1017–1030.
154. Zhou, Z. Z.; Guo, L. D.; Shiller, A. M.; Lohrenz, S. E.; Asper, V. L.; Osburn, C. L. Characterization of oil components from the Deepwater Horizon oil spill in the Gulf of Mexico using fluorescence EEM and PARAFAC techniques. *Mar. Chem.* **2013**, *148*, 10–21.
155. Wedborg, M.; Persson, T.; Larsson, T. On the distribution of UV-blue fluorescent organic matter in the Southern Ocean. *Deep Sea Res., Part I* **2007**, *54*, 1957–1971.
156. Heller, M. I.; Gaiero, D. M.; Croot, P. L. Basin scale survey of marine humic fluorescence in the Atlantic: Relationship to iron solubility and H_2O_2 . *Global Biogeochem. Cycles* **2013**, *27*, 88–100.
157. Kowaleczuk, P.; Tilstone, G. H.; Zablocka, M.; Rottgers, R.; Thomas, R. Composition of dissolved organic matter along an Atlantic Meridional Transect from fluorescence spectroscopy and Parallel Factor Analysis. *Mar. Chem.* **2013**, *157*, 170–184.
158. Omori, Y.; Hama, T.; Ishii, M.; Saito, S. Vertical change in the composition of marine humic-like fluorescent dissolved organic matter in the subtropical western North Pacific and its relation to photoreactivity. *Mar. Chem.* **2011**, *124*, 38–47.
159. Coble, P. G.; Del Castillo, C. E.; Avril, B. Distribution and optical properties of CDOM in the Arabian Sea during the 1995 Southwest Monsoon. *Deep Sea Res., Part II* **1998**, *45*, 2195–2223.
160. Yamashita, Y.; Tsukasaki, A.; Nishida, T.; Tanoue, E. Vertical and horizontal distribution of fluorescent dissolved organic matter in the Southern Ocean. *Mar. Chem.* **2007**, *106*, 498–509.
161. Rochelle-Newall, E. J.; Fisher, T. R. Chromophoric dissolved organic matter and dissolved organic carbon in Chesapeake Bay. *Mar. Chem.* **2002**, *77*, 23–41.
162. Yamashita, Y.; Tanoue, E. In situ production of chromophoric dissolved organic matter in coastal environments. *Geophys. Res. Lett.* **2004**, *31*, L14302.
163. Romera-Castillo, C.; Sarmento, H.; Alvarez-Salgado, X. A.; Gasol, J. M.; Marrase, C. Net Production and Consumption of Fluorescent Colored Dissolved Organic Matter by Natural Bacterial Assemblages Growing on Marine Phytoplankton Exudates. *Appl. Environ. Microb.* **2011**, *77*, 7490–7498.

164. Shimotori, K.; Watanabe, K.; Hama, T. Fluorescence characteristics of humic-like fluorescent dissolved organic matter produced by various taxa of marine bacteria. *Aquat. Microb. Ecol.* **2011**, *65*, 249–260.
165. Romera-Castillo, C.; Sarmento, H.; Alvarez-Salgado, X. A.; Gasol, J. M.; Marrase, C. Production of chromophoric dissolved organic matter by marine phytoplankton. *Limnol. Oceanogr.* **2010**, *55*, 446–454.
166. Tani, H.; Nishioka, J.; Kuma, K.; Takata, H.; Yamashita, Y.; Tanoue, E.; Midorikawa, T. Iron(III) hydroxide solubility and humic-type fluorescent organic matter in the deep water column of the Okhotsk Sea and the northwestern North Pacific Ocean. *Deep Sea Res., Part I* **2003**, *50*, 1063–1078.
167. Hansell, D. A.; Carlson, C. A.; Repeta, D. J.; Schlitzer, R. Dissolved Organic Matter in the Ocean a Controversy Stimulates New Insights. *Oceanography* **2009**, *22*, 202–211.
168. Muller, S.; Vahatalo, A. V.; Stedmon, C. A.; Granskog, M. A.; Norman, L.; Aslam, S. N.; Underwood, G. J. C.; Dieckmann, G. S.; Thomas, D. N. Selective incorporation of dissolved organic matter (DOM) during sea ice formation. *Mar. Chem.* **2013**, *155*, 148–157.
169. Stedmon, C. A.; Thomas, D. N.; Granskog, M.; Kaartokallio, H.; Papadimitriou, S.; Kuosa, H. Characteristics of dissolved organic matter in Baltic coastal sea ice: Allochthonous or autochthonous origins? *Environ. Sci. Technol.* **2007**, *41*, 7273–7279.
170. Stedmon, C. A.; Thomas, D. N.; Papadimitriou, S.; Granskog, M. A.; Dieckmann, G. S. Using fluorescence to characterize dissolved organic matter in Antarctic sea ice brines. *J. Geophys. Res.: Biogeosci.* **2011**, *116*, G03027.
171. Korak, J. A.; Dotson, A. D.; Summers, R. S.; Rosario-Ortiz, F. L. Critical analysis of commonly used fluorescence metrics to characterize dissolved organic matter. *Water. Res.* **2014**, *49*, 327–338.
172. Murphy, K. R.; Stedmon, C. A.; Wenig, P.; Bro, R. OpenFluor- an online spectral library of auto-fluorescence by organic compounds in the environment. *Anal. Methods* **2014**, *6*, 658–661.
173. Murphy, K. R.; Hambly, A.; Singh, S.; Henderson, R. K.; Baker, A.; Stuetz, R.; Khan, S. J. Organic Matter Fluorescence in Municipal Water Recycling Schemes: Toward a Unified PARAFAC Model. *Environ. Sci. Technol.* **2011**, *45*, 2909–2916.
174. Fellman, J. B.; Miller, M. P.; Cory, R. M.; D'Amore, D. V.; White, D. Characterizing Dissolved Organic Matter Using PARAFAC Modeling of Fluorescence Spectroscopy: A Comparison of Two Models. *Environ. Sci. Technol.* **2009**, *43*, 6228–6234.
175. Cory, R. M.; Miller, M. P.; McKnight, D. M.; Guerard, J. J.; Miller, P. L. Effect of instrument-specific response on the analysis of fulvic acid fluorescence spectra. *Limnol. Oceanogr.: Methods* **2010**, *8*, 67–78.

Chapter 4

Acidic Functional Groups of Suwannee River Natural Organic Matter, Humic Acids, and Fulvic Acids

Shamus J. Driver and E. Michael Perdue*

Department of Chemistry, Ball State University, Muncie, Indiana 47306

*E-mail: emperdue@bsu.edu.

Two samples each of natural organic matter, humic acids, and fulvic acids from the Suwannee River in southeastern Georgia were titrated with NaOH on a Mettler-Toledo autotitrator. An average of 1500 data points was collected for each titration. Charge densities were corrected for the concentrations of inorganic anions and cations in the original samples. The pH 8 and 10 method, the modified Henderson-Hasselbalch model, and the Gaussian distribution model were fit to the titration data, and fitting parameters were compared with fitting parameters from earlier manual titrations of the same samples. With the exception of the carboxyl contents of two samples, both the carboxyl and phenolic contents from the pH 8 and 10 method were noticeably higher in the 2003 paper. Similar results were obtained for fitting parameters of the modified Henderson-Hasselbalch model, where, with the exception of two samples, both carboxyl contents and $\log K_1$ values are lower in the current study.

Introduction

Since 1981, the International Humic Substances Society (IHSS) has provided samples of humic acids, fulvic acids, and natural organic matter (NOM) from locations all over the world. Among their collections are humic acids, fulvic acids, and NOM from the Suwannee River in southeastern Georgia, United States. Although these samples have been available since 1983, the first comprehensive analysis of the acid-base chemistry of these samples did not occur until 2003

(1). In this 2003 study, four Suwannee River standard and reference materials were analyzed, including two fulvic acids (1S101F and 1R101F), one humic acid (1S101H), and one NOM (1R101N). Since that time, one fulvic acid (2S101F), one humic acid (2S101H), and one NOM (2R101N) from the Suwannee River have been added to the IHSS collection.

The 2003 analysis relied on acid-base titrations in which approximately 0.1M NaOH was added manually to samples using a micropipette. Titrations were conducted on 10 mL aliquots of solutions containing 360 mg L⁻¹ of humic acids, fulvic acids, or NOM. Each titration was titrated over 30 minutes, producing no more than 120 data points. The samples were titrated in a background electrolyte of 0.1M NaCl to stabilize the ionic strength of the solution. When calculating the charge of the organic anions ($\Sigma[\text{Orgi}^-]$) in the solution, the only cations considered were H⁺ and the Na⁺ from the added titrant. The only anions considered were OH⁻ and Cl⁻. The concentrations of carboxyl groups and phenolic hydroxyl groups were derived from the data using the pH 8 and 10 method (2) and the modified Henderson-Hasselbalch model (3).

The focus of this research was to replicate the 2003 titrations of Suwannee River NOM, humic acids, and fulvic acids using an autotitrator capable of recording thousands of data points per titration. The three new Suwannee River samples were titrated alongside the older samples to complement the existing data for this set of important standard and reference samples.

The pH 8 and 10 model was used to derive concentrations of acidic functional groups from the data, and the modified Henderson-Hasselbalch model was used to fully model the pH dependence of organic charge density in each titration curve. The Gaussian distribution model (4) was also used to fit titration data and provide an additional point of comparison between the different models for the data. The Gaussian distribution model was developed in 1983, but has been used as recently as 2013 to study the acid-base chemistry of NOM samples from Barataria Bay, Louisiana, U.S.A. after the Deepwater Horizon MC252 oil spill (5).

All three of these models use the variation of $\Sigma[\text{Orgi}^-]$ with pH to calculate the concentrations of acidic functional groups and other relevant properties of those functional groups. The $\Sigma[\text{Orgi}^-]$ is calculated from the electroneutrality equation, given the concentrations of all other cations and anions in the solution. In the current research, a comprehensive effort has been made to quantify the contributions of all major inorganic cations and anions to the electroneutrality equation, thus enabling a more accurate estimate of the pH dependence of $\Sigma[\text{Orgi}^-]$ for each sample. The increased density of data from the autotitrator and the more complete accounting for major cations and anions should lead to a more accurate determination of acidic functional groups in these Suwannee River samples.

Experimental

Samples of IHSS reference NOM, standard humic acids, and standard fulvic acids were dissolved into 0.1M NaCl at a concentration of approximately 375 mg L⁻¹. A 40 mL aliquot of the sample was titrated to an endpoint of pH 10.5 with a Mettler Toledo G20 Compact Auto titrator. A Mettler Toledo DG115-SC pH

electrode was used to monitor pH during the potentiometric titration. The titrant was approximately 0.1M NaOH, standardized with dried potassium hydrogen phthalate. Titrations were carried out at a rate of 40 $\mu\text{L min}^{-1}$ with constant stirring. Each titration lasted 25-35 minutes. Titration data (volume of added titrant, pH, etc.) were recorded using LabX titration software version 3.1. All titrations were carried out under flowing, humidified nitrogen gas using a Haake G temperature bath to maintain the temperature of the sample at $25\pm0.2^\circ\text{C}$. All titrations were performed in triplicate.

The IHSS codes of the samples that were titrated were 1R101N, 2R101N, 1S101F, 1S101H, 2S101H, and 2S101F. All samples were collected from the Suwannee River in southeastern Georgia. 1R101N and 2R101N are samples of NOM that were isolated from the Suwannee River via reverse osmosis (6) in 1999 and 2012, respectively (7). The humic acid and fulvic acid samples (1S101F, 1S101H, 2S101H, and 2S101F) were isolated using the XAD-8 method (8). The 1S101F and 1S101H samples were collected in 1982, and the 2S101F and 2S101H samples were collected in 2003.

The concentrations of major cations (Na^+ , Ca^{2+} , Mg^{2+} , K^+ , and NH_4^+) and anions (SO_4^{2-} and Cl^-) were determined for each sample. Concentrations of cations and anions were measured on a Dionex ICS-5000 using a CS-19 IonPac Dionex column and an AS-15 Dionox IonPac column, respectively. Total nitrogen and non-purgeable organic carbon were measured using a Shimadzu TOC-L carbon analyzer that is equipped with a Shimadzu TNM-L nitrogen accessory. The concentration of silicic acid in each sample was determined using the heteropoly blue colorimetric method for the determination of silica in water. The organic charge (in eq L^{-1}) at any point in the titration was calculated using Equation 1.

$$\Sigma[\text{Orgi}^-] = [\text{H}^+] + [\text{Na}^+] + 2[\text{Ca}^{2+}] + 2[\text{Mg}^{2+}] + [\text{K}^+] + [\text{NH}_4^+] - [\text{OH}^-] - [\text{Cl}^-] - 2[\text{SO}_4^{2-}]$$

Equation 1

Ionic strength was calculated at each step of the titration using Equation 2. The hydrogen ion concentration was calculated using the Davies equation to calculate the activity coefficient. Because ionic strength depends on $\Sigma[\text{Orgi}^-]$, Equations 1 and 2 must be solved iteratively. The task is simplified by the presence of a high concentration of NaCl as a swamping background electrolyte that dominates ionic strength.

$$I = \frac{1}{2}(\Sigma[\text{Orgi}^-] + [\text{H}^+] + [\text{OH}^-] + [\text{Na}^+] + 4[\text{Ca}^{2+}] + 4[\text{Mg}^{2+}] + [\text{K}^+] + [\text{NH}_4^+] + [\text{Cl}^-] + 4[\text{SO}_4^{2-}])$$

Equation 2

The organic charge calculated in Equation 1 was divided by the concentration of organic carbon (DOC) in the solution to correct for dilution and give the experimental organic charge density (Q_{exp}) in units of meq gC^{-1} . This is shown in Equation 3.

$$Q_{exp} = 1000 \left(\frac{\sum [org_i^-]}{DOC} \right) \quad \text{Equation 3}$$

Three different methods were used to assign concentrations of carboxylic acid functional groups and phenolic groups for the samples. The simplest method used is the pH 8 and 10 method (9). In this method, it is assumed that all the carboxylic acids and no phenolic groups are titrated by pH 8. The carboxyl content is thus estimated to be equal to Q_{exp} at pH 8 (10). From pH 8 to pH 10, it is assumed that half of the phenolic groups have been titrated (2). The phenolic content is thus estimated to be double the difference in Q_{exp} between pH 8 and pH 10 (11).

The second method used to estimate the concentrations of acidic functional groups in the samples was the modified Henderson-Hasselbalch model. This model describes proton binding by two different types of proton binding sites using Equation 4 (3).

$$Q_{tot} = \left(\frac{Q_1}{1 + (K_1[H^+])^{1/n_1}} \right) + \left(\frac{Q_2}{1 + (K_2[H^+])^{1/n_2}} \right) \quad \text{Equation 4}$$

One of the two different types of binding sites is assumed to be carboxylic acid groups, with a concentration of Q_1 meq gC⁻¹, an average equilibrium constant of K_1 for proton binding, and width parameter (n_1) that increases with increased range of K values within the class of carboxyl groups. The second type of proton binding sites is assumed to be phenolic groups with a concentration of Q_2 meq gC⁻¹, an average equilibrium constant of K_2 for proton binding, and a width parameter (n_2). The Fletcher-Powell minimization algorithm was used to optimize the model fitting parameters and minimize the sum of squares of residuals (12).

The third method used to assign concentrations of carboxylic and phenolic groups for the sample is the Gaussian distribution model (13). In this model, the variation of Q_{exp} with pH is attributed to two Gaussian distributions of acidic functional groups. Each of these distributions can be described independently by a charge density (Q, meq gC⁻¹), an average log K for proton binding (μ), and a standard deviation of log K values within the distribution of proton binding sites (σ). The overall charge density (Q_{tot}) is described mathematically in Equation 5. The same minimization algorithm was used to fit the data.

$$Q_{tot} = \left(\frac{Q_1}{\sigma_1 \sqrt{2\pi}} \int_{-\infty}^{\infty} \left(\frac{1}{1 + K_1[H^+]} \right) e^{-\frac{(\mu - \mu K_1)^2}{\sigma_1^2}} d\log K_1 \right) + \left(\frac{Q_2}{\sigma_2 \sqrt{2\pi}} \int_{-\infty}^{\infty} \left(\frac{1}{1 + K_2[H^+]} \right) e^{-\frac{(\mu - \mu K_2)^2}{\sigma_2^2}} d\log K_2 \right) \quad \text{Equation 5}$$

When using these three means of estimating carboxyl content, the pH 8 and 10 method gives the lowest estimate, the modified Henderson-Hasselbalch model gives the highest estimate, and the Gaussian distribution model generally gives intermediate values (5).

Results

Titrations and Inorganic Contributions

All samples yielded titration curves with the characteristics of Figure 1. As seen in Figure 1, the titration curve slowly increases in pH until pH 6, where a steeper increase in pH is observed. The inflection point of the curve is around pH 7. The experimental data were converted using Equations 1, 2, and 3 and plotted as Q_{exp} versus pH. Figure 2 shows this plot for a titration of Suwannee River NOM (2R101N).

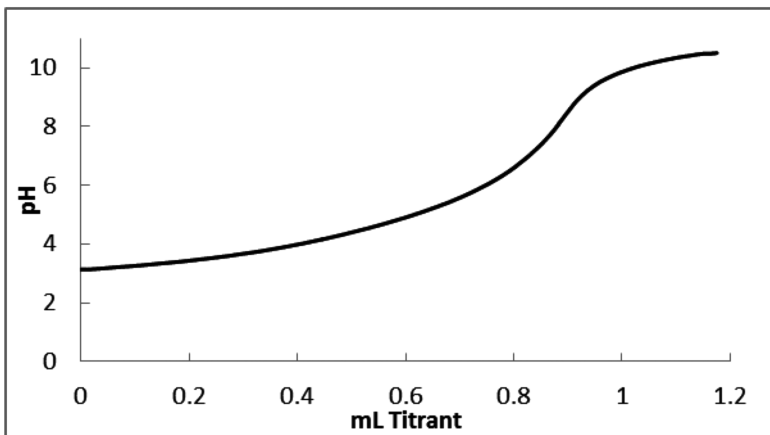


Figure 1. Titration of 2R101N.

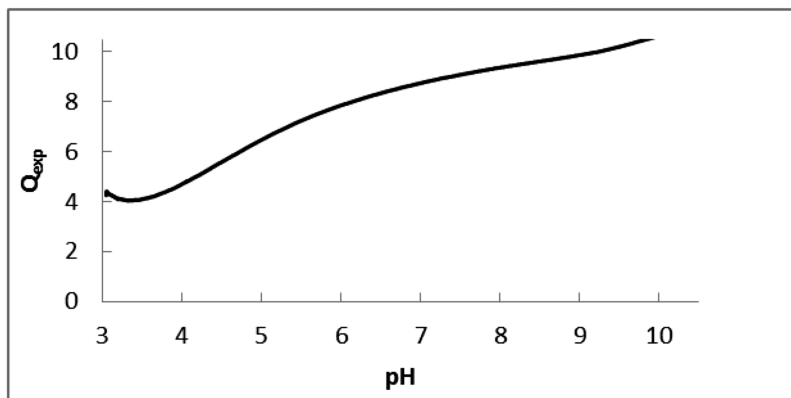


Figure 2. Titration on 2R101N in Q_{exp} v pH.

As planned, this study included a comprehensive accounting of the contributions to the electroneutrality equation of major cations and anions that were present as contaminants in the initial freeze-dried samples. Generally, Q_{exp} decreased by 0.2-1.4 meq gC⁻¹ when titration curves were corrected for background cations and anions, indicating that the initial samples typically contained more strong acid anions than strong base cations. The shift in the charge density curve was a vertical offset, so the shapes of titration curves were unaffected by the presence of background cations and anions in the initial sample. This offset was especially high in 2R101N, which has an unusually high concentration of sulfate.

In Figure 2, the organic charge density of the NOM increases throughout the pH range of the titration. The three different models discussed above were fit to data for the three replicate titrations of each sample. Model-derived parameters are reported as average values and standard deviations for each sample. The Gaussian distribution model returned unrealistically high values for both Q_2 and μ_2 for several titrations. In such instances, μ_2 was constrained to be 10 (an average log K for proton binding by phenolic groups). With this constraint, there was good general agreement between the Gaussian model and the Modified Henderson-Hasselbalch model in these cases. Table 1 contains the averages for data given by the pH 8 and 10 method.

Table 1. Carboxyl Content (Q_{exp} at pH 8) and Phenolic Content (2 Times the Change in Q_{exp} between pH 8 and pH 10)

<i>Sample</i>	<i>Carboxyl Content</i>	<i>Phenolic Content</i>
1R101N	9.07 ± 0.11	2.99 ± 0.11
2R101N	10.39 ± 0.94	2.86 ± 0.60
1S101H	7.98 ± 0.05	3.79 ± 0.01
2S101H	9.61 ± 0.32	3.48 ± 0.79
1S101F	10.40 ± 0.08	2.47 ± 0.10
2S101F	11.35 ± 0.10	2.32 ± 0.04

Model Fitting Parameters

Table 2 shows the averages and standard deviations for the six model fitting parameters of the Gaussian distribution model and the modified Henderson-Hasselbalch model for three titrations of the six samples. The data sets highlighted in grey are those for which μ_2 was constrained to a value of 10 for the phenolic groups.

Table 2. Results for the Gaussian Distribution Model (See Text for Explanation of Model)

<i>Sample</i>	<i>Carboxyl Groups</i>						<i>Phenolic Groups</i>					
	<i>Q₁</i>	<i>μ₁</i>	<i>σ₁</i>	<i>Q₂</i>	<i>μ₂</i>	<i>σ₂</i>	<i>Q₁</i>	<i>μ₁</i>	<i>σ₁</i>	<i>Q₂</i>	<i>μ₂</i>	<i>σ₂</i>
1R101N	9.51 ± 0.08	4.03 ± 0.08	2.39 ± 0.10	2.26 ± 0.03	10.00 ± 0.00	0.61 ± 0.17						
2R101N	10.70 ± 0.90	4.02 ± 0.18	2.10 ± 0.21	2.23 ± 1.09	9.94 ± 0.13	0.60 ± 0.18						
1S101H	7.94 ± 0.12	4.84 ± 0.01	1.58 ± 0.05	3.35 ± 0.14	9.75 ± 0.02	1.05 ± 0.07						
2S101H	10.01 ± 0.03	4.32 ± 0.06	2.30 ± 0.02	2.11 ± 0.19	10.00 ± 0.00	0.51 ± 0.13						
1S101F	10.84 ± 0.10	3.99 ± 0.06	2.18 ± 0.05	1.57 ± 0.34	9.91 ± 0.17	0.29 ± 0.21						
2S101F	11.87 ± 0.15	3.98 ± 0.04	2.23 ± 0.05	1.16 ± 0.03	9.82 ± 0.03	0.22 ± 0.06						

Table 3 shows the difference between root mean squared errors (RMSE) when the constrained and unconstrained Gaussian models are fit to titration data sets. For three of the data sets, the RMSE increases by less than 1% when the phenolic content in the model is constrained, and the largest increase in RMSE is less than 5% when phenolic content is constrained. The quality of fit is not seriously compromised by constraining phenolic content.

Table 3. Root Mean Squared Error for Restricted and Unrestricted Gaussian Data Sets

<i>Sample</i>	<i>Titration</i>	<i>Restricted</i>	<i>Unrestricted</i>	<i>Difference</i>
1R101N	1	0.0296	0.0294	2.14E-04
1R101N	2	0.0263	0.0250	1.29E-03
1R101N	3	0.0488	0.0474	1.39E-03
2R101N	2	0.0470	0.0465	4.33E-04
2S101H	1	0.0255	0.0249	6.38E-04
2S101H	2	0.0228	0.0226	2.17E-04
2S101H	3	0.0270	0.0266	3.99E-04

Table 4 shows the results for the modified Henderson-Hasselbalch model. When carboxyl contents (Q_1 in the Gaussian and modified Henderson-Hasselbalch models) are compared, the lowest carboxyl contents are obtained from the pH 8 and 10 method, and the highest values are predicted by the modified Henderson-Hasselbalch model, the only exception being a Suwannee River humic acid (1S101H). When phenolic contents (Q_2 in the Gaussian and modified Henderson-Hasselbalch models) are compared, the highest phenolic contents are obtained from the pH 8 and 10 method, and the lowest values are predicted by the modified Henderson-Hasselbalch model, again with 1S101H being the only exception.

The μ values in the Gaussian model and the $\log K$ values in the modified Henderson-Hasselbalch model are both average $\log K$ values for proton binding by a class of functional groups (carboxyl or phenolic), so they can also be compared directly. With the exception of the carboxyl groups of the 1S101H sample, $\log K$ values from the modified Henderson-Hasselbalch model are consistently greater than μ values in the Gaussian model. Both the modified Henderson-Hasselbalch model and the Gaussian model have fitting parameters that represent the spread of $\log K$ values around the average values (n and σ , respectively). Although both n and σ increase continuously as the width of a distribution of $\log K$ values increases, they approach different limits when the width of a distribution decreases to a single proton binding site ($n = 1$ and $\sigma = 0$). Consequently, the width parameters are not directly comparable.

Table 4. Results for the Henderson-Hasselbalch Model (See Text for Explanation of Model)

<i>Sample</i>	<i>Carboxyl Groups</i>						<i>Phenolic Groups</i>					
	<i>Q₁</i>		<i>LogK_I</i>		<i>n_I</i>		<i>Q₂</i>		<i>LogK₂</i>		<i>n₂</i>	
1R101N	10.81	±	0.13	4.26	±	0.05	4.04	±	0.27	1.92	±	0.55
2R101N	11.20	±	0.82	4.16	±	0.20	3.44	±	0.39	1.60	±	0.74
1S101H	7.85	±	0.15	4.82	±	0.01	2.50	±	0.06	3.84	±	0.25
2S101H	10.58	±	0.03	4.53	±	0.03	3.79	±	0.05	1.61	±	0.32
1S101F	11.32	±	0.10	4.13	±	0.06	3.54	±	0.08	1.27	±	0.26
2S101F	12.38	±	0.18	4.40	±	0.52	3.60	±	0.28	1.12	±	0.26
										10.18	±	0.12
										1.05	±	0.08
										1.03	±	0.06
										2.24	±	0.15
										1.00	±	0.00
										1.00	±	0.00
										1.00	±	0.00

Comparison with IHSS Fitting Parameters

The IHSS website contains estimates of carboxyl and phenolic content of the samples used in this study (except the 2R101N sample, which was collected in 2012). The pH 8 and pH 10 method and the modified Henderson-Hasselbalch model were used to generate those estimates of carboxyl and phenolic contents (1). Those carboxyl and phenolic contents and the other fitting parameters of the model are compared in Table 5 with the corresponding results from this study. Because Q_{exp} decreased by 0.2-1.4 meq gC⁻¹ when titration curves were corrected for background cations and anions, it was anticipated that the results in the 2003 paper would be generally higher than those obtained in this study. Both the carboxyl and phenolic contents from the pH 8 and 10 method were noticeably higher in the 2003 paper, with the exception of the 2S101H and 2S101F carboxyl contents. This relationship is also observed for the fitting parameters of the modified Henderson-Hasselbalch model, for which both carboxyl contents and $\log K_1$ values of the 2S101H and 2S101F samples are higher in the current study.

Table 5. Experimental Results and IHSS Results Comparison

	Sample	Carboxyl Groups				Phenolic Groups				
		pH 8	Q_1	$\log K_1$	n_1	pH 10	Q_2	$\log K_2$	n_2	N
IHSS	1R101N	9.85	10.57	3.94	3.60	3.94	2.61	9.74	1.19	112
Exp	1R101N	9.07	10.18	4.26	4.04	2.99	1.92	10.18	1.05	1554
IHSS	1S101F	11.44	12.00	3.80	3.21	2.91	1.48	9.52	1.00	109
Exp	1S101F	10.40	11.32	4.13	3.54	2.47	1.27	10.13	1.00	1670
IHSS	2S101F	11.17	11.66	3.76	3.24	2.84	2.05	9.84	1.45	123
Exp	2S101F	11.35	12.38	4.40	3.60	2.32	1.12	10.22	1.00	1775
IHSS	1S101H	9.59	10.69	4.42	3.79	4.24	2.28	9.68	1.11	113
Exp	1S101H	7.98	7.85	4.82	2.50	3.79	3.84	9.85	2.24	1222
IHSS	2S101H	9.13	9.74	4.35	3.30	3.72	4.48	10.44	1.73	171
Exp	2S101H	9.61	10.58	4.53	3.79	3.48	1.61	10.06	1.00	1533

Conclusions

The data-rich titration curves that were generated using an autotitrator do not substantially alter the estimates of concentrations of carboxyl and phenolic groups, their average log K values, or the width parameters that describe the distribution of log K values in each class of proton binding sites. The enhanced correction for the contribution of background contaminant cations and anions that was used in this study led to generally lower estimates of carboxyl content relative to values generated earlier from manual titrations in which such corrections were not made. The range of estimates of carboxyl and phenolic content are consistent with prior observations and reflect only the fundamental differences in the three modeling approaches.

References

1. Ritchie, J. D.; Perdue, E. M. Proton-binding study of standard and reference fulvic acids, humic acids, and natural organic matter. *Geochim. Cosmochim. Acta* **2003**, *67*, 85–96.
2. Thurman, E. M. *Organic Geochemistry of Natural Waters*; Martinus Nijhoff/Dr. W. Junk Publishers: Dordrecht, 1985.
3. Spitnik, A. K. a. P. Potentiometric Titrations of polymethacrylic acid. *J. Polym. Sci.* **1947**, *2*, 432–446.
4. Perdue, E. M.; Lytle, C. R. Distribution Model for Binding of Protons and Metal Ions by Humic Substances. *Environ. Sci. Technol.* **1983**, *17*, 654–660.
5. Zhang, Y.; Green, N. W.; Perdue, E. M. Acid-base properties of dissolved organic matter from pristine and oil-impacted marshes of Barataria Bay, Louisiana. *Mar. Chem.* **2013**, *155*, 42–49.
6. Serkiz, S. M.; Perdue, E. M. Isolation of Dissolved Organic Matter from the Suwannee River Using Reverse Osmosis. *Water Res.* **1990**, *24*, 911–916.
7. Sun, L.; Perdue, E. M.; McCarthy, J. F. Using Reverse Osmosis to Obtain Organic Matter from Surface and Ground Waters. *Water Res.* **1995**, *29*, 1471–1477.
8. Averett, R. C.; Leenheer, J. A.; McKnight, D. M.; Thorn, K. A. *Humic substances in the Suwannee River, Georgia; interactions, properties, and proposed structures*; U.S. Geological Survey: 1994; pp 23–35.
9. Perdue, E. M. *Modeling the Acid-Base Chemistry of Organic Acids in Laboratory Experiments and in Fresh Waters*. In *Organic Acids in Aquatic Ecosystems*; Perdue E. M., Gjessing, E. T., Eds.; Dahlem Konferenzen; John Wiley & Sons, Ltd.: Chichester, 1990; pp 111–126.
10. Cabaniss, S. E. Carboxylic-acid content of a fulvic-acid determined by potentiometry and aqueous fourier-transform infrared spectrometry. *Anal. Chim. Acta* **1991**, *255*, 23–30.
11. Santos, E. B. H.; Esteves, V. I.; Rodrigues, J. P. C.; Duarte, A. C. Humic substances' proton-binding equilibria: assessment of errors and limitations of potentiometric data. *Anal. Chim. Acta* **1999**, *392*, 333–341.

12. Fletcher, R.; Powell, M. J. D. A rapidly convergent descent method for minimization. *Comput. J.* **1963**, *6*, 163–168.
13. Perdue, E. M.; Reuter, J. H.; Parrish, R. S. A statistical-model of proton binding by humus. *Geochim. Cosmochim. Acta* **1984**, *48*, 1257–1263.

Chapter 5

Natural and Unnatural Organic Matter in the Atmosphere: Recent Perspectives on the High Molecular Weight Fraction of Organic Aerosol

Tiffany R. Duhl,^{1,*} Nicholas Clements,¹ Natalie Mladenov,²
Kaelin Cawley,³ Fernando L. Rosario-Ortiz,³
and Michael P. Hannigan¹

¹Department of Mechanical Engineering, University of Colorado,
Boulder, Colorado, 80309

²Department of Civil Engineering, Kansas State University,
Manhattan, Kansas, 66506

³Department of Civil and Environmental Engineering,
University of Colorado, Boulder, Colorado, 80309

*E-mail: duhl@colorado.edu.

This chapter provides an overview of research related to aerosol-derived HUmic-LIke Substances (HULIS) and the low volatility/high molecular weight organic aerosol fraction, from the comprehensive 2006 review by Gruber and Rudich of the similarities and differences between terrestrial/aquatic humic substances and HULIS, to new insights on the sources and formation, atmospheric distribution and climatic, ecological, and epidemiological influences of HULIS from more recent observations. HULIS are primarily formed through secondary oxidation of gaseous biogenic and anthropogenic precursors followed by oligomerization or polymerization reactions and atmospheric aging but can also be directly emitted e.g., from biomass burning smoke or airborne soil. These diverse processes and sources cause HULIS' physicochemical and optical characteristics to evolve over time and vary spatially,

making conclusions about its climate forcing effects uncertain. Recent evidence shows that HULIS is present world-wide and in both fine and coarse aerosol size fractions and can impact water optical qualities and nutrient cycling in some ecosystems, form complexes with metals or organic pollutants, and generate reactive oxygen species, which can harm exposed cells. A brief review of mass spectrometric techniques that have been applied to study HULIS or have been recently developed but not yet extensively utilized is included, as are possible future research directions.

Introduction

NOM (Natural Organic Matter) is the term used to describe degraded plant, animal, and microbial substances found ubiquitously in terrestrial and aquatic ecosystems. NOM includes humic and non-humic substances and its constituents play important roles in ecosystem dynamics, fate and transport of organic contaminants, metal speciation and formation of disinfection byproducts (via interactions with halogen species). Organic matter is also abundant in the atmosphere, where organic compounds comprise a large but variable fraction of aerosol mass (e.g., up to 70% of fine-mode aerosol (1); and are also found in rain and fog water (2, 3). An important component of atmospheric organic matter is the poly-acidic, chromophoric fraction, termed HUmic-LIke Substances (HULIS) by Havers et al. (4), since it has similar chemical and physical properties as terrestrial and aquatic humic substances. HULIS is occasionally also referred to as NOM although this is misleading since HULIS is mainly formed in the atmosphere via oxidation of both anthropogenic and biogenic precursor compounds (5, 6); therefore atmospheric organic matter has both natural and un-natural components, an observation that inspired this chapter's title.

The goals of this chapter are to provide an overview of HULIS-related research leading up to (and described in) the comprehensive review by Gruber and Rudich (5) of the similarities and differences between terrestrial/aquatic humic substances and HULIS, and to discuss new insights on the sources and formation, as well as climatic, ecological, and epidemiological influences of HULIS in atmospheric aerosol, and its atmospheric distribution based on more recent observations. Although Gruber and Rudich (5) included discussion of rain-, cloud-, and fog-water HULIS in addition to aerosol-derived HULIS in their review, our focus here is on HULIS in aerosol. It should be noted that many aerosol studies relevant to HULIS do not explicitly refer to, nor focus on HULIS per se, but instead have examined low volatility/high molecular weight organic aerosol (LV/HMWOA (7)); which includes and has been used to describe HULIS in a number of reviews (5–7), therefore insights gained from several of these investigations are discussed in this chapter.

Chemical and Physical Properties of HULIS Relative To Humic Substances

Atmospheric HULIS are optically active, polyacidic, medium- to high molecular weight (HMW) substances, which can modify aerosol properties including light absorption characteristics and formation of cloud condensation nuclei (CCN) or ice nuclei (IN); therefore HULIS can potentially impact cloud formation and properties, atmospheric radiation dynamics, and, like humic substances, possibly also play a role in complexation, transport, or processing of pollutants (5, 8). Compared to humic substances, HULIS tend to be more acidic, have lower average molecular weight distributions, less aromatic content and more surface area as well as better droplet activation ability and higher surface activity (5).

Several explanations for observed differences between HULIS and humic substances include (a) the possibility that the higher acidic content of HULIS impedes the formation of large “supramolecular associations” seen in humic substances, (b) that large macromolecules do form but are degraded by UV light and atmospheric oxidants, or (c) that investigators simply have not yet resolved and identified individual compounds contributing to multicomponent mixtures (5). Differences might also be attributed to contrasting formation pathways, as humic substances are formed on long (years) timescales through biologically-mediated reactions, while HULIS are formed over shorter (days) timescales, mainly via oxidation of gas-phase organics emitted from biogenic and/or anthropogenic sources and smoke from biomass burning, although other minor sources of HULIS have also been identified, including aeolian dust and degraded plant structural materials (2, 5, 9).

Some researchers, especially in early studies (e.g. (9, 10),) employed similar techniques to isolate and quantify HULIS as have been used to study humic substances, which are typically isolated and separated into their humic (base soluble), fulvic (water soluble at any pH), and humin (insoluble) fractions first using either non-ionic copolymer sorbents or anion exchange resins followed by elution in a basic solution, and then further fractionated using either ion exchange or macroporous non-ionic resins (11). Like humic substances, HULIS are operationally defined according to the isolation technique used, therefore variations in chemical and physical properties reported in the literature are partly due to the operational nature of the term (12). Attempts to isolate HULIS in aerosol samples have included some alkaline extractions followed by various fractionation techniques. However most recent studies have focused on the water soluble organic carbon (WSOC) fraction (e.g. (5), and many of the studies discussed in this chapter). Therefore results presented from such studies will mainly include fulvic acid-like materials, restricting conclusions regarding the chemical nature of HULIS to only the investigated fractions. For example, while aromatic carbon content is thought to be higher in terrestrial and aquatic humic substances than most reported values for aerosol-derived HULIS (5), as mentioned most of these studies have considered only the WSOC fraction. When the base-soluble (humic acid-like) fraction of HULIS was extracted and isolated from fresh urban aerosol samples by Subbalakshmi et al. (13), the

aromatic carbon content (on the order of 45%) was comparable to values observed in terrestrial and aquatic humic acids, which generally have higher aromatic fractions than terrestrial and aquatic fulvic acids (5). In this chapter, we do not attempt to exhaustively describe the various extraction and isolation techniques applied to HULIS, but instead refer the reader to Gruber and Rudich (5) who not only cover this topic in detail but also discuss some of the limitations associated with the different approaches.

When pondering the conclusions that can be made about the characteristics of HULIS based on the available literature, several additional caveats should be considered. Aside from choice of extraction method, individual analytical techniques have limitations in their abilities to detect some potentially important constituents of HULIS. For example a lack of signal in the humic-like region of a 3-D fluorescence spectrum for a given sample could indicate either the absence of humics or extensive complexation with metal ions or other organic compounds (which quench the fluorescence response and which would be expected to be present in ambient aerosol). As another example, $^1\text{H-NMR}$ (i.e., proton) spectra do not provide information on the carbon structure of analytes, nor are acidic hydrogen atoms detected in proton spectroscopy (5). The individual limitations of the various techniques do not all overlap, therefore numerous methods should be applied systematically to the analysis of atmospheric HULIS, and inter-compared to the best extent possible. The time period over which a given study is performed is also a consideration, as measurements conducted over limited time periods can miss seasonal variation in HULIS composition due to changing sources. In a study of rural aerosol samples, the aromatic carbon fraction was higher in WSOC-derived HULIS collected in autumn compared to summer (14), a phenomena which may be attributed to biomass-and/or wood-burning activities during autumn months, as biomass burning aerosol-derived HULIS have been observed to have significantly higher aromatic carbon fractions than urban aerosol-derived HULIS (15).

There have been few attempts to intercompare the myriad techniques that have been used to extract, isolate, fractionate, and analyze HULIS, and existing humic substance standards, such as Suwanee River Fulvic Acid (SRFA), Nordic Lake Fulvic Acid (NLFA) et al. appear to have substantially different carbon distributions and other properties compared to both biomass burning aerosol-derived HULIS and urban aerosol-derived HULIS (15). Although reference dust samples such as those available from NIST do exist, there are currently no HULIS standards available for systematic comparisons of the many approaches applied thus far to the study of HMW organic materials in the atmosphere. However Andracchio et al. (16), created surrogate aerosol standards consisting of humic and fulvic acids along with low molecular weight (LMW) organic acids and inorganic salts (both of which can be abundantly present in ambient aerosol and which would also be expected to contribute to results obtained in studies using bulk WSOC) for the purpose of evaluating a HULIS fractionation method.

Although intercomparisons are lacking, scores of analytical techniques have been used to study HULIS including both spectroscopic (e.g. UV-VIS with or without size-exclusion chromatography, Fluorescence, IR, ^1H - and

¹³C-NMR spectroscopy) and non-spectroscopic analyses (pyrolysis GC/MS, capillary electrophoresis, elemental analysis, etc. (5)). The application of various analytical approaches has fortunately led to some convergence in terms of the conceptualization of HULIS: Mukai and Ambe (10) proposed a chemical structure for HULIS consisting of a poly-cyclic aromatic core with substituted aliphatic chains bearing carboxyl, carbonyl, and hydroxyl moieties, which is still largely accepted today (5) although recent evidence suggests that aliphatic structures may constitute the hydrophobic core in some important HULIS components, such as organosulfates (17), and oligoesters (18). The presence of amine, methoxyl, and phenol groups has also been inferred in the hydrophobic acid fraction of aerosol-derived WSOC (19).

Despite some consensus regarding the chemical structure of HULIS, the question of its molecular weight distribution remains a contentious issue. Numerous HULIS investigations have demonstrated through ultrafiltration techniques that a large fraction of HULIS components have MW below 500 or 1000 Da, causing some to question whether HULIS actually consists of a complex mixture of LMW compounds rather than macromolecular components (5), although it should be noted that a similar debate continues regarding soil and aquatic humic substances (20, 21). Up to Gruber and Rudich's 2006 review, a number of studies had used mass spectrometry (MS) to estimate aerosol-derived HULIS MW distributions (e.g., (22–25), etc.), and suggested that average distributions range from 50–600 Da, substantially lower than what is typically observed in terrestrial and aquatic humic substances though many of these studies examined un-fractionated bulk samples expected to contain LMW constituents, potentially leading to underestimates of HULIS MW distributions. In addition to possible negative bias introduced with the use of un-fractionated samples, there are also several caveats associated with mass spectrometric approaches that could skew HULIS molecular weight estimates to the left, (as described below), therefore the reported HULIS MW range of 50–600 Da should be considered a lower limit. Since 2006, MS has been increasingly used to study aerosol HULIS and/or LV/HMWOC, so a brief review of mass spectrometry as applicable to the study of HULIS is presented below.

Mass Spectrometric Approaches for Analysis of HULIS and LV/HMWOC

Mass spectrometry is an analytical technique in which analytes are ionized and then accelerated through a low-pressure chamber with an oscillating magnetic field that allows selected ion masses to pass through to a detector; the oscillating field and detector can scan very quickly across a broad range of ion masses. The intensity of the signal is expressed across a range of mass to charge (m/z) ratios. Assuming that ions are singly-charged, m/z represents the molecular weight of the ions. Traditional 'hard' ionization approaches such as electron impact or chemical ionization cause compound fragmentation, which is desirable when analytes have known fragmentation spectra (as these are used for compound identification) and can be easily separated prior to analysis (for example through the use of liquid

or gas chromatography), but is problematic when studying humics since these substances are complex, difficult-to-separate mixtures of chemical components, many with similar chemical properties and unknown chemical formulae (26). One aerosol-relevant application of MS that typically uses hard ionization is aerosol mass spectrometry (AMS), in which entire particles are vaporized and the vapor subsequently ionized and detected (27). AMS can broadly describe aerosol composition but the multitude of organic compounds comprising OA typically undergo extensive fragmentation upon ionization with many overlapping ions, thus identification at the compound level is not possible using this approach (28).

Several soft ionization techniques have been developed which are designed to add a single electric charge to individual analytes without causing significant fragmentation, although formation of multiply-charged ions and/or fragmentation of ionized analyte compounds are both possible and can lead to underestimates in MW and misidentification of individual components (5), however several studies have demonstrated that upon ionization, most humic and fulvic acid spectra consist of singly-charged ions (29–31). Electrospray ionization (ESI) is one soft ionization approach that had already been used by numerous HULIS investigators leading up to Gruber and Rudich's 2006 review. In addition to the limitations (mentioned above) associated with soft ionization techniques in general, ESI has several other drawbacks. Evidence of ESI-induced fragmentation of humic components has been observed, as has ionization suppression caused by the presence of inorganic ions in the sample and reduced efficiencies in both ionization and detection of HMW compounds (5), making ESI undesirable for the study of HMW aerosol components. Additionally, like some other soft-ionization techniques including atmospheric pressure chemical ionization (APCI) and atmospheric pressure photoionization (APPI), ESI requires the use of a liquid solvent, and solvent-analyte reactions have been shown to significantly alter aerosol extract composition (28). Matrix-assisted laser desorption ionization (MALDI) eliminates the need to extract samples into solvent by allowing for samples to be analyzed directly on their collection substrate, however MALDI requires the use of a matrix to increase ionization efficiency, which creates problems as peaks associated with the matrix dominate low MW regions ($m/z < 250$; though this may be of less concern in the study of HMWOA species) and significant variability in signal intensities have been observed with MALDI; these relate to laser power, matrix to sample ratio, and sample preparation (27). Like MALDI, ESI-derived results can also be heavily influenced by a number of variables (e.g. pH, solution concentration and ionic strength, complexity, detection mode, cone voltage etc. (5);) therefore ESI-and MALDI-based MS results of HULIS analyses should be viewed cautiously.

Since approximately 2006, several soft ionization techniques have been developed to overcome the problems associated with the use of solvents and matrices; these are known as ambient surface ionization techniques and require neither solvent extractions nor matrices, instead allowing for direct analysis of a sample on its collection substrate without sample preparation (28). Examples of ambient surface ionization techniques include desorption electrospray ionization (DESI), direct analysis in real time (DART), desorption atmospheric pressure chemical ionization (DAPCI), electrospray-assisted laser

desorption and ionization (ELDI) and atmospheric solids analysis probe (ASAP), however these techniques have not yet been extensively applied to the study of atmospheric aerosols (27). When considering an ionization scheme for analysis of HULIS/LV/HMWOA it is also important to consider that different methods may preferentially ionize certain compound groups, for example ESI can be used to ionize polar compounds, while APCI and APPI are better suited for less-polar constituents (27).

By definition, soft ionization techniques provide only very simple spectra (ideally each compound present would be detected as a single ion of some given mass), thus offering limited information about analyte chemical structure. This approach can be complimented with tandem mass spectrometry (MS/MS), in which soft ionization is initially applied to both generate and detect parent ions (individual compounds), which are then ionized and subsequently fragment during sequential ionization and detection routines; thus providing information about individual precursor and product ions and offering far more information about the detected ions.

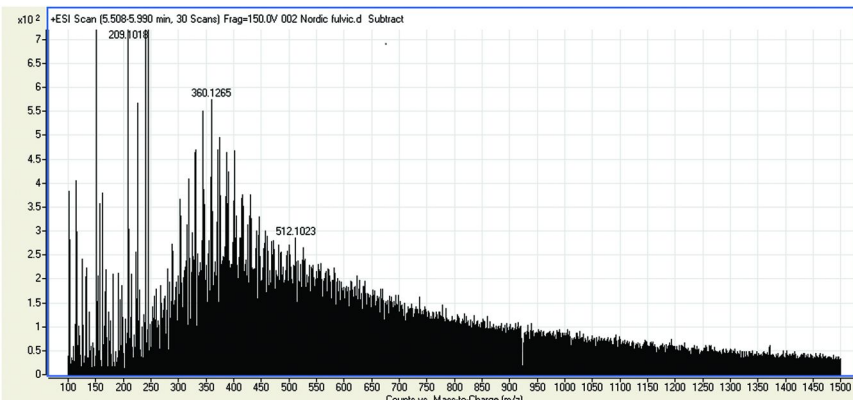


Figure 1. Portion of ESI-QTOF mass spectrum obtained from IHSS Nordic Fulvic Acid for 5.5-6.0 minute analysis window. (courtesy of D. Mawhinney, Southern Nevada Water Authority).

Historically, a major factor that has limited the ability of mass spectrometers to distinguish individual compounds contained in mixtures has been instrument resolution, in other words the ability to detect small mass differences between compounds. High resolution mass spectrometry (HRMS) has become increasing popular for the study of OA and describes a number of MS techniques that can resolve mass differences below $0.001\text{ }m/z$ and which have broad m/z detection ranges (analogous to MW ranges if one assumes ions are singly-charged), thereby discerning thousands of components typical of aerosol samples. HRMS combined with MS/MS is becoming increasingly popular for the study of organic aerosol, and the reader is referred to Nizkorodov et al. (27) for a compendium of HRMS studies of organic aerosol as well as relevant rain and fog water analyses, however it should be noted that ESI-based techniques have dominated these

investigations. Perhaps the HRMS technique best-suited to the analysis of HMW compounds is hybrid quadrupole time-of-flight (QTOF) mass spectrometry, due to its high sensitivity (27) and theoretically unlimited mass range. Figure 1 shows a 30-second subset of an ESI-QTOF mass spectrum obtained from an IHSS Nordic Fulvic Acid standard (provided courtesy of D. Mawhinney, Southern Nevada Water Authority). Other HRMS instruments include linear ion trap (LTQ) and Fourier transform ion cyclotron resonance (FT-ICR MS), both of which have already been applied in numerous studies of OA and its formation (27).

The application of HRMS approaches and many other analytical techniques to the study of LV/HMW OA and HULIS in recent years have resulted in new revelations regarding the composition, sources and formation of this fraction of aerosol, its distribution in the atmosphere, and its ecological, climatic, and epidemiological implications, all of which are discussed in the following sections.

New Insights into HULIS Composition, Sources, and Formation Pathways

Since Gruber and Rudich's 2006 review, there has been an explosion in studies of formation and composition of low volatility organic species in aerosol, many of them using HRMS. Ambient aerosol investigations as well as laboratory chamber experiments have illustrated that low volatility, HMW organic products can form in heterogeneous chemical reactions involving lower-weight volatile organic compound (VOC) precursors, both of anthropogenic (e.g. vehicle exhaust, VOC from paint) and biogenic (e.g. isoprene) origin, mainly through oxidation and subsequent oligomerization and oxidation reactions, although one important revelation of recent research is the observation that in-particle, non-oxidative reactions also contribute aerosol aging and composition (7). It is also now known that irrespective of source, both primary (e.g., smoke from biomass burning or fuel combustion) and secondary (e.g. VOC from vegetation or human emissions) organic aerosol all tend to undergo chemical transformations in the atmosphere on timescales of hours to days that result in a convergence towards low volatility, highly oxygenated OA products bearing many similar structural elements (6, 7).

Atmospheric aging of particles (especially in the presence of reduced nitrogen species) including anthropogenic and biogenic SOA has recently been shown to substantially increase aerosol light absorbance coefficients and fluorescence (28, 32–35), which has obvious implications on aerosol radiative forcing and other properties (see following sections). Laskin et al. (28) employed DESI-HRMS to identify several important imine aging reactions that result in the formation of chromophoric, highly-conjugated N-containing species from limonene-derived SOA, including carbonyl-imine transformation, intramolecular cyclization, and dimerization with other SOA carbonyl compounds.

Though it has long been postulated that oxidation of gaseous VOC precursors could lead to secondary organic aerosol (SOA) formation (36), many recent HRMS studies have elucidated the mechanisms by which HMW aerosol components form. For example, laboratory chamber and flow tube reactor studies of SOA formation from biogenic precursor compounds (which account

for 20-90% of surface SOA (37); such as isoprene (C_5H_8) and monoterpenes ($C_{10}H_{16}$) have indicated that upon oxidation, these compounds form SOA through oligomerization of reactive intermediates and/or stable monomer products (especially small carbonyl molecules) as well as repeating self-reactions of products such as alkoxy or peroxy radicals; polymerization of formaldehyde and acetaldehyde building blocks has also been observed (38-40). Nguyen et al. (41) studied SOA from high- NO_x isoprene oxidation using nano-DESI-HRMS under different humidities, and found that at high humidities, substantially fewer HMW oligomers were produced compared to drier reaction conditions, while in a study of SOA generated from α -pinene (a monoterpene) ozonolysis, Doezaem et al. (42) observed fewer HMW oligomeric compounds in dry air compared to air at 50% relative humidity.

Altieri et al. (18) applied ultra-high resolution FT-ICR mass spectrometry to show that in-cloud processing of methylglyoxal in the presence of OH ultimately resulted in the formation of organic acids as well as HMW oligoesters with similar chemical properties as HULIS and aged atmospheric aerosols. Oligomers and other first-generation reaction products form rapidly; subsequent aging processes slowly change certain chemical characteristics such as O:C ratios which have been reported to range from about 0.3-0.6 in biogenic VOC-derived SOA and to increase over time (38-40). Similar behavior has also been observed in VOC of anthropogenic origin (6, 43, 44).

Like SOA formed from biogenic and anthropogenic VOC, primary emissions from diesel combustion as well as from biomass burning have also been observed to evolve over time into low volatility, highly oxygenated OA products similar to those observed in ambient aerosol (6), although the oligomeric HMW fraction observed in ambient aerosol, which can comprise up to 20% of the total signal when analyzed using HR AMS (6) is typically lower than suggested by laboratory-based studies, in which HMW products can constitute the majority of SOA (40). Chamber and flow tube experimental conditions are generally not representative of realistic atmospheric conditions; i.e. levels of both oxidants (e.g. O_3 , OH) and VOC precursors tend to be artificially high therefore results obtained from these studies should be viewed accordingly.

Organosulfates, organonitrates and nitrooxy organosulfates, which have been observed to form in chamber studies of biogenic VOC oxidation in the presence of sulfate seed aerosol and NO_x (17), have also recently been reported in ambient aerosol (45, 46) as well as rainwater (47) and can comprise a significant fraction of HMW atmospheric organic matter, suggesting that both natural and anthropogenic SOA precursors interact to form HMWOA. Using HRMS and tandem MS, Surratt et al. (17) showed that organosulfates and nitrooxy organosulfates, formed mainly from the oxidation of biogenic VOC in the presence of acids, can contribute up to 30% of total organic mass in some locations and that both photo-oxidation as well as nighttime (i.e. NO_3 -mediated) oxidation can lead to the formation of these products. Mazzoleni et al. (48) made ~4000 molecular formula assignments in a composite aerosol-derived WSOC sample collected from a remote alpine high-elevation site using ultrahigh-resolution FT-ICR MS and observed S and N in over half of the compounds. Biogenic VOC were concluded to have acted as precursor compounds in a substantial fraction of the detected ions and

non-oxidative accretion-type formation was implied for a significant fraction of identified HMW components (48). Peng et al. (49) used radiocarbon and $\delta^{13}\text{C}$ information to determine that substances from biogenic sources comprised 44-62% of HULIS from TSP samples collected at urban, suburban, and forest sites in Guangzhou, China.

Fulvic acids that were indistinguishable from aquatic fulvic acids were reported for the first time in WSOC-derived aerosol by Reemtsma et al. (46), therefore these compounds can either form through atmospheric processing or (as inferred in earlier studies, e.g. (2, 9),) soil and/or aquatic sources also contribute to HULIS observed in aerosol. There are a multitude of potential reaction schemes that could lead to the formation of LV/HMWOA and HULIS, arising from hundreds or thousands of potential precursor compounds, oxidative and non-oxidative pathways, etc. (7); these are beyond the scope of this chapter. Kroll and Seinfeld (7) present an excellent and detailed review of formation mechanisms for LVOA/HMWOA, while in their review of HRMS techniques applied to the study of OA, Nizkorodov et al. (27) summarize HRMS investigations of the chemical characterization of ambient aerosol. Atkinson and Arey (50) present a detailed description and numerous schemes of atmospheric VOC degradation pathways, while Kroll and Seinfeld (7) focus on formation of low volatility SOA species, including schemes for particle-phase accretion reactions, alkoxy radical isomerization, and other processes involved in the formation of LV/HMWOA. Proposed reaction schemes showing formation of organosulfate and nitrooxy organosulfate compounds from the oxidation of biogenic VOCs are presented in Surratt et al. (17), while Tobias and Zieman (51) present schemes for particle-phase peroxy-hemiacetal formation from dry-air alkene ozonolysis. Garland et al. (52) depict aldol condensation and hemiacetal formation schemes from acid-catalyzed reactions of hexanal on sulfuric acid particles; Szmigielski et al. (53) present organic esterification pathways for high- NO_x isoprene photooxidation and Vione et al. (12) show HULIS formation schemes based on irradiation of aromatics and subsequent phenoxy radical reactions.

The sources of HULIS/HMWOA are known to have strong seasonal influences, and recent investigations (e.g. (19, 54-57),) have confirmed earlier observations (e.g. (14, 25),) that the composition of LV/HMWOA/HULIS varies seasonally, reflecting the relative importance of changing biogenic and anthropogenic sources at different times of the year, with biomass-burning being more important in colder months and SOA from VOC oxidation dominating in warmer months. Aromatic and aliphatic content of HULIS also tends to differ according to source (5, 14, 15, 19) as does WSOC hydrophobicity (56). Muller et al. (58) found a relationship between the fluorescence behavior of rainwater DOC and certain meteorological conditions and was also able to attribute some of the detected fluorophores to different sources and source regions (e.g. local, continental, etc.). Mladenov et al. (59) demonstrated that C and N stable isotopes and parameters from UV-Vis and fluorescence spectroscopy are able to discriminate between aerosols receiving substantial fossil fuel pollution and those influenced by Saharan dust in an urban area. The humification index (HIX), used predominantly to evaluate the degree of organic matter humification, was significantly related to the asymmetry parameter and the radius of fine mode

particles and may reflect aging of the Saharan dust-influenced aerosols (59). Duhl et al. (60) observed strong seasonal patterns in HIX and WSOC concentrations (Figure 2) from fine and coarse aerosol-derived bulk WSOC samples, including both aqueous- and base-extracted fractions, while little seasonality was apparent in fluorescence index (FI) values (not shown). Lee et al. (33) observed an increase in HIX as a function of aerosol aging in chamber experiments in which laboratory-generated SOA was aged with ammonia.

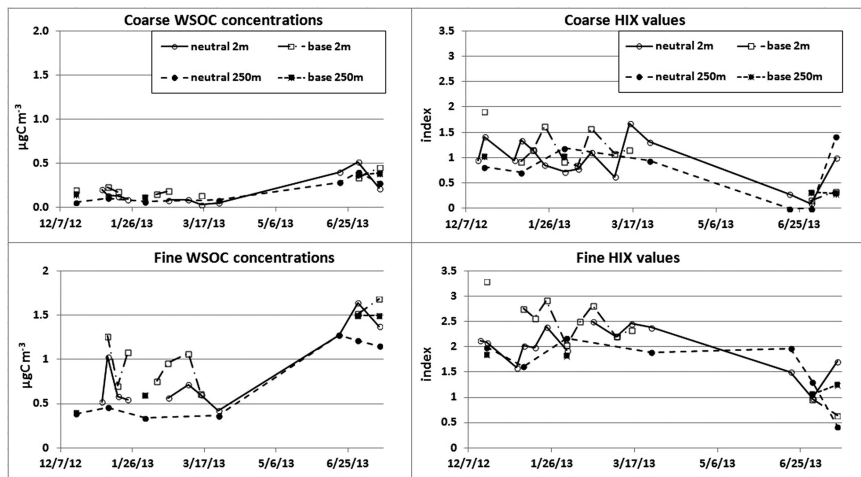


Figure 2. Time series of aerosol-derived bulk WSOC (“neutral”) and bulk base-extracted OC (“base”) fluorescence (FI; left) and humification (HIX; right) indices for coarse (top) and fine (bottom) aerosol samples collected at heights of 2m and 250m at a tower site in Colorado, U.S.A. between December 2012 and July 2013 (60).

Zhang et al. (61) characterized the spatial and temporal patterns of PM_{2.5} WSOC concentrations over the southeastern U.S. and observed that WSOC (as well as sulfate) concentrations were mainly correlated with ambient temperature year-round, therefore the authors concluded that photochemical and meteorological influences dictate WSOC concentrations moreso than biogenic release of VOC. This is notable since this region experiences substantial biogenic VOC emissions during summer months, and although observed WSOC concentrations were ~27% higher in locations with high predicted summertime isoprene emissions, concentrations were still rather homogenous over the region (61). Feczko et al. (62), isolated HULIS from both aqueous and alkaline extractions of fine PM samples collected from six sites spanning from west to east over Europe, and found that while relative amounts of water soluble and base-soluble HULIS were similar across the sites, there were large site-specific seasonal patterns in concentrations, for example total HULIS concentrations were highest in the summer in the Azores and high mountains, but peaked during winter at low elevation continental sites.

Distribution of HULIS in Aerosol and in the Atmosphere

Up to Gruber and Rudich's 2006 review and more recently, most investigations of aerosol-derived HULIS and/or bulk WSOC have focused on fine-mode particles (particles with average aerodynamic diameters $\leq 2.5 \mu\text{m}$ also known as $\text{PM}_{2.5}$) or PM_{10} (particles with average aerodynamic diameters $\leq 10 \mu\text{m}$) and have relied mainly on near-ground measurements. Fewer studies have examined the distribution of these substances in the coarse aerosol fraction ($\text{PM}_{2.5-10}$) or at various vertical heights in the atmosphere. Huang et al. (63) measured size distributions of WSOC, oxalate, and ionic species in a coastal city in China and observed both WSOC and oxalate had dominant droplet modes (with mass peaks observed at $1 \mu\text{m}$), and minor condensation ($0.4 \mu\text{m}$ mass peak) and coarse ($5.5 \mu\text{m}$ mass peak) modes. Biomass-burning and in-cloud processing contributed the most to fine WSOC, while soil dust and aged sea salt particles were the main components of coarse WSOC (63).

Lin et al. (64) measured the abundance and size distribution of aerosol-derived HULIS from a rural location in South China during a period of crop residue burning. $\text{PM}_{2.5}$ samples of direct (fresh) biomass burning emissions were also collected, and the investigators found HULIS to comprise ~60% of ambient and 30% of fresh biomass-burning WSOC, with a dominant droplet mode mass median aerodynamic diameter (MMAD) in the range of $\sim 0.63\text{--}0.87 \mu\text{m}$ in which 81% of total HULIS mass was found. HULIS also had minor condensation (at MMAD of $0.23\text{--}0.28 \mu\text{m}$ and with 12% of total HULIS mass) and coarse (MMAD: $4.0\text{--}5.7 \mu\text{m}$; 7% of HULIS mass) modes. Size distribution results suggested multiple formation pathways for HULIS including secondary (through formation in cloud droplets or via heterogeneous or solid-phase reactions) processes and primary (biomass burning, soil) sources.

Hiranuma et al. (65) characterized size-resolved PM emitted from a cattle feedlot in the Southwest US and found that coarse-mode particles dominated particle volume size distributions. PM_{10} concentrations up to $1200 \mu\text{g m}^{-3}$ were observed; these were primarily made up of carbonaceous materials and evidence suggested that a large fraction was contributed from soil-derived humic acids and that many of the organics were present in internal mixtures with salts.

HULIS appears to be a ubiquitous component of aerosol world-wide and has been observed to be present in concentrations of < 0.1 to $> 13 \mu\text{g m}^{-3}$ (66). Krivácsy et al. (67) detected HULIS in PM_{10} sampled at two urban marine sites in New Zealand, in $\text{PM}_{1.5}$ collected at a pristine oceanic site (Mace Head, Ireland), and in both coarse and fine PM from a continental urban site (Budapest), and found that at the site with both coarse and fine PM data (Budapest), HULIS concentrations in the fine mode samples were at least ten times higher than in coarse PM.

Feczko et al. (62) observed an exponential decrease in HULIS concentrations as a function of elevation in a study using fine PM samples from six European sites. Duhl et al. (60) collected rural/urban background fine and coarse aerosol samples over a 7 month period at heights of 2 m and 250 m above ground level at a tower site in CO, U.S.A. Water- and base-soluble carbon characteristics as well as concentrations of total organic carbon, elemental carbon, and aerosol mass were compared using bulk WSOC and base-soluble OC extracts. No

significant differences were observed between 2 m samples and 250 m samples for any of the coarse-mode parameters evaluated, while near-ground fine samples had significantly higher WSOC, EC, OC, and mass concentrations compared to samples collected at 250 m.

As mentioned previously, seasonal changes were observed in HIX values by Duhl et al. ((60); Figure 2) for all investigated aerosol fractions but not in FI values. Strong correlations were found between fine and coarse-mode WSOC and between WSOC and OC in both coarse and fine samples and in both neutral and basic extracts. Correlations were also found between HIX and both WSOC and OC in both size modes and pH values. Both fine and coarse neutral WSOC samples had significantly higher FI values than base-extracted samples, while fine-mode HIX values were significantly higher in the base-extracted samples from December through mid-March only, with patterns changing thereafter (Figure 2). Coarse versus fine FI and coarse versus fine HIX were well correlated in base-extracted samples but not in neutral extracts (but were correlated with each other in the fine samples). Base-extracted samples had significantly higher WSOC concentrations compared to neutral extracts in both size modes: base-extracted WSOC contributed ~6% more to total OC than neutral extracted WSOC in the coarse mode, and ~24% more in fine-mode samples. These results suggest that fine and coarse-mode soluble carbon are coupled or may have some common sources, and confirm previous observations that WSOC is an important fraction of total OC with seasonally varying source contributions and optical properties. Figure 3 shows sample EEMs typical of the fine- and coarse-mode near-ground and 250 m samples in winter and summer months along with (for comparison) EEMs representing fractionated SRFA and DOC from the Poudre River in CO (60).

Zhang et al. (61) found a good correlation between PM_{2.5} mass and WSOC concentrations in the southeast U.S., but only when aerosol was not influenced by biomass burning events. Duhl et al. (60) did not observe such a correlation in fine-mode samples but did observe a weak relationship between coarse PM mass and WSOC concentrations, though it should be noted that a number of forest fires were active in the region during several portions of the sampling period.

Hygroscopic, Cloud Nucleating, and Light-Absorbing Properties of HULIS

Investigations into the hygroscopic and cloud condensation nuclei (CCN) activating properties of HULIS leading up to Gruber and Rudich's 2006 review suggest that HULIS has similar or somewhat higher growth factors (68–70) and activates at lower diameters (71) compared to aerosolized aquatic fulvic and humic acids; growth rates may be synergistically enhanced in mixtures of inorganic salts (which would be expected to be present in ambient aerosol) and HULIS (72). Studies using surrogate HULIS (e.g. (69, 70, 73),) did not observe synergistic growth enhancement but did observe deliquescence to occur at similar RHs as those of pure inorganic substances with model HULIS being somewhat less hygroscopic than inorganic salts.

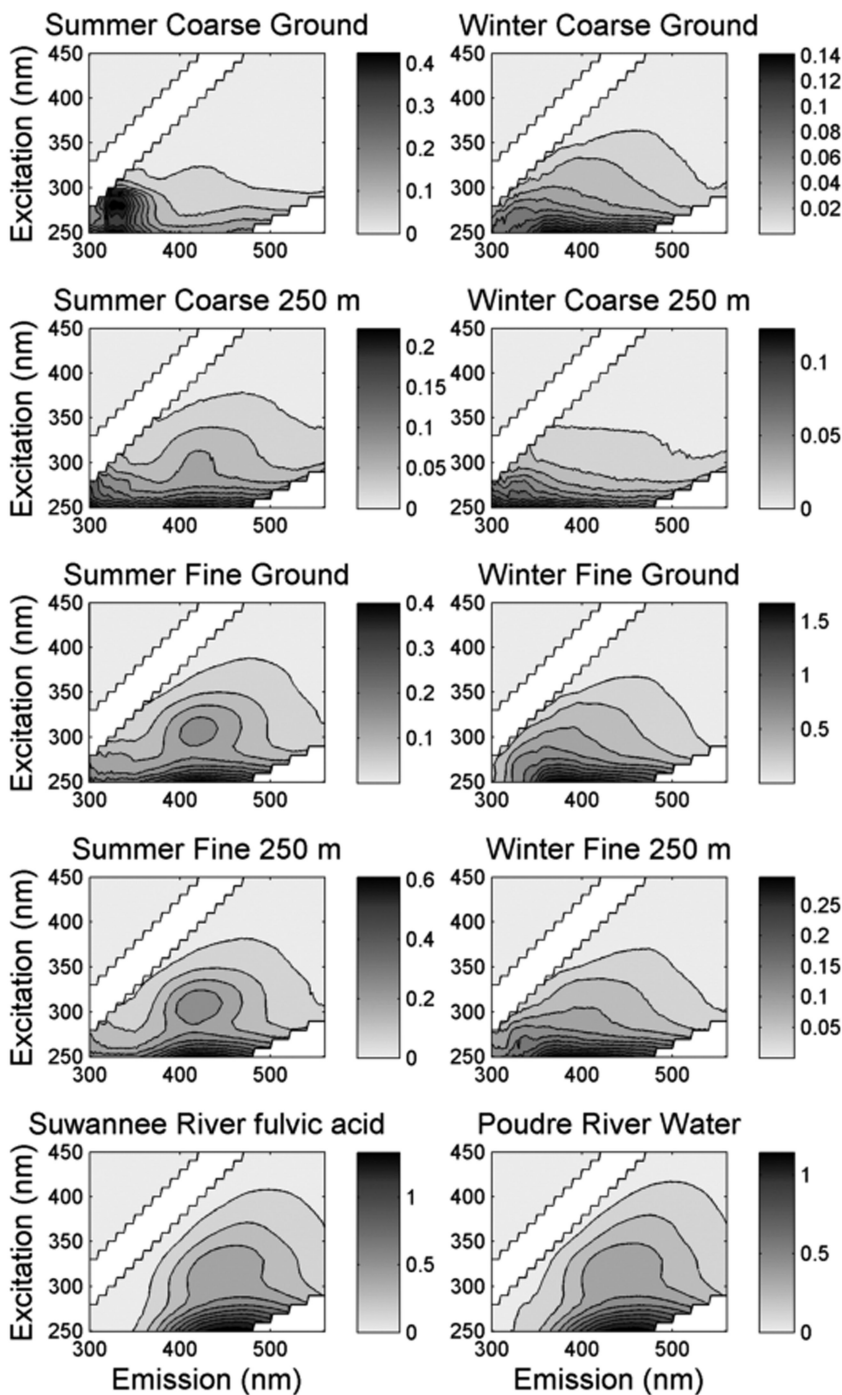


Figure 3. Representative EEMs obtained from WSOC extracts of coarse (rows 1, 2) and fine (rows 3, 4) aerosol samples collected near ground-level and at a height of 250 m from a tower site in CO, U.S.A. in summer (left) and winter (center). Shown for comparison are EEMs from SRFA (bottom, left) and Poudre River (bottom, right) samples (60).

Dinar et al. (71) compared droplet activation and surface properties of HULIS extracted from fresh and slightly aged biomass burning smoke and from urban pollution to various molecular weight fractions of SRFA, and observed that all HULIS samples activated at lower diameters and reduced surface tension more than any of the SRFA fractions investigated (at comparable concentrations), with the highest CCN activity observed in daytime biomass burning smoke samples. Several other studies (71, 74, 75) have also demonstrated the surface activity of HULIS, which can either enhance droplet activation and lower the critical supersaturation point (by lowering surface tension) or delay droplet activation (by forming surface organic films that impede the diffusion of water vapor into the droplet (5);). Surface tension has been observed to decline as total organic carbon content increases in both aerosol and fog water samples (74), and HULIS are likely to be more surface-active than smaller, more polar aerosol constituents (such as mono- and di-carboxylic acids) which have higher affinities for bulk solution as compared to droplet surfaces (76). HULIS extracted from rural aerosol in summer decreased the surface tension of water more so than samples collected in other seasons (as did the presence of inorganic salts) despite the fact that bulk elemental composition was indistinguishable across the samples (75).

Gysel et al. (68) separated WSOC from rural fine aerosol into a less hydrophilic fraction (which was a large component of the total WSOM) and an inorganic salts + hydrophilic organic matter fraction, and found that the less hydrophilic fraction had comparable deliquescence behavior as SOA from smog chambers, but lower than that of highly soluble organic acids. Asa-Awuku et al. (77) measured the CCN activity and surface activity of fractionated hydrophobic and hydrophilic components of WSOC from fine biomass burning aerosol, and found that the strongest surfactants were isolated in the more hydrophobic fraction while surface tension depression was minor in hydrophilics. The presence of inorganic salts in the hydrophobic fraction substantially lowered surface tension and enhanced CCN activity, exceeding that of pure salts (77).

Clearly, HULIS can exert considerable influence on aerosol droplet activation behavior, surface activity and hygroscopicity; these parameters modify cloud properties and can affect aerosol chemistry. One of the biggest sources of uncertainty in climate prediction is the direct effect of light absorbing organic compounds, (e.g., HULIS) on aerosol scattering and absorption (78). Baduel et al. (79) found that absorbance of UV and visible light increased along with pH, aromaticity, TOC content and MW of HULIS derived from PM₁₀ samples and

observed that the relative contribution of HULIS to light absorption ranged from 7-50% at 300 nm, while Hoffer et al. (80) examined the optical properties of PM_{2.5} from biomass burning and found that the relative contribution of HULIS to light absorption across the entire solar spectrum to be 6.4-8.6%. Baduel et al. (54) analyzed the WSOC fraction of PM₁₀ at several sites in France in summer and winter and found large differences in optical properties between the two seasons implying different seasonal sources. Dinar et al. (78) examined the refractive indices of HULIS from pollution, smoke, rural continental aerosol, and fractionated fulvic acid. Complex refraction behavior was observed and absorption increased in the direction of the UV-range as molecular weight and aromaticity increased; HULIS from pollution and smoke absorbed more light than rural aerosol HULIS and absorbed light in both the visible and UV regions (78). When HULIS absorption is accounted for in sensitivity calculations of aerosol radiative effects, single scattering albedo is significantly lowered and aerosol radiative forcing efficiency is increased, implying more atmospheric absorption and heating (78).

The effects of HULIS on aerosol-radiation interactions is poorly constrained but may be heavily influenced by the ability of self-assembling organic aggregates (pseudomicelles) to form in solution when solute concentrations exceed some critical threshold (similar to what has been observed for humic substances in solution (5));. As suggested by Tabazadeh (8), the presence of HULIS-derived amphiphilic substances and the concomitant potential for HULIS to form pseudomicelles or (depending on solution concentration) colloids in aerosol droplets could have important consequences for atmospheric chemistry/cloud properties via light-particle interactions as pseudomicelles increase droplet turbidity. Tabazadeh (8) also surmised that micelle formation would limit the ability of surface-active organics in aerosols to reduce the surface tension beyond 10 dyne/cm, and that these molecules enhance water uptake under dry conditions and reduce water uptake under humid conditions, as well as affect pollutant processing (see below). Despite the potential for aerosol effects on both radiative forcing and atmospheric chemistry by HULIS-derived organic aggregates, no studies that we are aware of have examined these effects in aerosol to date.

Ecological and Epidemiological Impacts of HULIS

Ecological influences of HULIS may be widespread across ecosystems, but difficult to observe because of the overprinting effects of catchment-derived terrestrial and microbial organic inputs (59). In remote and alpine (above treeline) ecosystems, which are often limited in terms of catchment inputs of organic matter, the influence of HULIS is more evident. In alpine lakes atmospheric inputs of organic aerosols associated with Saharan dust have been found to influence the pool of dissolved organic matter and biogeochemical processes in the water column (81, 82). Mladenov et al. (83) uncovered new evidence that significant latitudinal trends in dissolved organic matter quantity and quality were influenced

by dust deposition, flux of incident UV, and bacterial processing. Therefore, changes in land use and climate that result in increasing dust fluxes, UV, and air temperature may act to shift optical quality of DOC in alpine lakes. Atmospheric deposition also is an important input to barren soils in alpine catchments. In an alpine watershed of the Rocky Mountains, Colorado, wet deposition (9.9 kg C ha⁻¹ yr⁻¹) and dry deposition (6.9 kg C ha⁻¹ yr⁻¹) were a combined input of approximately 17 kg C ha⁻¹ yr⁻¹, which could be as high as 24 kg C ha⁻¹ yr⁻¹ in high dust years (84).

It was postulated that, given the role of humic substances in complexation of metals and organic pollutants, HULIS might perform similar functions in the atmosphere (8), although up to the 2006 HULIS review by Gruber and Rudich, only scant, indirect evidence of HULIS colloidal properties such as complexation with metals was available: extensive complexation was inferred for fog water by Gelencser et al. (85) and for rainwater by Spokes et al. (86). The presence of HULIS-derived pseudomicelles in aerosol could allow for the solubilization (and subsequent protection against oxidation) of hydrophobic organic pollutants (8). Although there are only a few recent reports available to date on this subject, it appears that HULIS does indeed contain numerous chemical sites that can serve as ligands where complexation with transition metals can and does occur, thus potentially influencing atmospheric metal redox chemistry, aerosol solubility and oxidative potential as well as human health effects from aerosol exposure (87, 88). HULIS extracted from wood burning and urban pollution enhanced aqueous phase oxidation of model organic contaminants by promoting the dark Fenton reaction, an important reaction for understanding in-cloud degradation of organic pollutants and for understanding the oxidation state of Fe (89). Dark Fenton oxidation was clearly enhanced in the presence of HULIS; HULIS and humic substances were equally as effective at accelerating the rate of pyrene oxidation, and while the initial rate of pyrene oxidation from daytime pollution aerosol was somewhat lower, the extent of oxidation was essentially the same (89). It was also noted that this process could involve low valency transition metals (e.g., Cu, Co, Mn, etc.), and observed that humic acids with copper ions produced more hydroxyl radical than with Fe ions (89).

Lin and Yu (88) observed that WSOC-derived HULIS (from rural and suburban aerosol) was the dominant redox active constituent of aerosol WSOC and can mediate the generation of reactive oxygen species (ROS) which cause oxidative stress and cell death in exposed cells. The ROS activity of the WSOC HULIS was 2% of that of a reference quinone compound, but was higher than the ROS activity of two different fulvic acid standards (88). Verma et al. (90) quantified the relative contributions to total ROS activity of fine aerosol-derived water soluble and insoluble compounds and their hydrophilic and hydrophobic subfractions. Hydrophobic subfractions of both water soluble and insoluble components made up a large portion of total PM oxidative potential, while insoluble compounds were significantly more ROS active than water-soluble materials. ROS activity was also correlated with soluble and insoluble organic carbon contents of the soluble and insoluble fractions, respectively, and with brown carbon (which is indicative of HULIS) in both fractions (90).

Conclusions and Future Research Directions

In the last decade, much has been learned about the formation of atmospheric HULIS/HMWOA while recent advancements in analytical capabilities offer numerous as yet unexplored opportunities to further characterize these substances. It's now well-accepted that HULIS are formed mainly through secondary oxidation of gaseous biogenic and anthropogenic precursors followed by oligomerization or polymerization reactions and atmospheric aging but can also be directly emitted e.g., from biomass burning smoke or airborne soil. There are large seasonal and spatial variations in HULIS both in terms of concentration as well as chemical and optical characteristics. The diverse sources and ever-changing nature of HULIS make determinations of its radiative forcing, light scattering, and cloud or ice nucleating effects difficult. Since essentially all of the radiative forcing effects of HULIS would theoretically be heavily influenced by the potential for pseudomicelle formation by HULIS in ambient aerosol solutions, future research into the likelihood of this phenomenon under ambient atmospheric conditions would be relevant.

Recent evidence shows that HULIS is present world-wide and in both fine and coarse aerosol size fractions and can impact water optical qualities and nutrient cycling in some nutrient-limited ecosystems, form complexes with metals or organic pollutants, and generate reactive oxygen species, which can harm exposed cells such as lung cells. Additional characterization of especially the hydrophobic organic aerosol fraction and isolated HULIS with respect to sources and toxicity is needed for a better understanding of the toxicological effects and magnitude of potential impacts. Emphasis should be placed on understanding the redox effects of these atmospheric components as well as on their relationships with metals. There is a clear need for an improved understanding of the vertical distribution of HULIS/LV/HMWOA as well as how this fraction of aerosol interacts with UV light and affects cloud properties. Future investigations might also explore whether HULIS has other ecological impacts and how these might change under scenarios of shifting climate and air quality. These lingering questions heighten uncertainties regarding aerosol climate forcing characteristics and effects on ecosystems and health; the knowledge gap is particularly large for coarse-mode PM. Future research might also benefit from application of recently-developed surface ionization techniques coupled with tandem HRMS to the characterization of HULIS and LV/HMWOA.

References

1. Saxena, P.; Hildemann, L. M. Water-soluble organics in atmospheric particles: a critical review of the literature and application of thermodynamics to identify candidate compounds. *J. Atmos. Chem.* **1996**, *24*, 57–109.
2. Likens, G. E.; Galloway, J. N. The composition and deposition of organic carbon in precipitation. *Tellus* **1983**, *35B*, 16–24.
3. Feng, J. S.; Moller, D. Characterization of water-soluble macro-molecular substances in cloud water. *J. Atmos. Chem.* **2004**, *48*, 217–233.

4. Havers, N.; Burba, P.; Lambert, J.; Klockow, D. Spectroscopic characterization of humic-like substances in airborne particulate matter. *J. Atmos. Chem.* **1998**, *29*, 45–54.
5. Gruber, E. R.; Rudich, Y. Atmospheric HULIS: How humic-like are they? A comprehensive and critical review. *Atmos. Chem. Phys.* **2006**, *6*, 729–753.
6. Jimenez, J. L.; Canagaratna, M. R.; Donahue, N. M.; Prevot, A. S. H.; Zhang, Q.; Kroll, J. H.; DeCarlo, P. F.; Allan, J. D.; Coe, H.; Ng, N. L.; Aiken, A. C.; Docherty, K. S.; Ulbrich, I. M.; Grieshop, A. P.; Robinson, A. L.; Duplissy, J.; Smith, J. D.; Wilson, K. R.; Lanz, V. A.; Hueglin, C.; Sun, Y. L.; Tian, J.; Laaksonen, A.; Raatikainen, T.; Rautiainen, J.; Vaattovaara, P.; Ehn, M.; Kulmala, M.; Tomlinson, J. M.; Collins, D. R.; Cubison, M. J.; Dunlea, E. J.; Huffman, J. A.; Onasch, T. B.; Alfarra, M. R.; Williams, P. I.; Bower, K.; Kondo, Y.; Schneider, J.; Drewnick, F.; Borrmann, S.; Weimer, S.; Demerjian, K.; Salcedo, D.; Cottrell, L.; Griffin, R.; Takami, A.; Miyoshi, T.; Hatakeyama, S.; Shimono, A.; Sun, J. Y.; Zhang, Y. M.; Dzepina, K.; Kimmel, J. R.; Sueper, D.; Jayne, J. T.; Herndon, S. C.; Trimborn, A. M.; Williams, L. R.; Wood, E. C.; Middlebrook, A. M.; Kolb, C. E.; Baltensperger, U.; Worsnop, D. R. Evolution of organic aerosols in the atmosphere. *Science (Washington DC, United States)* **2009**, *326*, 1525–1529.
7. Kroll, J. H.; Seinfeld, J. H. Chemistry of secondary organic aerosol: formation and evolution of low-volatility organics in the atmosphere. *Atmos. Environ.* **2008**, *42*, 3593–3624.
8. Tabazadeh, A. Organic aggregate formation in aerosols and its impact on the physicochemical properties of atmospheric particles. *Atmos. Environ.* **2005**, *39*, 5472–5480.
9. Simoneit, B. R. T.: Eolian particulates from oceanic and rural areas— their lipids, fulvic and humic acids and residual carbon. In *Advances in Organic Geochemistry*; Douglas, A. G., Maxwell, J. R., Eds.; Pergamon Press: Oxford, U.K., 1980; pp 343–352.
10. Mukai, H.; Ambe, Y. Characterization of a humic acid-like brown substance in airborne particulate matter and tentative identification of its origin. *Atmos. Environ.* **1986**, *20*, 813–819.
11. Thurman, E. M.; Malcolm, R. L. Preparative isolation of aquatic humic substances. *Environ. Sci. Technol.* **1981**, *15*, 463–466.
12. Vione, D.; Maurino, V.; Minero, C. Photosensitised humic-like substances (HULIS) formation processes of atmospheric significance: A review. *Environ. Sci. Pollut. R.* **2013** doi:10.1007/s11356-013-2319-0.
13. Subbalakshmi, Y.; Patti, A. F.; Lee, G. S. H.; Hooper, M. A. Structural characterisation of macromolecular organic material in air particulate matter using Py-GC-MS and solid state C-13-NMR. *J. Environ. Monitor.* **2000**, *2*, 561–565.
14. Duarte, R.; Pio, C. A.; Duarte, A. C. Spectroscopic study of the water-soluble organic matter isolated from atmospheric aerosols collected under different atmospheric conditions. *Anal. Chim. Acta.* **2005**, *530*, 7–14.
15. Sannigrahi, P.; Sullivan, A. P.; Weber, R. J.; Ingall, E. D. Characterization of water-soluble organic carbon in urban atmospheric aerosols using solid-state C-13 NMR spectroscopy. *Environ. Sci. Technol.* **2006**, *40*, 666–672.

16. Andracchio, A.; Cavicchi, C.; Tonelli, D.; Zappoli, S. A new approach for the fractionation of water-soluble organic carbon in atmospheric aerosols and cloud drops. *Atmos. Environ.* **2002**, *36*, 5097–5107.
17. Surratt, J. D.; Gómez-González, Y.; Chan, A. W. H.; Vermeylen, R.; Shahgholi, M.; Kleindienst, T. E.; Edney, E. O.; Offenberg, J. H.; Lewandowski, M.; Jaoui, M.; Maenhaut, W.; Claeys, M.; Flagan, R. C.; Seinfeld, J. H. Organosulfate formation in biogenic secondary organic aerosol. *J. Phys. Chem. A* **2008**, *112*, 8345–8378.
18. Altieri, K. E.; Seitzinger, S. P.; Carlton, A. G.; Turpin, B. J.; Klein, G. C.; Marshall, A. G. Oligomers formed through in-cloud methylglyoxal reactions: Chemical composition, properties, and mechanisms investigated by ultra-high resolution FT-ICR mass spectrometry. *Atmos. Environ.* **2008**, *42*, 1476–1490.
19. Duarte, R. M. B. O.; Santos, E. B. H.; Pio, C. A.; Duarte, A. C. Comparison of structural features of water-soluble organic matter from atmospheric aerosols with those of aquatic humic substances. *Atmos. Environ.* **2007**, *41*, 8100–8113.
20. Chin, Y.-P.; Alken, G.; O'Loughlin, E. Molecular weight, polydispersity, and spectroscopic properties of aquatic humic substances. *Environ. Sci. Technol.* **1994**, *28*, 1853–1858.
21. Schmidt, M. W. I.; Torn, M. S.; Abiven, S.; Dittmar, T.; Guggenberger, G.; Janssens, I. A.; Kleber, M.; Kögel-Knabner, I.; Lehmann, J.; Manning, D. A.; Nannipieri, P.; Rasse, D. P.; Weiner, S.; Trumbore, S. E. Persistence of soil organic matter as an ecosystem property. *Nature (New York)* **2011**, *478*, 49–56.
22. Krivácsy, Z.; Gelencser, A.; Kiss, G.; Meszaros, E.; Molnar, A.; Hoffer, A.; Meszaros, T.; Sarvari, Z.; Temesi, D.; Varga, B.; Baltensperger, U.; Nyeki, S.; Weingartner, E. Study on the chemical character of water soluble organic compounds in fine atmospheric aerosol at the Jungfraujoch. *J. Atmos. Chem.* **2001**, *39*, 235–259.
23. Kiss, G.; Tombacz, E.; Varga, B.; Alsberg, T.; Persson, L. Estimation of the average molecular weight of humic-like substances isolated from fine atmospheric aerosol. *Atmos. Environ.* **2003**, *37*, 3783–3794.
24. Samburova, V.; Kalberer, M.; Zenobi, R. Characterization of high molecular weight compounds in urban atmospheric particles. *Atmos. Chem. Phys.* **2005**, *5*, 2163–2170.
25. Samburova, V.; Szidat, S.; Hueglin, C.; Fisseha, R.; Baltensperger, U.; Zenobi, R.; Kalberer, M. Seasonal variation of high molecular weight compounds in the water-soluble organic fraction of urban aerosols. *J. Geophys. Res.: Atmos.* **2005**, *110* (D23), D23210.
26. Mawhinney, D. B.; Rosario-Ortiz, F. L.; Baik, S.; Vanderford, B. J.; Snyder, S. A. Characterization of fulvic acids by liquid chromatography-quadrupole time-of-flight mass spectrometry. *J. Chromatogr. A* **2009**, *1216*, 1319–1324.
27. Nizkorodov, S. A.; Laskin, J.; Laskin, A. Molecular chemistry of organic aerosols through the application of high resolution mass spectrometry. *Phys. Chem. Chem. Phys.* **2011**, *13*, 3561–4164.

28. Laskin, J.; Laskin, A.; Roach, P. J.; Slysz, G. W.; Anderson, G. A.; Nizkorodov, S. A.; Bones, D. L.; Nguyen, L. Q. High-resolution desorption electrospray ionization mass spectrometry for chemical characterization of organic aerosols. *Anal. Chem.* **2010**, *82*, 2048–2058.
29. Stenson, A. C.; Landing, W. M.; Marshall, A. G.; Cooper, W. T. Ionization and fragmentation of humic substances in electrospray ionization Fourier transform-ion cyclotron resonance mass spectrometry. *Anal. Chem.* **2002**, *74*, 4397–4409.
30. Reemtsma, T.; These, A. On-line coupling of size exclusion chromatography with electrospray ionization-tandem mass spectrometry for the analysis of aquatic fulvic and humic acids. *Anal. Chem.* **2003**, *75*, 1500–1507.
31. Rostad, C. E.; Leenheer, J. A. Factors that affect molecular weight distribution of Suwannee river fulvic acid as determined by electrospray ionization/mass spectrometry. *Anal. Chim. Acta.* **2004**, *523*, 269–278.
32. Bones, D. L.; Henricksen, D. K.; Mang, S. A.; Gonsior, M.; Bateman, A. P.; Nguyen, T. B.; Cooper, W. J.; Nizkorodov, S. A. Appearance of strong absorbers and fluorophores in limonene-O₃ secondary organic aerosol due NH₄⁺-mediated chemical aging over long time scales. *J. Geophys. Res.* **2010**, *115*, D05203.
33. Lee, H. J.; Laskin, A.; Laskin, J.; Nizkorodov, S. A. Excitation-emission spectra and fluorescence quantum yields for fresh and aged biogenic secondary organic aerosols. *Environ. Sci. Technol.* **2013**, *47*, 5763–5770.
34. Nguyen, T. B.; Lee, P. B.; Updyke, K. M.; Bones, D. L.; Laskin, J.; Laskin, A.; Nizkorodov, S. A. Formation of nitrogen- and sulfur-containing light-absorbing compounds accelerated by evaporation of water from secondary organic aerosols. *J. Geophys. Res.* **2012**, *117*, D01207.
35. Updyke, K. M.; Nguyen, T. B.; Nizkorodov, S. A. Formation of brown carbon via reactions of ammonia with secondary organic aerosols from biogenic and anthropogenic precursors. *Atmos. Environ.* **2012**, *63*, 22–31.
36. Went, F. W. Blue Hazes in the Atmosphere. *Nature (London, United Kingdom)* **1960**, *187*, 641–643.
37. Heald, C. L.; Henze, D. K.; Horowitz, L. W.; Feddema, J.; Lamarque, J.-F.; Guenther, A.; Hess, P. G.; Vitt, F.; Seinfeld, J. H.; Goldstein, A. H.; Fung, I. Predicted change in global secondary organic aerosol concentrations in response to future climate, emissions, and land use change. *J. Geophys. Res.* **2008**, *113*, D05211.
38. Bateman, A. P.; Nizkorodov, S. A.; Laskin, J.; Laskin, A. Time-resolved molecular characterization of limonene/ozone aerosol using high-resolution electrospray ionization mass spectrometry. *Phys. Chem. Chem. Phys.* **2009**, *11*, 7931–7942.
39. Heaton, K. J.; Sleighter, R. L.; Hatcher, P. G.; Hall, W. A., IV; Johnston, M. V. Composition domains in monoterpene secondary organic aerosol. *Environ. Sci. Technol.* **2009**, *43*, 7797–7802.
40. Nguyen, T. B.; Bateman, A. P.; Bones, D. L.; Nizkorodov, S. A.; Laskin, J.; Laskin, A. High-resolution mass spectrometry analysis of secondary organic aerosol generated by ozonolysis of isoprene. *Atmos. Environ.* **2010**, *44*, 1032–1042.

41. Nguyen, T. B.; Roach, P. J.; Laskin, J.; Laskin, A.; Nizkorodov, S. A. Effect of humidity on the composition of isoprene photooxidation secondary organic aerosol. *Atmos. Chem. Phys.* **2011**, *11*, 6931–6944.
42. Doezema, L. A.; Longin, T.; Cody, W.; Perraud, V.; Dawson, M. L.; Ezell, M. J.; Greaves, J.; Johnson, K. R.; Finlayson-Pitts, B. J. Analysis of secondary organic aerosols in air using extractive electrospray ionization mass spectrometry (EESI-MS). *RSC Adv.* **2012**, *2*, 2930–2938.
43. Gao, S.; Keywood, M.; Ng, N. L.; Surratt, J.; Varutbangkul, V.; Bahreini, R.; Flagan, R. C.; Seinfeld, J. H. Low-molecular-weight and oligomeric components in secondary organic aerosol from the ozonolysis of cycloalkenes and α -pinene. *J. Phys. Chem. A* **2004**, *108*, 10147–10164.
44. Bahreini, R.; Keywood, M. D.; Ng, N. L.; Varutbangkul, V.; Gao, S.; Flagan, R. C.; Seinfeld, J. H.; Worsnop, D. R.; Jimenez, J. L. Measurements of secondary organic aerosol from oxidation of cycloalkenes, terpenes, and m-xylene using an Aerodyne aerosol mass spectrometer. *Environ. Sci. Technol.* **2005**, *39*, 5674–5688.
45. Lin, P.; Yu, J. Z.; Engling, G.; Kalberer, M. Organosulfates in humic-like substance fraction isolated from aerosols at seven locations in east Asia: A study by ultra-high-resolution mass spectrometry. *Environ. Sci. Technol.* **2012**, *46*, 13118–13127.
46. Reemtsma, T.; These, A.; Venkatachari, P.; Xia, X. Y.; Hopke, P. K.; Springer, A.; Linscheid, M. Identification of fulvic acids and sulfated and nitrated analogues in atmospheric aerosol by electrospray ionization Fourier transform ion cyclotron resonance mass spectrometry. *Anal. Chem.* **2006**, *78*, 8299–8304.
47. Altieri, K. E.; Turpin, B. J.; Seitzinger, S. P. Oligomers, organosulfates, and nitrooxy organosulfates in rainwater identified by ultra-high resolution electrospray ionization FT-ICR mass spectrometry. *Atmos. Chem. Phys.* **2009**, *9*, 2533–2542.
48. Mazzoleni, L. R.; Saranjamour, P.; Dalbec, M. M.; Samburova, V.; Hallar, A. G.; Zielinska, B.; Lowenthal, D. H.; Kohl, S. Identification of water-soluble organic carbon in non-urban aerosols using ultrahigh-resolution FT-ICR mass spectrometry: organic ions. *Environ. Chem.* **2012**, 285–297.
49. Peng, P.; Zhao, J.; Song, J.; Ma, S. Humic acid, kerogen, and black carbon isolated from atmospheric Total Suspended Particulate from Guangzhou, China. *Aerosol Sci. Technol.* **2013**, *47*, 1342–1352.
50. Atkinson, R.; Arey, J. Atmospheric degradation of volatile organic compounds. *Chem. Rev.* **2003**, 4605–4638.
51. Tobias, H. J.; Ziemann, P. J. Thermal desorption mass spectrometric analysis of organic aerosol formed from reactions of 1-Tetradecane and O₃ in the presence of alcohols and carboxylic acids. *Environ. Sci. Technol.* **2000**, *34*, 2105–2115.
52. Garland, R. M.; Elrod, M. J.; Kincaid, K.; Beaver, M. R.; Jimenez, J. L.; Tolbert, M. A. Acid-catalyzed reactions of hexanal on sulfuric acid particles: Identification of reaction products. *Atmos. Environ.* **2006**, *40*, 6863–6878.
53. Szmigielski, R.; Surratt, J. D.; Vermeylen, R.; Szmigielska, K.; Kroll, J. H.; Ng, N. L.; Murphy, S. M.; Sorooshian, A.; Seinfeld, J. H.; Claeys, M. J.

Characterization of 2-methylglyceric acid oligomers in secondary organic aerosol formed from the photooxidation of isoprene using trimethylsilylation and gas chromatography/ion trap mass spectrometry. *J. Mass Spectrom.* **2007**, *42*, 101–116.

- 54. Baduel, C.; Voisin, D.; Jaffrezo, J. L. Seasonal variation of concentrations and optical properties of water soluble HULIS collected in urban environments. *Atmos. Chem. Phys.* **2010**, *10*, 4085–4095.
- 55. Zhao, J.; Peng, P.; Song, J.; Ma, S.; Sheng, G.; Fu, J. Characterization of organic matter in total suspended particles by thermodesorption and pyrolysis-gas chromatography-mass spectrometry. *J. Environ. Sci. (Beijing, China)* **2009**, *21*, 1658–1666.
- 56. Park, S. S.; Cho, S. Y.; Kim, K.-W.; Lee, K.-H.; Jung, K. Investigation of organic aerosol sources using fractionated water-soluble organic carbon measured at an urban site. *Atmos. Environ.* **2012**, *55*, 64–72.
- 57. Samburova, V.; Didenko, T.; Kunenkov, E.; Emmenegger, C.; Zenobi, R.; Kalberer, M. Functional group analysis of high-molecular weight compounds in the water-soluble fraction of organic aerosols. *Atmos. Environ.* **2007**, *41*, 4703–4710.
- 58. Muller, C. L.; Baker, A.; Hutchinson, R.; Fairchild, I. J.; Kidd, C. Analysis of rainwater dissolved organic carbon compounds using fluorescence spectrophotometry. *Atmos. Environ.* **2008**, *42*, 8036–8045.
- 59. Mladenov, N.; Alados-Arboledas, L.; Olmo, F. J.; Lyamani, H.; Delgado, A.; Molina, A.; Reche, I. Applications of optical spectroscopy and stable isotope analyses to organic aerosol source discrimination in an urban area. *Atmos. Environ.* **2011**, *45*, 1960–1969.
- 60. Duhl, T. R.; Hannigan, M. P.; Clements, N.; Department of Mechanical Engineering, University of Colorado, Boulder, CO, 80309; Lee, E.; Rosario-Ortiz, F. L.; Cawley, K. Department of Civil and Environmental Engineering, University of Colorado, Boulder, CO, 80309. Unpublished data.
- 61. Zhang, X.; Liu, Z.; Hecobian, A.; Zheng, M.; Frank, N. H.; Edgerton, E. S.; Weber, R. J. Spatial and seasonal variations of fine particle water-soluble organic carbon (WSOC) over the southeastern United States: implications for secondary organic aerosol formation. *Atmos. Chem. Phys.* **2012**, *12*, 6593–6607.
- 62. Feczkó, T.; Puxbaum, H.; Kasper-Giebl, A.; Handler, M.; Limbeck, A.; Gelencser, A.; Pio, C.; Preunkert, S.; Legrand, M. Determination of water and alkaline extractable atmospheric humic-like substances with the TU Vienna HULIS-analyser in samples from six background sites in Europe. *J. Geophys. Res.* **2007**, *112*, D23S10.
- 63. Huang, X.-F.; Yu, J. Z.; He, L.-Y.; Yuan, Z. Water-soluble organic carbon and oxalate in aerosols at a coastal urban site in China: Size distribution characteristics, sources, and formation mechanisms. *J. Geophys. Res.* **2006**, *111*, D22212.
- 64. Lin, P.; Huang, X.-F.; He, L.-Y.; Yu, J. Z. Abundance and size distribution of HULIS in ambient aerosols at a rural site in South China. *J. Aerosol Sci.* **2010**, *41*, 74–87.

65. Hiranuma, N.; Brooks, S. D.; Gramann, J.; Auvermann, B. W. High concentrations of coarse particles emitted from a cattle feeding operation. *Atmos. Chem. Phys.* **2011**, *11*, 8809–8823.
66. Zheng, G.; He, K.; Duan, F.; Cheng, Y.; Ma, Y. Measurement of humic-like substances in aerosols: a review. *Environ. Pollut.* **2013**, *181*, 301–314.
67. Krivácsy, Z.; Kiss, G.; Ceburnis, D.; Jennings, G.; Maenhaut, W.; Salma, I.; Shooter, D. Study of water-soluble atmospheric humic matter in urban and marine environments. *Atmos. Res.* **2008**, *87*, 1–12.
68. Gysel, M.; Weingartner, E.; Nyeki, S.; Paulsen, D.; Baltensperger, U.; Galambos, I.; Kiss, G. Hygroscopic properties of water-soluble matter and humic-like organics in atmospheric fine aerosol. *Atmos. Chem. Phys.* **2004**, *4*, 35–50.
69. Svenningsson, B.; Rissler, J.; Swietlicki, E.; Mircea, M.; Bilde, M.; Facchini, M. C.; Decesari, S.; Fuzzi, S.; Zhou, J.; Mønster, J.; Rosenørn, T. Hygroscopic growth and critical supersaturations for mixed aerosol particles of inorganic and organic compounds of atmospheric relevance. *Atmos. Chem. Phys.* **2006**, *6*, 1937–1952.
70. Badger, C. L.; George, I.; Griffiths, P. T.; Braban, C. F.; Cox, R. A.; Abbott, J. P. D. Phase transitions and hygroscopic growth of aerosol particles containing humic acid and mixtures of humic acid and ammonium sulfate. *Atmos. Chem. Phys.* **2006**, *6*, 755–768.
71. Dinar, E.; Taraniuk, I.; Gruber, E. R.; Katsman, S.; Moise, T.; Anttila, T.; Mentel, T. F.; Rudich, Y. Cloud Condensation Nuclei properties of model and atmospheric HULIS. *Atmos. Chem. Phys.* **2006**, *6*, 2465–2482.
72. Chan, M. N.; Chan, C. K. Hygroscopic properties of two model humic-like substances and their mixtures with inorganics of atmospheric importance. *Environ. Sci. Technol.* **2003**, *37*, 5109–5115.
73. Brooks, S. D.; DeMott, P. J.; Kreidenweis, S. M. Water uptake by particles containing humic materials and mixtures of humic materials with ammonium sulfate. *Atmos. Environ.* **2004**, *38*, 1859–1868.
74. Facchini, M. C.; Decesari, S.; Mircea, M.; Fuzzi, S.; Loglio, G. Surface tension of atmospheric wet aerosol and cloud/fog droplets in relation to their organic carbon content and chemical composition. *Atmos. Environ.* **2000**, *34*, 4853–4857.
75. Kiss, G.; Tombacz, E.; Hansson, H.-C. Surface tension effects of humic-like substances in the aqueous extract of tropospheric fine aerosol. *J. Atmos. Chem.* **2005**, *50*, 279–294.
76. Negre, M.; Vindrola, D.; Spera, S.; Ferraris, L.; Gennari, M. Effect of the chemical composition of soil humic acids on their viscosity, surface pressure, and morphology. *Soil Sci.* **2002**, *167*, 636–651.
77. Asa-Awuku, A.; Sullivan, A. P.; Hennigan, C. J.; Weber, R. J.; Nenes, A. Investigation of molar volume and surfactant characteristics of water-soluble organic compounds in biomass burning aerosol. *Atmos. Chem. Phys.* **2008**, *8*, 799–812.
78. Dinar, E.; Abo Riziq, A.; Spindler, C.; Erlick, C.; Kiss, G.; Rudich, Y. The complex refractive index of atmospheric and model humic-like substances

(HULIS) retrieved by a cavity ring down aerosol spectrometer (CRD-AS). *Faraday Discuss.* **2008**, *137*, 279–295.

79. Baduel, C.; Voisin, D.; Jaffrezo, J. L. Comparison of analytical methods for Humic Like Substance (HULIS) measurements in atmospheric particles. *Atmos. Chem. Phys.* **2009**, *9*, 5949–5962.
80. Hoffer, A.; Gelencser, A.; Guyon, P.; Kiss, G.; Schmid, O.; Frank, G. P.; Artaxo, P.; Andreae, M. O. Optical properties of humic-like substances (HULIS) in biomass-burning aerosols. *Atmos. Chem. Phys.* **2006**, *6*, 3563–3570.
81. Mladenov, N.; Pulido-Villena, E.; Morales-Baquero, R.; Ortega-Retuerta, E.; Sommaruga, R.; Reche, I. Spatiotemporal drivers of dissolved organic matter in high alpine lakes: Role of Saharan dust inputs and bacterial activity. *J. Geophys. Res.* **2008**, *113*, G00D01.
82. Mladenov, N.; López-Ramos, J.; McKnight, D. M.; Reche, I. Alpine lake optical properties as sentinels of dust deposition and global change. *Limnol. Oceanogr.* **2009**, *54*, 2386–2400.
83. Mladenov, N.; Sommaruga, R.; Morales-Baquero, R.; Laurion, I.; Camarero, L.; Diéguez, M. C.; Camacho, A.; Delgado, A.; Torres, O.; Chen, Z.; Felip, M.; Reche, I. Dust inputs and bacteria influence dissolved organic matter in clear alpine lakes. *Nat. Commun.* **2011**, *2*, 405.
84. Mladenov, N.; Williams, M. W.; Schmidt, S. K.; Cawley, K. Atmospheric deposition as a source of carbon and nutrients to an alpine catchment of the Colorado Rocky Mountains. *Biogeosciences* **2012**, *9*, 3337–3355.
85. Gelencser, A.; Sallai, M.; Krivácsy, Z.; Kiss, G.; Meszaros, E. Voltammetric evidence for the presence of humic-like substances in fog water. *Atmos. Res.* **2000**, *54*, 157–165.
86. Spokes, L. J.; Campos, M.; Jickells, T. D. The role of organic matter in controlling copper speciation in precipitation. *Atmos. Environ.* **1996**, *30*, 3959–3966.
87. Chang-Graham, A. L.; Profeta, L. T. M.; Johnson, T. J.; Yokelson, R. J.; Laskin, A.; Laskin, J. Case study of water-soluble metal containing organic constituents of biomass burning aerosol. *Environ. Sci. Technol.* **2011**, *45*, 1257–1263.
88. Lin, P.; Yu, J. Z. Generation of reactive oxygen species mediated by humic-like substances in atmospheric aerosols. *Environ. Sci. Technol.* **2011**, *45*, 10362–10368.
89. Moonshine, M.; Rudich, Y.; Katsman, S.; Gruber, E. R. Atmospheric HULIS enhance pollutant degradation by promoting the dark Fenton reaction. *Geophys. Res. Lett.* **2008**, *35*, L20807.
90. Verma, V.; Rico-Martinez, R.; Kotra, N.; King, L.; Liu, J.; Snell, T. W.; Weber, R. J. Contribution of water-soluble and insoluble components and their hydrophobic/hydrophilic subfractions to the reactive oxygen species-generating potential of fine ambient aerosols. *Environ. Sci. Technol.* **2012**, *46*, 11384–11392.

Chapter 6

NOM as Natural Xenobiotics

Christian E. W. Steinberg*

Faculty of Mathematics and Natural Sciences I, Institute of Biology,
Laboratory of Freshwater & Stress Ecology, Humboldt-Universität zu
Berlin, Arboretum, Späthstr. 80/81, 12437 Berlin, Germany

*E-mail: christian_ew_steinberg@web.de.

In all ecosystems, natural organic matter (NOM) comprises the major reservoir of organic carbon and contains a high proportion of humic substances (HSs). HSs are natural xenobiotics that exert indirect and direct chemical challenges to exposed organisms. Xenobiotics are chemicals that are found in, but are not produced by, an organism. Indirect xenobiotic interactions comprise the release of reactive oxygen species (ROS) from illuminated HSs in aquatic systems that in turn can place oxidative stress on exposed organisms. This oxidative stress can select robust over sensitive species and thereby structure the community, as shown by freshwater bacteria exposed to singlet oxygen. Furthermore, this oxidative stress can reduce the activity of viruses and pathogens and can oxidize various toxins released by cyanobacteria, and thereby reduce the chemical challenge of exposed organisms. Within freshwater phytoplankton, cyanobacteria appear to be more sensitive to such chemical stress than eukaryotic phototrophs. Due to the low persistence of polyphenols in eutrophic alkaline waters, it is questionable whether these xenobiotic NOM compounds are really effective.

Not all stress-responses of exposed organisms are adverse. For instance, due to the coevolution of plants and soil organic matter, HSs interact with higher plants by activating genes and complex regulation, resulting in increased stress resistance. One major phenotypic result of this interaction is the remodeling of root morphology, leading to an increased absorptive surface of

the root, which mycorrhizal fungi can attack and colonize. Most plants possess mycorrhiza that enable them to efficiently take up nutrients.

Exposed animals also respond to NOM on the gene, protein, and metabolic level. Low-molecular weight NOM can be internalized and can provoke oxidative stress, because animals attempt to rid themselves of natural xenobiotics. However, this oxidative stress can lead to an increased lifespan, body size, and offspring number, hence, stabilizing exposed populations. Another NOM-mediated population-stabilizing mechanism is the acquisition of multiple stress resistances where one stressor prepares the organism for another to cope with adverse effects. Evidence is accumulating that this applies to a variety of natural and anthropogenic environmental stressors, such as variations in osmotic conditions, acidity, or netting and predation. Stress-tolerance can be passed to succeeding generations by epigenetic mechanisms. Other apparently population-stabilizing mechanisms are weak feminization by NOM to reduce the maintenance costs for two separate parental bodies in ecosystems running close to their carrying capacity.

Several Quantitative-Structure-Activity-Relationships (QSAR) have shown that particularly phenolic, quinoid, and stable organic radicals account for various effects in organisms exposed to NOM, irrespective of its origin. The QSAR could be confirmed in tests with the nematode *Caenorhabditis elegans* by enriching a given HS-preparation artificially with hydroxybenzenes.

Overall, it appears that NOM is a major driving force of ecosystem functions, and we are only beginning to appreciate its ecological significance.

Introduction

In all ecosystems on earth, natural organic matter (NOM) is the major carbon reservoir, exceeding the total amount in living organisms. For instance, in oligotrophic freshwater ecosystems, with a dissolved organic carbon (DOC) concentration between 1 and 100 mg L⁻¹ and maximum values of 150 to 300 mg L⁻¹ (1, 2), NOM exceeds the amount of organic carbon in all living organisms by roughly one order of magnitude (3). NOM is a mixture of natural chemicals, mainly humic substances (HSs). Furthermore, on a global scale with huge geological formations, such as the bedrock shields in the Northern Hemisphere or the nutrient-poor regions in the tropics, non-calcareous, HS-rich freshwater type appears to predominate over calcareous, HS-poor ones (3). Practically all freshwater systems contain some NOM of allochthonous and certainly of autochthonous, origin (4).

Many studies deal with the interaction of NOM or HSs with xenobiotic chemicals and/or heavy metals and show a natural attenuation/quenching of potentially adverse chemicals (4, 5). The opposite occurs with metals that would not be bioavailable under prevailing toxic and circumneutral or slightly alkaline conditions: these metals, particularly Fe, are rendered bioavailable (6, 7). Furthermore, HSs can adversely impact the underwater light climate (8–12), reduce primary production (9) and subsequently the richness of herbivorous zooplankton (13). These issues, however, are not the focus of this study, which instead considers indirect and direct xenobiotic interactions with organisms. In this chapter, xenobiotics are understood as natural or synthetic chemicals that are found in or on an organism, but that are not normally produced by or expected to be present within it.

It is a fact that HSs are chemicals themselves, namely natural xenobiotic chemicals (14) and have the potential to indirectly and directly interact with organisms. Even low HS concentrations, typical of so-called clear-water lakes, interact with organisms (15). What kind of interactions are known so far and how do these interactions translate into individual and population integrity? Do HSs stabilize or destabilize populations? Does the HS-stress favor only euryoecious species that can survive virtually anywhere? Or is the stress by these natural xenobiotics a means to stabilize populations under fluctuating environmental conditions?

This study focuses on:

- NOM as a modulator of redox regimes;
- NOM as a means against harmful phototrophs;
- NOM interactions with higher plants;
- NOM interactions with animals;
- Do NOM origin and quality matter?

This study will pay particular, but not exclusive, attention to freshwater systems. However, we assume that many findings can be generalized and will apply to organisms and populations from other habitats.

NOM as a Modulator of Redox Regimes

Due to hydrophobic domains in its components (16), NOM can directly interact with bacteria and viruses, particularly with their membranes (17). The major fraction of NOM, which are HSs, have been shown to protect fish against bacterial pathogens by oral administration (Figure 1). However, it remains unclear whether this antibacterial activity is combined with an effect on bacterial membranes (18, 19) or with the acquisition of multiple stress resistance (20) (see below).

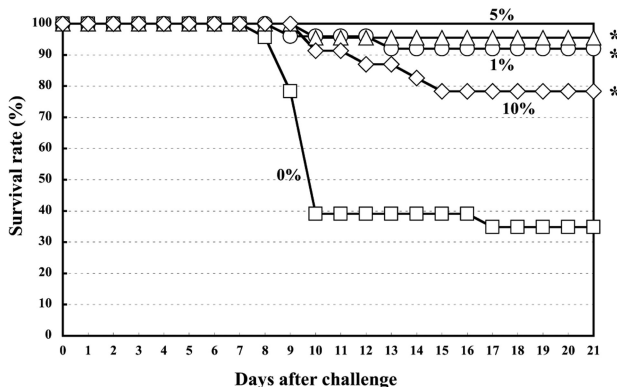


*Figure 1. Survival of ayu fish (*Plecoglossus altivelis*) challenged with *Flavobacterium psychrophilum* (cold-water disease) after treatment with 10% (◊), 5% (◇), or 1% (○) HS extract. The extract was administered for 30 days orally as a dry pellet (2% of total body weight per day) with or without (□) extract. Survival rates of fish in the HS-treated groups were significantly greater than in the control group. * = significant at $p < 0.01$ by the χ^2 test. Reproduced from ref. (18). Copyright 2009 Japanese Society of Veterinary Science.*

It has long been understood from medical studies that HSs display antiviral activity (21) against human pathogens, although the underlying mechanisms remain unclear. Recently, Posselt (22) extended this knowledge to aquaculture by studying the HS-mediated inactivation of koi herpes viruses. He reported that in the presence of various HSs and increasing concentrations, decreased intensities of infection, reduced virus DNA contents, and decreased virus counts occurred. Antiviral activity was also found with viruses from lake samples that were treated with fulvic acids (23). Because these experiments (22, 23) were carried out in darkness, an indirect photolytic mechanism can be excluded and a direct antiviral activity of HSs can not be ruled out. However, most interactions documented so far appear to be indirect.

Since the pioneering work of Zepp, et al. (24) and Cooper and Zika (25), it is known that illuminated HSs release a variety of reactive oxygen species and thereby change ambient redox conditions. Thus, they have the ability to indirectly structure the biocenoses as shown only in a few studies so far: for instance, with various *Daphnia* (Cladocera) species (26) and with freshwater bacteria (27, 28). Some HSs exhibited a slight antibiotic activity (29). ROS might act as a disinfectant towards pathogens as found by Liltved & Landfald (30) with the fish pathogenic bacteria *Aeromonas salmonicida* and *Vibrio anguillarum*. In contrast to Liltved & Landfald (30), Schreckenbach et al. (31) did not observe any growth inhibition of the fish-pathogenic bacteria *Aeromonas hydrophila*, *Pseudomonas fluorescens*, and *P. putida* in the presence of a synthetic HS preparation. It can be assumed that various laboratories applied HSs with different abilities to affect

bacterial growth. To obtain a detailed insight into a potential mode of action, a broader data base is required, with the aim to find a QSAR that statistically identifies the effective structures in the applied HSs.

Recently, singlet oxygen released from the illuminated NOM of a small humic lake (32) was identified as a neglected but important ecological driving force (27). The authors showed that bacterioplankton phylotypes favoured under moderate $^1\text{O}_2$ exposure, belonged to β -proteobacteria of the beta II cluster (e.g., *Polynucleobacter necessarius*) and to the beta I cluster related to *Limnohabitans* as well as to α -proteobacteria affiliated to *Novosphingobium acidiphilum*. In contrast, *Actinobacteria* of the freshwater acI-B cluster were sensitive even to moderate $^1\text{O}_2$ exposure. A subsequent study confirmed that UV in the presence of NOM selected for specific members of α -proteobacteria, β -proteobacteria, and Bacteriodetes (28).

It is highly probable that an oxidative stress mechanism in HS-containing water bodies controls the composition and abundance of viruses. This has recently been confirmed in a study that investigated the inactivation of two human viruses and two bacteriophages by sunlight in an array of coastal waters (33). When exposed to full-spectrum sunlight, the presence of photosensitizers increased the observed inactivation rates of three out of four viruses tested.

These findings provide evidence that the exogenous sunlight inactivation mechanism, involving damage by exogenously produced ROS, play a large role for the three viruses. Sunlight transforms the singlet groundstate of NOM (^1NOM) to its excited triplet state ($^3\text{NOM}^*$) that releases ROS. Inactivation of the fourth virus was observed to be regulated by endogenous mechanisms. These inactivation pathways are presented schematically in Figure 2.

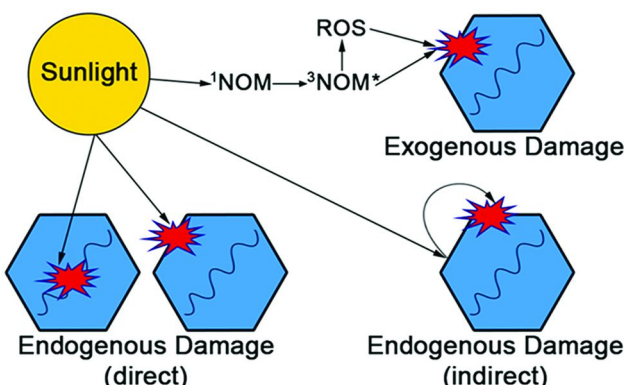


Figure 2. Scheme of direct and indirect sunlight inactivation of human viruses and bacteriophages in coastal waters containing natural photosensitizers.
Reproduced from ref. (33). Copyright 2013 ACS.

The ROS released from illuminated HSs not only attack viruses and organisms, but also oxidize any chemical compound that they encounter. By this means, HSs initiate indirect photolysis of the compound. In eutrophicated water bodies with blooms of harmful phototrophs, several of the encountered compounds are so-called allelochemicals—chemicals via which organisms of one species adversely affect the growth, health, behavior, or population biology of individuals of another species (34). In other words, allelochemicals are strong weapons against competitors, predators and non-target organisms. In aquatic systems, toxins are released from cyanobacteria (e.g., microcystins, cylindrospermopsin, anatoxin, saxitoxin), marine dinoflagellates (e.g., saxotoxin, brevetoxin), marine red algae and diatoms (domoic acid). Whereas a few toxins are directly photolabile, most require the presence of photosensitizers, such as HSs. Microcystin-LR (35), brevetoxin (36), or cylindrospermopsin (37) are allelochemicals. The degradation of cylindrospermopsin (CYN), an alkaloid guanidinium sulfated toxin, has recently been studied in detail and the ROS involved were identified (37) (Figure 3). Direct photolysis did not take place, but only HS-mediated indirect photolysis.

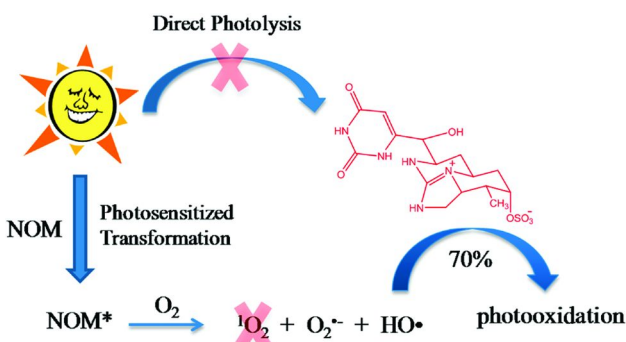
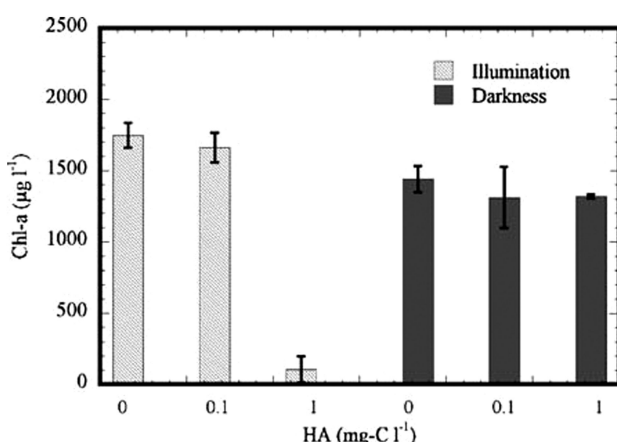


Figure 3. Cartoon of the photosensitized degradation of cylindrospermopsin. Excited NOM transfers its energy to oxygen that releases ROS. From ROS, hydroxyl radicals (HO^\bullet) appear to be most effective. Reproduced from ref. (37). Copyright 2012 ACS.

Product analyses indicated that the major products from the reaction of hydroxyl radicals with CYN involve attack of the hydroxyl radical (HO^\bullet) at the uracil ring and hydrogen abstraction from the hydroxy-methine bridge. The role of hydroxyl radical-initiated pathways in the NOM-photosensitized transformation of CYN accounted for approximately ~70% of CYN destruction in surface waters under solar irradiation in the presence of NOM. Singlet oxygen did not play a significant role in the NOM-sensitized transformation of CYN.

Overall, the role of illuminated NOM (HSs) appears to be two-fold. Firstly, ROS released from solar radiation can attack organisms directly, thereby separating robust species from sensitive species. Secondly, photo-products such as HO• can protect organisms by initiating indirect photolysis of harmful allelochemicals, such as cyanotoxins.

If NOM in general, and HSs in particular, are internalized, even the internal redox homeostasis of organisms will be drastically altered, because these substances are natural xenobiotics (14) and the organisms attempt to rid themselves of these metabolically. For instance, Sun, et al. (38) reported that a low concentration of a commercial humic acid (HA) preparation was effective in slightly reducing the cell yield of the cyanobacterium *Anabaena circinalis*. In a subsequent paper, the authors elucidated the underlying mechanism and reported that light was an important factor for the cell lysis (Figure 4), whereas intracellular H₂O₂ might be the chemical factor for this process (39). Furthermore, the results indicated that HA or its possible photodegradation product(s) can induce damage to the intracellular antioxidant system, which leads to abnormally high concentrations of intracellular H₂O₂, eventually resulting in cell death. The sensitivity of cyanobacteria to HSs might also explain patterns in the field. Thus, eutrophic humic-rich and slightly acidic lakes do not support the cyanobacterial blooms characteristic of eutrophic but humic-poor lakes (40), but humic-rich and alkaline lakes do (41). How this apparent contradiction can be resolved will be discussed in the following paragraphs.



*Figure 4. The effect of humic acid (HA) and light on the growth of *Anabaena circinalis*. All cultures were cultivated for 24 h from the same initial chlorophyll-a concentration under conditions of illumination (open columns) or darkness (closed columns). Values are means \pm SD of triplicate samples. Reproduced from ref. (39). Copyright 2006 Springer.*

The Effect of NOM against Harmful Phototrophs

Massive algal growth in eutrophicated lakes can lead to toxic cyanobacterial blooms and cause risk to wildlife and humans. To reduce these symptoms of eutrophication, several allelochemical strategies have been developed, based on the understanding that many plant secondary metabolites that later form parts of the NOM are effective against competitors (34). To keep treatment expenses low, agricultural byproducts have often been applied, especially barley (42) and rice straw (43).

For many years, polyphenols have been considered as the principal candidate allelochemicals to control cyanobacterial blooms. These chemicals are also thought to stabilize the clear, macrophyte-dominated state of shallow lakes (44). However, these studies on allelopathic action against algal blooms raise one key unanswered question that continues to be disregarded, namely, the persistence of the chemicals if applied under field conditions: What is the environmental fate of the polyphenols released into eutrophic water columns? Are they bioavailable for the phototrophs under discussion?

In eutrophic lakes, the ambient pH strongly modulates the persistence of polyphenolic allelochemicals. Most mechanistic studies have been carried out in the laboratory, often at a pH adjusted to circumneutral values, and extrapolated to field conditions where senders and receivers of allelochemicals are separated by considerable distances and where a moderately alkaline pH prevails. None of the published studies has shown that polyphenols were internalized and adversely affected the phototrophs in the field. In the “omics” age, this can easily be achieved by analyzing the transcribed products of genes that respond to polyphenols (45). Instead, many believe that laboratory findings apply even under field conditions (44). However, upscaling from laboratory trials to field applications is more than a simple magnification of scales; environmental mechanisms also apply. In particular, phototrophs are adversely affected by polyphenols only under circumneutral and slightly acidic pH values (46). However, if the ambient pH rises above 8.3, as is usual in eutrophicated freshwaters where pH-values even above 10.0 are common (47), polyphenol bioavailability and corresponding toxicity is significantly reduced by polymerization – an issue that has been well understood for a long time from studies on the stability of green tea polyphenols (48). In Figure 5, the efficacy of hydroquinone, a polyphenol released by macrophytes (49), is shown to depend on the pH during pre-exposure. Although the toxicity increases with exposure time at pH 7.0, the opposite occurs after pre-exposure at pH 11.0, when hydroquinone loses its toxicity within a few hours.

Recent studies have consistently shown that the long-held assumption has to be reconsidered and that other allelochemicals than polyphenols emerge as candidates and should be checked for stability under eutrophic lake conditions. Among these candidates, particularly alkaloids such as gramine (50) appear to be very promising algicidal compounds (51).

In contrast to unicellular, planktonic phototrophs discussed so far, terrestrial plants can uptake humic material and respond to it even on the transcriptional level.

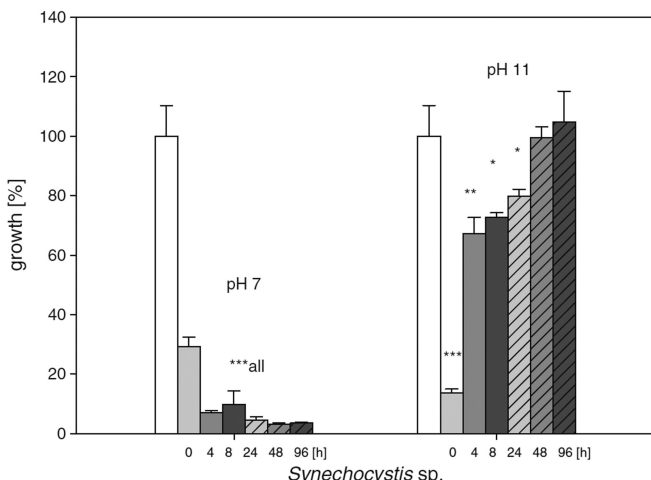


Figure 5. Growth inhibition of the cyanobacterium *Synechocystis* sp., using EC90 values, with hydroquinone pre-exposed at pH 7 (left) or pH 11 (right) for increasing periods of time. Non-hatched columns: white = Control; light gray = 0 h; gray = 4 h; dark gray = 8 h; hatched columns: light gray = 24 h; gray = 48 h; dark gray 96 h. Reproduced from ref. (46). Copyright 2013 Springer.

NOM Interactions with Higher Plants

For thousands of years, the positive effect of humic material on plant growth has been accepted by the observation that dark-colored soils are more productive than light-colored ones (6). Some reasons for this phenomenon are enhanced root growth and the development of secondary roots (52) (Figure 6), a subsequent increased uptake of macronutrients, and an enhanced bioavailability of trace elements, particularly iron (7). The modulated root morphology was at least partly due to the down-regulation of two genes that encode negative regulators of root-hair cell fate (53). The presence of HSs caused a subsequent ordered remodeling of root morphology, and led to an increased absorptive surface of the root (54). Furthermore, the enlarged root surface offers an enlarged space for mycorrhizal fungi to attack and colonize. However, mycorrhizal fungi themselves can be stimulated by HSs to colonize roots and produce extraradical mycelia (29).

It has been hypothesized that HSs might exert positive effects on plant growth and yield through an auxin-like activity (52, 56). Other authors have argued that the enhanced growth is attributable solely to the improved bioavailability of iron and other trace metals (7), since they could not find auxins, cytokinins, abscisic acid, or the transcription of auxin-responsive genes (53) in exposed *Arabidopsis thaliana* plants. Only recently, this controversy has been solved by ‘omics’ studies. For instance, Trevisan et al. (57) demonstrated by real-time quantitative RT-PCR, that the early auxin-responsive *IAA19* gene of *A. thaliana* was up-regulated after 30 min of treatment of *Arabidopsis* with either HSs or 34 nM auxin, and subsequently displayed a decline in transcription after 2 h of treatment with IAA, whereas a

steady increase was detected in the presence of HSs and to a lesser extent, in control plants (Figure 7). The transcription of *IAA19* was rapidly and transiently up-regulated by auxin; however, the lack of down-regulation of *IAA19* after 2 h by HSs might favour the hypothesis that additional factors other than IAA in HSs exist (57). The *IAA5* transcript was not induced by either IAA or HSs (Figure 7).

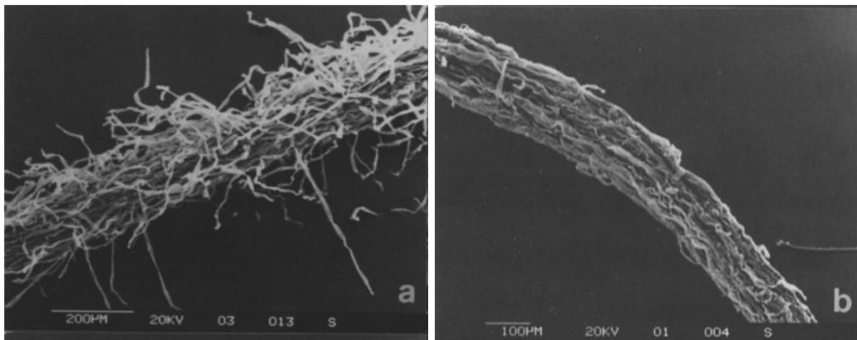


Figure 6. Scanning electron micrographs of seedling surface roots of wheat grown in HS-containing medium ($5 \text{ mg L}^{-1} \text{ C}$) (a) and HS-free medium (b).
Reproduced from ref. (55). Copyright 1996 Springer.

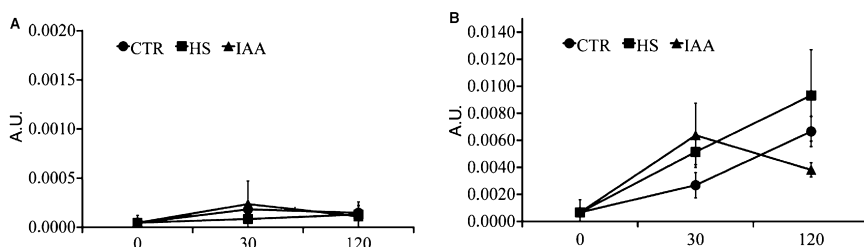


Figure 7. Expression of *IAA5* (A) and *IAA19* (B) in *Arabidopsis* upon exposure to HSs measured by real-time PCR using the *18S* gene as a reference. Seedlings were grown for 4 days on MS plates and then treated with water (CTR), HS (1 mg C L^{-1}) or IAA (34 nM) for 30 min or 2 h. Analyses were carried out in triplicate for each cDNA obtained from two independent RNA extractions. Specific transcript levels are expressed as arbitrary units (AU) of mean normalized expression. Bars represent SE. Reproduced from ref. (57). Copyright 2010 Wiley.

Carletti et al. (58) investigated the changes in expression patterns of root proteins in *Zea mays* seedlings using a proteomic approach and found 42 differentially expressed proteins, the majority of which were down-regulated by HS-treatment. The proteins identified included malate dehydrogenase, ATPases, cytoskeleton proteins, and different enzymes belonging to the glycolytic/gluconeogenic pathways and sucrose metabolism. These differentially regulated proteins were confirmed in *A. thaliana* by a transcriptomic study (59), which identified 133 genes putatively involved in the plant–HS interaction. Sequence analysis and Gene Ontology classification indicated that a large number of genes involved in developmental and metabolic processes, as well as in transcriptional regulation or RNA metabolism were identified as being regulated by HS. This study demonstrated that HSs exert their effects on plant physiology via complex transcriptional networks. From the overall transcriptomic results, we hypothesize that HSs exert their function via a multifaceted mechanism of action, partially connected to their well-demonstrated auxinic activity, but also involving IAA-independent signaling pathways. Overall, HSs functioned as nutrients and interfered with stress response signaling, resulting in increased stress resistance.

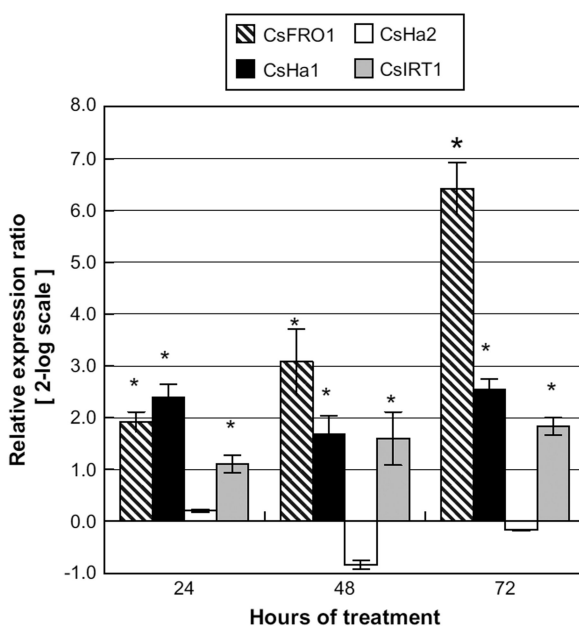


Figure 8. Time-course of the transcriptional expression of plasma membrane H^+ -ATPase genes (*CsHa1* and *CsHa2*), the Fe(III) chelate-reductase (*CsFRO1*), and the Fe(II) root transporter (*CsIRT1*) in apical roots of cucumber plants subjected to Fe deficiency. The values are means of three replicates. The mRNA levels are normalized with respect to the internal control alpha-tubulin; * significant at $p < 0.05$. Reproduced from ref. (60). Copyright 2009 Elsevier Masson.

To demonstrate that HSs not only increase the bioavailability of metals, particularly Fe, Aguirre et al. (60) investigated the effect of HSs that were free of measurable concentrations of the major plant hormones, on the transcriptional regulation of iron assimilation in cucumber plants. The mRNA transcripts of *CsFRO1*, which encodes Fe(III) chelate-reductase; *CsHa1* and *CsHa2* encoding plasma membrane H⁺-ATPases; and *CsIRT1* encoding a Fe(II) high-affinity transporter, were quantified by real-time RT-PCR. The results indicated that HSs-treatments of roots affected the transcriptional regulation of the studied genes, but this effect was transient and differed (up- or down-regulation), depending on the specific gene studied. Thus, higher doses of HSs caused a transient increase in the expression of the *CsHa2* isoform for 24 and 48 h, whereas expression of the *CsHa1* isoform was unaffected or downregulated (Figure 8). These effects were accompanied by an increase in plasma membrane H⁺-ATPase activity. These results emphasize the close relationships between the effects of HSs on plant development and iron nutrition.

NOM Interaction with Animals

High amounts of natural xenobiotic chemicals, particularly HSs, are contained within NOM. Using ¹⁴C-labelled HSs, it was shown that HSs, or at least their low-molecular weight fraction (approximately 0.5 kDa) (61, 62), can be internalized (14) by aquatic organisms. This can occur by uptake via membranes or epithelia and, in the case of animals, via food with adsorbed HSs. This is open to future studies, to identify which pathways prevail in animals.

Only very few organisms use internalized HSs as antioxidants, such as the freshwater macroalga *Chara hispida*, which is characteristic of humic habitats (63). The compost and soil-dwelling *C. elegans* is also able to utilize the antioxidant property of HSs under certain conditions, if exposed to relatively high, but still soil-relevant HS-concentrations (64).

Most organisms and almost all animals, attempt to rid themselves of HSs immediately after uptake, and the “first line of defense” (65) is the ABC-exporter system. However, this defense system might be blocked by dissolved HSs (66) and organisms then have to metabolize the internalized HSs (67–69). Once HSs are internalized, their metabolism begins by the activation of oxygen, releasing several ROS as products and can lead to oxidative stress, including lipid peroxidation, the induction of stress proteins and biotransformation enzymes (70). To overcome this stress, considerable amounts of energy have to be provided (71) and are reallocated from growth, reproduction, or body maintenance. Strikingly, however, the model invertebrate, *Caenorhabditis elegans*, prefers humic-rich and stressful environments, over humic-free environments (64) and benefits from an extended lifespan and increased offspring as long as the chemical stress remains mild (equivalent to 0.2 mM humic DOC). This indicates that not all stress is actually stressful – in contrast, it appears that mild (chemical) stress in the environment, below the mutation threshold, is essential for many subtle manifestations of population structures and biodiversity and might indeed have played a key role in evolution in adverse environments. It appears that due to

the long-term co-evolution of organisms and HSs, organisms have developed various means to reverse the original adverse stress into a positive outcome. Instead, this stress can improve the Darwinian fitness of an organism and is an essential prerequisite for existence in fluctuating environments. Major underlying mechanisms comprise the following physiological and molecular biological effects of HSs and of their major building blocks, natural polyphenols:

- (1) Health-promoting activity: The improved health of aquaculture and ornamental fish in humic-rich waters is well known. Recently, Chakrabarti et al. (72) reported the increased transcription of a major tumor-suppressor gene from the *p53* family in *Caenorhabditis elegans* exposed to HSs from two Brazilian coastal lagoons (Figure 9). Although *C. elegans* does not develop tumors, due to its cell constancy as an adult, it is now well understood that these genes and proteins additionally have multiple positive and stabilizing functions for health. For many species, one potential result of exposure to HSs is a prolonged lifespan, as reported for *C. elegans* (64), the cladocerans *Daphnia magna* (73), *Moina macrocopa* (74, 75) (but not its sister species *M. micrura*), and the threespine stickleback, *Gasterosteus aculeatus* (76). It was shown for the humic-tolerant charophyte, *Chara hispida*, that HSs delay the aging of its photosynthetic apparatus (63).
- (2) Female-bias in the sex ratio: Feminizing activity by both the estrogenic and the anti-androgenic pathway appears to be an intrinsic activity of HSs and humic-like substances (77, 78). Exposure to these natural xenobiotics decreases the m/f ratio and reduces the maintenance costs for two separate parental bodies in ecosystems that function close to their carrying capacity, such as brown water bodies. Using this strategy, the available biochemical energy of the ecosystem is reallocated to a reproductive trait. Feminization mediated by HSs has been reported in several lower vertebrates, such as the swordtail, *Xiphophorus helleri* (79), the molly, *Poecilia vivipara* (80), and the claw frog, *Xenopus laevis* (77). Hormone-like activities of natural xenobiotics, such as HSs or polyphenol-containing litter leachates are not restricted to vertebrates only; exposure of the hermaphrodite nematode, *C. elegans* to various humic preparations significantly induced the transcription of at least two vitellogenin genes, as exemplified by *vit-6*, which encodes a precursor of the yolk protein (Figure 10).
- (3) Hormetic modulation of life trait variables: Hormesis refers to a biphasic dose-response to an environmental agent characterized by low dose stimulation or a beneficial effect and a high-dose inhibitory or toxic effect. From the ecological perspective, hormesis is a mild stress that improves Darwinian fitness, rather than only a single life-trait variable. Specifically, the mitohormesis hypothesis states that a certain increase in reactive oxygen production leads to lifespan extension and for the

puddle cladoceran *Moina macrocopia*, also to an increased number of offspring (75). This study analyzed the temperature-dependence of the water-soluble antioxidant capacity of the puddle cladoceran *Moina macrocopia* and evaluated its life trait variables with increasing temperature and increasing HS concentrations as stressors. Temperatures below or above the apparent optimum (20 °C), reduced the antioxidative capacity. The addition of HSs increased body length, but decreased mean lifespan at 15 and 20 °C. There was no clear HS-effect on offspring numbers at 15, 20, or 30 °C. At 25 °C with increasing HS-concentration, lifespan was extended and offspring numbers increased enormously, reaching 250% of the control values. Overall, mitohormesis with all major life trait variables being positively affected, is a newly discovered pathway that might stabilize populations in fluctuating environments.

(4) Multiple stress resistance or cross-tolerance: Exposure to HSs induces a general multiple stress tolerance in animals. Examples include tolerance against predation (netting) stress on fish (79) or osmotic stress on *M. macrocopia* alone (74) (Figure 11) or combined with fluctuating temperature. It is very likely, but not yet proven, that the protection of fish against pathogenic bacteria (18, 19) is also based on such a mechanism, because the authors did not find any direct antibiotic activity of the HSs applied.

Cross experiments, e.g. initial exposure to a specific stressor, such as sea salt, and subsequent exposure to HSs did not show any multiple stress resistance in *M. macrocopia*.

In addition to these examples, evidence is accumulating that HS-exposure also increases the fitness of shrimps (Figure 12), copepods, mayflies, and fishes to survive in natural and man-made acidic waterways (81, 82). For instance, Hargeby and Petersen (82) reported that during 21 days of exposure of *Gammarus pulex* to acidity, with or without HS:

- the proton toxicity at pH 6 in the absence of HS led to 92% mortality. If HSs were added at a concentration of 7 and 20 mg L⁻¹, the mortality rates fell to 80% and 64% respectively (Figure 12);
- animals surviving at pH 6 exhibited a reduced growth rate, a lower nutrient use and a higher body water content than at pH 7.3 (control);
- the presence of HS significantly improved the survival rate in acidic conditions.

In a recent study, Holland et al. (83) confirmed the classical finding by Hargeby and Petersen (82) by exploring the ability of HSs in the form of Aldrich humic acid (AHA) to increase survivorship of the freshwater shrimp (*Caridina* sp. D) at low pH in artificial soft (representative of

naturally acidic environments) and hard waters (artificial and natural Dee River water). Freshwater shrimps were exposed to pH treatments ranging from pH 7 to pH 3.5, with or without 10 or 20 mg L⁻¹ HSs treatments. In low pH water, shrimp mortality was higher in artificial hard water (LC₅₀ at pH 4.95) and natural hard water (LC₅₀ at pH 4.74), compared with soft water (LC₅₀ at pH 4.27). The HSs substantially decreased the threshold at which pH caused 50% mortality to the freshwater shrimp, with this threshold shifting from 4.95 to 4.47 in artificial hard water, from 4.74 to 4.50 in natural hard water and from 4.27 to 4.18 in soft water (Figure 13).

(5) Transgenerational heritage of stress resistance: One of the most promising strategies to stabilise long-term populations in fluctuating environments is the transfer of acquired stress-tolerance to succeeding generations. Recent findings concerning salt-tolerance in *Moina macrocopa* show that stress-tolerance after HS-exposure is transmitted to filial generations (Figure 14). Strong indications suggest that this inheritance is based on epigenetics (most often gene silencing), since HS-exposure leads to DNA methylation (Figure 15). This example illustrates that environmental factors can lead to epigenetically mediated increased genomic flexibility even in successive, untreated generations, and thereby increase the potential for adaptation without changes in the DNA itself.

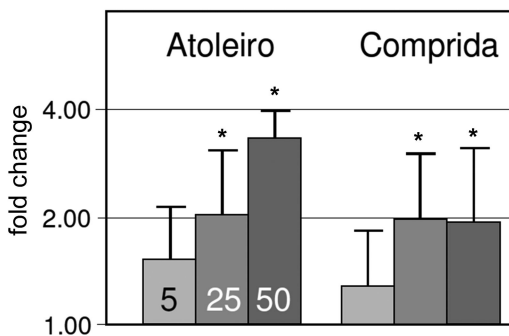
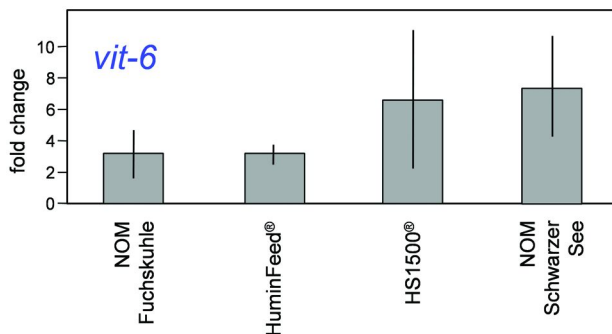
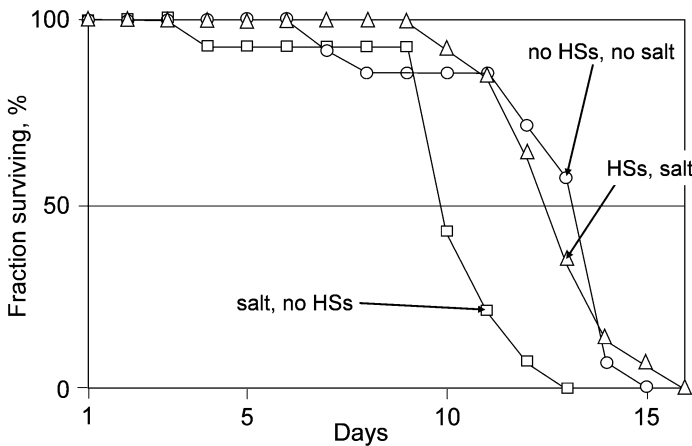


Figure 9. Relative expression of the *cep-1* gene in *Caenorhabditis elegans*, exposed to 5, 25, or 50 mg L⁻¹ DOC of natal humic substances from two Brazilian coastal lagoons (Lagoa Atoleiro, Lagoa Comprida). * indicates an increase in transcription >1.7-fold compared to the control and after normalization with the reference gene *act-1*. Reproduced in modified form from ref. (72). Courtesy of Northeastern University, Boston, MA.



*Figure 10. Relative expression of the vit-6 gene in *Caenorhabditis elegans* exposed to 2.08 mM DOC of each humic substance from two lakes in the vicinity of Berlin; one soil isolate (HuminFeed®) and one synthetic humic substance (HS1500®). NOM = Natural Organic Matter isolated by reverse osmosis from lakes. Transcript increases >1.7-fold compared to the control and after normalization with the act-1 gene, are considered significant. Reproduced from ref. (80).*



*Figure 11. Multiple stress tolerance to survive fluctuating osmotic conditions in a Brazilian coastal lagoon. The lagoon is separated from the Atlantic Ocean only by a small sandbar and saline water often intrudes into the lagoon. Lifespan modulation in *Moina macrocopa* occurs by intermittent exposure to salt (5.5 g L⁻¹) alone or salt + humic substances (HSSs, 0.83 mM DOC) from an adjacent lagoon in the national park. Reproduced from ref. (80).*

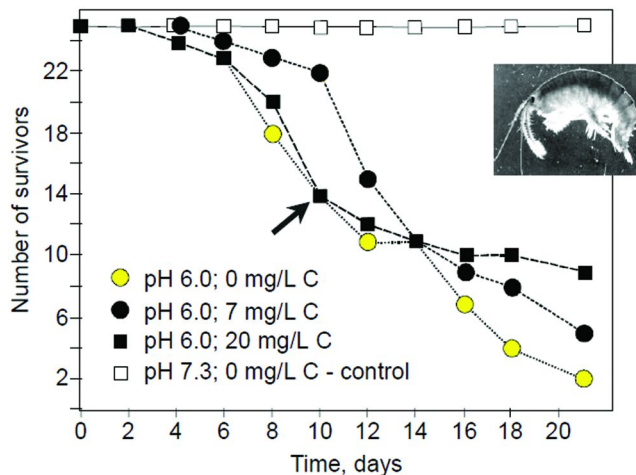


*Figure 12. Multiple stress tolerance to survive acidic conditions: Survival of *Gammarus pulex* during 21 days' exposure to pH 6.0 and 7.3, and HS concentrations of 7 and 20 mg L⁻¹ DOC. The arrow marks the adverse effect of an elevated HS concentration. Reproduced from ref. (82). Copyright 1988 Wiley.*

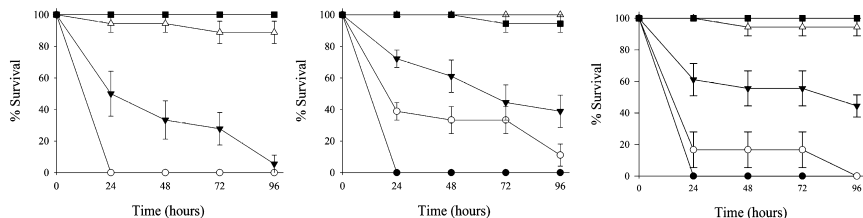


*Figure 13. Multiple stress tolerance to survive acidic conditions: Survival of *Caridina* sp. D in acidified Dee River water. Top: 0 mg L⁻¹ Aldrich Humic Acid, AHA, middle: 10 mg L⁻¹ AHA, bottom: 20 mg L⁻¹ AHA. ● = pH 3.5; ○ = pH 4.0; ▼ = pH 4.5; ▲ = pH 5.0; ■ = Control. Each point is the mean of six replicates from two trials ± SE. Reproduced from ref. (83). Courtesy of Northeastern University, Boston, MA.*

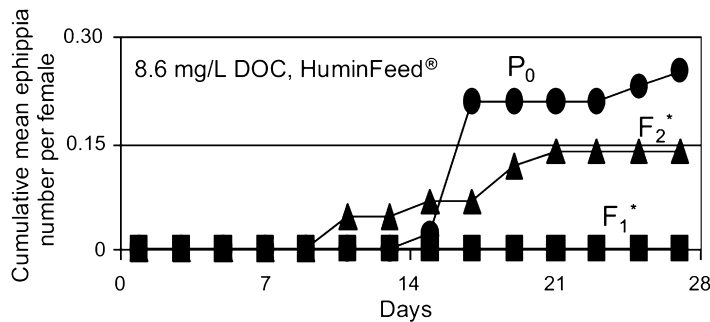


Figure 14. *Daphnia magna* mothers (P_0) transmit stress resistance to filial generations. Exposure for all generations was identical to 20 mg L^{-1} HuminFeed® (8.6 mg L^{-1} DOC). The exposed daughters from exposed mothers (F_1) do not produce ephippia, whereas exposed granddaughters from exposed daughters (F_2) start to produce ephippia again, in significantly lower numbers than their grandmothers. * = significantly different from P_0 at $p < 0.05$.

Reproduced from ref. (84). Copyright 2011 Elsevier.

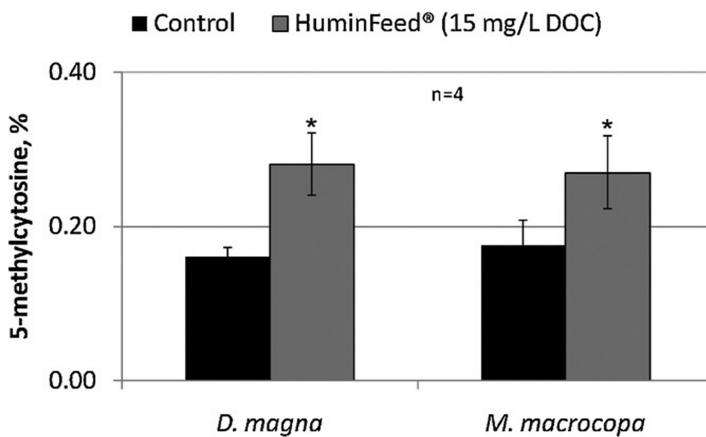


Figure 15. Increased cytosine-methylation in clones of two cladoceran species (*Daphnia magna*, *Moina macrocopia*) exposed to humic substances. * $p < 0.05$.

Reproduced from ref. (84). Copyright 2011 Elsevier.

Do NOM Origin and Quality Matter?

Both the origin and particularly the quality of NOM are extremely important. The measurement of DOC is an analytical one for the quantity of dissolved organic carbon, but does not contain any quality features. Hence, identical DOC quantities might reflect differing and even contrasting qualities. The governing

role of NOM origin can be observed in Figure 16, where the number of offspring of *C. elegans* is plotted as a function of the DOC concentration from various sources and preparation methods. Waste-water fulvic acids (FA), soil leachate FA, humic lake FA, and marsh ultra-filtrate increase nematode reproduction, whereas groundwater FA and industrial waste-water FA do not significantly modulate reproduction (85). It is clear that the origin of a NOM isolate controls its composition; however, so far it remains unclear which structural moieties provoke which effects.

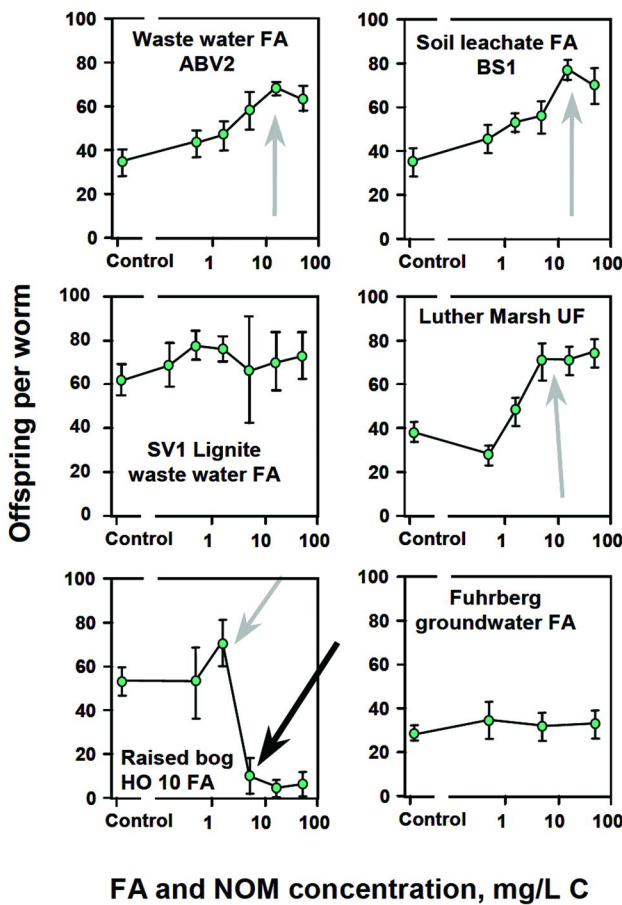


*Figure 16. The origin of NOM is important: Number of offspring per worm (mean \pm SD) of *C. elegans* after 72 h exposure to DOM from different sources and various concentrations: waste-water fulvic acid (FA), soil-leachate FA, raised-bog FA, raised-bog ultra-filtrate (UF), industrial waste-water FA, ground-water FA, marsh UF. Data are means \pm standard deviation. Significant increases in offspring numbers are indicated by grey arrows; significant decreases by black arrows. Reproduced from ref. (85). Copyright 2001 Wiley.*

The answer to this question was addressed by another survey that tested 20 chemically and physically well-characterized HS preparations of different qualities with respect to a reduction in the vegetative growth of the water mold, *Saprolegnia parasitica* (86). The results suggested that fungal growth was most efficiently reduced by HSs with a high aromaticity and was encouraged by NOMs with a high carbohydrate content (Figure 17).

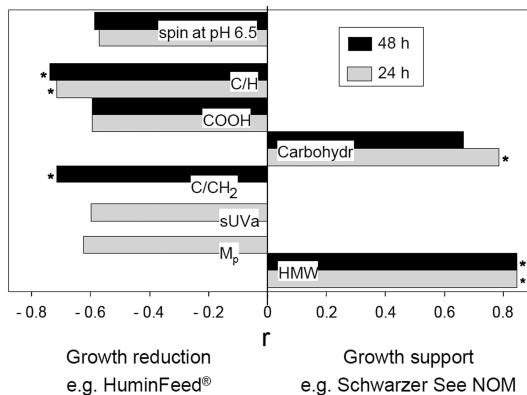


Figure 17. The quality of NOM matters: Correlations of the 24 h and 48 h EC₅₀ values of *Saprolegnia parasitica* growth modulation with structural features. Specific UV absorption (sUVa) and peak molar mass (M_p) were derived from HPSEC and point to aromatic humic compounds with a higher molar mass; COOH and CH₂ are relative measures of these functional groups derived from FTIR spectra; C and H were derived from elemental analysis and spin at pH 6.5 denotes the spin concentrations of stable organic radicals in HSs measured by EPR spectroscopy. HMW = high molar mass. Negative r -values signify a reduction in vegetative growth; a positive r -value means growth support as exemplified by two HSs of contrasting effects. Reproduced from ref. (87).

Courtesy of Northeastern University, Boston, MA.

This dualism continues to apply to the extension of the lifespan of *C. elegans* (Figure 18), however, in an inverse relationship. Here, the carbohydrate-rich NOM from the Schwarzer See did not affect the lifespan, whereas the preparation with a high aromaticity (HuminFeed®) extended the lifespan at low-to-medium concentrations.

When aquatic macrophytes, such as coontail (*Ceratophyllum demersum*) and Java moss (*Vesicularia dubyana*) were exposed to NOMs, a reduction in photosynthetic oxygen release occurred (88, 89), and a QSAR could be established. Particularly stable radicals that are indicative of quinone structures, statistically account for approximately 80% of the reduction in oxygen release (Figure 19). HSs might directly quench electrons or bind to the bio-quinones

in PSII and thereby block electron transfer. The development of an internal oxidative stress might also be a mode of action, which in primary producers, leads to a reduction in photosynthetic activity to avoid excess ROS production (90).

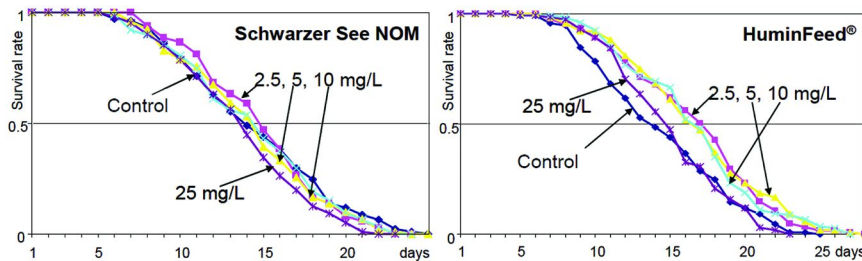


*Figure 18. The quality of NOM matters: The survival rate and lifespan of *C. elegans* exposed to Schwarzer See NOM and HuminFeed® at increasing concentrations (mg L⁻¹ DOC). Controls were without any NOM/HS addition. With Schwarzer See NOM, no exposure was significantly different from the controls. With HuminFeed®, the differences between control and 2.5, 5 and 20 mg L⁻¹ exposures were significant at the $p < 0.005$ level (log-rank test, $n = 94$ –120). There were no significant differences between the control and the 25 mg L⁻¹ DOC exposure. Reproduced from ref. (87). Courtesy of Northeastern University, Boston, MA.*

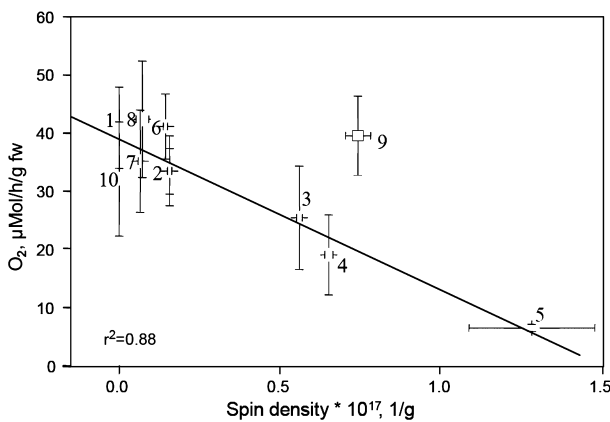


*Figure 19. The quality of NOM matters: Spin density of HS and NOM as a predictor for the reduction in photosynthetic oxygen release in Java moss (*Vesicularia dubyana*). 1: control; 2: Suwannee River NOM, 3: Suwannee River FA, 4: Suwannee River HA, 5: synthetic HS1500, 6: Hellerudmyra NOM, 7: Svartberget NOM, 8: Valkea-Kotinen NOM, 9: Hietajärvi NOM, 10: Birkenes NOM. Reproduced from ref. (89). Courtesy of the Akademie gemeinnütziger Wissenschaften Erfurt, Germany.*

To date, all structure–activity relationships indicate that particularly structures with high spin densities or with high hydroxybenzene moieties were effective in macrophytes and the nematode *C. elegans*. To test this experimentally, Menzel et al. (64) enriched HSs with hydroxybenzene moieties. Based on the leonardite preparation HuminFeed® (HF), Menzel et al. (64) followed a polycondensation reaction in which this natural HS preparation and a dihydroxybenzene (hydroquinone or benzoquinone) served as reaction partners. Several analytical methods showed the formation of the corresponding copolymers. The chemical modification boosted the antioxidant properties of HF both *in vitro* and *in vivo*. HSs enriched with hydroxybenzene moieties caused a significant increase in the tolerance to thermal stress in *C. elegans* and extended its lifespan. Exposed nematodes showed a delayed linear growth and onset of reproduction and a stronger pumping activity of the pharynx. Thus, treated nematodes behaved younger than they really were. In this respect, the modified HF replicated the biological impact of various plant polyphenol monomers. In fact, there was a strong transcriptional overlap in worms exposed to modified HF and plant polyphenols, thereby supporting the hydroxybenzene moieties of HSs as major effective structures for the physiological effects observed in *C. elegans*. With some plausibility, this statement can be extended to the other NOM and HS effects on organisms described above.

Conclusion

This study has shown that NOM is a major driving force in ecosystems. NOM and its major fraction, HSs, are natural xenobiotic chemicals that indirectly or directly interact with organisms. Polyphenols, quinones, or stable radicals appear to be the most effective NOM components, whereas polysaccharides appear to provoke opposite effects. Indirect interactions comprise changes in the external redox regime by released ROS upon illumination, with subsequent oxidative stress; however, if allelochemicals are the subject of attack by ROS, the allelochemical stress of exposed organisms is reduced. Direct interactions start with membranes, which is covered only by a few studies and deserves intensive future study.

The low-molecular weight HS fraction of NOM, with a molecular weight of approximately 0.5 kDa (61, 62), is taken up via epithelia/membranes or via food ingestion. To date, only very few organisms are known that make use of the antioxidative properties of the HSs; however, there is no reason to believe that other unidentified organisms could not also benefit from the antioxidative properties of HSs. For instance, organisms that inhabit humic-rich environments have co-evolved with these natural xenobiotics and have turned the original stress into a benefit. On a more comprehensive basis, this strategy could be identified with terrestrial plants, compost nematodes, or fishes and aquatic invertebrates. In conclusion, exposed organisms develop multiple stress resistances that might be epigenetically transmitted to succeeding generations, thereby enabling organisms

to maintain stable populations under fluctuating environmental conditions. In this respect, further strategies include increased lifespan, body growth and especially, an increase in offspring numbers or feminization of young males. The latter strategy makes optimal use of the available biochemical energy in an ecosystem that approaches its carrying capacity. Finally, we are hopeful that the scientific community will continue to make fascinating discoveries, although the recognition of the importance of the ecological significance of NOM as a natural xenobiotic is in its infancy.

Acknowledgments

This work was supported in part by the Deutsche Forschungsgemeinschaft, grants STE 673-16/1, STE 673/17-1, and STE 673-18/1. Thanks are also due to the anonymous supportive reviewers who helped to improve the manuscript.

References

1. Sobek, S.; Tranvik, L. J.; Prairie, Y. T.; Kortelainen, P.; Cole, J. J. Patterns and regulation of dissolved organic carbon: An analysis of 7,500 widely distributed lakes. *Limnol. Oceanogr.* **2007**, *52*, 1208–1219.
2. Farjalla, V. F.; Amado, A. M.; Suhett, A. L.; Meirelles-Pereira, F. DOC removal paradigms in highly humic aquatic ecosystems. *Environ. Sci. Pollut. Res.* **2009**, *16*, 531–538.
3. Wetzel, R. G. *Limnology. Lake and River Ecosystems*, 3rd ed.; Academic Press: San Diego, 2001.
4. Playle, R. C.; Dixon, D. G.; Burnison, K. Copper and cadmium binding to fish gills: Estimates of metal-gill stability constants and modelling of metal accumulation. *Can. J. Fish. Aquat. Sci.* **1993**, *50*, 2678–2687.
5. Pan, B.; Ning, P.; Xing, B. Humic substances (review series). Part IV – Sorption of hydrophobic organic contaminants. *Environ. Sci. Pollut. Res.* **2008**, *15*, 554–564.
6. Chen, Y.; Aviad, T. Effects of humic substances on plant growth. In *Humic Substances in Soil and Crop Sciences: Selected Readings*; MacCarthy, P., Clapp, C. E., Malcom, R. L., Bloom, P. R., Eds.; Soil Science Society of America: Madison, 1990; pp 161–186.
7. Chen, Y.; Clapp, C. E.; Magen, H. Mechanisms of plant growth stimulation by humic substances: The role of organo-iron complexes. *Soil Sci. Plant Nutr.* **2004**, *50*, 1089–1095.
8. Jackson, T. A.; Hecky, R. E. Depression of primary productivity by humic matter in lake and reservoir water of the boreal forest zone. *Can. J. Fish. Aquat. Sci.* **1980**, *37*, 2300–2317.
9. Leggieri, L.; Feijoó, C.; Giorgi, A.; Ferreiro, N.; Acuña, V. Seasonal weather effects on hydrology drive the metabolism of non-forest lowland streams. *Hydrobiologia* **2013**, *716*, 47–58.

10. Jones, R. I. The influence of humic substances on lacustrine planktonic food chains. *Hydrobiologia* **1992**, *229*, 73–91.
11. Reinart, A.; Paavel, B.; Pierson, D.; Strombeck, N. Inherent and apparent optical properties of Lake Peipsi, Estonia. *Boreal Environ. Res.* **2004**, *9*, 429–445.
12. Goldstone, J. V.; Del Vecchio, R.; Blough, N. V.; Voelker, B. M. A multicomponent model of chromophoric dissolved organic matter photobleaching. *Photochem. Photobiol.* **2004**, *80*, 52–60.
13. Shurin, J. B.; Winder, M.; Adrian, R.; Keller, W. B.; Matthews, B.; Paterson, A. M.; Paterson, M. J.; Pinel-Alloul, B.; Rusak, J. A.; Yan, N. D. Environmental stability and lake zooplankton diversity—contrasting effects of chemical and thermal variability. *Ecol. Lett.* **2010**, *13*, 453–463.
14. Steinberg, C. E. W.; Paul, A.; Pflugmacher, S.; Meinelt, T.; Klöcking, R.; Wiegand, C. Pure humic substances have the potential to act as xenobiotic chemicals – a review. *Fresenius Environ. Bull.* **2003**, *12*, 391–401.
15. Steinberg, C. E. W.; Ouerghemmi, N.; Herrmann, S.; Bouchnak, R.; Timofeyev, M. A.; Menzel, R. Stress by poor food quality and exposure to humic substances: *Daphnia magna* responds with oxidative stress, lifespan extension, but reduced offspring numbers. *Hydrobiologia* **2010**, *652*, 223–236.
16. Wershaw, R. L. New model for humic materials and their interactions with hydrophobic organic chemicals in soil-water or sediment-water systems. *J. Contam. Hydrol.* **1986**, *1*, 29–45.
17. Visser, S. A. Physiological action of humic substances on microbial cells. *Soil Biol. Biochem.* **1985**, *17*, 457–462.
18. Nakagawa, J.; Iwasaki, T.; Kodama, H. Protection against *Flavobacterium psychrophilum* infection (cold water disease) in ayu fish (*Plecoglossus altivelis*) by oral administration of humus extract. *J. Vet. Med. Sci.* **2009**, *71*, 1487–1491.
19. Kodama, H.; Denso; Nakagawa, T. Protection against atypical *Aeromonas salmonicida* infection in carp (*Cyprinus carpio* L.) by oral administration of humus extract. *J. Vet. Med. Sci.* **2007**, *69*, 405–408.
20. Meinelt, T.; Schreckenbach, K.; Pietrock, M.; Heidrich, S.; Steinberg, C. E. W. Humic substances (review series). Part 1: Dissolved humic substances (HS) in aquaculture and ornamental fish breeding. *Environ. Sci. Pollut. Res.* **2008**, *15*, 17–22.
21. Klöcking, R.; Sprössig, M. Antiviral properties of humic acids. *Experientia* **1972**, *28*, 607–608.
22. Posselt, M. *Antiviral activity of humic substances*, Study Project; Humboldt-Universität zu Berlin: Berlin, 2013.
23. Anesio, A. M.; Hollas, C.; Graneli, W.; Laybourn-Parry, J. Influence of humic substances on bacterial and viral dynamics in freshwaters. *Appl. Environ. Microbiol.* **2004**, *70*, 4848–4854.
24. Zepp, R. G.; Wolfe, N. L.; Baughman, G. L.; Hollis, R. C. Singlet oxygen in natural waters. *Nature (London)* **1977**, *267*, 421–423.

25. Cooper, W. J.; Zika, R. G. Photochemical formation of hydrogen peroxide in surface and ground waters exposed to sunlight. *Science (Washington, DC)* **1983**, *220*, 711–712.
26. Borgeraas, J.; Hessen, D. O. Variations of antioxidant enzymes in *Daphnia* species and populations as related to ambient UV exposure. *Hydrobiologia* **2002**, *477*, 15–30.
27. Glaeser, S. P.; Grossart, H. P.; Glaeser, J. Singlet oxygen, a neglected but important environmental factor: short-term and long-term effects on bacterioplankton composition in a humic lake. *Environ. Microbiol.* **2010**, *12*, 3124–3136.
28. Paul, A.; Dziallas, C.; Zwirnmann, E.; Gjessing, E. T.; Grossart, H. P. UV irradiation of natural organic matter (NOM): impact on organic carbon and bacteria. *Aquat. Sci.* **2012**, *74*, 443–454.
29. Gryndler, M.; Hrselova, H.; Sudova, R.; Gryndlerova, H.; Rezacova, V.; Merhautova, V. Hyphal growth and mycorrhiza formation by the arbuscular mycorrhizal fungus *Glomus claroideum* BEG 23 is stimulated by humic substances. *Mycorrhiza* **2005**, *15*, 483–488.
30. Liltved, H.; Landfald, B. Effects of high intensity light on ultraviolet-irradiated and non-irradiated fish pathogenic bacteria. *Water Res.* **2000**, *34*, 481–486.
31. Schreckenbach, K.; Meinelt, T.; Spangenberg, R.; Staaks, G.; Kaletka, T.; Spangenberg, M.; Stüber, A. *Untersuchungen zur Wirkung des Synthesehuminstoffes RHS 1500 auf Süßwasserfische der Aquakultur*; Institut für Binnenfischerei: Berlin, 1991.
32. Paul, A.; Hackbarth, S.; Vogt, R. D.; Röder, B.; Burnison, B. K.; Steinberg, C. E. W. Photogeneration of singlet oxygen by humic substances: comparison of humic substances of aquatic and terrestrial origin. *Photochem. Photobiol. Sci.* **2004**, *3*, 273–280.
33. Silverman, A. I.; Peterson, B. M.; Boehm, A. B.; McNeill, K.; Nelson, K. L. Sunlight inactivation of human viruses and bacteriophages in coastal waters containing natural photosensitizers. *Environ. Sci. Technol.* **2013**, *47*, 1870–1878.
34. Whittaker, R. H.; Feeny, P. P. Allelochemistry: chemical interactions between species. *Science (Washington, DC)* **1971**, *171*, 757–770.
35. Welker, M.; Steinberg, C. Rates of humic substance photosensitized degradation of microcystin-LR in natural waters. *Environ. Sci. Technol.* **2000**, *34*, 3415–3419.
36. Kieber, R. J.; Pitt, J.; Skrabal, S. A.; Wright, J. L. C. Photodegradation of the brevetoxin PbTx-2 in coastal seawater. *Limnol. Oceanogr.* **2010**, *55*, 2299–2304.
37. Song, W. H.; Yan, S. W.; Cooper, W. J.; Dionysiou, D. D.; O’Shea, K. E. Hydroxyl radical oxidation of cylindrospermopsin (cyanobacterial toxin) and its role in the photochemical transformation. *Environ. Sci. Technol.* **2012**, *46*, 12608–12615.
38. Sun, B. K.; Tanji, Y.; Unno, H. Influences of iron and humic acid on the growth of the cyanobacterium *Anabaena circinalis*. *Biochem. Eng. J.* **2005**, *24*, 195–201.

39. Sun, B. K.; Tanji, Y.; Unno, H. Extinction of cells of cyanobacterium *Anabaena circinalis* in the presence of humic acid under illumination. *Appl. Microbiol. Biotechnol.* **2006**, *72*, 823–828.
40. Steinberg, C. E. W.; Kamara, S.; Prokhotskaya, V. Y.; Manusadžianas, L.; Karasyova, T. A.; Timofeyev, M. A.; Jie, Z.; Paul, A.; Meinelt, T.; Farjalla, V. F.; Matsuo, A. Y. O.; Burnison, B. K.; Menzel, R. Dissolved humic substances – ecological driving forces from the individual to the ecosystem level? *Freshwater Biol.* **2006**, *51*, 1189–1210.
41. Löffler, H. *Neusiedlersee – The Limnology of a Shallow Lake in Central Europe*; Dr. W. Junk: The Hague, 1980; Vol. 37.
42. Newman, J. R.; Barrett, P. R. F. Control of *Microcystis aeruginosa* by decomposing barley straw. *J. Aquat. Plant Manage.* **1993**, *31*, 203–206.
43. Park, M. H.; Chung, I. M.; Ahmad, A.; Kim, B. H.; Hwang, S. J. Growth inhibition of unicellular and colonial *Microcystis* strains (Cyanophyceae) by compounds isolated from rice (*Oryza sativa*) hulls. *Aquat. Bot.* **2009**, *90*, 309–314.
44. Hilt, S.; Gross, E. M. Can allelopathically active submerged macrophytes stabilise clear-water states in shallow lakes? *Basic Appl. Ecol.* **2008**, *9*, 422–432.
45. Menzel, R.; Menzel, S.; Swain, S. C.; Pietsch, K.; Tiedt, S.; Witczak, J.; Stürzenbaum, S. R.; Steinberg, C. E. W. The nematode *Caenorhabditis elegans*, stress and aging: Identifying the complex interplay of genetic pathways following the treatment with humic substances. *Front. Genet.* **2012**, *3*, 50.
46. Bährs, H.; Putschew, A.; Steinberg, C. E. W. Toxicity of hydroquinone to different freshwater phototrophs is influenced by time of exposure and pH. *Environ. Sci. Pollut. Res.* **2013**, *20*, 146–154.
47. Moss, B.; Stephen, D.; Alvarez, C.; Becares, E.; Van De Bund, W.; Collings, S. E.; Van Donk, E.; De Eyto, E.; Feldmann, T.; Fernández-Aláez, C.; Fernández-Aláez, M.; Franken, R. J. M.; García-Criado, F.; Gross, E. M.; Gyllström, M.; Hansson, L. A.; Irvine, K.; Järvalt, A.; Jensen, J. P.; Jeppesen, E.; Kairesalo, T.; Kornijów, R.; Krause, T.; Künnap, H.; Laas, A.; Lill, E.; Lorens, B.; Luup, H.; Miracle, M. R.; Nõges, P.; Nõges, T.; Nykänen, M.; Ott, I.; Peczula, W.; Peeters, E. T. H. M.; Phillips, G.; Romo, S.; Russell, V.; Salujo, J.; Scheffer, M.; Siewertsen, K.; Smal, H.; Tesch, C.; Timm, H.; Tuvikene, L.; Tonno, I.; Virro, T.; Vicente, E.; Wilson, D. The determination of ecological status in shallow lakes - A tested system (ECOFRA) for implementation of the European Water Framework Directive. *Aquat. Conserv.* **2003**, *13*, 507–549.
48. Komatsu, Y.; Suematsu, S.; Hisanobu, Y.; Saigo, H.; Matsuda, R.; Hara, K. Studies on preservation of constituents in canned drinks. 2. Effects of pH and temperature on reaction kinetics of catechins in green tea infusion. *Biosci. Biotechnol. Biochem.* **1993**, *57*, 907–910.
49. Nakai, S.; Inoue, Y.; Hosomi, M. Algal growth inhibition effects and inducement modes by plant-producing phenols. *Water Res.* **2001**, *35*, 1855–1859.

50. Hong, Y.; Hu, H. Y.; Xie, X.; Sakoda, A.; Sagehashi, M.; Li, F. M. Gramine-induced growth inhibition, oxidative damage and antioxidant responses in freshwater cyanobacterium *Microcystis aeruginosa*. *Aquat. Toxicol.* **2009**, *91*, 262–269.
51. Laue, P.; Chakrabarti, S.; Bährs, H.; Steinberg, C. E. W. Natural xenobiotics to prevent cyanobacterial and algal growth in freshwater: Contrasting efficacy of tannic acid, gallic acid, and gramine. *Chemosphere* **2014** DOI: 10.1016/j.chemosphere.2013.11.029.
52. Jindo, K.; Martim, S. A.; Navarro, E. C.; Pérez-Alfocea, F.; Hernandez, T.; Garcia, C.; Aguiar, N. O.; Canellas, L. P. Root growth promotion by humic acids from composted and non-composted urban organic wastes. *Plant Soil* **2012**, *353*, 209–220.
53. Schmidt, W.; Santi, S.; Pinton, R.; Varanini, Z. Water-extractable humic substances alter root development and epidermal cell pattern in *Arabidopsis*. *Plant Soil* **2007**, *300*, 259–267.
54. Dobbss, L. B.; Canellas, L. P.; Olivares, F. L.; Aguiar, N. O.; Peres, L. E. P.; Azevedo, M.; Spaccini, R.; Piccolo, A.; Façanha, A. R. Bioactivity of chemically transformed humic matter from vermicompost on plant root growth. *J. Agric. Food Chem.* **2010**, *58*, 3681–3688.
55. Concheri, G.; Nardi, S.; Reniero, F.; Dell’Agnola, G. The effects of humic substances within the Ah horizon of a Calcic Luvisol on morphological changes related to invertase and peroxidase activities in wheat roots. *Plant Soil* **1996**, *179*, 65–72.
56. Dell’Agnola, G.; Nardi, S. Hormone-like effect and enhanced nitrate uptake induced by depolycondensed humic fractions obtained from *Allolobophora rosea* and *A. caliginosa* faeces. *Biol. Fertil. Soils* **1987**, *4*, 115–118.
57. Trevisan, S.; Pizzeghello, D.; Ruperti, B.; Franciosi, O.; Sassi, A.; Palme, K.; Quaggiotti, S.; Nardi, S. Humic substances induce lateral root formation and expression of the early auxin-responsive *IAA19* gene and *DR5* synthetic element in *Arabidopsis*. *Plant Biol.* **2010**, *12*, 604–614.
58. Carletti, P.; Masi, A.; Spolaore, B.; Polverino De Laureto, P.; De Zorzi, M.; Turetta, L.; Ferretti, M.; Nardi, S. Protein expression changes in maize roots in response to humic substances. *J. Chem. Ecol.* **2008**, *34*, 804–818.
59. Trevisan, S.; Botton, A.; Vaccaro, S.; Vezzaro, A.; Quaggiotti, S.; Nardi, S. Humic substances affect *Arabidopsis* physiology by altering the expression of genes involved in primary metabolism, growth and development. *Environ. Exp. Bot.* **2011**, *74*, 45–55.
60. Aguirre, E.; Leménager, D.; Bacaicoa, E.; Fuentes, M.; Baigorri, R.; Zamarreno, A. M.; García-Mina, J. M. The root application of a purified leonardite humic acid modifies the transcriptional regulation of the main physiological root responses to Fe deficiency in Fe-sufficient cucumber plants. *Plant Physiol. Biochem.* **2009**, *47*, 215–223.
61. Reemtsma, T.; These, A. On-line coupling of size exclusion chromatography with electrospray ionization-tandem mass spectrometry for the analysis of aquatic fulvic and humic acids. *Anal. Chem.* **2003**, *75*, 1500–1507.

62. Reemtsma, T.; These, A. Comparative investigation of low-molecular-weight fulvic acids of different origin by SEC-Q-TOF-MS: New insights into structure and formation. *Environ. Sci. Technol.* **2005**, *39*, 3507–3512.
63. Pörs, Y.; Steinberg, C. E. W. Humic substances delay aging of the photosynthetic apparatus of *Chara hispida*. *J. Phycol.* **2012**, *48*, 1522–1529.
64. Menzel, R.; Menzel, S.; Tiedt, S.; Kubsch, G.; Stösser, R.; Bährs, H.; Putschew, A.; Saul, N.; Steinberg, C. E. W. Enrichment of humic material with hydroxybenzene moieties intensifies its physiological effects on the nematode *Caenorhabditis elegans*. *Environ. Sci. Technol.* **2011**, *45*, 8707–8715.
65. Epel, D. Use of multidrug transporters as first lines of defense against toxins in aquatic organisms. *Comp. Biochem. Physiol. A* **1998**, *120*, 23–28.
66. Timofeyev, M. A.; Shatilina, Z. M.; Bedulina, D. S.; Menzel, R.; Steinberg, C. E. W. Natural organic matter (NOM) has the potential to modify the multixenobiotic resistance (MXR) activity in freshwater amphipods *Eulimnogammarus cyaneus* and *E. verrucosus*. *Comp. Biochem. Physiol., Part B: Biochem. Mol. Biol.* **2007**, *146*, 496–503.
67. Andersson, C.; Abrahamson, A.; Brunstrom, B.; Orberg, J. Impact of humic substances on EROD activity in gill and liver of three-spined sticklebacks (*Gasterosteus aculeatus*). *Chemosphere* **2010**, *81*, 156–160.
68. Matsuo, A. Y. O.; Woodin, B. R.; Reddy, C. M.; Val, A. L.; Stegeman, J. J. Humic substances and crude oil induce cytochrome P450 1A expression in the Amazonian fish species *Colossoma macropomum* (Tambaqui). *Environ. Sci. Technol.* **2006**, *40*, 2851–2858.
69. Meems, N.; Steinberg, C. E. W.; Wiegand, C. Direct and interacting toxicological effects on the waterflea (*Daphnia magna*) by natural organic matter, synthetic humic substances and cypermethrin. *Sci. Total Environ.* **2004**, *319*, 123–136.
70. Steinberg, C. E. W.; Meinelt, T.; Timofeyev, M. A.; Bittner, M.; Menzel, R. Humic substances (review series). Part 2: Interactions with organisms. *Environ. Sci. Pollut. Res.* **2008**, *15*, 128–135.
71. Cazenave, J.; Bistoni, M. d. I. Á.; Zwirnmann, E.; Wunderlin, D. A.; Wiegand, C. Attenuating effects of natural organic matter on microcystin toxicity in zebra fish (*Danio rerio*) embryos – benefits and costs of microcystin detoxification. *Environ. Toxicol.* **2006**, *21*, 22–32.
72. Chakrabarti, S.; Menzel, R.; Steinberg, C. E. W. Selected natural humic materials induce and char substrates repress a gene in *Caenorhabditis elegans* homolog to human anticancer *P53*. *Ann. Environ. Sci.* **2011**, *5*, 1–6.
73. Bouchnak, R.; Steinberg, C. E. W. Modulation of longevity in *Daphnia magna* by food quality and simultaneous exposure to dissolved humic substances. *Limnologica* **2010**, *40*, 86–91.
74. Suhett, A. L.; Steinberg, C. E. W.; Santangelo, J. M.; Bozell, R. L.; Farjalla, V. F. Natural dissolved humic substances increase the lifespan and promote transgenerational resistance to salt stress in the cladoceran *Moina macrocopa*. *Environ. Sci. Pollut. Res.* **2011**, *18*, 1004–1014.
75. Engert, A.; Chakrabarti, S.; Saul, N.; Bittner, M.; Menzel, R.; Steinberg, C. E. W. Interaction of temperature and an environmental stressor: *Moina*

macrocopa responds with increased body size, increased lifespan, and increased offspring numbers slightly above its temperature optimum. *Chemosphere* **2013**, *90*, 2136–2141.

76. Gambling, S. J.; Reimchen, T. E. Prolonged life span among endemic *Gasterosteus* populations. *Can. J. Zool.* **2012**, *90*, 284–290.
77. Lutz, I.; Jie, Z.; Opitz, R.; Kloas, W.; Ying, X.; Menzel, R.; Steinberg, C. E. Environmental signals: synthetic humic substances act as xeno-estrogen and affect the thyroid system of *Xenopus laevis*. *Chemosphere* **2005**, *61*, 1183–1188.
78. Hermelink, B.; Urbatzka, R.; Wiegand, C.; Pflugmacher, S.; Lutz, I.; Kloas, W. Aqueous leaf extracts display endocrine activities in vitro and disrupt sexual differentiation of male *Xenopus laevis* tadpoles in vivo. *Gen. Comp. Endocrinol.* **2010**, *168*, 245–255.
79. Meinelt, T.; Schreckenbach, K.; Knopf, K.; Wienke, A.; Stüber, A.; Steinberg, C. E. W. Humic substances affect physiological condition and sex ratio of swordtail (*Xiphophorus helleri* Heckel). *Aquat. Sci.* **2004**, *66*, 239–245.
80. Steinberg, C. E. W.; Dachsel, P.; Suhett, A. L.; Farjalla, V. F.; Petry, A. C.; Holland, A.; Protopopova, M. V.; Pavlichenko, V. V.; Meinelt, T.; Menzel, R.; Tartarotti, B.; Saul, N. Stress by natural xenobiotics enables freshwater animals to exist in fluctuating environments. *Freshwater Biol.* **2013**, in review.
81. Holland, A.; Duivenvoorden, L. J.; Kinnear, S. H. W. Humic substances increase survival of freshwater shrimp *Caridina* sp. D to acid mine drainage. *Arch. Environ. Contam. Toxicol.* **2013**, *64*, 263–272.
82. Hargeby, A.; Petersen, R. C. Effects of low pH and humus on the survivorship, growth and feeding of *Gammarus pulex* (L.) (Amphipoda). *Freshw. Biol.* **1988**, *19*, 235–247.
83. Holland, A.; Duivenvoorden, L. J.; Kinnear, S. H. W. Humic substances increase the survivorship rates of freshwater shrimp exposed to acidified waters of varying hardness. *Ann. Environ. Sci.* **2013**, *7*, 49–58.
84. Menzel, S.; Bouchnak, R.; Menzel, R.; Steinberg, C. E. W. Dissolved humic substances initiate DNA-methylation in cladocerans. *Aquat. Toxicol.* **2011**, *105*, 640–642.
85. Höss, S.; Bergtold, M.; Haitzer, M.; Traunspurger, W.; Steinberg, C. E. W. Refractory dissolved organic matter can influence the reproduction of *Caenorhabditis elegans* (Nematoda). *Freshw. Biol.* **2001**, *46*, 1–10.
86. Meinelt, T.; Paul, A.; Phan, T. M.; Zwirnmann, E.; Krüger, A.; Wienke, A.; Steinberg, C. E. W. Reduction in vegetative growth of the water mold *Saprolegnia parasitica* (Coker) by humic substance of different qualities. *Aquat. Toxicol.* **2007**, *83*, 93–103.
87. Steinberg, C. E. W.; Saul, N.; Pietsch, K.; Meinelt, T.; Rienau, S.; Menzel, R. Dissolved humic substances facilitate fish life in extreme aquatic environments and have the potential to extend lifespan of *Caenorhabditis elegans*. *Ann. Environ. Sci.* **2007**, *1*, 81–90.
88. Pflugmacher, S.; Pietsch, C.; Rieger, W.; Steinberg, C. E. W. Dissolved natural organic matter (NOM) impacts photosynthetic oxygen production

and electron transport in coontail *Ceratophyllum demersum*. *Sci. Total Environ.* **2006**, *357*, 169–175.

89. Paul, A.; Pflugmacher, S.; Steinberg, C. E. W. Correlation of spin concentration in humic substances with inhibitory effects on photosynthesis of aquatic macrophytes (In German). *Akad. gemeinnütziger Wiss. Erfurt, Sitzungsber. Math.-Natwiss. Kl.* **2003**, *12*, 205–217.

90. Mittler, R. Oxidative stress, antioxidants and stress tolerance. *Trends Plant Sci.* **2002**, *7*, 405–410.

Chapter 7

NMR Studies of Phosphorus Speciation and Carbon Humification in Wetland Soils

Aopeau Imvittaya, Rasha Hamdan, and William Cooper*

Department of Chemistry and Biochemistry, Florida State University,
Tallahassee, Florida 32306-4390

*E-mail: cooper@chem.fsu.edu.

Excessive phosphorus in surface waters can lead to significant changes in ecosystem characteristics. The Florida Everglades is a classic example of a phosphorus-impacted system. The “natural” state of the Everglades is highly oligotrophic, with dissolved total phosphorus levels less than 20 ppb in unimpacted areas in the south. However, in the northern Everglades, wetlands receive runoff rich in phosphorus and the normally open sawgrass plains have been converted into dense mono-species stands of cattail. In response, Water Conservation Areas (WCAs) have been established as buffer zones to protect pristine areas and prevent systemic eutrophication. Macrophytes, periphyton, and microbes in these wetlands take up part of the excess, labile inorganic phosphorus from the water column and convert it into organic forms. As these organisms decay, phosphorus is incorporated into the soil, essentially sequestering it as a part of the soil organic matter matrix. However, this sequestered phosphorus is subject to re-release back into the water column upon changes in nutrient status, hydrological regime or soil redox conditions. In this study we have used ^{31}P and ^{13}C NMR spectroscopy to estimate the extent of phosphorus sequestration in wetland soils. These estimates are based on previous studies using hydrofluoric acid treatments. Results from those studies suggest that phosphorus storage is linked to soil organic matter humification. Organic matter in soils in Everglades Water Conservation Area 2 are immature and poorly humified and thus phosphorus storage there may be at risk if hydrology or soil redox state changes.

Introduction

Phosphorus in wetland soils exists in both organic and inorganic forms. Inorganic phosphorus originates mainly from anthropogenic contamination, including fertilizers. Macrophytes, periphyton, and microbes in wetlands take up part of the labile inorganic phosphorus from the water column and convert it into organic compounds in their tissue. As these organisms decay, phosphorus is incorporated into the soil in the form of organic phosphorus. One major question in understanding phosphorus cycling in wetlands is the extent to which this natural organic matter in sediments might protect soil phosphorus from re-suspension back into the water column (1).

Soil organic phosphorus typically consists of three chemically distinct groups. Phosphate monoesters are thought to be the most abundant class in wetlands (2–4), although there is some evidence that diesters may hydrolyze in the alkaline solutions used in P-extraction resulting in an overestimation of monoester content (5). Phosphate monoesters originate from phosphate esters of sugar-like molecules and they occur mainly as inositol phosphates, with myo-inositol hexakisphosphate (phytic acid) the most prominent form in upland soils but not so in wetlands (4). The second group consists of phosphate diesters such as DNA and RNA. This group has been associated with sorption to silicate clays and humic acids. Phospholipids, a major component of cell membranes, form the final group.

Under the anaerobic conditions typically found in wetland soils, decomposition rates are slow and accumulation of moderately reactive phosphorous compounds occurs along with other refractory fractions. Thus, phosphorus will accumulate along with soil organic matter (SOM) from partially decomposed plant remains, providing long-term storage of phosphorus with a turnover time of ~ 100 years, in contrast to herbaceous plants where turnover times are on the order ~ two years (6). However, phosphorus sequestration is tightly linked to nutrient stoichiometry, and any shift in nutrient status or hydrological regime may affect the stability of the sequestered phosphorus (7).

Organic phosphorus from microbial and plant tissues requires enzymatic hydrolysis to liberate inorganic phosphate that then becomes bioavailable. When phosphorus is in excess, synthesis of the enzyme phosphatase by soil microorganisms will be suppressed and organic phosphorus will accumulate (8, 9). But the form of organic phosphorus produced under high pollutant loading might be readily degradable if bioavailable phosphorus inputs are reduced. Indeed, it has been reported that plants and microorganisms favor organic phosphorus under phosphorus limited conditions (10).

At the same time, phosphorus retention is tightly linked to soil physicochemical properties, mainly the oxidation-reduction status of the soil and the binding sites available for phosphorus adsorption (3). At the soil-water interface and under oxidation conditions, phosphates bind to ferric iron (Fe^{3+}) and precipitate into the soil (11). An aerobic to anaerobic shift may cause reduction of iron to ferrous form (Fe^{2+}), releasing previously bounded phosphorus (12). In highly acidic soils, aluminum is the main metal binding site for phosphorus, and the stability of the complex depends on the pH of the soil rather than the redox

state, while in more alkaline soils, phosphate is generally associated with calcium and magnesium carbonates (13).

Apart from metal complexes, significant amounts of organic phosphorus have been found to be associated with organic carbon compounds. Thus, the biodegradability of organic phosphorus is tightly linked to the stability of soil organic matter, and the nature of the soil organic material originating from plant and microbial remains plays a major role in determining the long term stability of phosphorus (14). Binding of organic phosphorus to relatively labile soil organic matter exposes it to degradation by microorganisms or solubilization due to changes in pH or redox state. Conversely, the accumulation of phosphorus associated with stable organic matter can be a major sink for phosphorus retention in wetlands (15).

The “natural” state of the Florida Everglades is highly oligotrophic, with dissolved total phosphorus levels less than 20 ppb in unimpacted areas in the south and an ecology dominated by broad, low-density sawgrass plains. However, in the northern Everglades, wetlands receive runoff rich in phosphorus, calcium and other essential nutrients. Water Conservation Areas (WCAs) have been established as buffer zones to protect pristine areas and prevent systemic eutrophication. For example, Water Conservation Area 2A (WCA 2A) has converted 44,800 hectares from a soft to hard water ecosystem, with a P gradient that extends 7 km into the interior of the marsh. P-enriched areas in WCA 2A are dominated by dense mono-species stands of cattail (*Typha spp.*), while the areas in between P-enriched and unenriched conditions have both cattail and sawgrass (*Cladium jamaicense* Crantz).

In this chapter we report on experiments designed to identify forms of phosphorus in soils from a treatment wetland in the Florida Everglades and link speciation and stability with soil organic matter composition and diagenetic state using NMR spectroscopy. Phosphorus speciation was determined by solution ^{31}P NMR after first extraction of P from the solid soil phase, while soil organic matter composition was determined by solid state ^{13}C NMR using cross polarization, magic angle spinning, high power decoupling and sideband suppression. Phosphorus stability was estimated based on a previous study that used a combination solution ^{31}P and solid state ^{13}C NMR spectroscopy before and after hydrofluoric acid treatment (1). Hydrofluoric acid pretreatment removes much of the soil inorganic matrix in soils, concentrating soil carbon, which is largely resistant to the acid (16). Our hypothesis was that phosphorus associated with metals (e.g. Fe) or in organic forms sorbed to anionic sorption sites (17) will be removed during HF treatment and thus represent phosphorus fractions that would be affected by environmental changes that disrupt these associations (e.g. changes in pH and redox conditions, flooding and/or re-wetting) (18). Conversely, phosphorus that persists following HF pretreatment must be part of the stable soil organic matter and therefore represents a pool of sequestered phosphorus that will be resistant to remobilization as long as the soil organic matter remains stable (19).

The principal assumptions and results from our original HF treatment study are summarized here in order to provide background on this approach. We then applied these same NMR techniques to define P speciation and SOM composition

along a hydraulic gradient in WCA 2A but without HF treatments which are laborious, time-consuming and not suitable for routine laboratory analyses. Our goal was to predict phosphorus stability in organic-rich Everglades soils based on our hypothesis that phosphorus sequestration is linked to organic matter stability, as well as to provide experimental evidence for future studies that address the validity of that hypothesis.

Methods and Sampling Sites

Phosphorus Extraction

Wetland soil samples were first freeze-dried (lyophilized), ground, and frozen. Phosphorus was extracted from each freeze-dried soil by a 2-step extraction using ethylenediaminetetraacetate (EDTA) and NaOH solutions. The first step involves a release of phosphorus from paramagnetic ions that can interfere with NMR spectral acquisition. Two grams of freeze-dried soil was mixed with 20 mL of 0.1 M EDTA, and then the soil mixture shaken for 30 minutes. The mixture was centrifuged for 15 mins and the supernatant discarded. Alkaline extraction was accomplished by adding 20 mL of 0.5 M NaOH to the precipitate, and the mixture was then shaken at room temperature for 16 hours. The supernatant (phosphorus extract) was then freeze-dried. The freeze-dried soil extracts were ground in a mortar and pestle to optimize their subsequent dissolution.

Elemental Analysis

Total phosphorus (TP) in soils was determined using a semi-automated molybdate colorimetry method according to EPA method 365.1. Total carbon (TC) was determined using a Thermo Finnigan Elemental Analyzer (Flash EA 1112).

^{31}P NMR Spectroscopy

A phosphorus extract solution for ^{31}P NMR analysis was prepared by dissolving 150-200 mg of P extract in 2 ml of a mixture of D_2O and 1 M NaOH. The base was used to increase the pH of the reconstituted extract to greater than 13. The mixture was vortexed for 2 minutes and then filtered through a 0.45- μm polyethersulfone (PES) membrane syringe filter. The filtered P extract solution was transferred to a 5-mm NMR tube. Spectra were acquired on a 600 MHz Bruker high resolution NMR spectrometer operating at 242.9 MHz for P. Acquisition parameters included a 90° pulse, 7.5-s pulse delay, 0.5-s acquisition time (AQ), and 100-ppm spectral width. The number of scans was 1,024 accumulated over approximately 11-12 hours. Proton decoupling was applied.

Chemical shifts (δ) in ^{31}P NMR spectra were referenced to an external standard of 85% H_3PO_4 set to $\delta = 0$ ppm. For quantitative analysis, methylene diphosphonic acid (MDPA), $\delta \sim 20$ ppm, was used as an internal standard. Peak assignments of P compounds include inorganic orthophosphate (5 to 9 ppm), orthophosphate monoesters (3 to 8 ppm), orthophosphate diesters (-1 to 5

ppm), pyrophosphate (-5 to -2 ppm), and polyphosphate (-21 to -16 ppm). For quantitation, spectral integration was performed over the chemical shift window corresponding to these peak assignments. A typical ^{31}P spectrum illustrating these assigned chemical shifts is included in Figure 1.

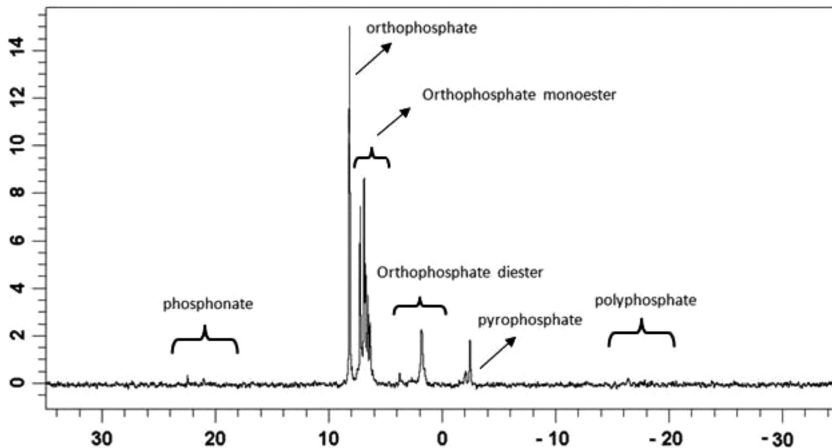


Figure 1. Typical ^{31}P NMR spectrum of NaOH extract from wetland soil.

^{13}C NMR Spectroscopy

Carbon composition of wetland soils was characterized using a 500 MHz Varian Unity-Inova spectrometer operating at 125 MHz for carbon. Approximately 500 mg of the freeze-dried soil sample was packed in a 7-mm solid state rotor and spun at of 14 kHz. Acquisition parameters included a 90° pulse, 3-s pulse delay, 750- μs cross polarization (CP) contact time, and 250-ppm spectral window. Spinning sidebands were eliminated using the total suppression of sidebands (TOSS) sequence. Between 32,000 and 45,000 scans were acquired. Chemical shifts (δ) in ^{13}C NMR spectra were referenced to an external standard of glycine at $\delta = 41.5$ ppm. Relative abundances of different carbon functional groups were determined by integrating the signal intensities over the defined chemical shift windows in the ^{13}C NMR spectra. These windows included 0-50 (alkyl C), 50-60 (N-alkyl C), 60-110 (O-alkyl C), 110-150 (aromatic C) and 160-220 ppm (carbonyl C).

Sampling Sites

Studies of phosphorus stability before and after HF treatment used soils collected from wetland sites chosen to represent a range of soil carbon sources and site nutrient status (1). These included a boreal Sphagnum dominated peatland (Alaska), a tropical *Raphia taedigera* palm swamp and tropical ombrotrophic peat

dome (Panama) (20), and subtropical ephemeral wetlands within an agricultural landscape (Florida) (2). All sites were highly organic peatlands except the Florida marsh, which has a relatively high mineral content consisting of uncoated Quartz grains (21).

Everglades soils were obtained from Water Conservation Area 2A. WCA 2A receives water rich in P and Ca via structures at the northern end of the marsh, which moves slowly southward via sheet flow. Phosphorus-enriched runoff also enters through a structure on the western boundary. Water leaves WCA 2A through a series of culverts along the southern boundary (5). P-enriched areas are dominated by dense mono-specific stands of cattail (*Typha spp.*), while the areas in between P-enriched and unenriched conditions have both cattail and sawgrass (*Cladium jamaicense* Crantz). All of the samples used in this study were obtained from the cattail-dominated, P-enriched sites, except for EG-7 which is a mix of cattail and sawgrass. The characteristics of these samples are summarized in Table I. While these sites represent a gradient in hydraulic residence time, because of multiple inputs they do not reflect a gradient in phosphorus surface water concentrations.

Table I. Sample Descriptions, Everglades Water Conservation Area 2

Sample ID	Sampling Depth (cm)	% C	Total P (mg P/kg dried soil)	Extractable P (mg P/kg dried soil)
EG1	2-10	51.0	1230	890
EG2	2-10	39.7	1430	670
EG3	2-10	46.1	2120	401
EG4	0-2	47.4	1580	1194
EG5	2-10	47.4	1810	587
EG6	10-30	44.6	1050	317
EG7	0-2	41.5	1090	544

Results

Phosphorus Stability as a Function of Soil Organic Matter Composition

Figure 2 summarizes the results of initial experiments to determine the effects of the acid treatments on phosphorus speciation in organic-rich soils. This study used soils from the four variable wetland sites (1). Phosphorus species identified include organic phosphonates (P-phonate), inorganic orthophosphate (O-P), orthophosphate monoesters (O-mono), orthophosphate diesters (O-diester), and

pyrophosphate (Pyro). Inorganic pyrophosphate was completely removed by the acid pretreatment, clearly indicating associations with anionic sorption sites or presence in live microbial cells. The most surprising aspect of our data is the amount of orthophosphate retained in the carbon matrix in these soils, decreasing by between 45 and 83%, indicating that relatively large amounts were physically/chemically stabilized through associations with soil organic matter. This differs markedly from a study of low organic matter pasture soils, in which HF treatment removed >98% of the inorganic orthophosphate (22). However, our results are consistent with a previous report of orthophosphate associated with organic matter in NaOH extracts of high organic matter wetland soils from the Florida Everglades (4).

After HF treatment the amounts of organic phosphate monoesters (O-mono) decreased only slightly in the Raphia swamp and Florida marsh soils. In contrast, significant decreases in these monoesters were observed in the sawgrass bog and Sphagnum bog soils. A significant decrease in organic phosphonates was observed in the Sawgrass bog as well. The stability of the organic phosphorus within the humic–phosphorus complex apparently depends mainly on the stability and degree of diagenesis of the organic matter in the accreted soil. Figure 3 includes the abundances of different carbon groups before and after acid treatment for the four soils. The tropical Raphia swamp and subtropical marsh soils in which the organic phosphorus is largely unaffected by the HF treatment are both dominated by alkyl functional groups that represent about 50% of the total soil organic carbon before the HF treatment, whereas O-alkyl groups represented only ~30% of soil carbon. The alkyl to O-alkyl ratio for these two soils was > 1 (Raphia swamp = 1.6, Florida marsh = 1.4), which indicates a preferential loss of carbohydrates and humification of the organic matter (23, 24). In contrast, the soils in which organic phosphorus was significantly reduced by HF treatment, tropical sawgrass bog and boreal Sphagnum bog, contained organic matter dominated by O-alkyl groups (~54% of the total ^{13}C NMR signal for the tropical bog soil and ~64% of the signal for the boreal bog soil). Relatively minor contributions from alkyl groups to the total organic carbon fraction were noted for these soils. For tropical sawgrass bog and boreal Sphagnum bog soils the alkyl to O-alkyl ratio was 0.5 and 0.4, respectively, reflecting weakly decomposed and less stable organic matter.

These results from solution ^{31}P and solid ^{13}C NMR revealed different behavior for soils sharing similar physical properties. Relatively little phosphorus was removed after HF treatment in soils dominated by alkyl groups compared to soils dominated by O-alkyl groups. These differences support the hypothesis that phosphorus will form associations with humified organic matter consisting primarily of alkyl and aromatic functional groups. Conversely, in soils dominated by O-alkyl groups (likely carbohydrates), phosphorus appears to be susceptible to leaching based on our hypothesis that HF treatment disrupts P-binding to free metal or mineral surfaces. Our data are consistent with those results and suggest that sequestration of phosphorus in wetlands may be tightly linked to soil carbon humification, the process that converts labile biopolymers into stable geopolymers. Once sequestered in this way, release of phosphorus into overlying water would be minimized as long as the soil organic matter was stabilized.

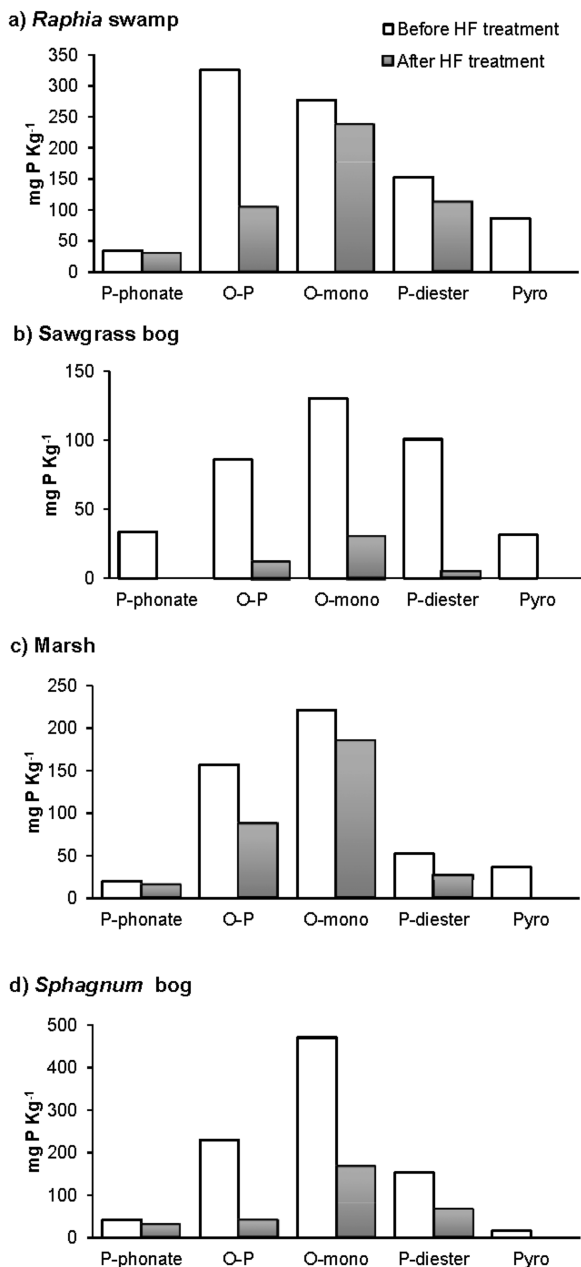


Figure 2. Distributions of phosphorus species (expressed as mg P/Kg dry soil) before and after HF treatment in soils from (a) tropical Raphia swamp (b) tropical sawgrass bog (c) subtropical marsh and (d) boreal Sphagnum bog sites. All values are expressed relative to the initial amount of soil in the extract.
Reproduced from reference (1). Copyright 2012 ACS.

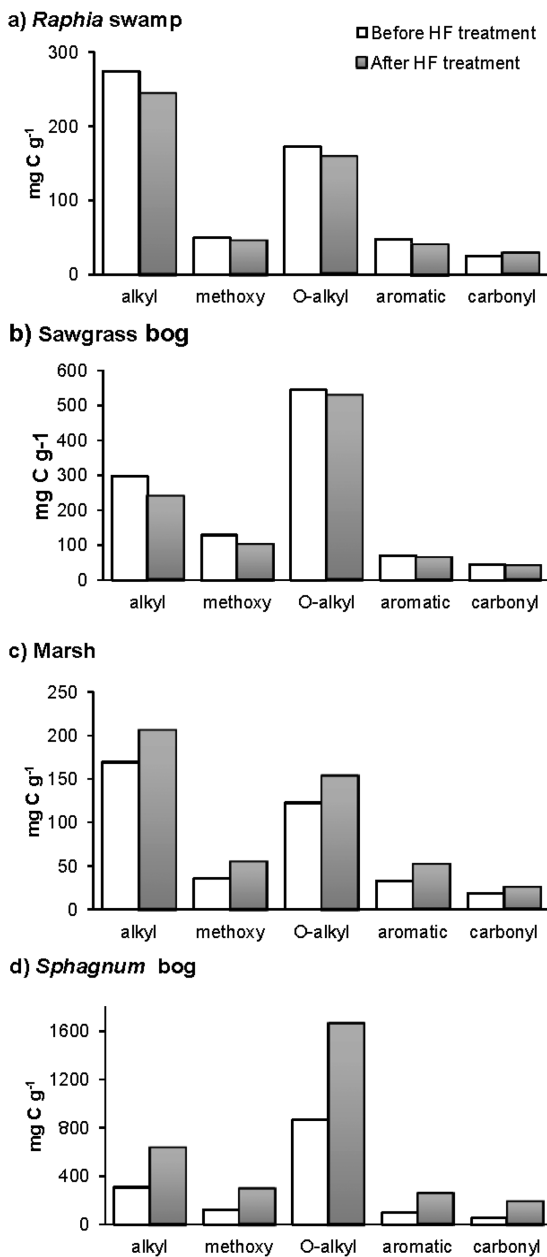


Figure 3. Distribution of major organic carbon species (expressed as mg C/g dry soil) before and after HF treatment in soils from (a) tropical Raphia swamp (b) tropical sawgrass bog (c) subtropical marsh and (d) boreal Sphagnum bog sites. Carbon concentrations are normalized for actual amount of soil and do not take into account enrichment due to removal of inorganic material after HF treatment. Reproduced from reference (1). Copyright 2012 ACS.

Phosphorus Speciation along a Gradient in WCA 2A

^{31}P and ^{13}C NMR were then used to characterize P-speciation and carbon functional group distributions in soils from Water Conservation Area 2A. The goal was to correlate these data with results of the acid stability study and predict the stability and potential re-suspension of phosphorus into WCA 2A surface waters. Figure 4 includes a representative ^{31}P NMR spectrum of phosphorus extracted from WCA 2A soils. Inorganic orthophosphate (9 ppm) and phosphate monoesters (7-8 ppm) are the dominant species in all samples. Phosphate diesters (0-2 ppm) are also present at much lower levels. Unfortunately, individual phosphate monoesters such as inositol phosphates or phosphate diesters such as phospholipids and nucleic acids cannot be clearly differentiated by ^{31}P NMR.

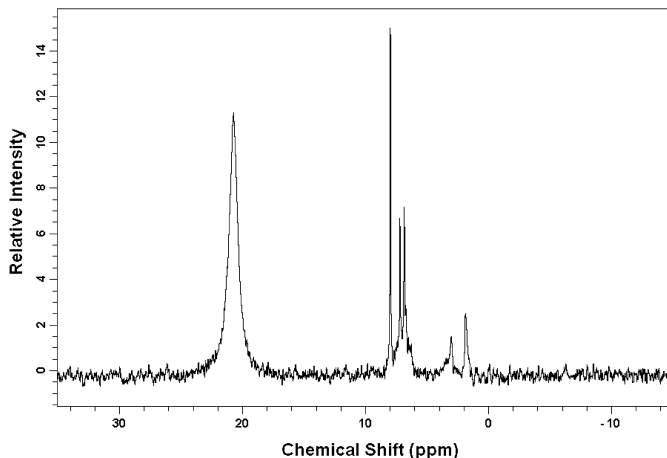


Figure 4. ^{31}P NMR spectrum of NaOH extract from WCA 2A sample EG4. The peak at ~ 20 ppm is methylene diphosphonic acid (MDPA) that is used as an internal standard.

Figure 5 includes quantitative distributions of these three forms of phosphate for the WCA 2A soils. While these sampling sites represent a hydrologic gradient, multiple inputs of surface runoff into WCA 2A yield phosphorus surface water concentrations that do not reflect this hydraulic gradient. This variability in surface P concentrations is reflected in variable soil P levels. However, in all of these soils, O-monoesters are the dominate P species, even in EG7 which is a mixed cattail/sawgrass site.

^{13}C NMR spectra of these Everglades soils reveal soil organic matter that is relatively “immature”, with alkyl (0 - 50 ppm) to O-alkyl ([50 - 60] + [60 - 110] ppm) ratios significantly less than one (Figures 6 and 7). Soil organic matter maturity can be quantified with a Humification Index (HI) calculated from the ratio of alkyl to O-alkyl carbon (23). HI values greater than 1 indicate preferential

loss of carbohydrates and “humified” organic matter (23, 25, 26). However, soils in WCA 2A appear only weakly decomposed. Our previous studies using HF pretreatments suggest that phosphorus associated with such immature organic matter (i.e. HI < 0.5) appears to be less stable and may well be prone to release back into the water column after drying - re-wetting cycles in the Water Conservation Areas. We therefore suggest that the excess dissolved phosphorus that is being biologically removed by marsh plants may not be truly sequestered until soil organic carbon becomes more humified in deeper soil horizons.

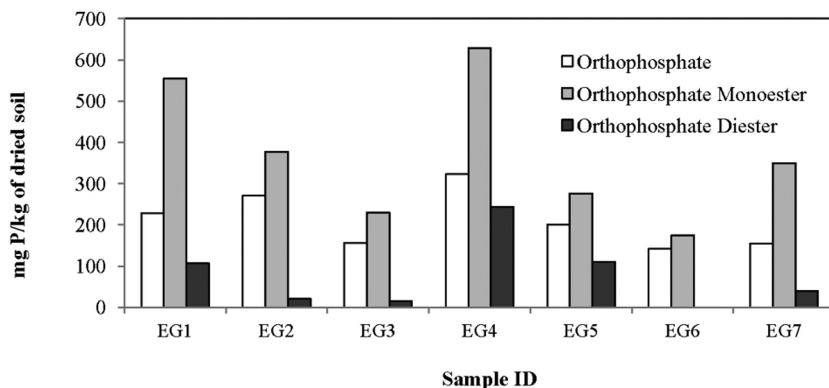


Figure 5. Summary of phosphorus speciation in WCA 2A soils determined by ^{31}P NMR.

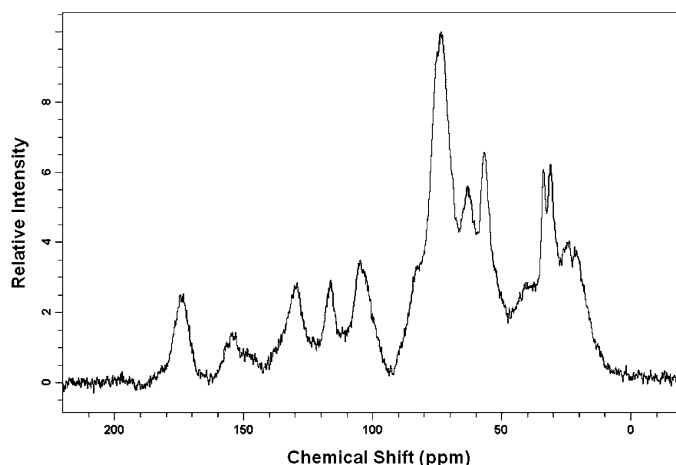


Figure 6. ^{13}C NMR spectrum of soil from WCA 2A site EG4.

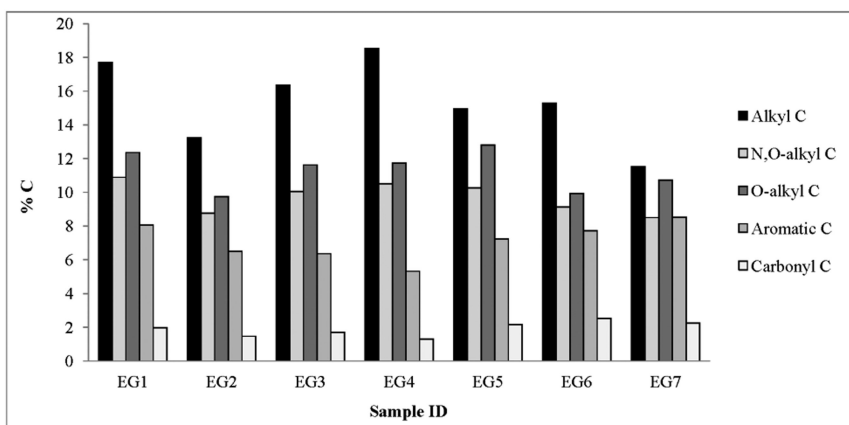


Figure 7. Summary of carbon speciation in WCA 2A soils determined by ^{13}C NMR.

Conclusions

The combination of ^{31}P and ^{13}C NMR spectroscopy was used to evaluate phosphorus speciation in wetland soils before and after HF treatment. Results identify inorganic and organic forms of phosphorus that are stabilized as a part of the organic matter matrix in soils that are highly humified (e.g. humification index $\text{HI} > 1$). In less mature soils where humification is much less extensive ($\text{HI} \leq \sim 0.5$), phosphorus appears to be susceptible to leaching into the overlying water column if soil wetting and/or redox conditions change. Application of the humification index threshold for predicting phosphorus leaching potentials to soils from Water Conservation Area 2A in the Florida Everglades suggests that phosphorus incorporated into WCA 2A soils may not be unequivocally sequestered and that future management plans should include consideration of this high phosphorus leaching potential.

Acknowledgments

NMR spectra were obtained in the FSU NMR Facility. The assistance of Dr. Banghao Chen, Facility Director, is greatly appreciated. Samples were provided by Dr. Ben Turner and Dr. Alexander Cheesman of the Smithsonian Tropical Research Institute, and Dr. Sue Newman of the South Florida Water Management District.

References

1. Hamdan, R.; El-Rifai, H. M.; Cheesman, A. W.; Turner, B. L.; Reddy, K. R.; Cooper, W. T. Linking Phosphorus Sequestration to Carbon Humification in Wetland Soils by ^{31}P and ^{13}C NMR Spectroscopy. *Environ. Sci. Technol.* **2012**, *46*, 4775–4782.

2. Cheesman, A. W.; Dunne, E. J.; Turner, B. L.; Reddy, K. R. Soil Phosphorus Forms in Hydrologically Isolated Wetlands and Surrounding Pasture Uplands. *J. Environ. Qual.* **2010**, *39*, 1517–1525.
3. Reddy, K. R.; Wang, Y.; DeBusk, W. F.; Fisher, M. M.; Newman, S. Forms of soil phosphorus in selected hydrologic units of the Florida everglades. *Soil Sci. Soc. Am. J.* **1998**, *62*, 1134–1147.
4. Turner, B. L.; Newman, S.; Newman, J. M. Organic phosphorus sequestration in subtropical treatment wetlands. *Environ. Sci. Technol.* **2006**, *40*, 727–733.
5. Turner, B. L.; Newman, S. Phosphorus cycling in wetland soils: The importance of phosphate diesters. *J. Environ. Qual.* **2005**, *34*, 1921–1929.
6. Johnston, C. A. Sediment and nutrient retention by fresh-water wetlands - effects on surface-water quality. *Crit. Rev. Environ. Control* **1991**, *21*, 491–565.
7. Richardson, C. J. Mechanisms controlling phosphorus retention capacity in fresh-water wetlands. *Science (Washington, D.C.)* **1985**, *228*, 1424–1427.
8. Newman, S.; Aldridge, F. J.; Phlips, E. J.; Reddy, K. R. Assessment of phosphorus availability for natural phytoplankton populations from a hypereutrophic lake. *Arch. Hydrobiol.* **1994**, *130*, 408–427.
9. Wright, A. L.; Reddy, K. R. Phosphorus loading effects on extracellular enzyme activity in everglades wetland soils. *Soil Sci. Soc. Am. J.* **2001**, *65*, 588–595.
10. Kuhn, N. L.; Mendelsohn, I. A.; McKee, K. L.; Lorenzen, B.; Brix, H.; Miao, S. L. Root phosphatase activity in Cladium jamaicense and Typha domingensis grown in everglades soil at ambient and elevated phosphorus levels. *Wetlands* **2002**, *22*, 794–800.
11. Patrick, W. H.; Khalid, R. A. Phosphate release and sorption by soils and sediments - effect of aerobic and anaerobic conditions. *Science (Washington, D.C.)* **1974**, *186*, 53–55.
12. Faulkner, S. P.; Richardson, C. J. In *Constructed Wetlands for Wastewater Treatment*; Hamner, D. A., Ed.; Lewis Publishers: Chelsea, MI, 1989; pp 41–72.
13. Richardson, C. J. In *Phosphorus Biogeochemistry in Subtropical Systems*; Reddy, K. R., O'Connor, G. A., Schelske, C. L., Eds.; Lewis Publishers: Boca Raton, FL, 1999; pp 47–68.
14. Chen, C. R.; Condron, L. M.; Turner, B. L.; Mahieu, N.; Davis, M. R.; Xu, Z. H.; Sherlock, R. R. Mineralisation of soil orthophosphate monoesters under pine seedlings and ryegrass. *Aust. J. Soil Res.* **2004**, *42*, 189–196.
15. Reddy, K. R.; DeLaune, R. D. *Biogeochemistry of Wetlands: Science and Applications*; CRC: Boca Raton, FL, 2008; p 328–330.
16. Schilling, M.; Cooper, W. T. Effects of chemical treatments on the quality and quantitative reliability of solid-state C-13 NMR spectroscopy of mineral soils. *Anal. Chim. Acta* **2004**, *508*, 207–216.
17. Celi, L.; Lamacchia, S.; Marsan, F. A.; Barberis, E. Interaction of inositol hexaphosphate on clays: Adsorption and charging phenomena. *Soil Sci.* **1999**, *164*, 574–585.

18. Moore, P. A.; Reddy, K. R.; Fisher, M. M. Phosphorus flux between sediment and overlying water in Lake Okeechobee, Florida: spatial and temporal variations. *J. Environ. Qual.* **1998**, *27*, 1428–1439.
19. Jordan, S.; Velty, S.; Zeitz, J. The influence of degree of peat decomposition on phosphorus binding forms in fens. *Mires Peat* **2007**, *2*, 1–10.
20. Sjogersten, S.; Cheesman, A. W.; Lopez, O.; Turner, B. L. Biogeochemical processes along a nutrient gradient in a tropical ombrotrophic peatland. *Biogeochemistry* **2011**, *104*, 147–163.
21. Harris, W. G.; Rhue, R. D.; Kidder, G.; Brown, R. B.; Littell, R. Phosphorus retention as related to morphology of sandy coastal plain soil materials. *Soil Sci. Soc. Am. J.* **1996**, *60*, 1513–1521.
22. Dougherty, W. J.; Smernik, R. J.; Bunemann, E. K.; Chittleborough, D. J. On the use of hydrofluoric acid pretreatment of soils for phosphorus-31 nuclear magnetic resonance analyses. *Soil Sci. Soc. Am. J.* **2007**, *71*, 1111–1118.
23. Baldock, J. A.; Oades, J. M.; Nelson, P. N.; Skene, T. M.; Golchin, A.; Clarke, P. Assessing the extent of decomposition of natural organic materials using solid-state C-13 NMR spectroscopy. *Aust. J. Soil Res.* **1997**, *35*, 1061–1083.
24. Gerke, J. Humic (Organic Matter)-Al(Fe)-phosphate complexes: An underestimated phosphate form in soils and source of plant-available phosphate. *Soil Sci.* **2010**, *175*, 417–425.
25. Hopkins, D. W.; Chudek, J. A.; Webster, E. A.; Barraclough, D. Following the decomposition of ryegrass labeled with ¹³C and ¹⁵N in soil by solid-state nuclear magnetic resonance spectroscopy. *Eur. J. Soil Sci.* **1997**, *48*, 623–631.
26. Zech, W.; Ziegler, F.; Kogel-Knabner, I.; Haumaier, L. Humic substances distribution and transformation in forest soils. *Sci. Total Environ.* **1992**, *118*, 155–174.

Chapter 8

Relation between Optical Properties and Formation of Reactive Intermediates from Different Size Fractions of Organic Matter

Simón Mostafa,* Julie A. Korak, Kyle Shimabuku,
Caitlin M. Glover, and Fernando L. Rosario-Ortiz

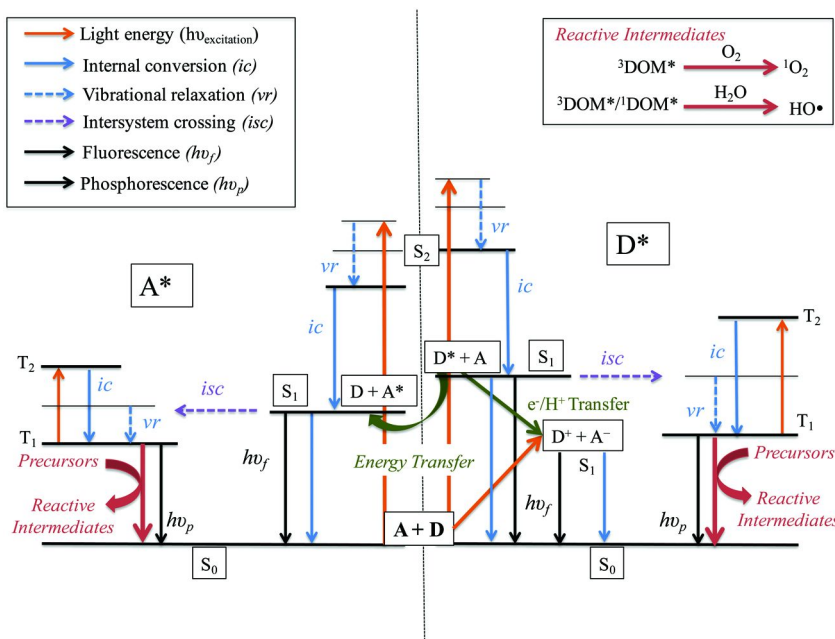
Department of Civil, Environmental and Architectural Engineering,
428 UCB, University of Colorado, Boulder, Colorado 80309, U.S.A.

*E-mail: simonmostafa@gmail.com.

The photophysics and photochemistry of aquatic organic matter (OM) are of interest due to their role in defining the reactivity of this material in the environment. Studies have demonstrated that molecular size and composition are important determinants of the photochemical behavior of OM, including the formation of reactive intermediates (RIs). The present study expands on previous works by evaluating both photophysical and photochemical processes of OM of distinct origins and molecular sizes through the analysis of absorbance and fluorescence along with the formation of various RIs of interest (^3OM , HO^\bullet , $^1\text{O}_2$). In general, larger size fractions displayed higher absorptivity that extends further into the visible region. On the other hand, smaller components displayed higher quantum yields for fluorescence and all RIs measured. In accordance with hypotheses previously formulated, possible explanations for the observed results are proposed based on the increased prevalence of non-radiative energy decay processes in larger OM molecules.

Introduction

Organic matter (OM) of various origins is present in all water bodies and plays an important role in a number of natural processes, affecting the fate and transport of water constituents (1–3), light absorption and the depth of the photic zone (4, 5) as well as the photochemical production of reactive intermediates (RIs) (6–9), including excited states, hydroxyl radicals (HO^{\cdot}) and singlet oxygen (${}^1\text{O}_2$). RIs are known to react at relatively high rates with various organic contaminants as well as microbes (3, 10–17). Following light-induced excitation, the excited state of an OM chromophore may return to its ground state via a radiative transition, i.e. luminescence, or undergo non-radiative processes (internal conversion, IC or intersystem crossing, ISC). ISC leads to the formation of a triplet excited state (${}^3\text{OM}$), which can be followed by phosphorescence or ${}^1\text{O}_2$ formation. These processes are illustrated in Scheme 1.



Scheme 1. Conceptual illustration of photoinduced processes within organic matter. Light excitation and various possible decay processes are shown, including vibrational relaxation (VR), intersystem crossing (ISC), radiationless decay via internal conversion (IC), luminescence ($h\nu_f$, $h\nu_p$), energy and charge transfer from donor (D) to acceptor (A) species, as well as formation of reactive intermediates. The relative position of the various energy levels is meant for illustration purposes only and does not represent energy values of specific excited state molecules.

The photochemistry and photophysics of OM are of interest to environmental scientists and engineers; yet, due to its molecular complexity, it is difficult to isolate and study individual compounds and their behavior. Instead, measuring

bulk characteristics and relevant processes offers an insight into the overall properties of the material. The relative efficiency at which each of these processes occurs is measured by its quantum yield (Φ), which is defined as the number of occurrences of a given process per photon absorbed (18).

Previous works have explored how photophysical behavior of OM is affected by its molecular size. In this regard, differences in absorbance spectra have been reported (and partially attributed to molecular size) and characterized by increased tailing into longer wavelength regions for larger molecules (19). Quantification of this optical phenomenon has been achieved by measuring the E4:E6 ratio (19–21), E2:E3 ratio (21–24), and spectral slope (S) (24–28). Early on, these observations were associated with intramolecular interactions and the formation of donor-acceptor complexes (19, 29). Such models have since been expanded, elucidating the types of species involved in the charge transfer (CT) donor-acceptor pairs (30–32). Consistent with the increase in CT processes expected from increased molecular size, decreases in the apparent fluorescence efficiency have been correlated to increasing OM size (29, 31, 33–37). Size effects have also been linked to the formation efficiencies of various RIs in the presence of OM. For example, previous studies by our group have shown that across size fractions of wastewater-derived OM (WWOM), fluorescence quantum yields correlate to those of HO[•] radicals (38) while E2:E3 ratios are positively correlated to singlet oxygen quantum yields (28). Similar correlations to singlet oxygen formation have been reported for fluorescence of various humic and fulvic acids (39) as well as for absorbance spectral characteristics (22–24). Furthermore, the formation of triplet states have also been reported to increase with decreasing size of OM (35, 40).

In this contribution, we expand on the work of our group and others by assessing the formation rates of various RIs and conducting detailed optical measurements simultaneously on various OM size fractions. Evaluating the behavior of OM samples with very different compositions (Suwannee River natural organic matter and WWOM) that still display similar trends as a function of size provides a more complete picture of the photophysics of these molecules and of the underlying mechanisms. These results are combined with previously proposed mechanisms to put forward an explanation of OM photophysical and photochemical behaviors based on relevant intramolecular processes. It is proposed here that increasing molecular size of OM leads to an increase in the prevalence of non-radiative decay relative to other processes, such as luminescence and the formation RIs.

Materials and Methods

Sample Collection and Preparation

Two different sets of samples were used for this study representing OM of different origins, namely Suwannee River natural organic matter (SRNOM) and treated wastewater effluent (BWW). SRNOM isolate was obtained from the International Humic Substances Society (catalog number 1R101N). After

dissolving the SRNOM, the stock solution was diluted to a final concentration of 8.8 mgC/L in a phosphate buffer solution (10 mM, pH 7.2). Wastewater effluent was obtained from the Boulder Wastewater Treatment Facility after undergoing complete treatment (no chemical disinfection, e.g. chlorination, was performed). Within 8 hours of collection, samples were filtered through 0.7 μ m glass fiber filters that were muffled at 550 °C for 3 hours and rinsed. Filtered samples were kept refrigerated at a temperature of 4 °C in the dark until further use.

Each source water was fractionated using ultrafiltration membranes into three size fractions: less than 1 kDa, 1-10 kDa, and greater than 10 kDa. To achieve this, the OM with MW < 1 kDa was separated in a Millipore tangential flow ultrafiltration system with an Amicon regenerated cellulose cartridge with a nominal molecular weight cut-off (NMWCO) of 1 kDa. The retentate was further fractionated in a solvent-resistant stir cell (Model XFUF 07601, Millipore, MA, USA) using a regenerated cellulose membrane with a NMWCO of 10 kDa (Millipore), resulting in a fraction with MW > 10 kDa (retentate) and an intermediate fraction with 1 kDa < MW < 10 kDa (permeate). Initially, retentate solutions were diluted by three times the initial volume with the phosphate buffer solution and then filtered so that the initial volume remained in the retentate. In an attempt to remove OM from the retentate that was less than the NMWCO, the retentate from each fractionation step was rinsed by diluting in 10 mM phosphate buffer and filtering again. The rinsing steps were repeated until there was a less than 5% change in the permeate absorbance at 254 nm (~ 4-5 rinses), but likely did not remove all the DOM that could potentially pass through the membrane. Concentrations of Cl⁻ and Br⁻ in the WW samples were measured by ICP-MS. All WW samples were adjusted to the same concentration of these ions (72.5 mg/L for Cl⁻ and 0.3 mg/L for Br⁻) by addition of NaCl and KBr to allow for an accurate inter-comparison of fractions considering the impact of halides on the formation of RIs (41).

Characterization and Optical Measurements

Dissolved organic carbon (DOC) measurements were conducted using a TOC-VCSH (Shimadzu Corp., Japan) analyzer while nitrite (NO₂⁻) and nitrate (NO₃⁻) were measured using FIA-IC (Lachat QuikChem 8500 Flow Injection Analyzer).

Size exclusion chromatography (SEC) was performed using an Agilent 1200 series high performance liquid chromatograph with a Waters Protein-PakTM 125 7.8 x 300 mm column (Milford, MA). The detector was an Agilent diode array that monitored UV absorbance at a wavelength of 254 nm. The mobile phase buffer consisted of 0.0024 M Na₂HPO₄, 0.0016 M Na₂HPO₄, and 0.025 M NaSO₄, and the flow rate was 0.7 ml/min.

For the optical measurements, the concentrated fractions were diluted with 10 mM phosphate buffer to an absorbance less than 0.05 at 350 nm. UV-Vis absorption was measured in triplicate from 200 to 600 nm in 1 nm increments in a 1 cm pathlength quartz cuvette (Cary 100, Agilent Technologies CA). The E₂:E₃ value denotes the ratio of absorbance at 254 nm and 365 nm. Absorption coefficient, $a(\lambda)$, was calculated according to equation 1, where A is the absorbance at wavelength λ in nanometers, and L is the path length in centimeters. The spectral

slope (S) was determined by fitting the non-linear regression to the absorption coefficients from 300 to 600 nm following equation 2, where λ_r is the reference wavelength (350 nm) (27, 42).

$$a(\lambda) = 2.303 A(\lambda)/L \quad (1)$$

$$a(\lambda) = a(\lambda_r) e^{-S(\lambda-\lambda_r)} \quad (2)$$

Fluorescence excitation-emission matrices (EEMs) were measured in triplicate for each sample (Fluoromax-4, John Yvon Horiba, NJ). Excitation wavelengths ranged from 240 to 450 nm in 5 nm increments, and the emission wavelengths ranged from 300 to 560 nm in 2 nm increments. Both the excitation and emission bandpasses were set to 4 nm, and the integration time was 0.25 s. Fluorescence intensities were measured in ratio mode (signal divided by reference). Lamp scans, cuvette contamination checks and Raman scans were performed daily to verify calibration. Fluorescence data were corrected for inner filter effects, normalized to the area under Raman peak for 18 MΩ lab-grade water at 370 nm excitation and blank subtracted, according to published methods (43).

The fluorescence quantum yields were determined for each sample relative to a 1 mg/L quinine sulfate standard in 0.1N H₂SO₄ following previously published methods except that the quinine sulfate absorbance and fluorescence were measured at the same excitation wavelength as the DOM sample (44–46). Quantum yields were calculated as a function of excitation wavelength from 290 to 380 nm. The calculation assumes a quinine sulfate quantum yield of 0.51, and the uncertainty reported is based on the error propagation of both fluorescence and absorption measurements between triplicates. The fluorescence index (FI) is reported for each fraction as a measure of compositional differences. FI is defined as the ratio of emission intensities at 470 and 520 nm at an excitation wavelength of 370 nm (47, 48).

Reactive Species Measurements

Furfuryl alcohol (FFA), benzene, and 2,4,6-trimethylphenol (TMP) were used as probes for reactive intermediates ¹O₂, HO[•], and ³OM, respectively (28, 49). FFA was added to the samples at an initial concentration of 22.5 μM along with methanol (0.1 M) in order to quench HO[•], which may be formed during light exposure. For the HO[•] experiments, benzene (99.8% Alpha Aesar, MA, USA) was added at a concentration of 3 mM, causing it to be the main HO[•] scavenger in the system (49) and leading to the formation of phenol. Bovine liver catalase (Sigma-Aldrich, MO, USA) was added at a concentration of 20 unit/mL to prevent the formation of hydrogen peroxide, thus preventing HO[•] formation via photo-Fenton processes. TMP was used as a probe to assess the formation of OM excited triplet states (35, 50–52), by measuring its degradation from an initial concentration of 3.67 μmol/L.

All samples were placed in 2-mL clear glass vials and kept in a water bath at 20 °C during exposure to simulated sunlight. A solar simulator (Model Sol1A, Oriel Instruments, Stratford, CT) was used for the exposure experiments, equipped with a 1000 W Xe lamp and 1.5 air mass filter. Probe concentrations were monitored after light exposure using liquid chromatography (Agilent, 1200 LC). Quantum yields for $^1\text{O}_2$ (Φ_{SO}), HO^\bullet (Φ_{HO}), and TMP degradation (Φ_{TMP} , indicative ^3OM formation) were calculated based on the ratio of the reactive species formed ($^1\text{O}_2$, HO^\bullet) or TMP degraded, divided by the total number of photons absorbed per unit time over the wavelength range of the polychromatic light source used in this study ($\lambda = 290\text{-}400\text{ nm}$). The contribution of nitrate to the formation of HO^\bullet was factored out for the calculation of Φ_{HO} . Details of the methodology used can be found in previous publications (28, 49), except for TMP degradation experiments. In this case, analysis was similar to that of FFA degradation, where pseudo-first order kinetics are assumed and the degradation rate, k_{TMP} , represents the slope of the linear regression curve of $\ln[\text{TMP}]/[\text{TMP}]_0$ versus irradiation time.

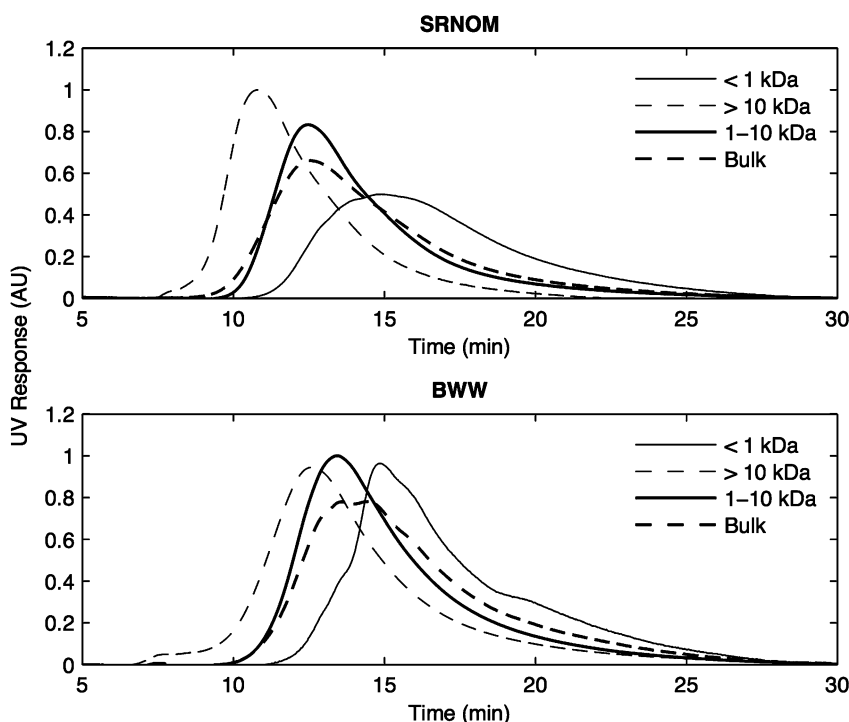


Figure 1. Size exclusion chromatograms with UV_{254} detection for SRNOM and BWW size fractions.

Results and Discussion

Water Quality and Molecular Size

The results of the water quality analyses, including pH and DOC concentration are shown in Tables 1 and 2 for SRNOM and BWW, respectively, along with optical parameters including spectral slope, E2:E3 ratio, and specific absorbance at 254 and 350 nm. Figure 1 displays the results of the SEC measurements normalized to the total area. The weighted average of the elution time (t_{SEC}) of the chromophoric dissolved OM, as calculated from the SEC measurements, is shown in Tables 1 and 2 with increasing times corresponding to decreasing OM size. While each fraction has a different t_{SEC} , there is overlap between the spectra due to the heterogeneity of DOM. Ultrafiltration membranes are typically designed to retain 90% of a protein solution near the reported NMWCO. Considering that DOM is chemically different from the proteins used by the manufacturer for size calibration, it is expected that a portion of DOM greater than the NMWCO will still pass through the filters. As a result, some of the OM molecules will reside outside of the stated NMWCOs following ultrafiltration (53).

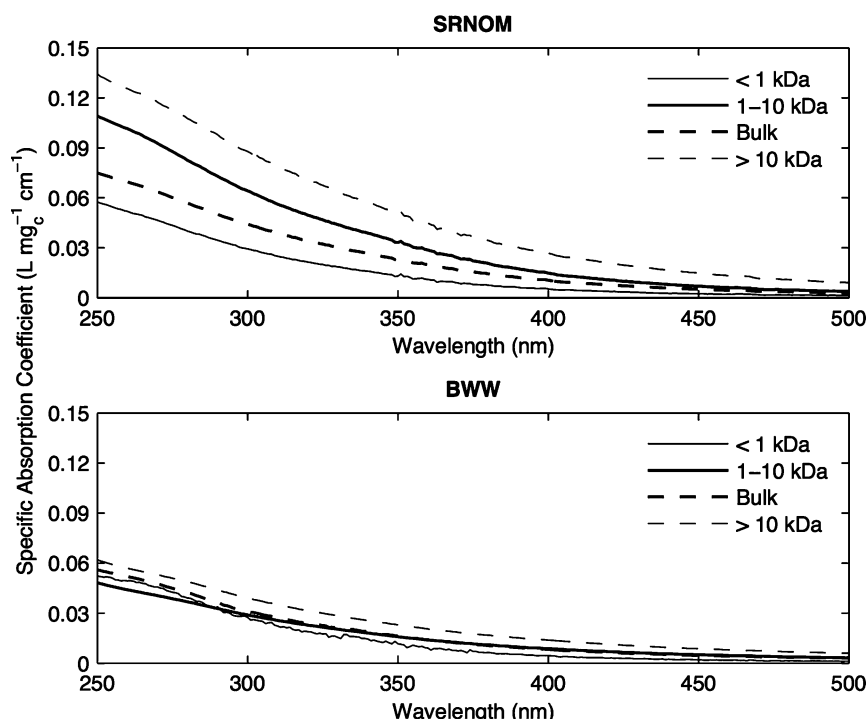


Figure 2. Specific absorption spectra for each size fraction. Absorption coefficients calculated using equation 1 are normalized to the sample DOC concentration.

Optical Properties

Absorbance spectra for all the samples studied are presented in Figure 2 and display typical featureless curves of decreasing absorbance with increasing wavelength.

Table 1. SRNOM Samples Characteristics and Quantum Efficiencies of Various Processes. The Standard Deviation between Analytical Triplicates Is Listed in Parentheses

Sample	SRNOM			
Fraction	Bulk	> 10 kDa	1-10 kDa	< 1 kDa
pH	7.2	7.2	7.2	7.2
DOC (mg C/L) ^a	4.9	1.9	3.5	3.0
SUVA ₂₅₄ (L/mg C-m)	3.16	5.65	4.60	2.40
SUVA ₃₅₀ (L/mg C-m)	0.99	2.17	1.44	0.56
S	0.014	0.012	0.014	0.017
E2:E3	4.11	3.25	4.18	5.83
FI	1.29	1.06	1.19	1.47
t _{SEC} (min)	14.8	12.4	14.0	16.1
Φ _{FL}	0.007 (0.00017)	0.001 (0.00004)	0.005 (0.00014)	0.023 (0.00063)
Φ _{SO} (%)	1.85 (0.15)	0.44 (0.05)	1.44 (0.11)	4.39 (0.33)
Φ _{HO} (%)	0.0041 (0.0020)	0.0035 (0.0013)	0.0028 (0.0008)	0.0068 (0.0015)
Φ _{TMP} (%)	0.0131 (0.0009)	0.0049 (0.0003)	0.0062 (0.0005)	0.0284 (0.0029)

^a The DOC values for the size fractions do not add up to the bulk concentration since volume of each fraction was different.

For both OM sources, smaller molecular size fractions had higher spectral slope values (0.024 and 0.017 for the <1 kDa fraction of BWW and SRNOM, respectively) compared to the bulk, unfractionated samples (~ 0.014 for both), as shown in the tables below. Furthermore, specific absorbance at 254 and 350 nm generally increased with increasing size, in agreement with previous reports

(53, 54), except for the specific absorbance at 254 nm being higher for the smallest than for the mid fraction in BWW. These results could be explained in part by differences in composition across the various fractions, with increasing concentration of phenolic groups in the larger size fractions as has been reported, for example, in the case of Laurentian fulvic acid (29).

Table 2. BWW Samples Characteristics and Quantum Efficiencies of Various Processes. The Standard Deviation between Analytical Triplicates Is Listed in Parentheses

Sample	BWW			
Fraction	Bulk	> 10 kDa	1-10 kDa	< 1 kDa
pH	7.4	7.3	7.2	7.7
DOC (mg C/L) ^a	5.0	10.0	11.7	1.5
SUVA ₂₅₄ (L/mg C-m)	2.43	2.59	2.01	2.48
SUVA ₃₅₀ (L/mg C-m)	0.70	0.99	0.69	0.50
S	0.014	0.010	0.012	0.024
E2:E3	4.62	3.19	3.70	7.80
FI	2.05	1.51	1.54	2.14
t _{SEC} (min)	16.0	13.9	15.2	17.8
Φ _{FL}	0.027 (0.00102)	0.004 (0.00015)	0.008 (0.00037)	0.048 (0.00190)
Φ _{SO} (%)	3.29 (0.63)	1.15 (0.07)	1.91 (0.16)	6.18 (0.64)
Φ _{HO} (%)	0.0032 (0.0005)	0.0018 (0.0003)	0.0016 (0.0001)	0.0497 (0.0111)
Φ _{TMP} (%)	0.0435 (0.0034)	0.0014 (0.0001)	0.0027 (0.0002)	0.1327 (0.0130)

^a The DOC values for the size fractions do not add up to the bulk concentration since volume of each fraction was different.

The fluorescence EEMs for all samples are shown in Figures 3 and 4. Since the DOC concentration of each fraction was different, the intensities were normalized per unit carbon to be able to directly compare them. On a per unit carbon basis, the smallest molecular size fraction has the highest intensities compared to the large size fractions. For SRNOM, the bulk sample intensities fall closest to the the 1-10 kDa fraction whereas the bulk BWW sample intensity falls between those of the <1 kDa and 1-10 kDa fractions.

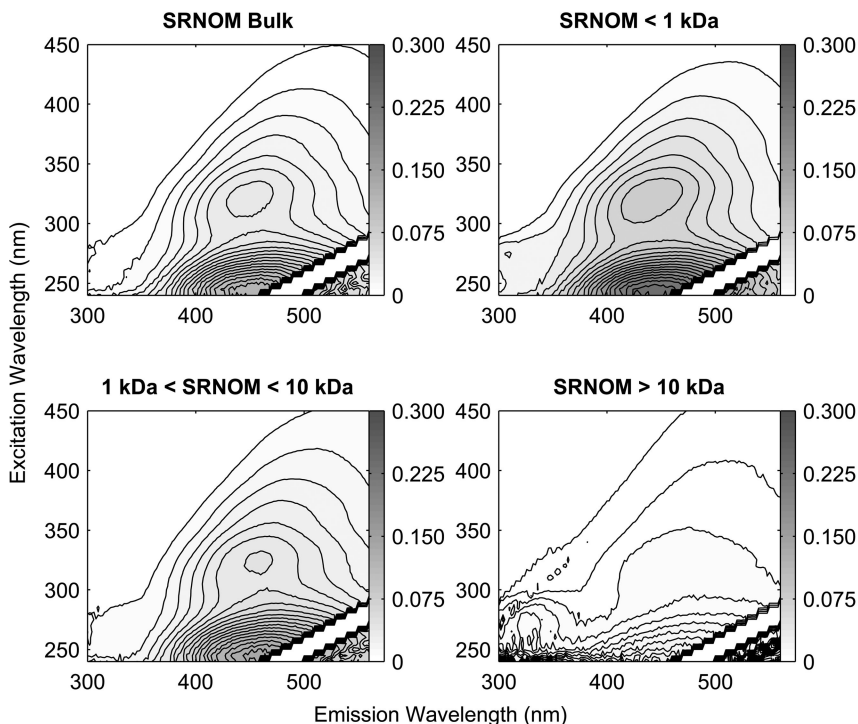


Figure 3. Fluorescence EEMs for SRNOM and each size fraction. Each EEM is the average EEM from three replicates. The intensities have been normalized to the DOC concentration.

The fluorescence quantum yields (Φ_f) as a function of excitation wavelength are presented in Figures 5a and 5b and show that for both OM sources the Φ_f increases with decreasing molecular size. The bulk quantum yield is influenced by the relative contribution of each size fraction. Low molecular weight species make the greatest relative contribution towards the overall fluorescence of unfractionated BWW and the Φ_f of this unfractionated sample falls in between that of the <1 kDa and 1-10 kDa fractions. Unfractionated SRNOM Φ_f , however, is closer to that of the mid-size fraction. The maximum Φ_f occurred at an excitation of 350 nm for all samples except for the <1 kDa BWW (360 nm). The position of max Φ_f with respect to excitation energy appears to be independent of size, as suggested elsewhere (31).

The correlation between excitation wavelength (λ_{ex}) and peak emission wavelength (λ_{em}) has been suggested as evidence for CT interactions as the source of fluorescence in the visible range (30, 31) and is depicted in Figures

5c and 5d. Such interpretation is derived from the assumption that a red shift in the peak emission with increasing excitation wavelength indicates that the set of fluorophores emitting upon excitation with longer wavelengths represents a subgroup of those excited at shorter wavelengths. This behavior is in contrast to regions where λ_{em} is independent of λ_{ex} and is attributed to individual fluorophores that behave independently from other processes, i.e., emission from local excited states (30, 31). All fractions exhibit a region where excitation and emission wavelengths are correlated. The larger molecular weight fractions (>10 kDa and 1-10 kDa) both show a region where λ_{em} is independent of λ_{ex} , which occurs at $\lambda_{ex} < 350$ nm. Both <1 kDa fractions show a continued correlation at $\lambda_{ex} < 350$ nm. The bulk waters display characteristics of both size fraction behaviors. Past work suggests that the region where λ_{em} is independent of λ_{ex} occurs at excitation wavelengths less than that of the maximum Φ_f (30, 31). These samples suggest that this trend is violated in the low molecular weight fractions, which may be an indication of different fluorescence mechanisms.

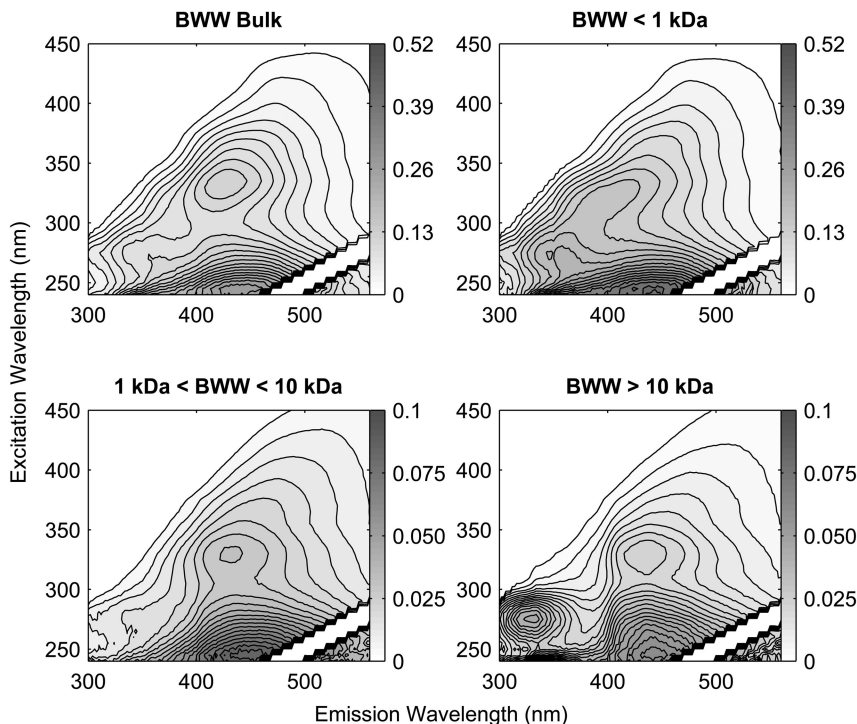


Figure 4. Fluorescence EEMs for BWW and each size fraction. Each EEM is the average EEM from three replicates. Note the different scales used for the various samples.

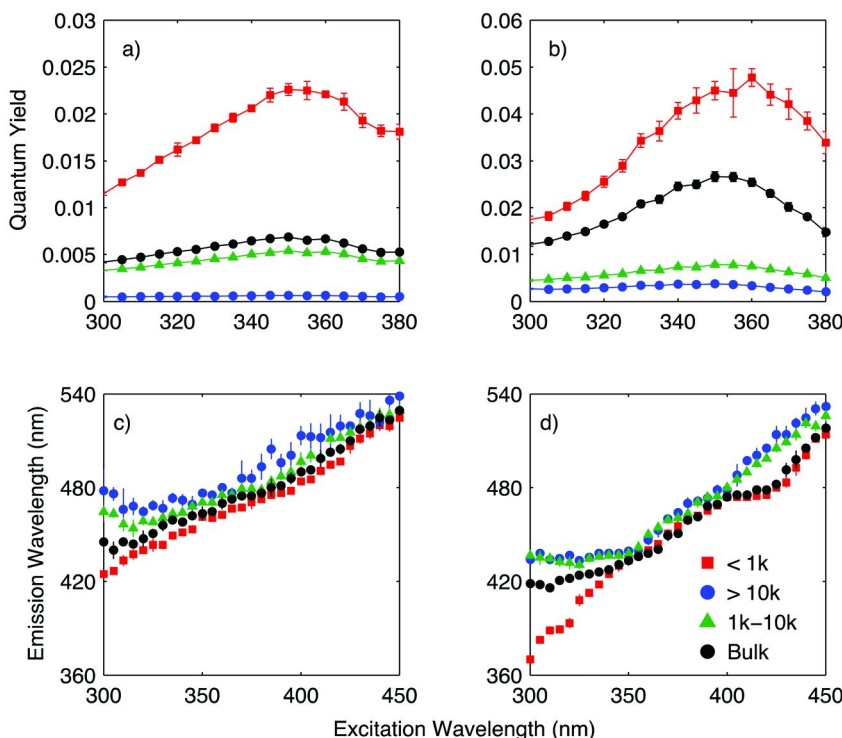


Figure 5. Fluorescence quantum yields as a function of excitation wavelength is presented for each size fraction in a) SRNOM and b) BWW. Peak emission wavelength as a function of excitation wavelength is depicted for each size fraction for c) SRNOM and d) BWW.

The wastewater samples exhibit a behavior not reported elsewhere. The BWW <1 kDa fraction has a small shoulder at λ_{ex} of 310–320 nm (Figure 5d), which may be due to local state emissions from the blue-shifted fluorescence commonly attributed to the Peak M region (55). A fluorescence plateau in the Peak M region is apparent in Figure 4. Finally, both the unfractionated and <1 kDa BWW fraction exhibit a region where emission wavelength is independent of λ_{ex} between 400 and 420 nm, suggesting the presence of low molecular weight species emitting from local states that dominate the fluorescence relative to charge transfer interactions.

Formation of Reactive Intermediates

Figure 6 shows the Φ for the reactive intermediates measured (HO^{\cdot} , ${}^1\text{O}_2$) and TMP degradation (${}^3\text{OM}$) as well as the maximum fluorescence quantum yield. In this figure, quantum yields for each photochemical process have been normalized to the quantum yield measured in the corresponding bulk water for comparison on the same numeric scale (all Φ values are shown in Tables 1 and 2).

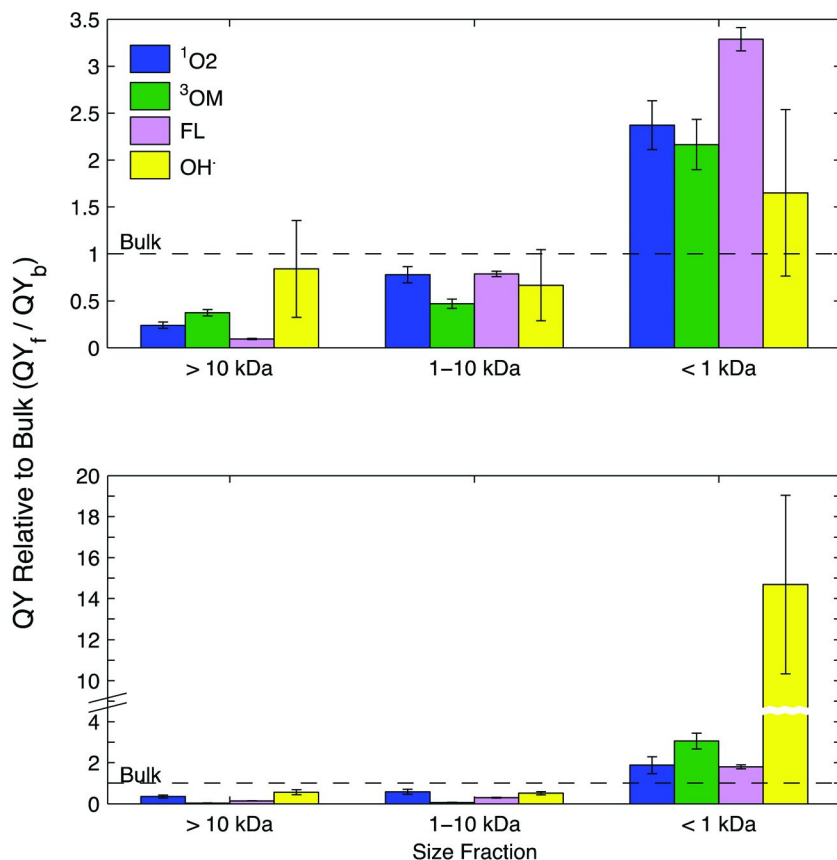


Figure 6. Quantum yields for the formation of reactive intermediates ($^1\text{O}_2$, HO^\cdot), TMP degradation (^3OM), and maximum fluorescence for the different size fractions normalized to the values of the unfractionated samples of SRNOM and BWW. Quantum yields for bulk samples are assigned a value of 1 for each specific species and the relative values for the fractions are displayed.

Clear trends emerge for both sets of samples (SRNOM, BWW) where quantum yields increase with decreasing size. In all cases, the <1 kDa fraction shows the highest value and the >10 kDa the lowest. These trends for HO^\cdot and $^1\text{O}_2$ have previously been reported for similar samples (28, 38) and the same behavior is shown here for the ^3OM , consistent with results reported for fulvic acid (40) and humic acid triplet states (35). These results, together with fluorescence, suggest that the lower MW fractions are more reactive in terms of fluorescence relaxation and photochemical production of RIs.

Relation between Measured Properties

Since the various parameters discussed above increase with decreasing size, it is not surprising that monotonic positive relations emerge when comparing the formation efficiency of the various reactive species and optical properties. Such trends are shown in Figures 7 and 8, where the efficiency of the various photochemical processes positively correlates to S and fluorescence index (FI) values, respectively (similar trends were found for E2:E3, not shown).

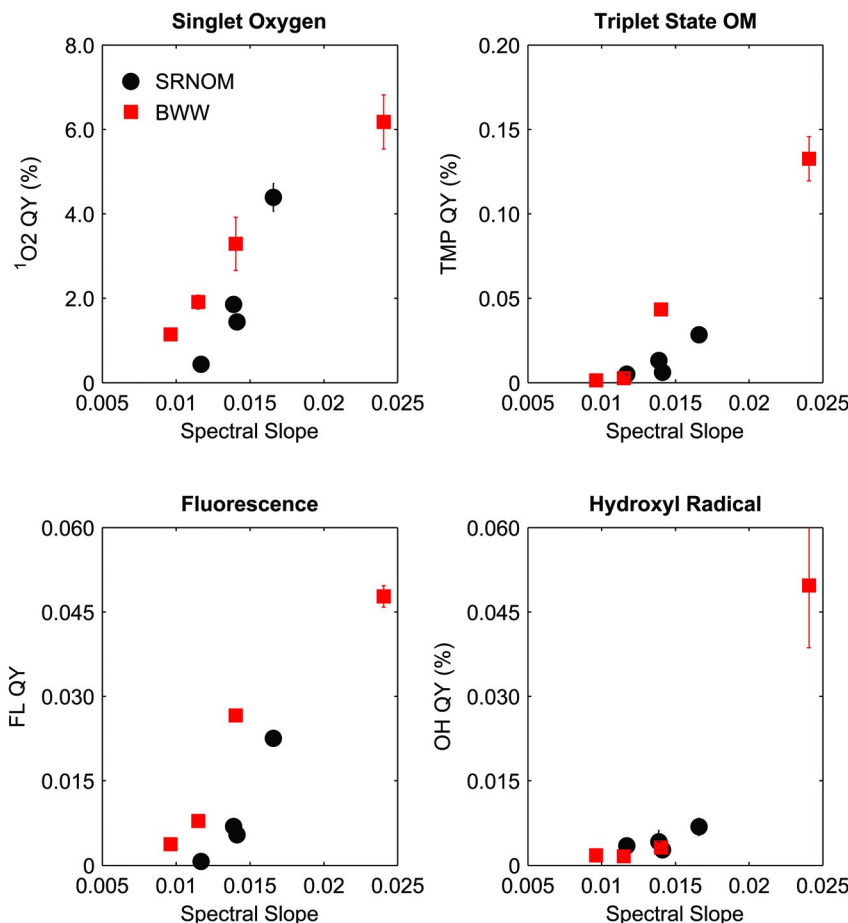


Figure 7. Quantum yields of the various processes measured as a function of sample spectral slope. Values for the unfractionated samples and three size fractions for both SRNOM and BWW are displayed.

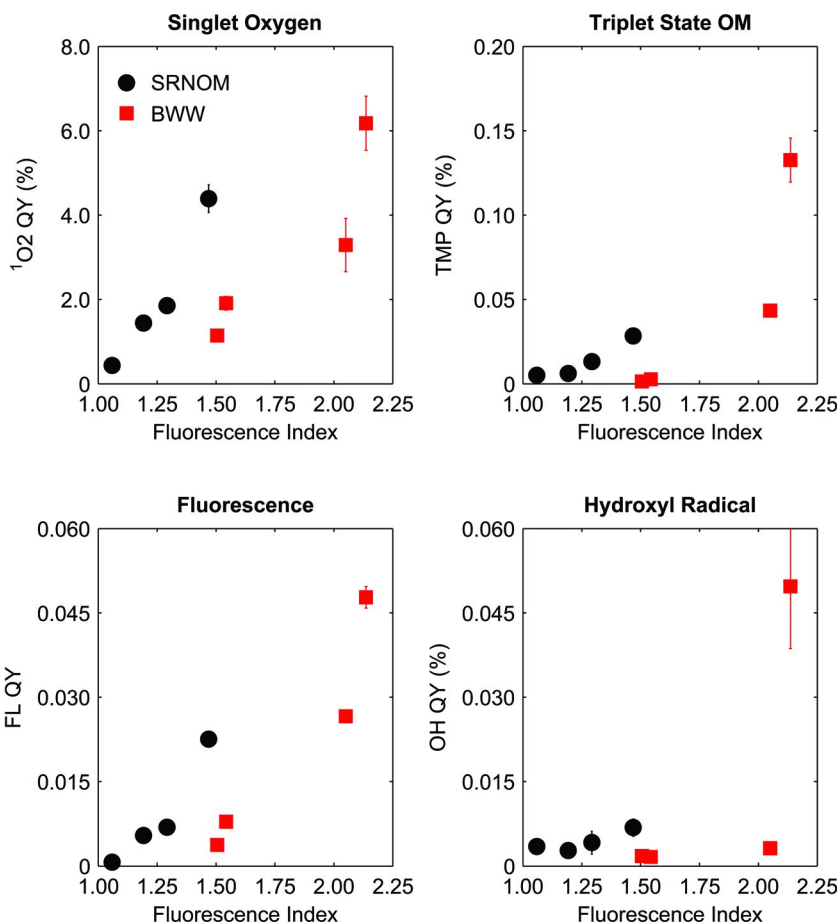


Figure 8. Quantum yields as a function of fluorescence index. Values for the unfractionated samples and three size fractions for both SRNOM and BWW are displayed.

While the trends observed across sample sets may vary, the emergence of such clear trends within each set of size fractions suggests that similar underlying mechanisms are involved. Furthermore, Figure 9 shows the efficiency of the various processes as a function of average elution time for the SEC measurements. A clear positive relationship is observed where increasing elution time (indicating lower average sizes) corresponds to higher quantum efficiencies. It should be noted that both sets of samples show very similar changes as a function of elution time, despite their distinct composition, indicating that size plays a major role in the fate of light-induced processes.

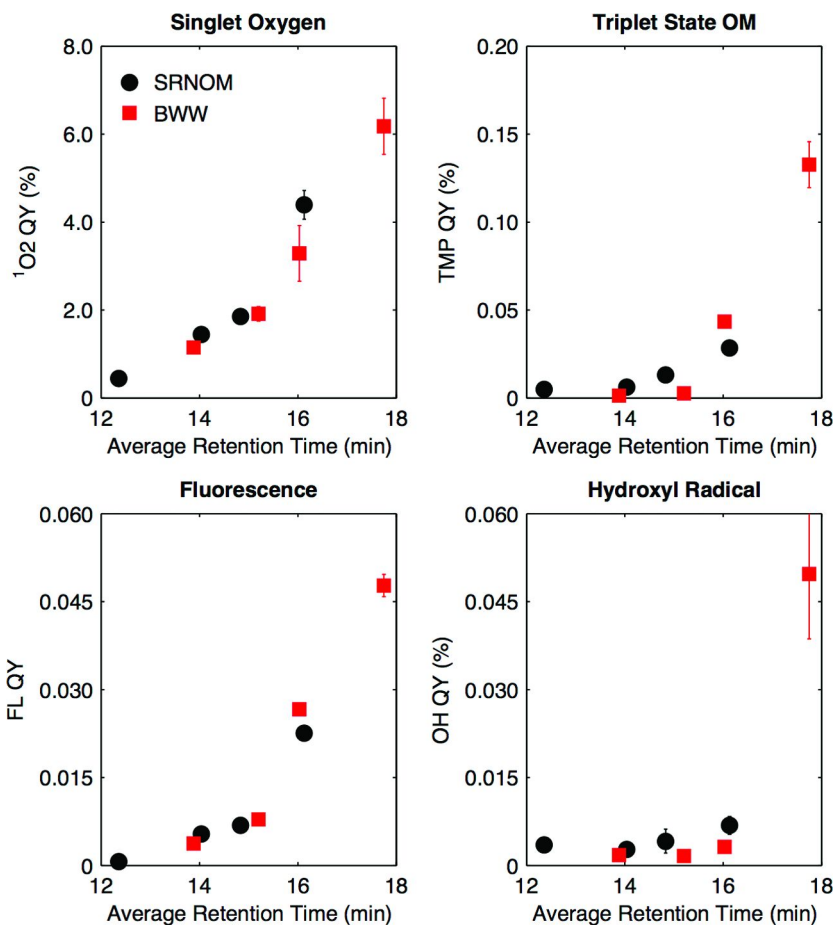


Figure 9. Quantum yields as a function of SEC retention time weighted average. Values for the unfractionated samples and three size fractions for both SRNOM and BWW are displayed.

Interpretation of Observed Results

Various conceptual interpretations could satisfactorily explain the results presented here. First, differences in the photophysics of large and small size fractions could be attributed simply to differences in composition among the different fractions. In this case, it could be argued that chromophoric species displaying high absorbance but relatively low fluorescence yields are preferentially found in the larger size fractions with the opposite trend expected in the lower fractions. While this phenomenon could have an impact, it is unlikely to be the only factor at play, considering how consistent the correlations between size and photochemical activity appear to be, even when considering OM samples of very different origins.

Another possible explanation derives from the fact that DOM has exhibited correlations between molecular weight fractions and aromaticity, which may be an indication of greater degrees of conjugation in the higher molecular weight fraction (56). Such increased conjugation would lead to the formation of singlet excited states that possess lower energies as compared to those present in smaller molecules. Such lower energy states are more prone to non-radiative decay (30) and are also expected to have shorter lifetimes (31). Furthermore, the ^3OM formed are likely to have lower energies as well since they are formed via ISC from singlets of relatively low energy. Thus, they will display shorter lifetimes than those of smaller molecules, which decreases the probability of reacting with species of interest before decaying to the ground state. This would lead to the lower formation rates of $^1\text{O}_2$ and lower TMP degradation rates observed.

Another factor contributing to the observed results is that increasing size may lead to an increased number of donor-acceptor pairs, leading to enhanced CT processes (see Scheme 1). Such transfers would be reflected in longer absorbance spectrum tailing and associated decreased S values, as observed here, indicating that spectral characteristics could serve as indicators of increased prevalence of such processes. It should be noted, however, that CT processes are likely still present in lower MW fractions as suggested by the fluorescence data. Such processes may compete with both fluorescence and ISC, in accordance with the model developed by Sharpless (22, 23) for explaining the observed relation between E2:E3 ratio and $^1\text{O}_2$ quantum yields. This model is further supported by a decrease in fluorescence quantum yields for larger size fractions, while the impact on the relative prevalence of ISC is reflected by a decrease in the formation of not only $^1\text{O}_2$ but also triplets (i.e. lower TMP decay rates). Similarly, HO^\bullet formation decreases with increasing size due to an increase in radiationless decay and CT processes, since this leads to lower probability of excited species (whether in the singlet or triplet state) forming HO^\bullet radicals before decaying to the ground state.

It is likely that a combination of these factors affect the OM photophysics to different degrees. The conceptual explanations presented allow for a new way of understanding the intramolecular photophysics of OM where fluorescence and ISC are not competing processes to the extent that one would significantly inhibit the other. Instead, they may both be similarly affected by the increase in radiationless decay (i.e. IC processes) or other processes (e.g. CT) observed to increase with increasing size and that inhibit the occurrence of measurable (and generally more environmentally relevant) photophysical and photochemical processes. While precise quantification of the phenomena discussed above remains elusive, the qualitative descriptions presented provide a satisfactory explanation to the general trends observed here and elsewhere.

Acknowledgments

The authors gratefully acknowledge support from the United States EPA STAR Fellowship for Simón Mostafa (FP91748801) and the National Science Foundation Graduate Research Fellowship Program for Caitlin M. Glover (115198) and Julie A. Korak (1144083). Support is also acknowledged from

the National Science Foundation (CBET #1235288). We also thank Sarah Al-Mutlaq and Cristina Tillberry for their assistance with laboratory procedures. Water quality analyses were performed at the Kiowa Environmental Chemistry Laboratory in Boulder, CO and the Laboratory for Environmental and Geological Studies at CU-Boulder.

References

1. Barber, L. B.; Leenheer, J. A.; Noyes, T. I.; Stiles, E. A. Nature and transformation of dissolved organic matter in treatment wetlands. *Environ. Sci. Technol.* **2001**, *35*, 4805–16.
2. Fimmen, R.; Cory, R.; Chin, Y.; Trout, T.; McKnight, D. Probing the oxidation–reduction properties of terrestrially and microbially derived dissolved organic matter. *Geochim. Cosmochim. Acta* **2007**, *71*, 3003–3015.
3. Hassett, J. P. Dissolved natural organic matter as a microreactor. *Science* **2006**, *311*, 1723–4.
4. Bidigare, R. R.; Ondrusk, M. E.; Brooks, J. M. Influence of the Orinoco River Outflow on Distributions of Algal Pigments in the Caribbean Sea. *J. Geophys. Res.* **1993**, *98*, 2259–2269.
5. Arrigo, K.; Brown, C. Impact of chromophoric dissolved organic matter on UV inhibition of primary productivity in the sea. *Mar. Ecol.: Prog. Ser.* **1996**, *140*, 207–216.
6. Canonica, S.; Jans, U. R. S.; Stemmler, K.; Hoigne, J. Transformation Kinetics of Phenols in Water: Photosensitization by Dissolved Natural Organic Material and Aromatic Ketones. *Environ. Sci. Technol.* **1995**, *29*, 1822–1831.
7. Cooper, W. J.; Zika, R. G. Photochemical Formation of Hydrogen Peroxide in Surface and Ground Waters Exposed to Sunlight. *Science* **1983**, *220*, 711–712.
8. Mopper, K.; Zhou, X. Hydroxyl radical photoproduction in the sea and its potential impact on marine processes. *Science* **1990**, *250*, 661–4.
9. Zepp, R. G.; Baughman, G. L.; Schlotzhauer, P. F. Comparison of Photochemical Behavior of Various Humic Substances in Water: II. Photosensitized Oxygenations. *Chemosphere* **1981**, *10*, 119–126.
10. Scully, F. E.; Hoigne, J. Rate constants for reactions of singlet oxygen with phenols and other compounds in water. *Chemosphere* **1987**, *16*, 681–694.
11. Al Housari, F.; Vione, D.; Chiron, S.; Barbat, S. Reactive photoinduced species in estuarine waters. Characterization of hydroxyl radical, singlet oxygen and dissolved organic matter triplet state in natural oxidation processes. *Photochem. Photobiol. Sci.* **2010**, *9*, 78–86.
12. Zhan, M.; Yang, X.; Xian, Q.; Kong, L. Photosensitized degradation of bisphenol A involving reactive oxygen species in the presence of humic substances. *Chemosphere* **2006**, *63*, 378–86.
13. Zepp, R. G.; Schlotzhauer, P. F. Influence of algae on photolysis rates of chemicals in water. *Environ. Sci. Technol.* **1983**, *17*, 462–468.

14. Kohn, T.; Nelson, K. L. Sunlight-mediated inactivation of MS2 coliphage via exogenous singlet oxygen produced by sensitizers in natural waters. *Environ. Sci. Technol.* **2007**, *41*, 192–7.
15. Romero, O. C.; Straub, A. P.; Kohn, T.; Nguyen, T. H. Role of temperature and Suwannee River natural organic matter on inactivation kinetics of rotavirus and bacteriophage MS2 by solar irradiation. *Environ. Sci. Technol.* **2011**, *45*, 10385–93.
16. Davies-Colley, R. J.; Bell, R. G.; Donnison, a M. Sunlight inactivation of enterococci and fecal coliforms in sewage effluent diluted in seawater. *Appl. Environ. Microbiol.* **1994**, *60*, 2049–58.
17. Curtis, T. P.; Mara, D. D.; Silva, S. A. Influence of pH, Oxygen, and Humic Substances on Ability of Sunlight To Damage Fecal Coliforms in Waste Stabilization Pond Water. *Appl. Environ. Microbiol.* **1992**, *58*, 1335–43.
18. IUPAC. *Compendium of Chemical Terminology*, 2nd ed. (the “Gold Book”); Compiled by McNaught, A. D., Wilkinson, A.; Blackwell Scientific Publications: Oxford, 1997; XML on-line corrected version: <http://goldbook.iupac.org> (2006).
19. Power, J. F.; Langford, C. H. Optical Absorbance of Dissolved Organic Matter in Natural Water Studies Using the Thermal Lens Effect. *Anal. Chem.* **1988**, *60*, 842–846.
20. Summers, R. S.; Cornel, P. K.; Roberts, P. V. Molecular size distribution and spectroscopic characterization of humic substances. *Sci. Total Environ.* **1987**, *62*, 27–37.
21. Cottrell, B. A.; Timko, S. A.; Devera, L.; Robinson, A. K.; Gonsior, M.; Vizenor, A. E.; Simpson, A. J.; Cooper, W. J. Photochemistry of excited-state species in natural waters: A role for particulate organic matter. *Water Res.* **2013**, *47*, 5189–99.
22. Sharpless, C. M. Lifetimes of triplet dissolved natural organic matter (DOM) and the effect of NaBH4 reduction on singlet oxygen quantum yields: implications for DOM photophysics. *Environ. Sci. Technol.* **2012**, *46*, 4466–73.
23. Dalrymple, R. M.; Carfagno, A. K.; Sharpless, C. M. Correlations between dissolved organic matter optical properties and quantum yields of singlet oxygen and hydrogen peroxide. *Environ. Sci. Technol.* **2010**, *44*, 5824–9.
24. Peterson, B. M.; McNally, A. M.; Cory, R. M.; Thoemke, J. D.; Cotner, J. B.; McNeill, K. Spatial and temporal distribution of singlet oxygen in Lake Superior. *Environ. Sci. Technol.* **2012**, *46*, 7222–9.
25. Fichot, C. G.; Benner, R. The spectral slope coefficient of chromophoric dissolved organic matter (S275–295) as a tracer of terrigenous dissolved organic carbon in river-influenced ocean margins. *Limnol. Oceanogr.* **2012**, *57*, 1453–1466.
26. Helms, J. R.; Stubbins, A.; Ritchie, J. D.; Minor, E. C.; Kieber, D. J.; Mopper, K. Absorption spectral slopes and slope ratios as indicators of molecular weight, source, and photobleaching of chromophoric dissolved organic matter. *Limnol. Oceanogr.* **2008**, *53*, 955–969.

27. Twardowski, M. S.; Boss, E.; Sullivan, J. M.; Donaghay, P. L. Modeling the spectral shape of absorption by chromophoric dissolved organic matter. *Mar. Chem.* **2004**, *89*, 69–88.
28. Mostafa, S.; Rosario-Ortiz, F. L. Singlet oxygen formation from wastewater organic matter. *Environ. Sci. Technol.* **2013**, *47*, 8179–86.
29. Wang, Z.-D.; Pant, B. C.; Langford, C. H. Spectroscopic and structural characterization of a Laurentian fulvic acid: notes on the origin of the color. *Anal. Chim. Acta* **1990**, *232*, 43–49.
30. Del Vecchio, R.; Blough, N. V. On the origin of the optical properties of humic substances. *Environ. Sci. Technol.* **2004**, *38*, 3885–91.
31. Boyle, E. S.; Guerriero, N.; Thiallet, A.; Del Vecchio, R.; Blough, N. V. Optical properties of humic substances and CDOM: relation to structure. *Environ. Sci. Technol.* **2009**, *43*, 2262–8.
32. Ma, J.; Del Vecchio, R.; Golosinski, K. S.; Boyle, E. S.; Blough, N. V. Optical properties of humic substances and CDOM: effects of borohydride reduction. *Environ. Sci. Technol.* **2010**, *44*, 5395–402.
33. Stewart, A. J.; Wetzel, R. G. Fluorescence : absorbance ratios - a molecular-weight tracer of dissolved organic matter. *Limnol. Oceanogr.* **1980**, *25*, 559–564.
34. Stewart, A. J.; Wetzel, R. G. Asymmetrical relationships between absorbance , fluorescence , and dissolved organic carbon. *Limnol. Oceanogr.* **1981**, *26*, 590–597.
35. Richard, C.; Trubetskaya, O.; Trubetskoy, O.; Reznikova, O.; Afanas'eva, G.; Aguer, J. P.; Guyot, G. Key role of the low molecular size fraction of soil humic acids for fluorescence and photoinductive activity. *Environ. Sci. Technol.* **2004**, *38*, 2052–7.
36. Richard, C.; Coelho, C.; Guyot, G.; Shaloiko, L.; Trubetskoy, O.; Trubetskaya, O. Fluorescence properties of the <5kDa molecular size fractions of a soil humic acid. *Geoderma* **2011**, *163*, 24–29.
37. Trubetskoy, O. a.; Trubetskaya, O. E.; Richard, C. Photochemical activity and fluorescence of electrophoretic fractions of aquatic humic matter. *Water Resour.* **2009**, *36*, 518–524.
38. Lee, E.; Glover, C.M.; Rosario-Ortiz, F.L. Photochemical Formation of Hydroxyl Radical from Effluent Organic Matter: Role of Composition. *Environ. Sci. Technol.* **2013**, *47*, 12073–12080.
39. Coelho, C.; Guyot, G.; ter Halle, A.; Cavani, L.; Ciavatta, C.; Richard, C. Photoreactivity of humic substances: relationship between fluorescence and singlet oxygen production. *Environ. Chem. Lett.* **2010**, *9*, 447–451.
40. Brucolieri, A.; Pant, B. C.; Sharma, D. K.; Langford, C. H. Evaluation of Primary Photoproduct Quantum Yields in Fulvic Acid. *Environ. Sci. Technol.* **1993**, *27*, 889–894.
41. Glover, C.M.; Rosario-Ortiz, F.L. Impact of Halides on the Photoproduction of Reactive Intermediates from Organic Matter. *Environ. Sci. Technol.* **2013**, *47*, 13949–13956.
42. Stedmon, C. a.; Markager, S.; Kaas, H. Optical Properties and Signatures of Chromophoric Dissolved Organic Matter (CDOM) in Danish Coastal Waters. *Estuarine, Coastal Shelf Sci.* **2000**, *51*, 267–278.

43. Murphy, K. R.; Butler, K. D.; Spencer, R. G. M.; Stedmon, C. A.; Boehme, J. R.; Aiken, G. R. Measurement of dissolved organic matter fluorescence in aquatic environments: an interlaboratory comparison. *Environ. Sci. Technol.* **2010**, *44*, 9405–12.
44. Lakowicz, J. R. *Principles of Fluorescence Spectroscopy*; Springer: New York, 2006.
45. Green, S. A.; Blough, N. V. Optical absorption and fluorescence properties of chromophoric dissolved organic matter in natural waters. *Limnol. Oceanogr.* **1994**, *39*, 1903–1916.
46. Vodacek, A.; Green, S. A.; Blough, N. V. An experimental model of the solar-stimulated fluorescence of chromophoric dissolved organic matter. *Limnol. Oceanogr.* **1994**, *39*, 1–11.
47. McKnight, D. M.; Boyer, E. W.; Westerhoff, P. K.; Doran, P. T.; Kulbe, T.; Andersen, D. T. Spectrofluorometric characterization of dissolved organic matter for indication of precursor organic material and aromaticity. *Limnol. Oceanogr.* **2001**, *46*, 38–48.
48. Cory, R. M.; Miller, M. P.; McKnight, D. M.; Guerard, J. J.; Miller, P. L. Effect of instrument-specific response on the analysis of fulvic acid fluorescence spectra. *Limnol. Oceanogr. Methods* **2010**, *8*, 67–78.
49. Dong, M. M.; Rosario-Ortiz, F. L. Photochemical formation of hydroxyl radical from effluent organic matter. *Environ. Sci. Technol.* **2012**, *46*, 3788–94.
50. Canonica, S.; Freiburghaus, M. Electron-rich phenols for probing the photochemical reactivity of freshwaters. *Environ. Sci. Technol.* **2001**, *35*, 690–5.
51. Golanoski, K. S.; Fang, S.; Del Vecchio, R.; Blough, N. V. Investigating the mechanism of phenol photooxidation by humic substances. *Environ. Sci. Technol.* **2012**, *46*, 3912–20.
52. Cawley, K. M.; Hakala, J. A.; Chin, Y. P. Evaluating the triplet state photoreactivity of dissolved organic matter isolated by chromatography and ultrafiltration using an alkylphenol probe molecule. *Limnol. Oceanogr. Methods* **2009**, *7*, 391–398.
53. Belzile, C.; Guo, L. Optical properties of low molecular weight and colloidal organic matter: Application of the ultrafiltration permeation model to DOM absorption and fluorescence. *Mar. Chem.* **2006**, *98*, 183–196.
54. Ged, E. C.; Boyer, T. H. Molecular weight distribution of phosphorus fraction of aquatic dissolved organic matter. *Chemosphere* **2013**, *91*, 921–7.
55. Coble, P. G. Characterization of marine and terrestrial DOM in seawater using excitation-emission matrix spectroscopy. *Mar. Chem.* **1996**, *51*, 325–346.
56. Chin, Y. P.; Aiken, G.; O'Loughlin, E. Molecular weight, polydispersity, and spectroscopic properties of aquatic humic substances. *Environ. Sci. Technol.* **1994**, *28*, 1853–8.

Chapter 9

Using Polyethylene Glycols To Understand the Temperature Dependence of the Dissolved Organic Matter- HO^\bullet Reaction

Garrett McKay and Stephen P. Mezyk*

Department of Chemistry and Biochemistry, California State University at Long Beach, 1250 Bellflower Boulevard, Long Beach, California, 90840

*E-mail: Stephen.Mezyk@csulb.edu.

The temperature-dependent bimolecular rate constants for the reaction of the hydroxyl radical (HO^\bullet) with a series of polyethylene glycol (PEG) polymers ($k_{\text{PEG-HO}^\bullet}$) have been measured in order to better understand the reaction of this radical with naturally occurring dissolved organic matter (DOM). Rate constants were measured using electron pulse radiolysis and thiocyanate competition kinetics. Values for $k_{\text{PEG-HO}^\bullet}$ were effectively diffusion controlled ($\sim 10^9 \text{ M}^{-1}\text{s}^{-1}$), approximately an order of magnitude faster than rate constants for the reaction of HO^\bullet with DOM ($\sim 10^8 \text{ M}^{-1} \text{ s}^{-1}$). Temperature dependent $k_{\text{PEG-HO}^\bullet}$ measurements show that the reaction is Arrhenius, with activation energies of $\sim 15 \text{ kJ mol}^{-1}$ for the 100 and 1000 Da PEGs, as expected for diffusion-controlled reactions. However, the 5000, 9000, and 15,000 Da PEGs exhibited activation energies greater than 20 kJ mol^{-1} , suggesting that additional reaction mechanisms, potentially polymer linearization, are also occurring.

Introduction

The hydroxyl radical (HO^\bullet) is an important oxidant in both engineered and natural aquatic systems. In natural systems, the reaction of photolytically produced HO^\bullet with organic compounds is a significant pathway for pollutant degradation (1–4). HO^\bullet also plays a role in the oxidative transformation of naturally occurring dissolved organic matter (DOM). Additionally, HO^\bullet is used as the main reactive species in advanced oxidation processes² (AOPs) treatment of drinking and waste water (5–7). At large-scale, AOPs typically generate HO^\bullet radicals using mixtures of O_3/UV , $\text{O}_3/\text{H}_2\text{O}_2$, or $\text{H}_2\text{O}_2/\text{UV}$. The produced HO^\bullet radical reacts quickly ($k > 108 \text{ M}^{-1}\text{s}^{-1}$) with organic pollutants (8), to ultimately result in biologically inactive products (9).

The presence of HO^\bullet scavengers in the water matrix impacts both the efficiency of AOPs and the steady state concentration of photolytically produced HO^\bullet in natural systems. These scavengers include nitrite (NO_2^-), carbonates ($\text{HCO}_3^-/\text{CO}_3^{2-}$), ammonia (NH_3), and DOM. While rate constants for the reaction of HO^\bullet with inorganic species are well-established (8), the values for the DOM- HO^\bullet reaction ($k_{\text{DOM-HO}^\bullet}$) are not as well characterized due to the complexity and heterogeneous nature of DOM. Despite this, many rate constants have been reported for the reaction between DOM and HO^\bullet , with values ranging from $k_{\text{DOM-HO}^\bullet} \sim 1 - 12 \times 10^8 \text{ M}^{-1}\text{s}^{-1}$ depending on the type of DOM, notably whether it is natural organic matter (NOM) or effluent organic matter (EfOM) (10–13). Previous work has shown that the magnitude of $k_{\text{DOM-HO}^\bullet}$ can be correlated with the sample's physicochemical properties (12, 14) and apparent molecular weight (15). It is also known that the temperature-dependence of $k_{\text{DOM-HO}^\bullet}$ exhibits Arrhenius-type behavior, likely due to the diffusion-controlled nature of the reaction (16).

Nuclear Magnetic Resonance (NMR) characterization of the mixture of chemical compounds that constitutes DOM has been reported by several workers (17, 18). In freshwater DOM, for example, major components found included multiple carboxyl-rich alicyclic molecules, heteropoly-saccharides (17), and polymeric material derived mainly from microorganisms including peptidoglycans, lipoproteins, large polymeric carbohydrates and other proteinaceous material (18). Earlier studies had also suggested that humic substances were comprised of randomly coiled macromolecules with mass-weighted average molecular masses of 20–50 kDa and radii of gyration (distance from the coil center that has the highest probability of finding a monomer unit) of 4–10 nm (19). HO^\bullet can undergo a number of different reactions with these types of organic/polymer molecules, including addition to carbon and/or nitrogen double bonds, hydrogen-atom abstraction reactions from carbon (CH_x) and nitrogen (NH_y) moieties, and addition to aromatic ring compounds (20).

Thus utilizing the HO^\bullet oxidation of different molecular weight polymers as model systems could provide insight into the important mechanisms occurring for DOM. Work by Bartoszek et al. (21) has shown that the rate constant for the reaction of HO^\bullet with Poly(N-Vinylpyrrolidone) (PVP), a coiled polymer in aqueous solution, depends both on its concentration and molecular weight. Both

of these observations were explained by the diffusion-controlled nature of this reaction. At lower polymer concentrations, HO[•] radicals diffuse longer distances before contacting a polymer unit, thus reacting slower on a diffusion-controlled basis than at higher concentrations of PVP where the polymer coils start to interpenetrate each other. The molecular weight effect was explained by the direct relationship between PVP molecular weight and average radius of gyration, with lower molecular weight PVP samples found to have a lower average radius of gyration. Therefore, on a per monomer unit basis, HO[•] radicals should react faster with lower molecular weight PVP molecules as they have less distance to travel before contacting a polymer unit.

Though DOM is not strictly a polymer, it is described as a supramolecular assembly of lower molecular weight organic molecules (22). Moreover, the dependence of the reaction of HO[•] radicals with size-fractionated EfOM (15) shows a similar trend to HO[•] radical's reaction with PVP. Unlike PVP though, EfOM is thought to exist more as an aggregate, where with increasing molecular weight, some oxidation sites would become inaccessible. While DOM does not have a defined molecular weight, total organic carbon (TOC) is used to express DOM concentration in terms of moles of carbon per liter. Recently, there has been a report that the reactivity between HO[•] radicals and EfOM is inversely correlated to TOC (14). This is thought to be due to a decrease in EfOM molecular weight with lower TOC values as a result of increased microbial degradation of EfOM.

The goal of this study was to gain a deeper understanding of the reaction of HO[•] radicals with DOM using standard polyethylene glycol (PEG) polymers of different molecular weights as a model system. To do this, absolute rate constants for the reaction between HO[•] radical and these polymers were measured as a function of temperature in aqueous solution. Though PEGs are not a complete representation of DOM structure and chemical composition, the distinct molecular weight ranges is expected to mimic what is produced by size-fractionation of organic matter in water. Our previous research has shown a direct relationship between EfOM's apparent molecular weight and its activation energy for reaction with HO[•] radicals (16). Furthermore, PEGs have been specifically identified in wastewaters (Thurman and Ferrer personal communication), which is not surprising based on their ubiquitous usage. By investigating the temperature dependence of $k_{\text{PEG-HO}^{\bullet}}$ for these polymers with known, more well-defined, (relative to DOM) molecular weights, further insight can be gained into whether the molecular weight of the macromolecule is the cause of this increase in activation energy.

Experimental

Standard PEG samples of known molecular weight (100 – 15,000 Da) were obtained from PolySciences Inc. (Warrington, PA) and had dispersities (M_w/M_n) < 1.1. All solutions were prepared by dissolving the PEGs in Millipore Milli-Q water (> 18.2 MΩ x cm). PEG solutions were prepared at 10 mg L⁻¹ in order to stay below the critical hydrodynamic concentration, the point at which polymer

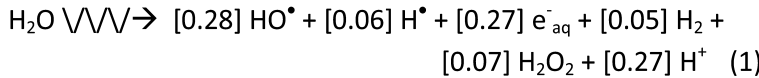
coils start to interpenetrate one another. These concentrations were not measured for our PEGs, but are based on the values reported by Bartoszek et al. (21) for PVP, which is also an uncharged polymer.

The linear accelerator electron pulse radiolysis facility at the University of Notre Dame Radiation Laboratory was used for the quantification of the reaction rate constants. This irradiation and transient absorption detection system has been previously described in detail (23). Briefly, the PEG solutions were pre-saturated with N₂O gas to isolate HO[•] upon radiolysis. [PEG] refers to the PEG concentration in moles of monomer units per liter, and $k_{\text{PEG-HO}^{\bullet}}$ is calculated on the basis of monomer units. Standard dosimetry was performed using N₂O-saturated, 1.00 × 10⁻² M KSCN solutions at $\lambda = 475$ nm, ($Ge = 5.2 \times 10^{-4} \text{ m}^2 \text{ J}^{-1}$) with average doses of 2-5 Gy per 3-4 ns pulse resulting in initial HO[•] concentrations of 1-3 μM . During kinetic measurements, solutions were continuously sparged with the minimum amount of N₂O necessary to prevent air ingress, and experiments were carried out at four or five controlled temperatures for each sample in at least triplicate. The quoted errors for the reaction rate constants are a combination of the measurement precision and concentration errors.

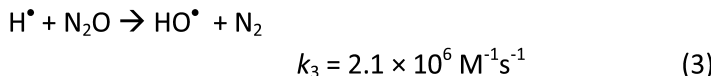
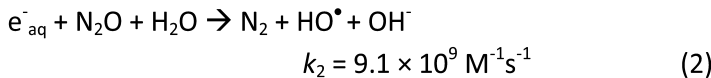
Results and Discussion

PEG-HO[•] Kinetics

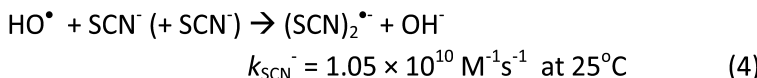
The radiolysis of pure water or low concentration solutions produces a suite of radicals and other species according to the stoichiometry (8):



where the bracketed numbers are G-values (yields in $\mu\text{mol J}^{-1}$) for each species produced. The N₂O pre-saturation of all solutions was performed in order to quantitatively convert the e⁻_{aq} and H[•] radicals to HO[•] (8):



Due to the lack any absorbing species following the PEG-HO[•] reaction, rate constants in this study were measured using thiocyanate competition kinetics, which has previously been used to measure HO[•] reactions with polymers (21). The overall HO[•] loss rate was due to competing reactions:





The temperature-dependence of k_{SCN^-} has been previously established (8). Integrating these equations gives the competition kinetics expression:

$$\frac{1}{\text{Abs}_{(\text{SCN})_2^\bullet}} = \frac{1}{\text{Abs}^0_{(\text{SCN})_2^\bullet}} + \left(\frac{k_{\text{PEG-HO}^\bullet} [\text{PEG}]}{k_{\text{SCN}^-} \text{Abs}^0_{(\text{SCN})_2^\bullet}} \right) \left(\frac{1}{[\text{SCN}^-]} \right) \quad (6)$$

where $\text{Abs}^0_{(\text{SCN})_2^\bullet}$ is the limiting $(\text{SCN})_2^\bullet$ absorbance in the absence of any competitor (such as PEG), and $\text{Abs}_{(\text{SCN})_2^\bullet}$ is the corresponding decreased absorbance in its presence. Plotting $1/\text{Abs}_{(\text{SCN})_2^\bullet}$ against $1/[\text{SCN}^-]$ yields a straight line, the slope being equal to $k_{\text{PEG-HO}^\bullet} [\text{PEG}] / (k_{\text{SCN}^-} \text{Abs}^0_{(\text{SCN})_2^\bullet})$, and the y-intercept is equal to $1/\text{Abs}^0_{(\text{SCN})_2^\bullet}$. Division of the slope by the intercept yields the ratio $k_{\text{PEG-HO}^\bullet} [\text{PEG}] / k_{\text{SCN}^-}$.

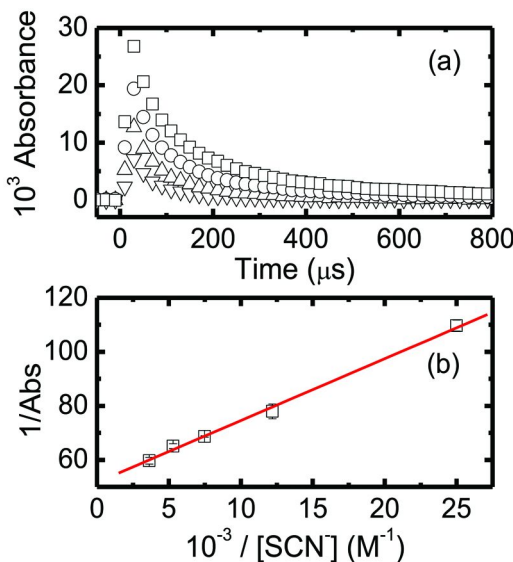


Figure 1. Typical kinetic data for PEG-HO[•] experiments. (a) Decay of the $(\text{SCN})_2^\bullet$ transient for N_2O -saturated 5000 Da PEG at 29.2 °C. Symbols represent 40.0 (∇), 81.7 (Δ), 133 (\circ), and 275 μM (\square) added SCN^- . Mixed order decays were fitted to each trace in order to obtain initial absorbance intensities, corresponding to $\text{Abs}_{(\text{SCN})_2^\bullet}$. (b) Transformed competition-kinetics plot for this sample based on extrapolated initial intensities obtained from (a). Error bars correspond to one standard deviation from repeat value intensities. Solid line is a weighted linear fit, with a slope of $(2.30 \pm .01) \times 10^{-3}$ and an intercept of 51.6 ± 0.2 , corresponding to $k_{\text{PEG-HO}^\bullet} [\text{PEG}] = (6.01 \pm 0.04) \times 10^5 \text{ s}^{-1}$.

Table 1. Temperature-Dependent $k_{\text{PEG-HO}^{\cdot}}$ Values Measured in This Study

Sample	Temp (°C)	$K_{\text{Peg-HO}^{\cdot}} \times 10^{-9} (M^{-1}S^{-1})$
100 Da	10.0	3.35 ± 0.48
	21.0	4.52 ± 0.24
	30.0	5.30 ± 0.20
	38.8	6.42 ± 0.14
1000 Da	9.8	1.26 ± 0.06
	10.0	1.38 ± 0.41
	14.5	1.42 ± 0.05
1000 Da	21.2	1.87 ± 0.01
	22.5	1.56 ± 0.02
	34.2	2.32 ± 0.26
	39.9	2.59 ± 0.09
5000 Da	10.8	1.20 ± 0.04
	20.5	1.79 ± 0.07
	29.2	2.42 ± 0.19
	34.2	2.47 ± 0.26
9000 Da	11.7	1.08 ± 0.10
	19.0	1.21 ± 0.11
	24.5	1.44 ± 0.08
	29.3	1.65 ± 0.09
15,000 Da	38.5	2.19 ± 0.16
	9.5	0.64 ± 0.08
	18.8	1.21 ± 0.02
	24.6	1.45 ± 0.03
	29.2	2.31 ± 0.12
	35.5	3.19 ± 0.28

Additional division by the PEG concentration and multiplying the temperature-dependent $k_{\text{SCN}^{\cdot}}$ value produces the bimolecular rate constant, $k_{\text{PEG-HO}^{\cdot}}$. Typical raw kinetic data for 5000 Da PEG obtained in this study and the corresponding transformed analysis plot are shown in Figure 1a and 1b, respectively.

Temperature-dependent rate constants were measured for the reaction between HO^{\cdot} and a series of varying molecular weight PEGs by this approach. These rate constants at all temperatures are given in Table 1 in terms of the concentration of monomer units, which is typical for polymers.

Representative Arrhenius data for the 100 and 15,000 Da PEG is shown in Figure 2 and in general the reaction exhibited good linearity. Most $k_{\text{PEG-HO}^{\cdot}}$ values measured were greater than $10^9 \text{ M}^{-1}\text{s}^{-1}$ in terms of monomer concentration at room temperature, indicating that this reaction is effectively diffusion-controlled. Although apparent activation energies for the reaction of HO^{\cdot} with most of the PEGs were below or $\sim 20 \text{ kJ mol}^{-1}$, the highest value of $44.68 \pm 3.21 \text{ kJ mol}^{-1}$ for the 15,000 Da sample is not characteristic of a diffusion-controlled reaction.

Comparison of PEG and DOM Kinetics – Molecular Weight

The observed inverse correlation of $k_{\text{PEG-HO}^{\cdot}}$ to PEG molecular weight (Figure 3) has been reported for HO^{\cdot} radical reactions with other polymers (21, 24) and is also consistent with the reactivity of size-fractionated DOM (15). However, this reactivity correlation is absent for non-size-fractionated DOM samples (12, 13). This difference may be due to the significant apparent molecular weight differences that result from size-fractionation, which in turn may have a more pronounced effect on $k_{\text{DOM-HO}^{\cdot}}$. Conversely, bulk DOM is more consistent in apparent molecular weight across different samples, resulting in no effect on HO^{\cdot} reactivity. Furthermore, comparing multiple DOM samples in order to correlate molecular weight and $k_{\text{DOM-HO}^{\cdot}}$ is complicated by other competing factors in these samples, such as geographical source and chemical composition.

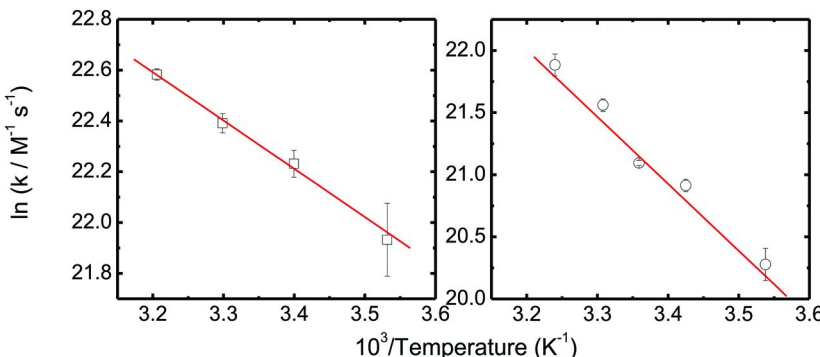
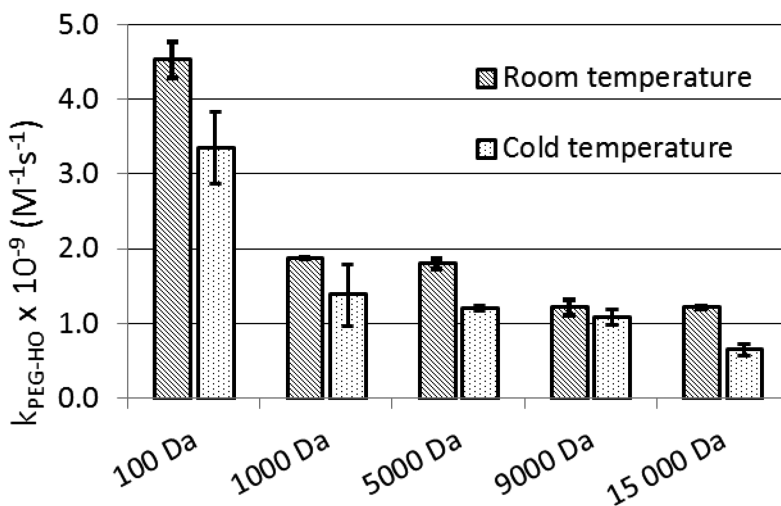


Figure 2. Arrhenius plots for the HO^{\cdot} radical reaction with 100 Da (left) and 15,000 Da PEG (right). Activation energies and Arrhenius pre-factors based on a linear fit of the data are shown in Table 2. Courtesy of Garrett McKay, M.S. Thesis, 2013.

Table 2. Summary of Arrhenius Parameters Established in This Study

Sample	E_a (kJ mol ⁻¹)	$\ln(A)$
100 Da	15.61 ± 2.27	28.6 ± 0.9
1000 Da	16.78 ± 1.91	28.1 ± 0.8
5000 Da	23.41 ± 3.05	30.9 ± 1.2
9000 Da	19.86 ± 1.71	29.1 ± 0.7
15,000 Da	44.68 ± 3.21	39.3 ± 1.3

*Figure 3. Plot of $k_{PEG-HO\cdot}$ versus PEG molecular weight at room (18.8 - 21.5 °C) and cold temperatures (9.5-10.8 °C).*

Bartoszek et al. (21) have suggested that the magnitude of the rate constant for the reaction between HO[·] and PVP is controlled by the average radius of gyration, which is a function of sample molecular weight. The radius of gyration increases with increasing polymer molecular weight, which results in a lower reactivity on a per monomer basis due to the radical having to diffuse a longer distance to contact a polymer unit. Based on our results for the PEGs, it is likely that a similar mechanism is responsible for the inverse correlation of $k_{PEG-HO\cdot}$ with molecular weight. While DOM is not strictly a polymer, it is possible that there is a similar effect occurring in its reaction with HO[·].

Comparison of PEG and DOM Kinetics – Temperature Dependence

Arrhenius parameters for the reaction between HO[•] and the PEGs measured in this study are shown in Table 2. Activation energies ranged from 15.61-44.68 kJ mol⁻¹ and there is a general increase from the 100 to 15,000 Da PEG. This higher-than-expected activation energy for the 15,000 Da sample can be attributed to two effects: 1) an intrinsic increase in $k_{\text{PEG-HO}^{\bullet}}$ with increasing temperature (i.e. normal Arrhenius behavior) and 2) uncoiling or linearization with increasing temperature. Linearization would increase the polymer's chain length, and therefore its reactivity to HO[•].

We have previously shown that the reaction between HO[•] and DOM is also Arrhenius, with activation energies ranging from 10-30 kJ mol⁻¹ (16). These values are similar to the lower molecular weight PEGs, but much lower than the 15,000 Da sample. Interestingly, the DOM sample that had the largest activation energy in the previous study (Elliot Soil Humic Acid (ESHA) – 30.7 kJ mol⁻¹) also had the largest average molecular weight (3100 Da) as determined by size exclusion chromatography, while Suwanee River Fulvic Acid and Pony Lake Fulvic Acid both had values of ~ 15 kJ mol⁻¹ (with average molecular weights of 2800 and 2400 Da, respectively).

For ESHA, a similar linearization of coil-like moieties could be occurring with increasing temperature, explaining its high apparent activation energy. Further kinetic experiments over a larger temperature range could show whether the change in $k_{\text{DOM-HO}^{\bullet}}$ with temperature is due only to Arrhenius behavior, or also includes linearization. If the measured apparent activation energy is significantly different depending on the temperature range, e.g. over 30-60 °C versus 10-50 °C, then it is likely that there is some non-Arrhenius-based reason for the rate of change of $k_{\text{OM-HO}^{\bullet}}$.

Conclusions

Temperature dependent rate constants for the reaction between HO[•] and varying molecular weight PEGs have been measured in order to model the reactivity of this radical with DOM. Rate constants for the PEG-HO[•] reaction were generally faster than the DOM-HO[•] reaction (10⁹ vs. 10⁸ M⁻¹s⁻¹). The value of $k_{\text{PEG-HO}^{\bullet}}$ increased with decreasing PEG molecular weight, similar to measurements on size-fractionated DOM samples previously. This is believed to arise from the large molecular weight differences between PEG samples. In addition, the activation energy for the PEG-HO[•] reaction increased with increasing molecular weight, which is attributed to increased linearization of the polymer at higher temperatures. These results yield insight into what mechanisms may be occurring in the reaction between HO[•] and DOM.

Acknowledgments

Rate constants measurements were performed at the Radiation Laboratory, University of Notre Dame, which is supported by the Office of Basic Energy Sciences, U.S. Department of Energy.

References

1. Zepp, R. G.; Hoigne, J.; Bader, H. Nitrate-induced photooxidation of trace organic chemicals in water. *Environ. Sci. Technol.* **1987**, *21*, 443–450.
2. Brezonik, P. L.; Fulkerson-Brekken, J. Nitrate-induced photolysis in natural waters: Controls on concentrations of hydroxyl radical photo-intermediates by natural scavenging agents. *Environ. Sci. Technol.* **1998**, *32*, 3004–3010.
3. Brekken, J. F.; Brezonik, P. L. Indirect photolysis of acetochlor: Rate constant of a nitrate-mediated hydroxyl radical reaction. *Chemosphere* **1998**, *36*, 2699–2704.
4. Zhan, M. J.; Yang, X.; Xian, Q. M.; Kong, L. G. Photosensitized degradation of bisphenol A involving reactive oxygen species in the presence of humic substances. *Chemosphere* **2006**, *63*, 378–386.
5. Legrini, O.; Oliveros, E.; Braun, A. M. Photochemical processes for water-treatment. *Chem. Rev.* **1993**, *93*, 671–698.
6. Wert, E. C.; Rosario-Ortiz, F. L.; Snyder, S. A. Effect of ozone exposure on the oxidation of trace organic contaminants in wastewater. *Water Res.* **2009**, *43*, 1005–1014.
7. Mezyk, S. P.; Rickman, K. A.; Hirsch, C. M.; Dail, M. K.; Scheeler, J.; Foust, T. Advanced oxidation and reduction process radical generation in the laboratory and on a large scale: An overview. *Monit. Water Qual.* **2012**, 227–248.
8. Buxton, G. V.; Greenstock, C. L.; Helman, W. P.; Ross, A. B. Critical review of rate constants for the reactions of hydrated electrons, hydrogen atoms, and hydroxyl radicals ($\bullet\text{OH}/\text{O}\bullet$) in aqueous solution. *J. Phys. Chem. Ref. Data.* **1988**, *17*, 513–886.
9. Mezyk, S. P.; Otto, S. C. Quantitative removal of M-lactam antibiotic activity by hydroxyl radical reaction in water: How much oxidation is enough? *J. Adv. Oxid. Technol.* **2013**, *16*, 117–122.
10. Westerhoff, P.; Aiken, G.; Amy, G.; Debroux, J. Relationships between the structure of natural organic matter and its reactivity towards molecular ozone and hydroxyl radicals. *Water Res.* **1999**, *33*, 2265–2276.
11. Westerhoff, P.; Mezyk, S. P.; Cooper, W. J.; Minakata, D. Electron pulse radiolysis determination of hydroxyl radical rate constants with Suwannee River fulvic acid and other dissolved organic matter isolates. *Environ. Sci. Technol.* **2007**, *41*, 4640–4646.
12. Rosario-Ortiz, F. L.; Mezyk, S. P.; Doud, D. F. R.; Snyder, S. A. Quantitative correlation of absolute hydroxyl radical rate constants with non-isolated effluent organic matter bulk properties in water. *Environ. Sci. Technol.* **2008**, *42*, 5924–5930.
13. McKay, G.; Kleinman, J. L.; Johnston, K. M.; Dong, M. M.; Rosario-Ortiz, F. L.; Mezyk, S. P. Kinetics of the reaction between the hydroxyl radical and organic matter standards from the International Humic Substance Society. *J. Soils Sediments.* **2014**, *14*, 298–304.
14. Keen, O. S.; McKay, G.; Mezyk, S. P.; Linden, K. G.; Rosario-Ortiz, F. L. Identifying the factors that influence the reactivity of effluent organic matter with hydroxyl radicals. *Water Res.* **2013**, *50*, 408–419.

15. Dong, M. M.; Mezyk, S. P.; Rosario-Ortiz, F. L. Reactivity of effluent organic matter (EfOM) with hydroxyl radical as a function of molecular weight. *Environ. Sci. Technol.* **2010**, *44*, 5714–5720.
16. McKay, G.; Dong, M. M.; Kleinman, J. L.; Mezyk, S. P.; Rosario-Ortiz, F. L. Temperature dependence of the reaction between the hydroxyl radical and organic matter. *Environ. Sci. Technol.* **2011**, *45*, 6932–6937.
17. Lam, B.; Baer, A.; Alaee, M.; Lefebvre, B.; Moser, A.; Williams, A.; Simpson, A. J. Major structural components in freshwater dissolved organic matter. *Environ. Sci. Technol.* **2007**, *41*, 8240.
18. McCaul, M. V.; Sutton, D.; Simpson, A. J.; Spence, A.; McNally, D. J.; Moran, B. W.; Goel, A.; O’Conner, B.; Hart, K.; Kelleher, B. P. Composition of dissolved organic matter within a lacustrine environment. *Environ. Chem.* **2011**, *8*, 146–154.
19. Swift, R. S. Macromolecular properties of soil humic substances: Fact, fiction and opinion. *Soil Sci.* **1999**, *164*, 790–802.
20. Cooper, W. J.; Cramer, C.; Martin, N. H.; Mezyk, S. P.; O’Shea, K. E.; von Sonntag, C. Free Radical Mechanisms for the Destruction of Methyl tert-Butyl Ether (MTBE) via Advanced Oxidation Processes. *Chem. Rev.* **2009**, *109*, 1302–1345.
21. Bartoszek, N.; Ulański, P.; Rosiak, J. M. Reaction of a low-molecular-weight free radical with a flexible polymer chain: Kinetic studies on the OH + Poly(N-Vinylpyrrolidone) model. *Int. J. Chem. Kin.* **2011**, *43*, 474–481.
22. Sutton, R.; Sposito, G. Molecular structure in soil humic substances: The new view. *Environ. Sci. Technol.* **2005**, *39*, 9009–9015.
23. Whitham, K.; Lyons, S.; Miller, R.; Nett, D.; Treas, P.; Zante, A.; Fessenden, R. W.; Thomas, M. D.; Wang, Y. Linear accelerator for radiation chemistry research at Notre Dame; IEEE Proceedings Particle Accelerator Conference and International Conference on High Energy Accelerators; Dallas, TX, 1995; pp 131–133.
24. Behzadi, A.; Schnabel, S. Kinetic studies on the influence of conformation and chain length on the reaction of hydroxyl radicals with poly (acrylic acid) in solution. *Macromolecules.* **1973**, *6*, 824–826.

Chapter 10

The Use of Perylene as a Probe To Determine the Ability of Dissolved Organic Matter in the Aquatic Environment To Associate with Hydrophobic Organic Pollutants

M.-H. (Chris) Hsu and I. H. (Mel) Suffet*

Environmental Science and Engineering Program,
University of California at Los Angeles, School of Arts and Sciences,
Room 61-295, CHS, Charles E. Young Drive South,
Los Angeles, California 90095, U.S.A.

*E-mail: msuffet@ucla.edu.

Hydrophobic organic pollutants (HOPs), with a $\log K_{\text{OW}}$ (octanol/water partition coefficient) of >5 , have the ability to sorb to dissolved organic matter (DOM). This process can enhance the solubility as well as decreased uptake to biota (i.e. less bioavailability) of HOPs. It has been shown that $\log K_{\text{DOM}}$ (HOP/DOM partition coefficient) for a particular HOP will vary in different natural waters with different DOM present. Thus, an HOP probe could be used to characterize the differences between aquatic DOM in different natural waters. Perylene appears to be an excellent probe to use as an HOP to characterize the differences between aquatic DOM in different natural waters. The objective of this paper was to consider adding another method to the categorize DOM reactivity related to an environmental concern by measuring sorption to the exemplary HOP probe perylene. This method could be used to determine the potential free hazardous HOP that would be present in any natural water.

As an application of this method, the sorption of Perylene to stormwater DOM was assessed. Stormwater runoff samples showed 58 % and 28 % free perylene for one Fall and one Spring stormwater runoff sample, respectively. This indicates

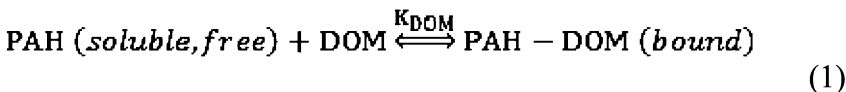
that the relationship between DOM and HOPs in equilibrium with DOM-HOPs might need definition on a temporal basis and even different flow regimes to understand the bioavailability of HOPs in stormwater.

Introduction

Dissolved organic matter (DOM) is a mixture of hundreds of anionic molecules of <1 to >15 kilodaltons that are composed of aromatic and aliphatic organic compounds found in natural waters (1–3). DOM can be classified into two main groups: humic and non humic substances. The humic fraction includes humic and fulvic acids whereas the non humic fraction includes amino acids, proteins, sugars, and polysaccharides (2–4). DOM is functionally defined as < 0.45 μm in size (5). In this chapter, we used a non-organic glass membrane filter of < 0.7 μm to define DOM. DOM is measured as dissolved organic carbon (DOC) in mgC/L.

Hydrophobic organic pollutants (HOPs) are compounds with log K_{ow} (octanol/water partition coefficient) of >5. HOPs, such as chlorinated pesticides, polychlorinated biphenyls, pyretheroids and polyaromatic hydrocarbons (PAHs), generally pose the largest toxicity risk to aquatic organisms in the environment. The important impact of DOM association (sorption) to HOPs is observed by the additional transport in the aqueous soluble phase (i.e. more solubility) and decreased uptake to biota (i.e. less bioavailability) of the HOPs (6). This indicates the need to characterize the ability of DOM from different aqueous environments to understand the potential impact of HOPs on the aquatic environment.

DOM can bind with HOPs in the aquatic environment and affect their bioavailability and ultimately lower their toxicity. In other words, when DOM associates with HOPs (bound form; DOM-HOPs), HOPs are not able to pass through biological membranes (i.e. not bioavailable). The free HOPs are toxic to biota (7, 8). The free and bound portions of HOPs in the water can be described by the partition coefficient, K_{DOM} between the DOM AND HOPs (7). Equation 1 describes the binding behavior between DOM and HOPs via K_{DOM} . A PAH is used as an example.



The percentage of bound PAH can be further determined by equation 2 knowing the concentration of DOM in the water (7):

$$\%bound = \frac{K_{DOM}[DOM]}{1 + K_{DOM}[DOM]} \times 100 \quad (2)$$

Knowing this information can guide water agencies to control water quality and minimize the effects of HOPs.

The pollution levels and the form of HOPs, and how DOM characteristics affect the fate and transport of HOPs in the environment has not been clarified. The free soluble form of an HOP is hazardous because it is bioavailable. However, the bound form is not, but it increases the solubility of HOPs, from sediments and enables the mobility of the HOPs in aquatic environments. Subsequently, the bound HOPs then at a location downstream equilibrate and become partially free, soluble and available for biological uptake. Thus, in the aquatic environment, knowing true free concentration of HOPs is necessary to effectively determine the bioavailable quantity of HOPs at any location. Then the issue becomes what kind of DOM characteristics affect binding and the bioavailability of HOPs.

Table 1 presents different methods used to characterize DOM for different objectives. The objective of determining the ability of DOM's "Reactivity Related to an Environmental Concern", such as formation potential of trihalomethanes and nitrosoamines is directed to under-standing actual environmental concerns (9–12).

The objective of this paper is to consider adding another method to categorize DOM reactivity related to an environmental concern by measuring sorption to an exemplary HOP probe. This method could be used to determine the potential free hazardous HOP that would be present in any natural water (6, 7).

It has been shown that $\log K_{DOM}$ for a particular HOP will vary in different natural waters with different DOM present (13). Thus, an HOP probe could be used to characterize the differences between aquatic DOMs in different natural waters.

The HOP probe should have the following characteristics:

1. A $\log K_{DOM}$ of >5
2. A chemical of high purity that is readily available
3. A chemical with minimal toxicity
4. A chemical able to use the quick and precise method of fluorescent quenching to determine the $\log K_{DOM}$.

The chemical perylene was chosen as the HOP indicator based upon these criteria.

As an application of this method, the sorption of Perylene to stormwater DOM was assessed to observe if there were temporal differences in Fall and Spring. UV₂₅₄, UF, and the polarity rapid assessment method (PRAM), for aromaticity, molecular structures size, and polarity, respectively were measured to define basic DOM characteristics.

Table 1. Summary of Many Characterization Methods for NOM [Based upon Reference (4)]

<i>Character</i>	<i>Examples</i>
Elemental Analysis	Total or Dissolved a) Organic Carbon b) Organic Nitrogen
Size	a) Filtration – Simple and Ultrafiltration (UF) b) Size Exclusion Chromatography
Polarity	a) XAD-ractionation b) Polarity Rapid Assessment Method (PRAM)
Functional Groups	a) Titration b) Infared Spectroscopy c) NMR Spectroscopy d) Oxidation-Reduction (Chemolysis, Pyrolysis) e) Mass Spectroscopy
Aromaticity	a) UV(254) b) Specific UV Absorbance
Kind of NOM (e.g. Humic, Fulvic etc.)	a) Solubility in Acid and Base b) Fluorescence Spectroscopy
Reactivity Related to an Environmental Concern	a) Trihalomethane Formation Potential (9–11) b) Nitrosoamine Formation c) Biological Organic Carbon (4) d) Sorption To Hydrophobic Organic Pollutants (HOPs)

Experimental

Sample Collection

Samples of stormwater runoff were collected from the storm drains within the City of Anaheim tributary to Anaheim Bay and Huntington Harbour. Two stormwater runoff samples, one in the Spring and one in the Fall were collected in the beginning of rain events during the first hour of discharge that are required in NPDES permits in California (14) to catch the “first flush” of pollutants. The first flush of runoff has been found to deliver most of the contaminants to the storm drains (15).

Sample Preparation

Water samples were filtered through 0.7 µm glass fiber membranes (Whatman Corp, Sanford, ME) prior to any analysis to remove filterable organic matter and microorganisms that may consume DOM. Before using, membranes were baked for 24 hours at 100 °C to reduce leaching of organics during filtration. This step is to ensure that the study is only measuring the dissolved form of natural organic matter.

Water Quality

Water quality measurements were completed according to standard methods of water and wastewater (5). Parameters include dissolved organic carbon (DOC, Method 5310B), ultraviolet absorbance at 254nm (UV₂₅₄, Method 5910), pH (Method 4500), conductivity (Method 2510), and specific UV absorbance (SUVA) which is the ratio of UV absorption to DOC concentration. DOM is measured as DOC in mgC/L.

Ultrafiltration To Measure Size Fraction of DOM

DOM was size fractionated by UF through Millipore YM (regenerated cellulose, negatively charged) 1000 (1k), 10,000 (10k) molecular weight cut off (MWCO), and PB (polyethersulfone, negatively charged) 5,000 (5k) MWCO membranes (Millipore Corp., Billerica, MA) that are recommended for the size characterization of DOM (16). To reduce leaching of DOC from the UF membranes, they were soaked three times in deionized (DI) water (30 min per time), from a (Milli-Q Plus water system, (Millipore Corp., Bedford, MA) and then in 5% NaCl solution over night. UF was performed in Millipore solvent-resistant stirred cells (XFUF 076 01). The final step was to rinse the membranes with 100 ml Deionized water (DI) water just before filtration. Two hundred ml of sample solution was added to the cell and 100 ml was filtered through under 55 psi nitrogen gas pressure. Each membrane was discarded after one use. Fractions were analyzed by a Shimadzu total organic carbon (TOC) 5050 Analyzer and a Shimadzu UV-1700 Pharmaspec UV-Vis spectrophotometer (Shimadzu Corp. Columbia, MD). All samples were completed in duplicate.

Polarity Rapid Assessment Method (PRAM)

DOM polarity is identified by the polar rapid assessment method under ambient water quality conditions without any pretreatment (17). Analysis takes into account the effect of pH and ionic strength on the structure of DOM under ambient conditions. Solid phase extraction (SPE) cartridges are cleaned by passing Milli-Q water to remove UV absorbing impurities. Parallel SPE cartridges with different sorbent polarities are used to adsorb DOM. The SPE cartridges include C18 (non-polar, hydrophobic), Diol (polar, hydrophilic), and NH₂ (weak anion exchanger with a, negative charge). The retention coefficient is defined as $1 - (C_{\max}/C_0)$ in percentages describing the specific polarity characteristics (polar, non-polar, and negative charges) retained on the cartridges, where C_{\max} is the maximum UV absorbance at 254 nm of the samples after breakthrough and C_0 is the UV absorbance at 254 nm of the absorbing impurities. The samples are analyzed in triplicate.

Fluorescence Quenching

The sorption coefficient, K_{DOM} was determined by fluorescence quenching (FQ) by the method of Schlautman and Morgan (18). Perylene was diluted in methanol to 4 mg/L and stored in an amber bottle at 4 °C. The stock solution was diluted to 0.3 µg/L perylene and added to DOM diluted samples to a final concentration of three-fourths of the reported solubility 0.4 µg/L in water. To control for the loss of perylene from the cuvette system, 12 measurements were made at defined time points (2 min intervals) to allow for extrapolation to initial conditions. Experiments were performed in a dimmed environment to prevent the photodegradation of perylene. A previous evaluation of the fluorescence method showed that the Log K_{DOM} was equivalent to values obtained from the solid phase extraction method (19). Thus, this indicates that the partitioning of PAHs between water and DOM was fast compared to the adsorption of PAHs to the cuvette wall. Sorption behavior can be modeled by:



where PAH_d is the dissolved portion of the total PAH concentration, PAH -wall is the portion adsorbed on the wall, and k_w and k_{-w} are first-order forward and backward rate constants for wall adsorption. Fluorescence intensity can be obtained by:

$$F = \frac{k_{-w} F_0'}{k_w + k_{-w}} + \frac{k_w F_0'}{k_w + k_{-w}} e^{-(k_w + k_{-w})t} \quad (4)$$

where F_0' is the free PAH intensity at time zero. Nonlinear curve-fitting program (SigmaPlot) was used to get F_0' , k_w , and k_{-w} . K_{DOM} values were determined by the Stern-Volmer equation which can be described as

$$\frac{F_0'}{F} = 1 + K_{DOM}[\text{DOM}] \quad (5)$$

where F_0' and F are the fluorescence intensities in the absence and presence of DOM. $[\text{DOM}]$ is the concentration of DOM measured as mgC/L. MilliQ water adjusted with 0.02 molar phosphate buffer adjusted to the pH and general conductivity of the stormwater was the comparison case when no quencher was present. The percentage of bound PAH was determined by equation 2 as described previously (13).

All measurements of fluorescence intensities were obtained by a fluorescence spectrophotometer (Varian, R3896) at an excitation-emission wavelength pair of 434 and 467 nm. Absorbance values at 434 and 467 nm were corrected for inner filtering effects (IFEs). UV Absorbance at 254 nm were usually below 1.2 L/mg⁻¹cm⁻¹ (Shimadzu UV-1700, Pharmaspec Columbia MD). The experimental procedure and precision were presented by Hsu and Suffet (19).

Results and Discussion

Water Quality Data

The water quality data for this study are listed in Table 2. The DOC concentration of stormwater runoff samples were 11.5 mgC/L (Fall) and 6.6 mgC/L (Spring) which were consistently higher than studies of raw and drinking water samples (1.9-3.2 mgC/L (19),) (1.3-7.0 mgC/L (20),). UV₂₅₄ varied from 0.193 to 0.330 cm⁻¹. SUVA was consistent at 2.9 L mg⁻¹cm⁻¹. pH ranged from 7.4 to 7.6 which were within the National Pollutant Discharge Elimination System (NPDES) permit limit (6.5-8.5). In stormwater runoff samples, conductivity fluctuated from 276 to 427 μ s/cm. The intensity of rain events and dilution could cause this variability.

PRAM Analysis

PRAM results of stormwater runoff were shown in Figure 1. Non-polar fractions (C18) of stormwater runoff were 26% and 33% for Fall and Spring, respectively. In comparison, previous studies of raw and drinking water showed the non-polar fraction can range from 2 to 25% (19, 20).

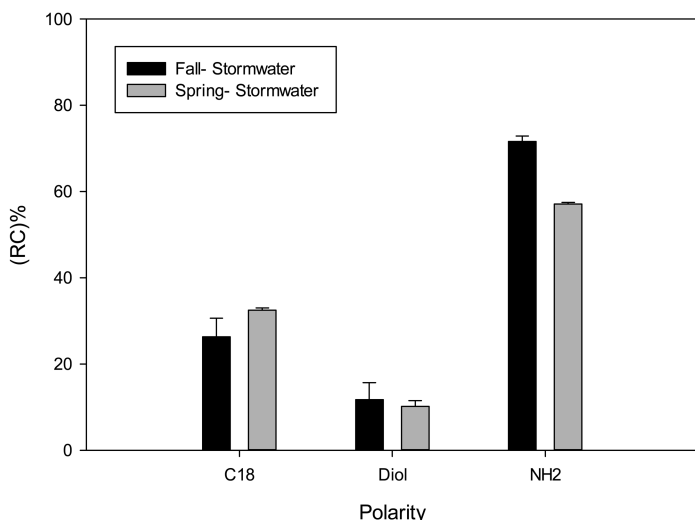


Figure 1. Polarity rapid assessment method analysis of stormwater runoff samples. (The values represent average of 3 analyses.)

Polar fractions isolated by the glycol SPE of stormwater runoff were 10% and 12% for Fall and Spring, respectively. In comparison, previous studies of raw and drinking water samples, polar fractions can range from 2 to 20% (19, 20). Negative charge portions of stormwater runoff measure by a weak anion exchanger were 72% and 57% for Fall and Spring, respectively. In comparison, raw and drinking water as well as other natural waters for the negative charges

DOM were reported at (39%-96% (19) and 28%-80% (20)). The results of PRAM analysis showed that season variations resulted in different polarity distribution. Specifically, the negative charge portions of DOM in stormwater runoff measured by a weak anion exchanger were significantly different 72% and 57% for Fall and Spring, respectively.

Table 2. Water Quality Parameters for Stormwater Runoff Samples

Sampling Date	Season	DOC	UV ₂₅₄	SUVA	pH	Conductivity
11/21/2011 P: 0.44 in	Fall	11.5	0.3297	2.9	7.4	276
04/11/2012 P: 0.22 in	Spring	6.6	0.1934	2.9	7.6	427

Units: DOC (mg L⁻¹); UV₂₅₄ (cm⁻¹); SUVA (L mg⁻¹cm⁻¹); Conductivity (μs cm⁻¹). P: precipitation. Rain fall intensity were 0.44 inches and 0.22 inches for Fall and Spring, respectively.

Size Characterization by Ultrafiltration

Figure 2 presents the UF results of stormwater runoff in Fall and Spring by DOC by (a) mgC/L and by (b) UV₂₅₄ absorbance. Figure 2(a) shows Fall stormwater had higher >10k and <1k fractions than Spring stormwater. There were no 10k-5k and 5k-1k fractions in Fall stormwater. Spring stormwater had a 10k-5k fraction.

Figure 2(b) shows that Fall stormwater runoff had higher <1k fraction than Spring stormwater runoff samples which was consistent as Figure 2(a). It appears that UF analysis measured by UV₂₅₄ is more sensitive than measured by DOC since there were measurements of 5k-1k fraction in Spring stormwater and 10k-5k fraction in Fall which were not shown in Figure 2(a). Spring stormwater runoff also had relative higher UV₂₅₄ absorbance in the molecular weight fractions (> 5 kDa) than Fall stormwater runoff. For > 10k fraction, Spring stormwater runoff has higher distribution than Fall stormwater which was not consistent as Figure 2(a). Thus, the DOM distribution was different for DOC that measures all the organic carbon in a sample and UV₂₅₄ analysis that measures the aromatic and double bond character of the DOC.

The results of UF analysis showed that size distributions of DOM were dependent on temporal variations. The variability in these samples could be ascribed to the changes in different environments such as weather resulting in different sources of DOM. The analysis of UF for DOM size distribution requires to monitor both DOC and UV₂₅₄ to continue build data to understand the size distribution for different physical meanings and samples.

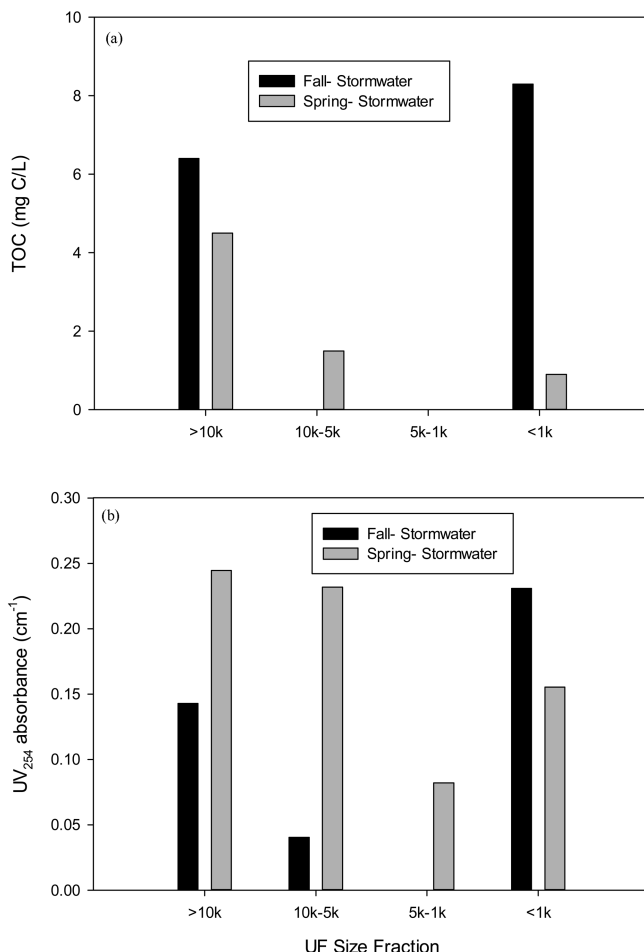


Figure 2. Ultrafiltration (UF) analysis of stormwater runoff samples: (a) DOC in mg C/L and (b) UV₂₅₄. (The values represent average, n=2.)

In total, the NOM in the Spring and Fall stormwater runoff showed differences in DOC, UV, UF and PRAM methods. Thus, one would expect a difference in the perylene log K, i.e. the log K_{DOM} for the Spring and Fall storm water runoff.

A comparison of log K_{DOM} values for perylene by fluorescence quenching and the PRAM showed no significant difference for log K_{DOM} from 4-6 at the 95% confidence interval (21). The Fluorescence quenching life time of perylene is only 5.5 nanoseconds (22), which would prevent errors due to other quenchers as oxygen to inflate the log K_{DOM}. Thus, perylene appears to be an excellent probe for assessing interactions between DOM and a HOP. The log K_{DOM} represents the ability of DOM to bind with Perylene. Equation 2 was used to calculate the free concentration of perylene as the probe method (7). The higher the K_{DOM} values of stormwater runoff samples represent the PAHs in the water that are potentially less

hazardous because more PAHs are bound to DOM. The probe perylene can be used to predict the free concentration of a related cancer causing PAH, as the human carcinogen, benzo(a)pyrene by using perylene as an indicator. This is done by transferring the % free portions of perylene into % free portions of BaP according to the proportion of the hydrophobicity using relative Log K_{ow} (7).

Table 3 shows that within Anaheim area, stormwater runoff contained free fraction distribution of Perylene from 28% to 58% for Fall and Spring, respectively. Birch et al. (23) also found that free fraction 27% - 36% in stormwater runoff in terms of fluoranthene (Log K_{ow} = 5.22) which was comparable to our results. Spring stormwater runoff had the higher Log K_{DOM} and thus had the lower free Perylene (28%) and free BaP (34%) distribution. It shows that Spring stormwater runoff had more ability to bind with HOPs and thus had a higher ability to decrease hazardous potential. Only 28% HOPs in terms of perylene is bioavailable. Fall stormwater had more free perylene (58%) and BaP distribution (60%). The difference of hazardous potential of free perylene and BaP during runoff in Fall and Spring is probably due to different DOM components present in the runoff.

Table 3. Free Fraction of Perylene Determined by Fluorescence Quenching and Calculated Fraction of Benzo(a)pyrene (BaP) of Stormwater Runoff Samples

Sampling Date	Season	DOC	UV ₂₅₄	SUVA	Log K_{DOM}	Free Perylene	Free BaP
11/21/2011 (P: 0.44 in)	Fall	11.5	0.3297	2.9	4.8	58	60
04/11/2012 (P: 0.22 in)	Spring	6.6	0.1934	2.9	5.6	28	34

Units: DOC (mg L⁻¹); UV₂₅₄ (cm⁻¹); SUVA (L mg⁻¹ cm⁻¹); Free Perylene and Free BaP (%). P: precipitation. Rain fall intensity were 0.44 inches and 0.22 inches for Fall and Spring, respectively.

Table 3 shows that although fall stormwater runoff had a higher DOC, it did not represent the higher K_{DOM} values (Log K_{DOM} = 4.8) indicating the poorer binding ability of DOM. In contrast, Fall stormwater runoff had the higher binding ability (Log K_{DOM} = 5.6) but with the lower DOC concentration. This indicates the binding ability of DOM (Log K_{DOM}) is not mainly dominated by the total amount of DOM in the water, but affected much more by different characteristics of DOM. Spring stormwater also had higher non-polar fraction (Figure 1), and higher molecular weight distribution (Figure 2b). These factors might also lead to Spring stormwater runoff had higher Log K_{DOM} values.

The fluorescent procedure developed in this chapter can identify the bioavailability of HOPs in the dissolved phase of urban runoff in a short time (within 30 mins). Thus, the method could be used to define the hazardous potential of free Perylene and BaP during runoff and possibly be used for site-specific

partition coefficient under ambient background conditions such as pH and organic carbon as metal pollution is defined by California “State Implementation Plan” (24). Also, understand the fate and transport of HOPs in urban runoff can help optimize the Toxicity Identification Evaluation (TIE) process required in the NPDES permit by relating the toxic free PAHs from the non-toxic bound DOM-PAH complex and develop better best management practices (BMPs) to treat HOPs in urban runoff as done for metals (14).

Conclusions

The objective of this paper was to consider adding another method to categorize “DOM Reactivity Related to an Environmental Concern” by measuring sorption to an HOPs and determining the free hazardous HOP. It has been shown that $\log K_{DOM}$ for a particular HOP will vary in different natural waters with different DOM constituents present (13). Perylene appears to be an excellent probe for an HOP. The $\log K_{DOM}$ represents the ability of DOM to bind with Perylene. An HOP probe could be used to characterize the differences between different aquatic DOMs in different natural waters.

HOPs exist in the aquatic environment coming from diverse sources like pavements, atmospheric deposition, and anthropogenic spilling, and can cause hazards to biota. Researches have estimated that urban runoff results in 14-36% of the total PAHs loading into aquatic ecosystems (25). The procedure developed in this chapter can identify the bioavailability of HOPs in the dissolved phase of urban runoff in a short time (within 30 mins) by the fluorescent method. The method could be used for site-specific partition coefficient under ambient background conditions such as pH and organic carbon as metal pollution is defined by California “State Implementation Plan” (24).

This study found that DOM in Spring stormwater runoff has better ability to bind with HOPs resulting in just 34% free portion of HOP versus 60 % free portion of HOP in Fall runoff. It is obvious that DOM characteristics were different due to temporal variations and thus lead to different potential hazards caused by HOPs. More monitoring needs to be completed in different locations, runoff types (e.g. stormwater runoff and dry weather flow), and different seasons to potentially build correlations between DOM characteristics and K_{DOM} values.

Also, understand the fate and transport of HOPs in urban runoff can help optimize the Toxicity Identification Evaluation (TIE) process required in the NPDES permit by relating the toxic free PAHs from the non-toxic bound DOM-PAH complex and develop better best management practices (BMPs) to treat HOPs in urban runoff as done for metals on a site specific basis (24).

Acknowledgments

The authors wish to thank the following individuals for their specific contributions to this study: Frank dela Vara, Janina Jarvis, and Carlos Campos for helping to get runoff samples from the fields; and Carmen Seetho and Hazel Cheung for support in the laboratory at UCLA.

References

- Chen, W.; Westerhoff, P.; Leenheer, J. A.; Booksh, K. Fluorescence excitation-emission matrix regional integration to quantify spectra for dissolved organic matter. *Environ. Sci. Technol.* **2003**, *37*, 5701–5710.
- Stevenson, F. J. *Humus Chemistry. Genesis, Composition, Reaction*, 2nd ed.; John Wiley & Sons: New York, NY, 1994.
- Thurman, E. M. *Developments in Biochemistry: Organic Geochemistry of Natural Waters*; Nijhoff & Junk Publishers: Dordrecht, The Netherlands, 1985.
- Reckhow, D. A.; Rees, P. L.; Nusslein, K.; Makdissi, G.; Devine, G.; Conneely, T.; Boutin, A.; Bryan, D. *Long-Term Variability of BDOM and NOM as Precursors in Watershed Sources*; AWWA Research Foundation Report, Denver, CO, 2007.
- APHA (American Public Health Association), American Water Works Association, and Water Environmental Federation. *Standard Methods for the Examination of Water and Wastewater*, 22nd ed.; Rice, E. W., Baird, R. B., Eaton A. D., Clesceri, L. S., Eds.; American Public Health Association: Washington DC, 2012.
- Lin, C. H.; Pedersen, J.; Suffet, I. H. Influence of Aeration on Hydrophobic Organic Contaminant Distribution and Diffusive Flux in Estuarine Sediments. *Environ. Sci. Technol.* **2003**, *37*, 3547–3554.
- Carter, C. W.; Suffet, I. H. Binding of DDT to dissolved humic materials. *Environ. Sci. Technol.* **1982**, *16*, 735–740.
- Chiou, C. T.; Malcolm, R. L.; Brinton, T. I.; Kile, D. E. Water solubility enhancement of some organic pollutants and pesticides by dissolved humic and fulvic-acids. *Environ. Sci. Technol.* **1986**, *20*, 502–508.
- Amy, G. L.; Thompson, J. M.; Tan, L.; Davis, M. K.; Krasner, S. W. Evaluation of THM precursor contributions from agriculture drains. *J. Am. Water Works Assoc.* **1990**, *82*, 57–64.
- Zhang, X. G.; Minear, R. A. Characterization of high molecular weight disinfection byproducts resulting from chlorination of aquatic humic substances. *Environ. Sci. Technol.* **2002**, *36*, 4033–4038.
- Singer, P. C. Humic Substances as precursors for potentially harmful disinfection by-products. *Water Sci. Technol.* **1999**, *40*, 25–30.
- Mitch, W. A.; Gerecke, A. C.; Sedlak, D. L. A N-Nitroso-dimethylamine (NDMA) Precursor Analysis for Chlorination of Water and Wastewater. *Water Res.* **2003**, *37*, 3733–3731.
- Carter, C. W.; Suffet, I. H. Interactions Between Dissolved Humic and Fulvic Acids and Pollutants in Aquatic Environments. In *Models for Predicting Fate of Chemicals in the Environment*; Swann, R. L., Eschenroeder, A., Eds.; ACS Symposium Series 225; American Chemical Society: Washington, DC, 1983; Chapter 11, pp 216–228.
- Waste Discharge Requirements For California as in Order No. R8-2008-0001, NPDES NO. CA0106283; California Regional Water Quality Control Board Santa Ana Region, 2008.

15. Li, Y.; Kang, J.-H.; Lau, S.-L.; Kayhanian, M.; Stenstrom, M. K. *J. Environ. Eng., ASCE* **2008**, *134*, 885–894.
16. Revchuk, A. D.; Suffet, I. H. Ultrafiltration separation of aquatic natural organic matter: Chemical probes for quality assurance. *Water Res.* **2009**, *43*, 3685–3692.
17. Rosario-Ortiz, F. L.; Snyder, S.; Suffet, I. H. Characterization of the polarity of natural organic matter under ambient conditions by the polarity rapid assessment method (PRAM). *Environ. Sci. Technol.* **2007**, *41*, 4895–4900.
18. Schlautman, M. A.; Morgan, J. J. Effects of aqueous chemistry on the binding of polycyclic aromatic hydrocarbons by dissolved humic materials. *Environ. Sci. Technol.* **1993**, *27*, 961–969.
19. Hsu, M.-H.; Suffet, I. H. The relationship between free and bound hydrophobic organic pollutants and dissolved organic matter in drinking water. In *It's All in the Water: Studies of Materials and Conditions in Fresh and Salt Water Bodies*; Benvenuto, M. A., Roberts-Kirchhoff, E. S., Murray, M. N., Garshott, D. M., Eds.; ACS Symposium Series 1086; American Chemical Society: Washington, DC, 2011; Chapter 5, pp 51–60.
20. Rosario-Ortiz, F. L.; Snyder, S.; Suffet, I. H. Characterization of dissolved organic matter in drinking water sources impacted by multiple tributaries. *Water Res.* **2007**, *41*, 4115–4128.
21. Gauthier, T. D.; Shane, E. D.; Guerin, W. F.; Sitz, W. R.; Grant, C. L. Fluorescence quenching method for determining equilibrium constants for polycyclic aromatic hydrocarbons binding to dissolved humic materials. *Environ. Sci. Technol.* **1986**, *20*, 1162–1166.
22. Backhus, D. A.; Golini, C.; Castellanos, E. Evaluation of fluorescence quenching for assessing the importance of interactions between nonpolar organic pollutants and dissolved organic matter. *Environ. Sci. Technol.* **2003**, *37*, 4717–4723.
23. Birch, H.; Gouliarmou, V.; Lutzhof, H.-C. H.; Mikkelsen, P. S.; Mayer, P. Passive dosing to determine the speciation of hydrophobic organic chemicals in aqueous samples. *Anal. Chem.* **2010**, *82*, 1142–1146.
24. The California “*State Implementation Plan*” (SIP), *Policy for Implementation of Toxics Standards for Inland Surface Waters Enclosed Bays, and Estuaries*, from the California State Water Resources Control Board, Section 1.4 “Calculation of Effluent Limitations”, February 24, 2005 (http://www.waterboards.ca.gov/water_issues/programs/state_implementation_policy/docs/final.pdf).
25. Hoffman, E. J.; Mills, G. L.; Latimer, J. S.; Quinn, J. G. Urban runoff as a source of polycyclic aromatic hydrocarbons to coastal waters. *Environ. Sci. Technol.* **1984**, *18*, 580–587.

Chapter 11

Characterization of the Molecular Weight and Reactivity of Natural Organic Matter in Surface Waters

Ina Kristiana,* Jace Tan, Suzanne McDonald, Cynthia A. Joll, and Anna Heitz

Curtin Water Quality Research Centre Department of Chemistry,
Curtin University Perth, Western Australia
*E-mail: I.Kristiana@curtin.edu.au.

Natural organic matter (NOM) can impact on all aspects of water treatments processes. Understanding the physical and chemical characteristics of NOM is essential to improving drinking water treatment processes. The size of NOM has important implications for drinking water treatment and the formation of DBPs, where the high molecular weight, hydrophobic components of NOM have been found to be effectively removed by conventional drinking water treatment processes, while the lower molecular weight and certain hydrophilic components of NOM are more difficult to remove using these processes. In our study, we collected raw (untreated) waters from three different drinking water reservoirs, characterised the molecular weight (MW) distribution of the NOM in these waters using analytical scale high performance size exclusion chromatography (HPSEC), and isolated apparent MW (AMW) fractions of the NOM using preparative scale HPSEC. We also investigated the reactivity of the AMW fractions of NOM in terms of disinfection by-products (DBP) formation potential from chlorination and chloramination. We focused on the formation potential of halogen-specific adsorbable organic halogen (AOX) and nitrogen-containing DBPs (N-DBPs), since brominated and iodinated DBPs and N-DBPs have been reported to be significantly more cytotoxic, genotoxic, and carcinogenic than the regulated DBPs. Our study found that the

AMW fractions of NOM with higher SUVA₂₅₄ values generally produced higher concentrations of halogenated DBPs, measured as halogen-specific AOX. Halogenated N-DBPs formed only a small fraction of AOX in both chlorination and chloramination, with higher relative contributions from halogenated N-DBPs in chloraminated samples. The propensity of the formation of N-DBPs, especially *N*-nitrosamines and haloacetamides, was higher in chloramination. Since these DBPs are more toxic than the regulated DBPs, further evaluation of the health risk trade-offs when selecting chlorine or chloramine as a disinfectant is essential. The size of NOM had little influence on the formation of halogenated N-DBPs, but the low to medium AMW fractions of NOM tended to form higher concentrations of *N*-nitrosamines. Chlorine tended to be incorporated into the higher AMW fractions of NOM, while bromine and iodine seemed to be preferentially incorporated into the lower AMW fractions of NOM. Since conventional water treatment processes are ineffective for the removal of the low to medium MW fractions of NOM, improved water treatment processes may be needed to minimise the formation of brominated and iodinated DBPs, as well as *N*-nitrosamines, especially for source waters that contain significant amounts of organic matter of low to medium MW.

Introduction

Organic matter is present in aquatic systems, including drinking water sources, and may originate from allochthonous and autochthonous sources. These organic materials are commonly referred to as natural organic matter (NOM). NOM is a complex, heterogeneous mixture of biogenic materials with a variety of molecular weights and chemical functional groups. The quality of a source water is closely linked to the nature and characteristics of NOM, and NOM can impact on all elements of water treatment processes. Many water treatment technologies are essentially focused on the removal of NOM and therefore the requirements for water treatment chemicals are closely related to the characteristics and concentrations of NOM in the source water. Typically, higher concentrations of NOM lead to increased requirements for water treatment chemicals such as coagulant and disinfectant, which in turn can lead to increased sludge formation and disinfection by-product (DBP) formation.

Considering the implications of NOM in the production of safe drinking water, understanding the physical and chemical characteristics of NOM is an important factor in improving drinking water treatment processes. Simple characterisation of NOM can be carried out using measurement of DOC concentration and UV absorbance at 254 nm (UV₂₅₄). Together, they provide an index of the extent of aromatic and other conjugated functional groups within the NOM structure. This index is termed 'specific UV₂₅₄ absorbance' (SUVA₂₅₄) and is derived by the

following equation: $UV_{254} (m^{-1}) / DOC (mg L^{-1}) \times 100 (I)$. More sophisticated methods are required to probe the characteristics of NOM molecules and their structures, both at bulk (e.g. size and functionality of NOM) and molecular (e.g. chemical composition of NOM) levels.

NOM characterisation studies have revealed useful information for designing NOM removal strategies in drinking water treatment. For example, it has been found that high molecular weight, hydrophobic components of NOM are effectively removed by conventional drinking water treatment processes (i.e. coagulation and filtration), while lower molecular weight and certain hydrophilic components of NOM are more difficult to remove using these processes (2–4). The hydrophilic fraction of NOM has also been implicated as containing the most precursors of nitrogenous DBPs (5, 6). Particular size fractions of NOM have been reported to have higher DBP formation potentials for the regulated DBPs, the trihalomethanes (THMs) and haloacetic acids (HAAs), than other fractions. For example, Hua and Reckhow (7) reported that NOM with molecular weight between 0.5 and 3 kDa produced the highest yield of THMs, while the low molecular weight NOM fractions (< 0.5 kDa) contained more abundant dichloroacetic acid precursors than the other molecular weight fractions studied.

There have been many reports of studies investigating the characteristics and reactivity of hydrophobic and hydrophilic fractions of NOM, however, the characteristics and reactivity of molecular weight (MW) fractions of NOM have been less extensively investigated. As demonstrated by the above examples, the molecular size distribution of NOM can have important implications for drinking water treatment and the formation of DBPs. Size exclusion chromatography (SEC) is commonly used to determine the MW distribution of NOM. It is a separation method based on the hydrodynamic molecular size of the material being analyzed (8). In the chromatography column, small molecules can access more of the internal pore volume than larger molecules, thus, ideally, larger molecules are excluded from the pores and elute first, followed by smaller components (8). SEC can be done at an analytical or preparative scale. Preparative SEC allows the isolation of organic rich apparent MW fractions of NOM through repeated injections of the water sample onto a preparative scale column, followed by collection of each fraction (9). Preparative scale sample volumes and column sizes are typically much larger than those used for analytical scale SEC, but comparable separation of components can be achieved, allowing direct comparison between the analytical scale results and fractions obtained using the preparative system.

In this study, we collected raw (untreated) waters from three different drinking water reservoirs, characterised the MW distribution of the NOM in these surface waters using analytical scale high performance size exclusion chromatography (HPSEC), and isolated apparent MW (AMW) fractions of the NOM using preparative scale HPSEC. We then investigated the reactivity of the AMW fractions of NOM in terms of DBP formation potential from chlorination and chloramination. Considering that the focus of investigations on the formation of DBPs in drinking water has shifted from the regulated DBPs (i.e. THMs and HAAs) to other emerging DBPs that are suspected to be more relevant from a human health perspective (e.g. nitrogen-containing DBPs, iodinated DBPs) (10, 11), we examined the formation of halogen-specific adsorbable organic

halogen (AOX) (i.e. AOCl, AOBr, and AOI), as bulk measures of the overall formation of halogenated DBPs, and nitrogen-containing DBPs (N-DBPs), as representatives of DBPs that are significantly more cytotoxic and genotoxic than the regulated DBPs. This study allowed an examination of the trends in the formation of halogenated DBPs and N-DBPs with respect to the size fractions of NOM, to provide insights into the reactivity of the complex mixture of organic compounds contained in NOM. It is the first comprehensive study of the formation of halogen-specific AOX and 27 species of N-DBPs from chlorination and chloramination of MW fractions of NOM from diverse surface waters, collected using preparative scale HPSEC.

Materials and Methods

Chemicals and Standards

All chemicals, standards, and organic solvents used in this study were of analytical grade purity (AR grade $\geq 99\%$ pure) or better (e.g. HPLC grade), and were used without further purification. Commercially available haloacetonitriles (HANs) standards were of analytical grade purity, and were used without further purification. Monochloroacetonitrile (MCAN), monobromoacetonitrile (MBAN), dichloroacetonitrile (DCAN), dibromoacetonitrile (DBAN), and trichloroacetonitrile (TCAN) were obtained from Sigma Aldrich as neat standards. Bromochloroacetonitrile (BCAN) was obtained from AccuStandard® as a solution in acetone (5 mg mL⁻¹). Trichloronitromethane (TCNM) standard was obtained from AccuStandard®. Other halonitromethanes (HNMs) standards were each obtained as single neat compound from Orchid Cellmark. Chloroacetamide (MCAM) standard was obtained from ChemService, while dibromoacetamide (DBAM) standard was obtained from Orchid Cellmark. Other haloacetamides (HAMS) standards were each obtained as single neat compound from Sigma Aldrich. 1,2-Dibromopropane-d₆ used as surrogate standard in the analysis of HANs, HNMs, and HAMS was obtained from CDN Isotopes. 1,1,2,2-Tetrachloroethane-d₂ used as internal standard in the analysis of HANs, HNMs, and HAMS was obtained from Sigma Aldrich. Native *N*-nitrosamines standards were obtained as a mixture (EPA 8270 Nitrosamine Mix) from Supelco. Deuterated *N*-nitrosamines standards used as internal and surrogate standards for quantification purposes were obtained from CDN Isotopes. The resins used in the solid phase extraction of nitrosamines, LiChrolut® EN and Carboxen™ 572, were purchased from Merck and Supelco, respectively. HPLC-grade solvents were obtained from Mallinckrodt, while inorganic salts were purchased from Sigma-Aldrich. Sodium hypochlorite solution (12.5% w/v) was obtained from APS Ajax.

Sample Collection and Preparation

Three surface waters from three different climatic regions in Western Australia were selected for this study (North West, Great Southern, and South West regions). These surface waters represent key drinking water sources for

the respective regions. Raw (untreated) water samples were collected from these locations: North West reservoir (Reservoir NW), Great Southern reservoir (Reservoir GS), and South West reservoir (Reservoir SW). At each location, 1000 L of water was collected and filtered through a 0.45 μm membrane, and then subjected to reverse osmosis (RO) to concentrate the organic matter in the sample to a final volume of approximately 1 L.

Fractionation of the NOM Concentrate

The NOM concentrate (~ 1 L) obtained for each sample was desalinated using dialysis bags (Spectra/Por® Biotech cellulose ester dialysis membranes; MWCO 100 Da) to remove the concentrated inorganic salts. A portion of the desalinated NOM concentrate was subjected to preparative scale HPSEC, following the method described by Peuravuori and Pihlaja (9). The high pressure liquid chromatography (HPLC) system was an Agilent 1100 equipped with a dual-loop autosampler, a diode array detector collecting data at 254 nm, and an automated fraction collector. The eluent comprised a 20 mM phosphate buffer with a flow rate of 4 mL min⁻¹ and the injection volume was 2 mL. Separation of NOM was achieved using a BioSep-SEC-S 3000 column (300 x 21.2 mm i.d., Phenomenex), equipped with a BioSep SEC-S 3000 guard column (75 x 21.2 mm i.d., Phenomenex). The system was calibrated using PSS standards (MW 208 – 81800 Da; Polymer Scientific Services, USA). Each apparent MW fraction corresponds to a molecular weight range as represented by a specific peak in the HPSEC chromatogram of the desalinated NOM concentrate. Since the diode array detector was set to 254 nm (the commonly used wavelength for the characterisation of NOM), 'NOM' in this manuscript refers to UV₂₅₄-absorbing NOM.

Analytical Scale HPSEC

Analytical scale HPSEC analysis of the samples used an HPLC system (Agilent 1100) equipped with a dual-loop autosampler and a diode array detector collecting data at 254 nm. The eluent was comprised of a 20 mM phosphate buffer with a flow rate of 1 mL min⁻¹ and the injection volume was 100 μL . Separation of NOM was achieved using a TSKgel™ G3000SW_{xl} column (300 x 7.8 mm i.d., TOSOH Bioscience, Supelco) preceded by a TSKgel™ SW_{xl} guard column (40 x 6.0 mm i.d., TOSOH Bioscience, Supelco). The analytical scale column has a similar phase to that of the preparative scale HPSEC column. The system was also calibrated using PSS standards (MW 208 – 81800 Da; Polymer Scientific Services, USA).

Water Quality Analysis

The raw water samples were analyzed for dissolved organic carbon (DOC) concentration, UV₂₅₄ absorbance, bromide and iodide ions concentrations, and total organic nitrogen content. The MW fractions of NOM were analyzed for DOC concentration and UV₂₅₄ absorbance. The DOC concentration of

the samples was determined by the UV/persulfate oxidation method, using a Shimadzu TOC Analyser TOC-VWS, according to the Standard Method 5310C (12). The UV₂₅₄ absorbance of the samples was determined using a HP 8452A Diode Array Spectrophotometer with a 5 cm quartz cell. The bromide and iodide ions concentrations were determined by ion chromatography according to the Standard Method 4110B (12), while the total nitrogen content was determined by flow injection analysis following persulphate digestion according to the Standard Method 4500N-C (12).

Disinfection Experiments

The MW fractions of NOM (each diluted to an identical DOC concentration of 2 mg L⁻¹) were each subjected to chlorination (8 mg L⁻¹ Cl₂) or chloramination (4 mg L⁻¹ NH₂Cl as Cl₂) in the presence of bromide ion (0.5 mg L⁻¹) and iodide ion (60 µg L⁻¹). Chlorine and chloramine doses were selected to provide disinfectant residuals greater than 0.5 mg L⁻¹ and 1 mg L⁻¹ in chlorination and chloramination, respectively, at the end of the experimental period. The samples were buffered to pH 7 in chlorination experiments and to pH 8 in chloramination experiments, using phosphate buffer. All experiments were carried out at 20 °C, for 72 hours. At the end of the experimental period, the disinfectant residual in each sample was quenched with excess ascorbic acid or sodium sulphite, and the sample was then analyzed for halogen-specific AOX and N-DBPs.

Analysis of Halogen-Specific AOX

Samples to be analyzed for halogen-specific AOX were acidified to pH 2 using concentrated nitric acid and passed through two activated carbon columns for adsorption of the organic halogens using a Mitsubishi TX-3AA adsorption module. The adsorbed sample was combusted in the presence of oxygen for 10 min at 1000 °C using a Mitsubishi AQF-100 Automated Quick Furnace system, and the produced hydrogen halide gas was collected in Milli-Q water in the Mitsubishi GA-100 absorption unit. The aqueous sample was then transferred online and analyzed for chloride, bromide, and iodide using a Dionex ICS-3000 dual-channel ion chromatograph system. The concentrations of the measured chloride, bromide, and iodide correspond to the concentrations of adsorbable organic chloride (AOCl), bromide (AOBr), and iodide (AOI), respectively.

Analysis of N-DBPs

A list of all the species of N-DBPs analyzed in this study is given in Table 1.

Table 1. List of N-DBPs Species Analysed

<i>N-DBPs</i>
Haloacetonitriles (HANs)
Chloroacetonitrile (MCAN)
Bromoacetonitrile (MBAN)
Dichloroacetonitrile (DCAN)
Trichloroacetonitrile (TCAN)
Bromochloroacetonitrile (BCAN)
Dibromoacetonitrile (DBAN)
Halogenated methanes (HNMs)
Dichloronitromethane (DCNM)
Bromochloronitromethane (BCNM)
Bromodichloronitromethane (BDCNM)
Dibromochloronitromethane (DBCNM)
Trichloronitromethane (TCNM)
Tribromonitromethane (TBNM)
Haloacetamides (HAMs)
Chloroacetamide (MCAM)
Bromoacetamide (MBAM)
Dichloroacetamide (DCAM)
Dibromoacetamide (DBAM)
Trichloroacetamide (TCAM)
<i>N</i> -Nitrosamines
<i>N</i> -Nitrosodimethylamine (NDMA)
<i>N</i> -Nitroso- <i>N</i> -methylethylamine (NMEA)
<i>N</i> -Nitrosodiethylamine (NDEA)
<i>N</i> -Nitrosodibutylamine (NDBA)
<i>N</i> -Nitrosodipropylamine (NDPA)
<i>N</i> -Nitrosopyrrolidine (NPYR)
<i>N</i> -Nitrosopiperidine (NPIP)
<i>N</i> -Nitrosomorpholine (NMOR)

Analysis of Haloacetonitriles (HANs)

The chlorinated and chloraminated samples were analyzed for 6 species of haloacetonitriles (MCAN, MBAN, DCAN, DBAN, BCAN, and TCAN). HANs were extracted from the samples by liquid-liquid extraction using methyl-*tert*-butyl ether (MTBE) and analyzed by gas chromatography/mass spectrometry (GC-MS) following the method described in Kristiana et al. (13). The GC-MS system was a Hewlett Packard 7890A GC interfaced to Hewlett Packard 5975C Mass Selective Detector, equipped with a 30 m x 0.25 mm ID ZB5-MS (Agilent) column with a film thickness of 0.25 μm .

Analysis of Halonitromethanes (HNMs) and Haloacetamides (HAMS)

The chlorinated and chloraminated samples were analyzed for 6 species of halonitromethanes (DCNM, TCNM, BCNM, BDCNM, CDBNM, and TBNM) and 5 species of haloacetamides (MCAM, MBAM, DCAM, DBAM, TCAM). HNMs and HAMS were extracted from the samples by liquid-liquid extraction using methyl-*tert*-butyl ether (MTBE) and analyzed by gas chromatography/mass spectrometry (GC-MS) following the method described in Liew et al. (14). The GC-MS system was a Hewlett Packard 7890A GC interfaced to Hewlett Packard 5975C Mass Selective Detector, equipped with a 30 m x 0.25 mm ID ZB5-MS (Agilent) column with a film thickness of 0.25 μm .

Analysis of N-Nitrosamines

The chlorinated and chloraminated samples were analyzed for 8 species of *N*-nitrosamines (NDMA, NMEA, NDEA, NDBA, NDPA, NPYR, NPIP, and NMOR). *N*-Nitrosamines were extracted from the samples by solid phase extraction and analyzed by gas chromatography/mass spectrometry (GC-MS) following a previously described method (15, 16). This method used in-house solid phase extraction (SPE) cartridges packed with LiChrolut® EN and Carboxen™ 572 resins (extraction rate: 2 mL min⁻¹), followed by elution of the nitrosamines from the cartridge using dichloromethane (elution rate: 1 mL min⁻¹), and concentration of the dichloromethane extract to approximately 300 μL . The concentrated extract was subsequently analyzed by GC-MS in electron impact (EI) mode, using a Hewlett Packard 7890A GC interfaced to Hewlett Packard 5975C Mass Selective Detector equipped with a 30 m x 0.25 mm ID HP-INNOWAX (Agilent) column with a film thickness of 0.25 μm .

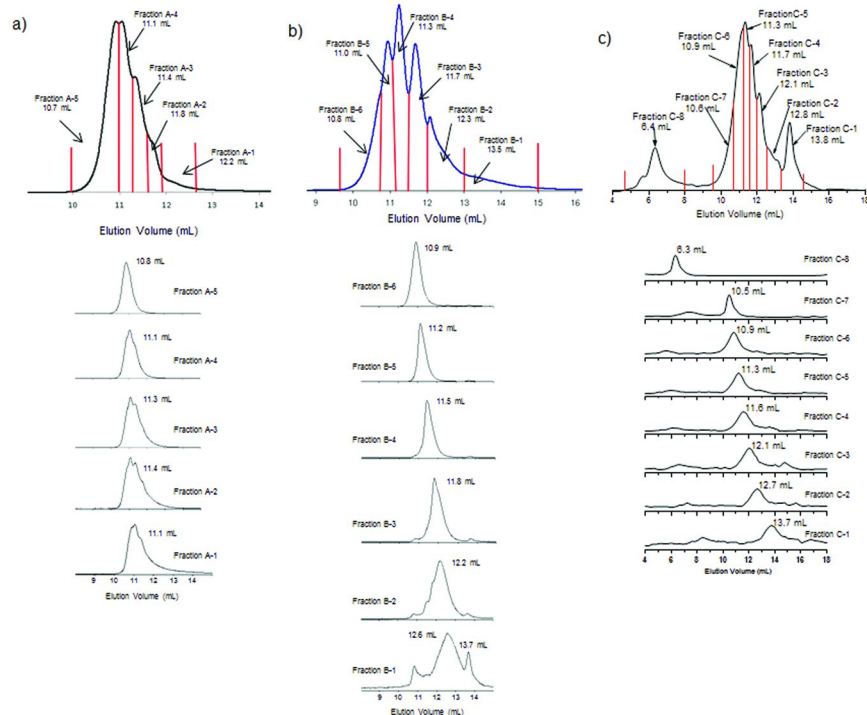


Figure 1. Analytical HPSEC chromatograms of the raw (untreated, unfractionated) waters from a) Reservoir NW, b) Reservoir GS, and c) Reservoir SW, after RO concentration and dialysis; and their corresponding fractions collected from subsequent preparative scale HPSEC.

Results and Discussion

Water Quality and Molecular Weight Characteristics of Surface Waters and NOM Concentrates

The three surface water samples studied (untreated, unfractionated), had significantly different water quality characteristics, as shown in Table 2, reflecting the different environmental (geological and ecological) conditions at each of the reservoir locations. Surface waters from locations NW and GS had similar DOC concentrations and UV_{254} absorbance. However, surface water from the NW reservoir had a higher concentration of bromide ion and a higher nitrogen content. The surface water from the SW reservoir was very different to those from NW and GS, since the SW sample had an extremely high DOC concentration, UV_{254} absorbance, and bromide ion concentration. The NOM collected from each surface water also had a different apparent MW (AMW) range according to UV_{254} detection in both analytical and preparative scale HPSEC (Figure 1, Table 3). The surface water from reservoir NW contained NOM with lower AMW range (< 2.6 kDa) than NOM from reservoir GS (< 4 kDa). The surface water from reservoir SW contained NOM with a wider MW range, with a fraction having MW > 20 kDa also collected. These differences can be attributed to the different geographical location of the reservoirs and the varying input of organic matter into the reservoirs. The differences in the climate, the factors influencing water inflow into the reservoirs, and the vegetation in the catchments surrounding the reservoirs all contributed to the differences in the water quality and the characteristics of NOM in the source waters.

Table 2. Water Quality Characteristics of the Raw Surface Waters (Untreated, Unfractionated) Collected from Three Regions in Western Australia

Sample	DOC (mg L ⁻¹)	UV ₂₅₄ (cm ⁻¹)	SUVA ₂₅₄ (L mg ⁻¹ m ⁻¹)	Total N (mg L ⁻¹)	Bromide (μ g L ⁻¹)	Iodide (μ g L ⁻¹)
Reservoir NW	4.05	0.073	1.30	0.5	480	20
Reservoir GS	4.28	0.075	1.75	0.3	350	60
Reservoir SW	23.7	0.178	3.77	1.0	803	20

The UV_{254} absorbance and DOC concentration of each collected AMW fraction of NOM were also measured and SUVA₂₅₄ calculated. The AMW fractions of NOM from each surface water had varying SUVA₂₅₄ values, demonstrating the range of reactivities within NOM in a specific water sample. SUVA₂₅₄ has been associated with the reactivity and aromatic character of NOM (1, 17). NOM fractions with higher SUVA₂₅₄ values have been shown to contain more aromatic moieties and structures with conjugated double bonds, all of which are reactive towards chlorine and chloramine (1, 17). For example, waters with higher SUVA₂₅₄ values have been reported to produce higher concentrations

of HAAs and THMs (18); while the aromatic moieties of NOM as indicated by SUVA₂₅₄ was found to play important role in the formation of total organic halogen (TOX) (19). The AMW fractions from reservoir SW had higher SUVA₂₅₄ values relative to the AMW fractions from the other reservoirs, indicating that these fractions have higher aromaticity than the other MW fractions, and hence they were expected to be more reactive towards the formation of DBPs. There seemed to be a trend of increasing SUVA₂₅₄ values with increasing AMW. However, the largest AMW fractions of NOM from reservoirs GS and SW did not follow this trend, having relatively low SUVA₂₅₄ values. This indicates that the NOM in these fractions contained significantly lower aromatic moieties relative to the other fractions.

Fractionation of NOM Concentrates by Preparative Scale HPSEC

The NOM in the three surface water samples was concentrated by reverse osmosis, desalinated using dialysis and then subjected to both analytical scale and preparative scale HPSEC with UV₂₅₄ detection. Analytical scale HPSEC was carried out to check the homogeneity and uniformity of the collected NOM fractions. Several AMW fractions of NOM were obtained from each surface water sample using the preparative scale HPSEC system. Each fraction of NOM corresponded to an apparent MW range as represented by a particular range of elution volume in the HPSEC chromatogram of the NOM concentrate. Chromatograms obtained for the NOM concentrates of the three surface waters are shown in Figure 1, which also shows the elution volume cutoffs of the collected fractions as represented by the vertical lines. The chromatograms obtained using analytical scale column were directly comparable to those obtained by preparative scale column. The AMW range of each collected fraction was calculated from the corresponding elution volumes, based on calibration of the preparative scale HPSEC system using a series of PSS MW standards. The elution volume ranges and calculated AMW ranges of the collected fractions are presented in Table 3. As a result of the inherent limitations of HPSEC separation of NOM (i.e. the size exclusion fractionation process does not separate samples based only on the molecular hydrodynamic size of the sample, but separation is also influenced by other factors including stationary phase, composition of mobile phase, ionic strength, hydrophobicity, hydrophilicity, molecular structure, and steric effects (9)), and the fact that the hydrodynamic and chemical properties of PSS MW standards are not directly comparable to NOM, the calculated AMW range does not represent an exact MW cutoff, but rather an approximation of the MW range of NOM contained in the fraction. Moreover, it is important to note that the NOM measured by the HPSEC system is only the UV₂₅₄-absorbing NOM.

Despite its limitations, the preparative scale HPSEC method showed relatively good recovery of NOM contained in the concentrated samples, as measured by the dissolved organic carbon (DOC) concentrations in the samples. Comparison between the total DOC in the initial, concentrated sample (prior to dialysis) and the total DOC in the corresponding fractions gave recoveries of 86%, 92%, and 94% for concentrated samples from reservoirs NW, GS, and SW, respectively.

Table 3. Elution Volumes and the Calculated Molecular Weight Cutoffs of the Collected Fractions of NOM (Based on Calibration Using Polystyrene Sulfonate Standards), and SUVA₂₅₄ of the Fractions

Sample	Elution Volume	Apparent MW Range	SUVA ₂₅₄ (L mg ⁻¹ m ⁻¹)
Reservoir NW			
Fraction 6	48.8 – 53.8 mL	0.1 – 0.3 kDa	1.44
Fraction 5	46.8 – 48.8 mL	0.3 – 0.5 kDa	1.75
Fraction 4	45.6 – 46.8 mL	0.5 – 0.6 kDa	1.68
Fraction 3	44.1 – 45.6 mL	0.6 – 0.9 kDa	1.55
Fraction 2	39.1 – 44.1 mL	0.9 – 2.6 kDa	2.10
Reservoir GS			
Fraction 7	47 – 50 mL	0.5 – 0.9 kDa	0.28
Fraction 6	46.2 – 47 mL	0.9 – 1 kDa	1.10
Fraction 5	45.5 – 46.2 mL	1 – 1.2 kDa	1.39
Fraction 4	44.1 – 45.5 mL	1.2 – 1.6 kDa	1.72
Fraction 3	42.9 – 44.1 mL	1.6 – 2 kDa	2.0
Fraction 2	39 – 42.9 mL	2 – 4 kDa	0.73
Reservoir SW			
Fraction 9	47.5 – 51.8 mL	0.3 – 1 kDa	3.28
Fraction 8	45 – 47.5 mL	1 – 1.5 kDa	4.33
Fraction 7	42.5 – 45 mL	1.5 – 2 kDa	4.42
Fraction 6	41.2 – 42.5 mL	2 – 2.5 kDa	5
Fraction 5	40 – 41.2 mL	2.5 – 3 kDa	5.22
Fraction 4	38.8 – 40 mL	3 – 5 kDa	5.22
Fraction 3	32 – 38.8 mL	5 – 20 kDa	6.28
Fraction 2	22.5 – 32 mL	> 20 kDa	2.92

In order to further evaluate the reliability of the MW fractionation process, a sub-sample of each collected fraction was analyzed using analytical scale HPSEC (Figure 1). The specified ‘elution volumes’ in Figure 1 correspond to the volume at which the mid-point of the fraction or the maximum peak height occurs. A single Gaussian-shaped peak with no overlapping peaks, that elutes near the elution volume where they were originally collected would signify that the separation during the fractionation process was the result of ideal SEC behaviour (20). A few fractions (fractions 4–6 from Reservoir NW; fractions 6 and 7 from Reservoir GS) showed some overlapping peaks upon analytical

scale HPSEC analysis, suggesting some substances with similar MW, but slightly different chemical and physical characteristics, elute at similar elution volumes. This observation may be caused by non-ideal interactions that have been known to occur between the sample and the stationary phase during the fractionation process. Within NOM, there are various functional groups that may be responsible for these non-ideal interactions. For example, carboxylic acid groups are negatively-charged at the pH used in the fractionation process (pH 6.85) and are thus subject to ion-exclusion interactions, while amino groups with a partial positive charge can undergo ion exchange (21). However, for these fractions with overlapping peaks, the main peaks still eluted near the elution volume where they were originally collected. For most fractions, single Gaussian peaks were obtained, eluting at the expected elution volume, demonstrating the uniformity and homogeneity of these fractions in relation to the unfractionated sample, and that discrete AMW fractions had been collected during the fractionation process. These signify the reliability of the MW fractionation process used, and that most of the AMW fractions of NOM collected in this study contained the majority of NOM in the calculated MW range.

Reactivity of Molecular Weight Fractions of NOM towards the Formation of Halogenated DBPs during Chlorination and Chloramination

The AMW fractions of NOM from the three surface waters (each diluted to an identical DOC concentration of 2 mg L⁻¹) were subjected to 72-h chlorination (8 mg L⁻¹ Cl₂; pH 7) and chloramination (4 mg L⁻¹ NH₂Cl as Cl₂; pH 8) in the presence of bromide (0.5 mg L⁻¹) and iodide (60 µg L⁻¹). The reactivity of the AMW fractions of NOM towards the formation of halogenated DBPs was determined by measurement of halogen-specific AOX concentrations (i.e. AOCl, AOBr, and AOI) in the chlorinated and chloraminated samples. The concentrations of halogen-specific AOX are presented in Figure 2. Relatively high concentrations of AOCl and AOBr were formed during chlorination, with MW fractions from Reservoir SW producing the highest concentrations. The highest chlorine demands (Table 4) were also observed in MW fractions from Reservoir SW. These demonstrate the higher reactivity of the MW fractions of NOM from Reservoir SW, relative to the other MW fractions, towards the consumption of chlorine and the formation of halogenated DBPs, which corresponded well with the higher SUVA₂₅₄ values of these fractions. During chloramination, significantly lower concentrations of AOCl and AOBr were formed than in chlorination, which is consistent with the relative reactivities of these disinfectants. The concentrations of AOCl and AOBr from chloramination, as well as the chloramine demand (Table 4), were also highest in MW fractions from Reservoir SW, which further demonstrates the higher reactivity of these fractions. The concentrations of AOCl were consistently higher than those of AOBr in both chlorinated and chloraminated samples, reflecting the relatively high initial ratio of Cl⁻ : Br⁻ in these samples.

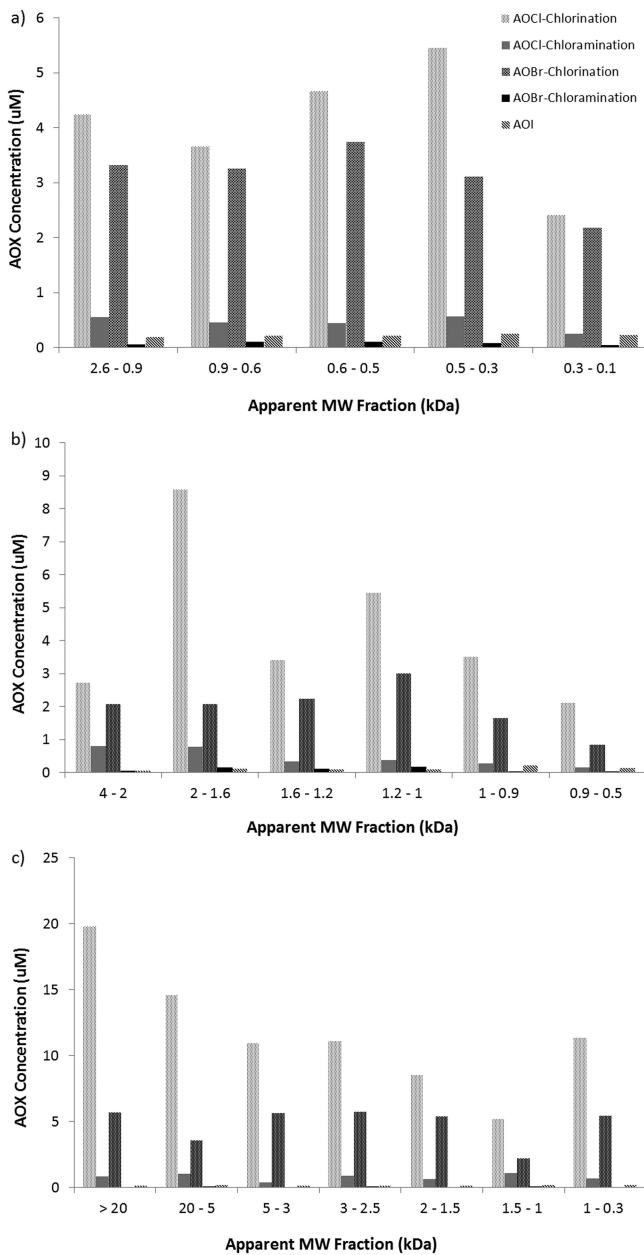


Figure 2. Molar concentrations of halogen-specific AOX after 72-hr chlorination (Cl_2 : 8 mg L^{-1} , pH 7) and chloramination (NH_2Cl : 4 mg L^{-1} as Cl_2 , pH 8) of MW fractions of NOM (DOC: 2 mg L^{-1} , Br^- : 0.5 mg L^{-1} , I^- : $60\text{ }\mu\text{g L}^{-1}$) from a) Reservoir NW, b) Reservoir GS, and c) Reservoir SW.

AOI was only detected in chloraminated samples, which is consistent with the chemistry of the oxidation of iodide. As a disinfectant with lower oxidising capacity than chlorine, chloramine can only oxidise iodide to HOI, rather than further to IO_3^- as chlorine can do, promoting the formation of iodinated DBPs from reaction of HOI with NOM (22). Furthermore, during chloramination, the formation of AOI was favoured over AOBr, as indicated by the lower concentrations of AOBr than AOI in the chloraminated samples. Once formed, HOI reacts faster with NOM than HOBr, resulting in the higher rate of formation of AOI than AOBr which leads to higher concentrations of AOI. HOI is the most reactive of the hypohalous acids (order of reactivity: $\text{HOI} \gg \text{HOBr} \gg \text{HOCl}$ (23, 24)). The concentrations of AOI were found to be highest in AMW fractions from Reservoir NW, which corresponds to lower AMW fractions (0.9 – 2.6 kDa) relative to the AMW fractions from Reservoir GS (0.5 – 4 kDa) and Reservoir SW (0.3 – > 20 kDa), suggesting that iodine may be preferentially incorporated into the lower MW fractions of NOM.

Although the concentrations of AOCl were consistently higher than AOBr in all chlorinated samples, the extent of bromine incorporation into NOM, as measured by the % incorporation of halogen (i.e. $[\text{AOX}] / [\text{X}_{\text{consumed}}]$), was significantly higher than that of chlorine. The % incorporation of chlorine into the AMW fractions of NOM varied from 3 – 20 %, while the % incorporation of bromine was 35 – 98% (Table 4). This observation can be explained by the fact that HOBr reacts approximately ten times faster than HOCl (25), and that bromide ion in the system can be recycled in reduction-oxidation reactions and further substituted into NOM forming brominated DBPs (26). In the chloraminated samples, the % incorporation of iodine (16 – 68%) was significantly higher than the % incorporation of chlorine (1 – 7%) and bromine (2 – 7%), which is consistent with the fact that HOI is the most reactive of the hypohalous acids (23, 24). The % incorporation of chlorine was generally higher in the AMW fractions from Reservoir SW, while the % incorporations of bromine and iodine were generally higher in the AMW fractions from Reservoir NW (Table 4). Although there was no clear trend in the formation of AOBr and AOI over the whole MW ranges, these observations indicate that chlorine tends to be incorporated into the higher MW fractions of NOM, while bromine and iodine may be preferentially incorporated into the lower MW fractions of NOM.

Reactivity of Molecular Weight Fractions of NOM towards the Formation of N-DBPs during Chlorination and Chloramination

The reactivity of the AMW fractions of NOM towards the formation of N-DBPs was determined by measurements of 6 species of haloacetonitriles (HANs), 6 species of halonitromethanes (HNMs), 5 species of haloacetamides (HAMs), and 8 species of *N*-nitrosamines. The concentrations of these N-DBPs, as total group molar concentrations are presented in Figures 3-5. To date, there are no reported studies of the formation of N-DBPs from size fractions of NOM collected using preparative-scale HPSEC. Previous studies have only been conducted on fractions that were collected based on polarity, which found that the hydrophilic fraction of NOM was responsible for the formation of N-DBPs (5, 6). The results

from our study showed that AMW fractions of NOM from Reservoir GS tended to form higher concentrations of HANs relative to the AMW fractions from the other reservoirs. However, there was no clear trend in the reactivity of the AMW fractions of NOM in the formation of HNMs, HAMs, and *N*-nitrosamines.

Table 4. Disinfectant Consumption and the Incorporation of Halogens into Dbps from Chlorination and Chloramination of AMW Fractions of NOM

Sample (AMW range)	CHLORINATION			CHLORAMINATION			I ^c
	Cl ₂ demand (mg L ⁻¹)	Cl ^a	Br ^b	NH ₂ Cl demand (mg L ⁻¹)	Cl ^a	Br ^b	
Reservoir NW							
0.1 – 0.3 kDa	1.0	8	69	0.4	2	2	68
0.3 – 0.5 kDa	5.8	3	77	1.6	1	3	68
0.5 – 0.6 kDa	2.6	6	98	0.7	2	5	53
0.6 – 0.9 kDa	2.0	6	87	0.7	2	5	58
0.9 – 2.6 kDa	3.5	4	83	0.3	7	2	51
Reservoir GS							
0.5 – 0.9 kDa	1.1	7	35	0.4	1	2	35
0.9 – 1 kDa	2.0	6	54	0.3	3	2	56
1 – 1.2 kDa	1.7	11	93	1.2	1	7	22
1.2 – 1.6 kDa	2.1	6	58	1.2	1	4	23
1.6 – 2 kDa	2.0	16	51	1.2	2	6	25
2 – 4 kDa	1.2	8	64	0.7	4	2	16
Reservoir SW							
0.3 – 1 kDa	4.7	9	72	0.7	4	2	37
1 – 1.5 kDa	2.5	7	47	0.6	6	4	39
1.5 – 2 kDa	2.0	15	75	0.8	3	2	31
2.5 – 3 kDa	2.1	20	74	0.5	6	4	30
3 – 5 kDa	2.3	17	63	0.7	2	2	27
5 – 20 kDa	3.5	15	52	0.8	5	3	37
> 20 kDa	7.5	9	57	2.1	1	2	33

^a % Cl incorporation = [AOCl] / [Cl₂ consumed]. ^b % Br incorporation = [AOBr] / [Br₂ consumed]. ^c % I incorporation = [AOI] / [I₂ consumed].

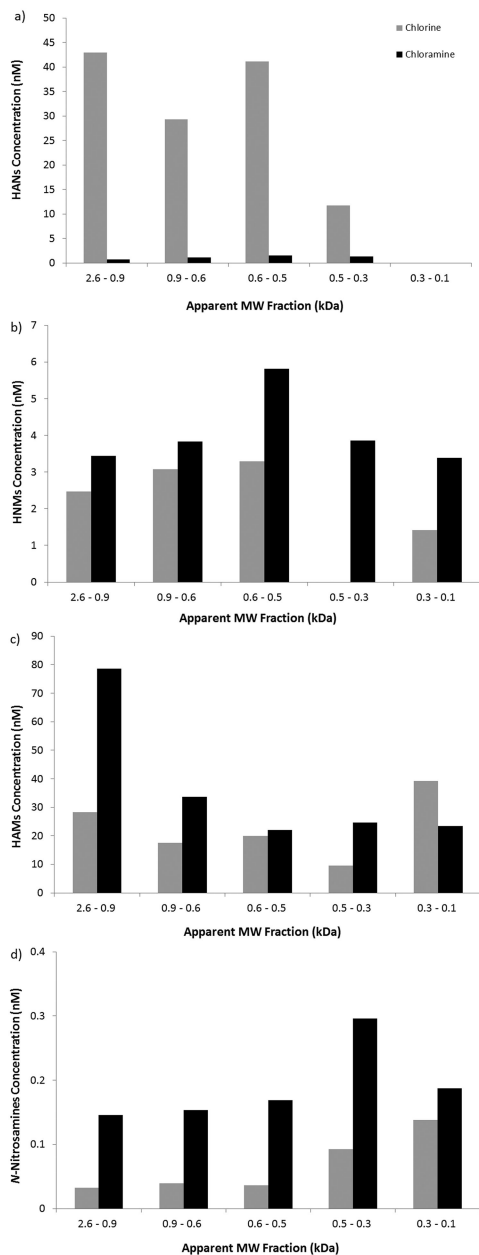


Figure 3. Molar concentrations of a) HANs, b) HNMs, c) HAMs, and d) N-nitrosamines after 72-hr chlorination (Cl_2 : 8 mg L⁻¹, pH 7) and chloramination (NH_2Cl : 4 mg L⁻¹ as Cl_2 , pH 8) of MW fractions of NOM (DOC: 2 mg L⁻¹, Br⁻: 0.5 mg L⁻¹, I⁻: 60 μ g L⁻¹) from Reservoir NW.

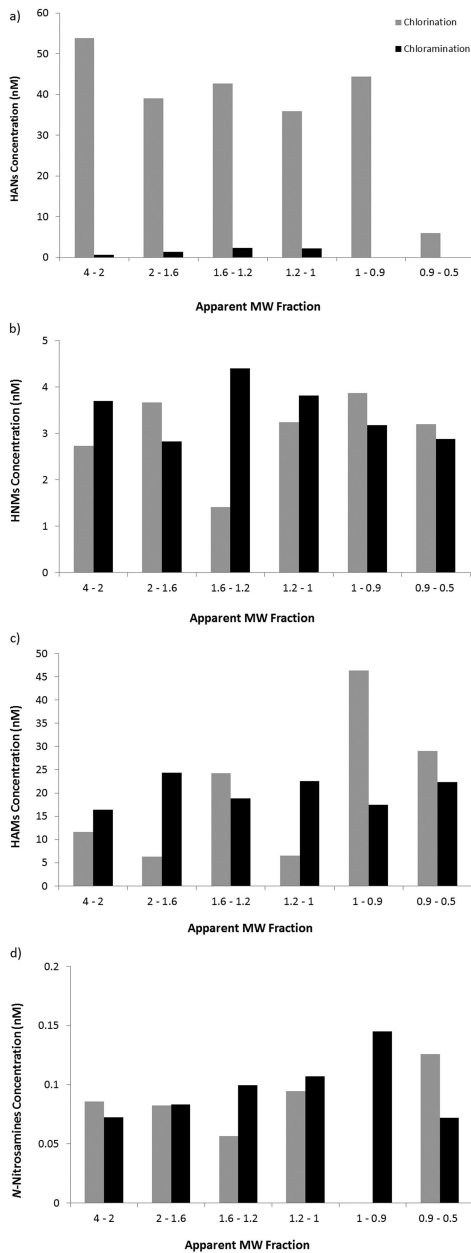


Figure 4. Molar concentrations of a) HANs, b) HNMs, c) HAMs, and d) N-nitrosamines after 72-hr chlorination (Cl_2 : 8 mg L^{-1} , pH 7) and chloramination (NH_2Cl : 4 mg L^{-1} as Cl_2 , pH 8) of MW fractions of NOM (DOC: 2 mg L^{-1} , Br^- : 0.5 mg L^{-1} , I^- : 60 $\mu\text{g L}^{-1}$) from Reservoir GS.

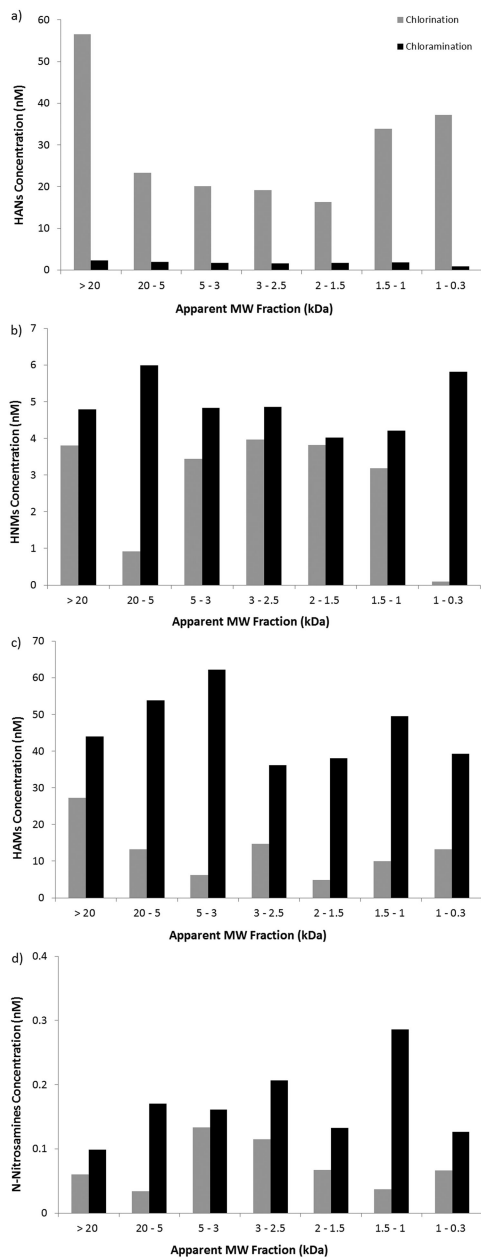


Figure 5. Molar concentrations of a) HANS, b) HNMs, c) HAMs, and d) N-nitrosamines after 72-hr chlorination (Cl_2 : 8 mg L^{-1} , pH 7) and chloramination (NH_2Cl : 4 mg L^{-1} as Cl_2 , pH 8) of MW fractions of NOM (DOC: 2 mg L^{-1} , Br^- : 0.5 mg L^{-1} , I⁻: 60 $\mu\text{g L}^{-1}$) from Reservoir SW.

Each group of N-DBPs had different formation potential in chlorination and in chloramination (Figures 3-5). HANs were consistently formed at higher concentrations in the chlorinated samples than in the chloraminated samples. Slightly higher concentrations of HNMs and HAMs were found in the chloraminated samples than in the chlorinated samples, while *N*-nitrosamines were consistently formed at higher concentrations in the chloraminated samples. In the chlorinated samples, 15-99% of the N-DBPs measured were HANs, while the corresponding range in the chloraminated samples was 1-10%. Similar proportions of HNMs were observed in chlorinated (0.2-15% of overall N-DBPs) and chloraminated (4-20% of overall N-DBPs) samples, which was in agreement with previously reported studies. Lee et al. (27) reported similar concentrations of trichloronitromethane in chlorinated and chloraminated NOM isolates, while Goslan et al. (28) found that there was no change in the median concentration of trichloronitromethane in chlorinated and chloraminated drinking waters in Scotland. In chloraminated samples, HAMs were produced at highest concentrations relative to the other groups of N-DBPs. Higher proportions of HAMs were also formed in chloraminated samples (74-95%) than in chlorinated samples (13-96%). Similar to HAMs, higher proportions of *N*-nitrosamines were observed in chloraminated samples (0.16-0.90%) than in chlorinated samples (0.04-0.45%). These data clearly highlight the preferential formation of HAMs and *N*-nitrosamines in chloramination compared to chlorination.

Halogenated N-DBPs dominate in both chlorinated and chloraminated samples, accounting for > 99% of N-DBPs measured. Relative to the concentrations of AOX, which represent the overall formation of halogenated DBPs, halogenated N-DBPs measured in this study only accounted for 0.2 – 2 % of AOX in chlorination, while the corresponding proportions for chloraminated samples are higher at 2 – 12% of AOX. Halogenated N-DBPs form only a small proportion of the overall halogenated DBPs, however, they are more cytotoxic and genotoxic than the regulated DBPs, the THMs and HAAs, which can form up to 50% of AOX (e.g. (13), (29)).

There was no clear trend in the formation potential of halogenated N-DBPs (i.e. HANs, HNMs, and HAMs) from AMW fractions of NOM. This suggests that, for these samples, the size of NOM had little influence on the formation potential of halogenated N-DBPs. N-containing NOM has been reported to be an important precursor of N-DBPs (30, 31). Thus, the functional groups (chemical characteristics) within NOM may be more important than size (i.e. molecular weight) in determining the formation potential of halogenated N-DBPs. NOM of any size may contain important functional groups for N-DBP formation, functional groups which will react with chlorine or chloramine to form halogenated N-DBPs.

The low to medium AMW fractions of NOM generally produced higher concentrations of *N*-nitrosamines in both chlorination and chloramination. In the chloraminated samples, the highest concentrations of *N*-nitrosamines were found in the lower AMW fractions of NOM (≤ 1.5 kDa). The results were less consistent in the chlorinated samples, but generally higher concentrations of *N*-nitrosamines were found in samples with higher AMW (< 5 kDa). Thus, precursor materials of *N*-nitrosamines appeared to be more abundant in the low to medium MW fractions NOM, in this case, less than 5 kDa. Since *N*-nitrosodimethylamine (NDMA) was

the *N*-nitrosamine species with the highest concentrations in most of the samples measured, this observation is consistent with reported studies of chlorination and chloramination of wastewaters, where effluent organic matter with MW < 3 kDa contained the majority of NDMA precursors (32, 33).

Considering all samples, the results showed that the concentrations of N-DBPs from chlorinated samples did not correlate with SUVA₂₅₄, while there was possible correlation between the concentrations of halogenated N-DBPs and SUVA₂₅₄ in chloraminated samples (Table 5). Previously reported studies have also found that there was no correlation between SUVA₂₅₄ and the concentrations of N-DBPs (30, 34, 35), which suggests that UV₂₅₄-active NOM has relatively low potential to form N-DBPs. Secondary aliphatic amines have been identified as organic nitrogen precursors for *N*-nitrosamines (36), while amino-nitrogen present in the form of proteinaceous material or within humic structures has been known to be a precursor of HANs (30, 37, 38). Primary amines have been associated with the formation of HNMs (39), while HAMs have been proposed to be degradation products of their corresponding HANs (40).

Table 5. Pearson Correlation Coefficients for Relationships between the Concentrations of N-DBPs and SUVA₂₅₄

<i>N</i> -DBPs	<i>r</i> (chlorination)	<i>r</i> (chloramination)
HANs	0.02	0.05
HNMs	0.01	0.37
HAMs	0.20	0.42
<i>N</i> -nitrosamines	0.03	0.11
Total halogenated N-DBPs (HANs+HNMs+HAMs)	0.10	0.47

Conclusions

Preparative scale HPSEC was successfully used to characterise the molecular weight distribution of NOM collected from diverse surface waters, and allowed for the collection of apparent MW (AMW) fractions of NOM. The measurement of SUVA₂₅₄ on the AMW fractions of NOM provided some information on the reactivity and the aromatic character of the samples. Evaluation of the reactivity of the AMW fractions of NOM towards the formation of DBPs during chlorination and chloramination showed that the AMW fractions with higher SUVA₂₅₄ values generally produced higher concentrations of halogenated DBPs, measured as halogen-specific AOX. These fractions also had the highest chlorine and chloramine demands. Halogenated N-DBPs formed only a small fraction of AOX in both chlorinated and chloraminated samples, with higher relative contributions from halogenated N-DBPs in chloraminated samples. Among the N-DBPs analyzed, HAMs and *N*-nitrosamines were preferentially formed in chloramination, measured at higher concentrations and formed the highest

proportions of N-DBPs. The higher propensity of the formation of N-DBPs in chloramination, especially HAMs and *N*-nitrosamines, which are significantly more toxic than the regulated DBPs, should prompt further evaluation of the health risk trade-offs when selecting chlorine or chloramine as a disinfectant.

The size of NOM had little influence on the formation of halogenated N-DBPs, but the low to medium AMW fractions of NOM tended to form higher concentrations of *N*-nitrosamines. Chlorine tended to be incorporated into higher MW fractions of NOM, while bromine and iodine seemed to be preferentially incorporated into the lower AMW fractions of NOM. Considering that brominated and iodinated DBPs have been reported to be more toxic than chlorinated DBPs, that *N*-nitrosamines are more toxic and carcinogenic than the regulated DBPs, and that conventional water treatment processes are ineffective for the removal of the low to medium MW fractions of NOM, improved water treatment processes may be needed to minimise the formation of brominated and iodinated DBPs, as well as *N*-nitrosamines, especially for source waters that contain significant amounts of organic matter of low to medium MW.

Acknowledgments

We thank the Australian Research Council (LP0882550), the Water Corporation of Western Australia, GHD Pty Ltd, and Curtin University for funding this work. We also thank Geoff Chidlow, Deborah Liew, Bradley Allpike, and Andrew Chan for their assistance in the laboratory.

References

1. Croué, J.-P.; Korshin, G. V.; Benjamin, M. *Characterisation of Natural Organic Matter in Drinking Water*; Report #159; American Water Works Association Research Foundation: Denver, CO, 2000; 324 pp.
2. Allpike, B. P.; Heitz, A.; Joll, C. A.; Kagi, R. I.; Abbt-Braun, G.; Frimmel, F. H.; Brinkmann, T.; Her, N.; Amy, G. L. Size exclusion chromatography to characterise DOC removal in drinking water treatment. *Environ. Sci. Technol.* **2005**, *39*, 2334–2342.
3. Drikas, M.; Chow, C. W. K.; Cook, D. The Impact of recalcitrant organic character on disinfection stability, trihalomethane formation and bacterial regrowth: An evaluation of magnetic ion exchange (MIEX) and alum coagulation. *J. Water Supply: Res Technol.* **2003**, *52*, 475–487.
4. Chow, C. W. K.; van Leeuwen, J. A.; Drikas, M.; Fabris, R.; Spark, K. M.; Page, D. W. The impact of the character of natural organic matter in conventional treatment with alum. *Water Sci. Technol.* **1999**, *40*, 97–104.
5. Chu, W. H.; Gao, N. Y.; Deng, Y.; Krasner, S. W. Precursors of dichloroacetamide, an emerging nitrogenous DBP formed during chlorination or chloramination. *Environ. Sci. Technol.* **2010**, *44*, 3908–3912.
6. Hu, J.; Song, H.; Addison, J. W.; Karanfil, T. Halonitromethane formation potentials in drinking waters. *Water Res.* **2010**, *44*, 105–114.

7. Hua, G.; Reckhow, D. A. Characterisation of disinfection byproduct precursors based on hydrophobicity and molecular size. *Environ. Sci. Technol.* **2007**, *41*, 3309–3315.
8. Pelekani, C.; Newcombe, G.; Snoeyink, V. L.; Hepplewhite, C.; Asemi, S.; Beckett, R. Characterisation of natural organic matter using high performance size exclusion chromatography. *Environ. Sci. Technol.* **1999**, *33*, 2807–2813.
9. Peuravuori, J.; Pihlaja, K. Preliminary study of lake dissolved organic matter in light of nanoscale supramolecular assembly. *Environ. Sci. Technol.* **2004**, *38*, 5958–5967.
10. Richardson, S. D. In *The Encyclopedia of Environmental Health*; Nriagu, J. O., Ed.; Elsevier: Burlington, 2011; Vol. 2, pp 110–136.
11. Richardson, S. D.; Plewa, M. J.; Wagner, E. D.; Schoeny, R.; DeMarini, D. M. Occurrence, genotoxicity, and carcinogenicity of regulated and emerging disinfection by-products in drinking water: A review and roadmap for research. *Mutat. Res.* **2007**, *636*, 178–242.
12. Clesceri, L. S.; Greenberg, A. E.; Eaton, A. D. *Standard Methods for the Examination of Water and Wastewater*, 20th ed.; American Public Health Association: Washington DC, 1998; 1325 pp.
13. Kristiana, I.; Allpike, B. P.; Joll, C. A.; Heitz, A.; Trolio, R. Understanding the behaviour of molecular weight fractions of natural organic matter to improve water treatment processes. *Water. Sci. Technol.* **2010**, *10*, 59–68.
14. Liew, D.; Linge, K. L.; Joll, C. A.; Heitz, A.; Charrois, J. W. A. Determination of halonitromethanes and haloacetamides: An evaluation of sample preservation and analyte stability in drinking water. *J. Chromatogr. A* **2012**, *1241*, 117–122.
15. Charrois, J. W. A.; Arend, M. W.; Froese, K. L.; Hrudey, S. E. Detecting N-nitrosamines in drinking water at nanogram per liter levels using ammonia positive chemical ionization. *Environ. Sci. Technol.* **2004**, *38*, 4835–4841.
16. Department of Health (DOH). *Characterising treated wastewater for drinking purposes following reverse osmosis treatment, Premier's Collaborative Research Program (2005-2008) Technical Report*; Department of Health: Perth, Western Australia, 2009; 370 pp.
17. Korshin, G.; Chow, C. W. K.; Fabris, R.; Drikas, M. Absorbance spectroscopy-based examination of effects of coagulation on the reactivity of fractions of natural organic matter with varying apparent molecular weights. *Water Res.* **2009**, *43*, 1541–1548.
18. Liang, L.; Singer, P. C. Factors influencing the formation and relative distribution of haloacetic acids and trihalomethanes in drinking water. *Environ. Sci. Technol.* **2003**, *37*, 2920–2928.
19. Kristiana, I.; Gallard, H.; Joll, C. A.; Croué, J-P. The formation of halogen-specific TOX from chlorination and chloramination of natural organic matter isolates. *Water Res.* **2009**, *43*, 4177–4186.
20. Muller, M. B.; Schmitt, D.; Frimmel, F. H. Fractionation of natural organic matter by size exclusion chromatography – properties and stability of fractions. *Environ. Sci. Technol.* **2000**, *34*, 4867–4872.

21. Specht, C. H.; Frimmel, F. H. Specific interactions of organic substances in size exclusion chromatography. *Environ. Sci. Technol.* **2000**, *34*, 2361–2366.
22. Bichsel, Y.; von Gunten, U. Formation of iodo-trihalomethanes during disinfection and oxidation of iodide-containing waters. *Environ. Sci. Technol.* **2000**, *34*, 2784–2791.
23. Smith, M. B.; March, J. *March's Advanced Organic Chemistry*, 5th ed.; John Wiley and Sons Inc.: New York, 2001; 2080 pp.
24. Kumar, K.; Margerum, D. W. Kinetics and mechanism of general-acid-assisted oxidation of bromide by hypochlorite and hypochlorous acid. *Inorg. Chem.* **1987**, *26*, 2706–2711.
25. Westerhoff, P.; Chao, P.; Mash, H. Reactivity of natural organic matter with aqueous chlorine and bromine. *Water Res.* **2004**, *38*, 1502–1513.
26. Song, R.; Westerhoff, P.; Minear, R. A.; Amy, G. L. Interaction between bromine and natural organic matter. In *Water Disinfection and Natural Organic Matter: Characterisation and Control*; Minear, R. A., Amy, G. L., Eds.; American Chemical Society: Washington DC, 1996; pp 322–349.
27. Lee, C.; Schmidt, C.; Yoon, J.; von Gunten, U. Oxidation of N-nitrosodimethylamine (NDMA) precursors with ozone and chlorine dioxide: Kinetics and effect on NDMA formation potential. *Environ. Sci. Technol.* **2007**, *41*, 2056–2063.
28. Goslan, E. H.; Kraner, S. W.; Bower, M.; Rocks, S. A.; Holmes, P.; Levy, L. S.; Parsons, S. A. A comparison of disinfection by-products found in chlorinated and chloraminated drinking waters in Scotland. *Water Res.* **2009**, *43*, 4698–4706.
29. Farré, M. J.; Day, S.; Neale, P. A.; Stalter, D.; Tang, J. Y. M.; Escher, B. I. Bioanalytical and chemical assessment of the disinfection by-product formation potential: Role of organic matter. *Water Res.* **2013**, *47*, 5409–5421.
30. Dotson, A.; Westerhoff, P.; Krasner, S. W. Nitrogen enriched dissolved organic matter (DOM) isolates and their affinity to form emerging disinfection by-products. *Water Sci. Technol.* **2009**, *60*, 135–143.
31. Shah, A. D.; Mitch, W. A. Halonitroalkanes, halonitriles, haloamides, and N-nitrosamines: A critical review of nitrogenous disinfection byproduct formation pathways. *Environ. Sci. Technol.* **2012**, *46*, 119–131.
32. Pehlivanoglu-Mantas, E.; Sedlak, D. Measurement of dissolved organic nitrogen from in wastewater effluents: Concentrations, size distribution and NDMA formation potential. *Water Res.* **2008**, *42*, 3890–3898.
33. Mitch, W. A.; Sedlak, D. L. Characterization and fate of N-nitrosodimethylamine precursors in municipal wastewater treatment plants. *Environ. Sci. Technol.* **2004**, *38*, 1445–1454.
34. Bouegard, C. M. M.; Goslan, E. H.; Jefferson, B.; Parsons, S. A. Comparison of the disinfection by-product formation potential of treated waters exposed to chlorine and monochloramine. *Water Res.* **2010**, *44*, 729–740.
35. Zhao, Y. Y.; Boyd, J. M.; Woodbeck, M.; Andrews, R. C.; Qin, F.; Hruday, S. E.; Li, X. F. Formation of N-nitrosamines from eleven disinfection

treatments of seven different surface waters. *Environ. Sci. Technol.* **2008**, *42*, 4857–4862.

- 36. Gerecke, A. C.; Sedlak, D. L. Precursors of N-nitrosodimethylamine in natural waters. *Environ. Sci. Technol.* **2003**, *37*, 1331–1336.
- 37. Reckhow, D. A.; Singer, P. C.; Malcolm, R. L. Chlorination of humic materials: By-product formation and chemical interpretations. *Environ. Sci. Technol.* **1990**, *24*, 1655–1664.
- 38. Oliver, B. G. Dihaloacetonitriles in drinking water: Algae and fulvic acid as precursors. *Environ. Sci. Technol.* **1983**, *17*, 80–83.
- 39. Joo, S. H.; Mitch, W. A. Nitrile, aldehyde, and halonitroalkane formation during chlorination/chloramination of primary amines. *Environ. Sci. Technol.* **2007**, *41*, 1288–1296.
- 40. Glezer, V.; Harris, B.; Tal, N.; Iosefzon, B.; Lev, O. Hydrolysis of haloacetonitriles: Linear free energy relationship, kinetics, and products. *Water Res.* **1999**, *33*, 1938–1948.

Chapter 12

Fate of Characterized and Uncharacterized Halogenated Organic Matter during Coagulation of Natural Waters with Chlorine or Chlorine Dioxide Application

Miguel S. Arias^{*,1,2} and R. Scott Summers¹

¹Department of Civil, Environmental and Architectural Engineering,
ECOT 441 CB 428, University of Colorado – Boulder,
Boulder, Colorado 80309

²Orica Watercare, 33101 East Quincy Avenue, Watkins, Colorado 80137
*E-mail: miguel.arias@orica.com.

Chlorine and chlorine dioxide react with source water organic matter to form halogenated organic matter (HOM), often termed organic disinfection byproducts (DBPs), some of which are characterized, e.g., the regulated trihalomethanes (THMs) and haloacetic acids (HAAs), and others that can be assessed with the adsorbable organic halogen (AOX) measurement. The fate of HOM was addressed during alum coagulation of five natural waters. THMs and HAAs preformed in the raw waters were not removed by coagulation (< 9%), while the uncharacterized AOX (AOX-U), calculated as the difference between AOX concentration and THM and HAA concentrations, was removed by 55% on average over all coagulant doses and 75% at highest doses, with near complete AOX-U removal for three waters. Turbidity influenced the removal of AOX-U, where the most turbid waters demonstrated 100% removal of AOX-U and one water spiked with kaolin at 100 mg/L also demonstrated a similar removal efficiency; 98%. Once incorporated into the floc, AOX was found not to release back to the water. Once flocs formed, no removal of HOM occurred, indicating that sorption on aluminum hydroxide precipitate was not the AOX removal

mechanism. The suggests that other removal mechanisms, such as co-precipitation and metal HOM complexation reactions, dominated, although they were not directly measured in this study. Chlorine was found to react directly with the flocs to produce 40% of the THMs and HAAs formed during coagulation, but not to produce AOX-U. Use of chlorine dioxide produced less HOM, and formed TTHMs and HAAs were less than 10% of the AOX-U. Coagulation only removed about 20% of the AOX-U. No quantifiable levels of AOX were formed when chlorine dioxide reacted with flocs containing organic matter.

Introduction

The application of chlorine prior to or during the coagulation is commonplace in drinking water treatment to disinfect water and control iron, manganese, taste, odor, biogrowth and aid particle filtration. Chlorine also reacts with organic matter (OM) present in source waters via substitution reactions to form halogenated organic matter (HOM), termed organic disinfection by-products (DBPs), which are of health concern (1). Extensive organic structures that can be halogenated via chlorine substitution have been identified (2). Substitution reactions involving chlorine are usually electrophilic and form significant amounts of chlorinated organic compounds (3). A collective measurement for the characterized and uncharacterized HOM formed is total organic halogen (TOX). However, the analytical process used to characterize this parameter in bulk water only measures the adsorbable organic halogen (AOX) fraction through the use of adsorption to activated carbon. Approximately 50% or greater of the HOM can be characterized including the predominantly formed trihalomethanes (THMs) and haloacetic acids (HAAs), with lesser quantities of haloacetonitriles, halo ketones and chloropicrin (4). The regulated parameters in the U.S. are total THMs (TTHM) [chloroform, dichlorobromomethane, chlorodibromomethane and bromoform] and the summation of five species of HAA (HAA5) [mono-, di-, tri-chloroacetic acid, mono- and di-bromoacetic acid]. The heterogeneous nature of source water OM yields a large distribution of HOM with a range of molecular weight (MW). The reported molecular weight distributions (MWD) of AOX show that approximately 50% of the AOX has a MW > 500 Da (5, 6), which would correspond to the AOX fraction of HOM.

Chlorine dioxide is a disinfectant/oxidant that has the many of the same benefits as chlorine, as well as the added benefits of lower organic DBP formation and greater effect on protozoan disinfection. The application of chlorine dioxide through oxidation reactions causes NOM to break into smaller fragments and decrease aromaticity as measured through fluorescence emission – excitation plots (7). The (+4) valence of the chlorine in chlorine dioxide makes it a strong oxidizing agent and limits substitution and addition reactions that form

halogenated DBPs. Chlorine dioxide dose is limited by the formation of chlorite, in applications where reducing agents; such as ferrous salts, are not used to reduce chlorite; a regulated inorganic DBP with a maximum contaminant level (MCL) of 1.0 mg/L.

Source water OM is comprised of particulate and dissolved organic matter (DOM) and is ubiquitous in natural surface water bodies; rivers, streams, lakes and reservoirs. It can contain OM from anthropogenic sources; waste water discharges, as well as natural organic matter (NOM). Coagulation of surface waters was initially used to facilitate particle removal, as destabilized particles coalesce and are more easily settled and filtered (8, 9). Coagulation has been recognized as a DBP control process as substantial OM removal: 15 to >50% as measured by total organic carbon (TOC), can be achieved via adsorption and co-precipitation (10, 11). Coagulation of natural waters is complex with the interactions of particles, coagulants, DOM and water chemistry (12). TOC removal requirements are regulated by the USEPA and often require coagulant doses that are greater than those for particle removal and can dictate coagulant requirements in water treatment plants (12).

An effective DBP control strategy for utilities that use chlorine is to minimize the exposure of chlorine to OM (13). This can be achieved by reducing the chlorine dose prior to coagulation and by maximizing the OM removal by coagulation. Solarik et al. (14) conducted bench coagulation experiments in which the point of chlorination was moved from the rapid mix to mid-flocculation to post-sedimentation, which yielded progressively fewer DBPs, yet the kinetics of OM removal are rapid and removal by coagulation occurs by mid-flocculation (15). Similar results have been found at the pilot and full scale (16).

Humic substances (HS) are of specific concern because they are often the predominant DOM fraction and may have higher DBP formation potential than non-HS DOM (17, 18). HS are the primary NOM fraction that is adsorbed during coagulation. HS have molecular weights of several hundred or larger and carry weakly acidic and phenolic functional groups (19), which give the molecules properties of weak anionic polyelectrolytes (10). When hydrolyzing metal salts, such as aluminum sulfate, are used as a coagulant, the anionic humic polyelectrolytes complex onto positively charged sites on the aluminum hydrolysis species (20). Co-precipitation and/or adsorption on aluminum hydroxide solids follow. Higher concentrations of suspended matter can be beneficial for increasing the concentration of nucleating and binding sites both for adsorbing and co-precipitating OM (21).

The pathway for removal of organic DBPs during coagulation depends on the DBP structure; as either a high or low MW HOM. Through IR spectroscopy of chlorinated molecular weight fractions Tsai et al. (22) concluded that chlorination did not significantly alter the functional groups (carbonyl, $C_{sp^3}-H$, C-O-H and O-H) present in the NOM. This result indicates that the NOM fraction that would adsorb prior to chlorination retains the functional groups that can attach to aluminum hydroxide surfaces post-chlorination. Therefore, even after chlorination, AOX compounds may adsorb much like an NOM molecule. Zhang and Minear (23) evaluated a large MW NOM fraction, > 3000 Da, and showed a similar molecular weight distribution between DOC and AOX.

When NOM adsorbs onto floc it can be modeled as a series of (1) trains, which are NOM segments adsorbed to the surface, (2) tails, which are segments that terminate in aqueous solution and (3) loops, which have both ends attached to trains (9, 24). Such coiling is brought about by functional groups bonding to the surface and the NOM minimizing the hydrophobic surface area it exposes to the water. For hydrophobic NOM remaining in solution, a hydrophobic surface on the floc, such as the surface of a mineral or organic particle (25, 26) would be an energetically favorable location to attach to by not having to displace water (25).

Chi and Amy (27) identified several mechanisms for NOM sorption onto mineral surfaces. They found that hydrophobic partitioning effects followed by ligand exchange were the dominant contributing mechanisms for sorption of DOM to mineral surfaces. Furthermore, NOM with large molecular weights were shown to exhibit higher affinities for mineral surfaces and the higher content of carboxylic acid and phenolic acid groups were concluded to be the factors contributing to partitioning to aluminum and iron surfaces in natural streams (28, 29).

The molecular forces between the NOM on the surface and the aqueous NOM or halogenated molecule could be weak attraction forces, such as hydrophobic – hydrophobic interactions, as previously stated, indicating that this sorption could be reversible. The reversibility of the sorption reaction has been seen for numerous compounds: trichloroethylene, toluene, polychlorinated biphenyls, polycyclic aromatic hydrocarbons and insecticides (25). As previously stated NOM and HOM likely compete for the same surface sites in terms of adsorption if similar functional groups are present for both molecules, yet the NOM may already be irreversibly bound to the surface (30). Gu et al. (30) looked at adsorption and desorption of NOM onto iron oxide surfaces and observed very slow desorption kinetics, even at extended desorption times (up to 63 days) there was little desorption of NOM (27). Explanations that were offered were the possibility of multiple chemical binding sites from the NOM to the surface, requiring simultaneous detachment of all sites that had undergone ligand exchange for the NOM to desorb. Sorption could be reversible if the molecular forces that are binding the NOM to the surface are those of hydrophobic – hydrophobic interactions.

The objectives of this study were to quantify and understand the fate of HOM and its precursors during coagulation, flocculation and sedimentation while dosing chlorine and chlorine dioxide. The specific objectives were to: a) quantify the adsorptive and desorptive interactions between HOM and coagulant flocs, and b) determine the availability of OM sorbed to flocs to react to form aqueous HOM. The approach was to pre-form HOM and assess sorption and desorption during coagulation, and to pre-adsorb DOM onto flocs and assess the reactivity with chlorine or chlorine dioxide and solid phase OM to form HOM.

In this study the authors utilize the nonspecific term sorption to describe the removal of AOX by coagulation, as the pathway of OM or HOM removal is not resolved. The authors also use the term coagulation in this manuscript to refer to the coagulation/ flocculation/ sedimentation process.

Materials and Methods

Materials

Raw water samples were shipped to the University of Colorado at Boulder and stored at 4°C in containers pretreated to minimize leaching contamination. Raw waters were sampled for TOC, dissolved organic carbon (DOC), UV absorbance (UVA₂₅₄), bromide, pH, turbidity, alkalinity and hardness.

The chlorine stock solution was prepared using 10.5 percent sodium hypochlorite (NaOCl) stock solution, which was buffered to a pH of 8.0 using a pH 6.7 borate buffer (ACS Grade) and 0.11 M sodium hydroxide (ACS Grade) in laboratory clean water. The stock strength of the dosing solution was measured using the titrimetric iodometry method Standard Method (SM) 4500-Cl₂ B (31). Chlorine residuals were measured using the DPD-FAS Method, SM 4500-Cl₂ D (31); with a detection limit of 0.024 mg/L. A high purity chlorine dioxide stock solution concentration, 2000 mg/L, was generated on site at Colorado State University, Fort Collins, Colorado using a CDG™ generator. Chlorine dioxide stock concentration was measured using SM 4500-ClO₂ E (31) and residual was measured using EPA Method 327.

Methods

Coagulation Testing

The bench-scale simulation of coagulation, flocculation and sedimentation was performed using a programmable jar testing apparatus (Phipps and Bird – 900™) with 2 liters of water. To minimize the loss of volatile DBPs to the atmosphere, jars were covered with custom made plexi-glass lids that were suspended 1 to 2 cm above the water surface not to disturb mixing and settling. Chemical doses were administered through the lid using a 1 cm opening. Jar tests were operated at 20°C ± 1°C with aluminum sulfate; Al₂(SO₄)₃•18H₂O, (ACS Grade) as the coagulant. Jar tests were operated under the following mixing conditions: rapid mix 250 rpm for 3 minutes, three stages of flocculation at 30, 20 and 10 rpm, each for 10 minutes, and sedimentation for 90 minutes.

The effect of turbidity was also tested for one water, where kaolin was added at 100 mg/L for comparison to naturally high turbid waters tested in the water set.

Halogenated Organic Matter Analysis

THMs and HAAs were measured with a gas chromatograph (Agilent 6890), using a high-resolution column (J&W Scientific 124-1032 DB-1) and an electron capture device following a modified US EPA Method 551.1 and modified Standard Method 6251B, respectively (31, 32). Nine HAA species, HAA5 plus bromochloro-, bromodichloro- dibromochloro- and tribromo-acetic acid were measured and the mass sum; HAA9 and TTHM were reported. Aqueous AOX

was measured with a AOX instrument (Mitsubishi TOX-10 Σ following Standard Method 5320B (31). Ten percent of all samples were run in duplicate, which yielded an average analytical error (AE) of 3.8 $\mu\text{g/L}$ for TTHM, 1.4 $\mu\text{g/L}$ for HAA9 and 8.0 $\mu\text{g Cl/L}$ for both aqueous and solid phase AOX.

A TOX measurement of the solid floc required 2 liters of coagulated and settled raw water (dosed with chlorine or chlorine dioxide). The supernatant water was decanted post sedimentation. The remaining contents of the jar (flocs and interstitial water) were vacuum filtered with a 1.0 μm glass fiber filter (GFF, Whatman). The flocs captured on the GFF were rinsed with 10 mL of pH 2 nitric acid acidified nitrate (NO_3^-) (5 g/L) to displace any chloride ions and rinsed with 10 mL of pH 2 nitric acid acidified laboratory clean water. The filtered floc, complete with GFF were placed in the TOX instrument. Blank GFFs measured below limit TOX concentrations. The flocs were run in 8 to 10 segments, since the halogen concentrations on the flocs were often above quantifiable range of the instrument. Electrodes were cleaned and filled with electrolyte solution following every sample due to heavy silver halide precipitation. The sum of the mass $\mu\text{g Cl}^-$ measured from the flocs was normalized by the 2 liter volume of coagulated water for a TOX solid phase floc concentration in $\mu\text{g Cl/L}$. Reporting the solid phase TOX floc concentration in this manner facilitated the comparisons to the aqueous phase AOX concentrations.

Halogenated Organic Matter Sorption by Flocs

Raw waters were chlorinated in the jar test vessels at a 0.6:1 to 0.8:1 chlorine to TOC ratio. After 24 hours the chlorine decayed to an undetectable residual and HOM samples, AOX, TTHM and HAA9, were taken. Coagulation was performed as aforementioned and following sedimentation, samples of aqueous AOX, solid phase TOX, TTHM and HAA9 were taken.

Desorption of Halogenated Organic Matter from Flocs

Two equivalent parallel jars containing coagulated HOM / OM flocs were re-suspended to observe desorptive behavior. One jar was used for initial HOM measurements and solid phase floc HOM measurements (already outlined), since the method was destructive. The second jar yielded the flocs with HOM for desorption experiments. Flocs were harvested using a separatory funnel. A third jar without chlorine was used where the treatment process proceeded to the 1/3-floc point and the water was filtered using a 1.0 μm cartridge filter. The harvested flocs from the second jar were re-suspended in the filtered water. This re-suspension water was selected to ensure that the solids contacted water of similar overall composition to minimize HOM desorption due to changing water quality. The flocs were re-suspended using the jar tester and mixed using flocculation conditions, so the formed flocs would not be destroyed. The last stage of tapered flocculation continued until liquid-phase samples were taken at two, twenty-four and seventy-two hours for HOM analysis.

Halogenated Organic Matter Formation from Flocs

Three experiments, each in a different jar, were run in parallel to determine floc contributions to HOM formation. Waters were dosed with chlorine at the 1/3-flocculation point (after the first stage of tapered flocculation). The chlorinated waters included raw, coagulated (water containing flocs) and water coagulated and filtered at the 1/3 flocculation point with no flocs present. The raw water was the only one to be dosed at the 0.6:1 to 0.8:1 chlorine to TOC ratio and the coagulated and coagulated / filtered water chlorine doses had to be adjusted to ensure that all waters had equivalent residuals at mid-sedimentation. The mid-sedimentation residual was used for comparison between the three experiments to determine the contributions of HOM from the flocs. HOM measurements were taken at post-sedimentation.

Halogenated Organic Matter Sorption onto Existing Flocs

Preformed HOM was created using a high OM water (~ 200 mg /L TOC reverse osmosis membrane concentrated from Manatee Lake Water (MLW) in Florida) reacted at a 1:1 chlorine to TOC ratio and a contact time of 24 hours, which yielded a zero chlorine residual. Unchlorinated water was coagulated and at the 1/3 flocculation point the MLW preformed DBPs were added. Samples for solid and aqueous phase DBPs were taken at post-sedimentation.

High-Performance Size Exclusion Chromatography (HPSEC)

The HPSEC used for analysis was calibrated using Suwannee River humic acid (SRHA) reference material (1R101H) and Suwannee River fulvic acid (SRFA) standard material (1S101F) obtained from the International Humic Substances Society. The HPSEC used a TSK-50S column (35 mm Toyopearl HW resin) with a length of 25 cm and an ID of 2 cm. Sample buffering and ionic strength adjustment was as detailed by Her et al. (33).

Results and Discussion

Raw Water Characteristics and HOM Formation

The waters selected for this study; Table 1, included a range of water quality, geographic regions and sources; ground water, river and reservoir. The raw water TOC concentration ranged from 2.7 to 14.7 mg/L, the specific ultra-violet absorption (SUVA) ranged from 2.2 to 3.7 L/mg-m, and the turbidities ranged from 1.2 to 123 NTU. The KY river water had the lowest TOC and SUVA and highest turbidity, while the FL reservoir water had the highest TOC and SUVA and lowest turbidity. By design the chlorine doses applied to each water; 0.6:1 to 0.8:1 Cl₂:TOC mass ratios, did not yield detectable residuals after 24 hours. The formed HOM from the raw water are shown in Table 1.

Table 1. Raw Water Quality and HOM Formation

Source Water	TOC (mg/L)	SUVA (L/mg-m)	Turbidity (NTU)	pH	Chlorine Dose (mg/L)	TTHM (µg/L)	HAA9 (µg/L)	AOX (µg Cl/L)	AOX-C (µg Cl/L)	AOX-U (µg Cl/L)	Yield (µg Cl-/mg DOC)		AOX Yields (µg Cl-/mg DOC)			
											TTHM	HAA9	AOX	AOX-C	AOX-U	
CO- canal	3.4	2.9	11.4	7.7	2.5	74	52	272	97	175	22	15	80	29	51	
OH-reservoir	5.8	2.6	3.5	7.8	3.8	97	58	255	118	137	17	10	44	20	24	
NY- river	3.9	3.4	9.2	7.9	3.0	98	81	330	135	195	25	21	85	35	50	
FL-reservoir	14.7	3.7	1.2	7.0	9.0	371	216	1180	569	611	25	15	80	39	42	
KY- river	2.7	2.2	123	7.5	2.1	40	25	143	49	94	15	9	53	18	35	
											Mean	21	14	68	28	40

The TTHM and HAA9 characterized portion of AOX (AOX-C) is defined in this manuscript as follows:

$$\text{AOX-C} = \text{TTHM} + \text{HAA9} \text{ } (\mu\text{g Cl}^-/\text{L})$$

where the TTHM and HAA9 values are expressed on a chloride mass basis to yield units of $\mu\text{g Cl}^-/\text{L}$. The uncharacterized AOX (AOX-U) portion is defined as the difference between the AOX and AOX-C.

The AOX, TTHM and HAA9 yields, Table 1, were, as expected, less than that under chlorination conditions which yield a 1.0 mg/L residual after 24 hours; 100 $\mu\text{g AOX} / \text{mg TOC}$, 30 $\mu\text{g TTHM} / \text{mg TOC}$, 20 $\mu\text{g HAA9} / \text{mg TOC}$ (34). The OH reservoir and KY river waters had the lowest SUVA values, lowest yields of HOM and therefore were the least reactive of the five sources.

Table 2. TTHM and HAA9 Sorption to Flocs

Water Source	DBP Species	Location – (Time)				
		Raw Water (<i>t</i> = 0 min)	Post-Floc (<i>t</i> = 30 min)	Post-Sed (<i>t</i> = 120 min)		
		μL	μL	Remov- ed (%)	μL	Remov- ed (%)
CO	TTHM	74	63	15	71	4
	HAA9	52	54	-4	54	-4
OH	TTHM	97	89	8	81	16
	HAA9	58	55	5	55	5
NY	TTHM	98	94	4	95	3
	HAA9	81	84	-4	81	0
FL	TTHM	371	361	3	335	10
	HAA9	216	230	-6	243	-13
KY	TTHM	40	34	15	36	10
	HAA9	25	26	-4	29	-10

TTHM and HAA9 Sorption to Flocs

The chlorinated raw water, without chlorine residual, was coagulated and following flocculation and sedimentation, samples for THM and HAA were taken (Table 2). Compared to the raw water, the TTHM values averaged 9% lower for both the post-flocculation and post-sedimentation sample points. Chloroform, the most volatile and hydrophobic THM, accounted for most of the decrease. While

the jar test vessels were modified with lids, some volatilization was possible over the 2 hour experiment. Using the same apparatus in the University of Colorado lab, Cho (35) found MIB losses with no adsorbent present to be 4.0% on average for six runs. The HAA9 results show no discernible change, less than 2%, over the course of the experiment, as HAAs are less hydrophobic and volatile relative to the THMs.

AOX-U and TOC Behavior During Coagulation

Chlorination

The removal of TOC and AOX-U increased with increasing coagulant dose, as shown in Table 3, for the four waters where several coagulant concentrations were dosed. While not all OM can be removed by coagulation, the coagulant doses were not increased to the point that all of the sorbable OM was removed. The TOC fraction that can be removed, termed sorbable TOC, was estimated using a model (11) that uses raw water TOC, SUVA and coagulated pH values as inputs, also shown in Table 3. The measured TOC removed at the maximum coagulant dose tested for each water, averaged 66% of the model prediction for the maximum sorbable TOC. Thus, if coagulant doses had been increased more TOC removal would be expected for all five waters.

Coagulation yielded significant removal of AOX-U for all waters and averaged 75% at the maximum coagulant dose of each water, compared to 44% removal for TOC. For three waters, OH, FL and KY, the highest coagulant doses removed more than 90% of the raw water AOX-U. Removal greater than 100% was found for the KY water and was attributed to the AOX-U calculation method; where TTHM and HAA9 concentrations were subtracted from the initial AOX value. The near complete removal of AOX-U for these three waters indicates that the remainder of total AOX in aqueous solution is primarily THMs and HAAs.

The amount of TOX partitioned to flocs per liter of coagulated water was measured and reported in Table 3 as 'Floc TOX'; this measured floc partitioned TOX increased with coagulant dose. The Floc TOX was compared to the calculated AOX-U removed, $\Delta\text{AOX-U}$. A mass balance using the raw (initial), post-sed AOX-U and solid phase floc TOX, yielded losses that averaged 13% for all waters, indicating that removed AOX-U can be accounted for in the floc.

The AOX-U removal was found to be linearly correlated to TOC removal, when results from two high turbidity KY coagulation tests that yielded AOX-U removals greater than 100%, were not included. The AOX-U removal was also well correlated, $r^2 = 0.72$, with the maximum sorbable TOC removed, as shown in Figure 1, including the FL Turb water sample, which had kaolin added to it at 100 mg/L. The general trend shown in Figure 1 suggests a threshold of approximately 20% TOC removal before any AOX-U is removed. This indicates the OM initially removed does not contain significant amounts of AOX-U and at low coagulant doses TOC is preferentially removed and at high coagulant doses AOX-U is preferentially removed. The ratio of $\Delta\text{AOX-U}$ to ΔTOC was calculated and increases with increasing coagulant dosage for three waters; OH, FL and KY.

Table 3. AOX-U and TOC Behavior during Coagulation

Source Water	Raw DOC (mg/L)	Coag Dose (mg/L)	Coag pH	Coag TOC (mg/L)	Percent Sed TOC Removal (%)	Sorbed TOC (mg/L)	Predicted maximum sorbable TOC ² (mg/L)	Percent of maximum sorbable removed ³ (%)	Raw AOX-U (µg Cl ⁻ /L)	Post-Sed AOX-U		ΔAOX -U (µg Cl ⁻ /L)	ΔAOX -U / ΔTOC (µg Cl ⁻ /mg)	Floc TOX (µg Cl ⁻ /L)	Losses (%)
										µg Cl ⁻ /L	% Removed				
CO	3.4	35	6.7	2.0	41	1.4	2.2	64	175	92	47	83	59.3	37	26
OH	5.8	45	7.1	3.8	34	2.0	3.7	54	137	105	23	32	16.0	26	4
		90	6.8	3.1	47	2.7	3.7	73		5	98	132	48.9	133	1
NY	3.7	30	7.4	2.8	24	0.9	2.8	32	195	140	28	55	61.1	30	13
		50	7.3	2.5	32	1.2	2.8	43		131	33	64	53.3	43	11
		70	7.1	2.4	35	1.3	2.8	46		124	36	71	54.6	54	9
		25	7.0	10.0	32	4.7	11.4	41		496	19	115	24.5	4	18
FL	14.7	50	6.8	10.0	32	4.7	11.4	41	611	472	23	139	29.6	107	5
		100	6.7	5.8	61	8.9	11.4	78		238	61	373	41.9	189	30
		12.7	150 ¹	6.7	4.6	64	8.1	9.8		327	6	98	321	39.6	290
KY	2.7	5	7.0	2.1	22	0.6	1.6	38	94	61	35	33	55.0	26	7
		10	7.0	1.8	33	0.9	1.6	56		-2	102	96	106.7	77	20
		20	6.8	1.8	33	0.9	1.6	56		-14	115	108	120.0	89	18

¹ Sample with kaolin added at 100 mg/L; a raw TOC of 12.7 mg/L and AOX-U of 327 µg Cl⁻/L. ² Maximum sorbable TOC predicted from Edwards Model (II). ³ Measured sorbed TOC relative to predicted maximum sorbable TOC.

Table 4. AOX-U Sorption/Incorporation (Chlorine Dioxide)

Source Water	Raw AOX-U ($\mu\text{g Cl}^-/\text{L}$)	AOX-U yield ($\mu\text{g Cl}^-/\text{mg DOC}$)	Coagulant Dose (mg/L)	Coag pH	Sorbable TOC (mg/L)	Post-Sed TOC (mg/L)	Post-Sed AOX-U		ΔAOX -U ($\mu\text{g Cl}^-/\text{L}$)	ΔAOX -U / ΔTOC ($\mu\text{g Cl}^-/\text{mg}$)	Floc TOX ($\mu\text{g Cl}^-/\text{L}$)	Losses (%)
							$\mu\text{g Cl}^-/\text{L}$	% Removed				
OH	57	9.9	90	6.8	3.7	3.1	36	37%	21	8	18	5%
FL	92	6.3	100	6.7	11.4	5.1	47	49%	45	5	43	2%
KY	40	14.8	10	7	1.6	1.6	15	63%	25	23	25	0

The results with the KY water deviate to some degree from the general trend in Table 3. The KY water required very low coagulant doses (10 to 20 mg/L) to achieve significant removals of AOX-U as compared to the other waters and at higher doses yielded AOX-U removals greater than 100% as shown in Table 3. This may be attributed to the high raw water turbidity; 123 NTU. The turbidity may have provided additional sorption sites for the AOX-U compounds (21, 27, 29), this is supported by the FL water samples, in which the addition of 100 mg/L of kaolin increased the AOX-U removal from 61% to 98% at about the same maximum sorbale DOC removal (Figure 1). The KY water demonstrated preferential removal of AOX-U over TOC at coagulation doses over 5 mg/L. The results from the NY water yielded lower than expected TOC and AOX-U removal, even as coagulant doses were increased to 70 mg/L.

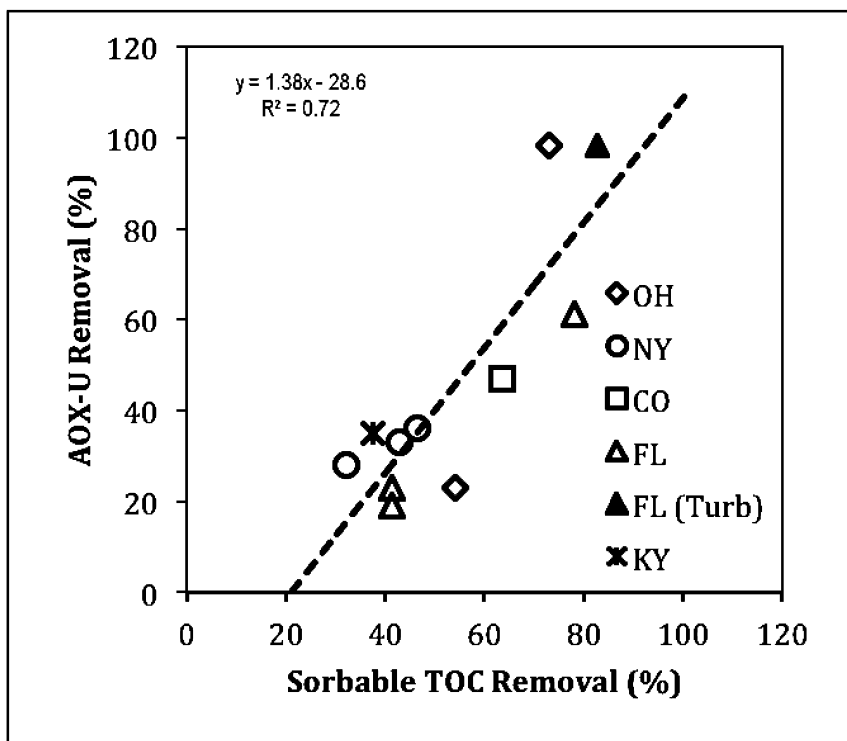


Figure 1. AOX-U Removal versus Sorbable TOC Removal.

The most easily coagulated OM is hypothesized to be the large molecular weight, hydrophobic compounds (6). Studies have shown that the MW distribution of the AOX yields smaller sizes compared to the TOC MWD (4, 5, 7), mainly through oxidation reactions, especially with stronger oxidants such as chlorine dioxide (7), where the hydrophobicity of NOM also decreases. These findings

support the preferential removal of TOC over AOX-U at low coagulant doses. Additionally, the HPSEC-DOC profile of the OH water sample after chlorine or chlorine dioxide application, Figure 2, shows a shift to the lower molecular weight range for the fractions with molecular weight greater than 500, relative to the samples that were not oxidized.

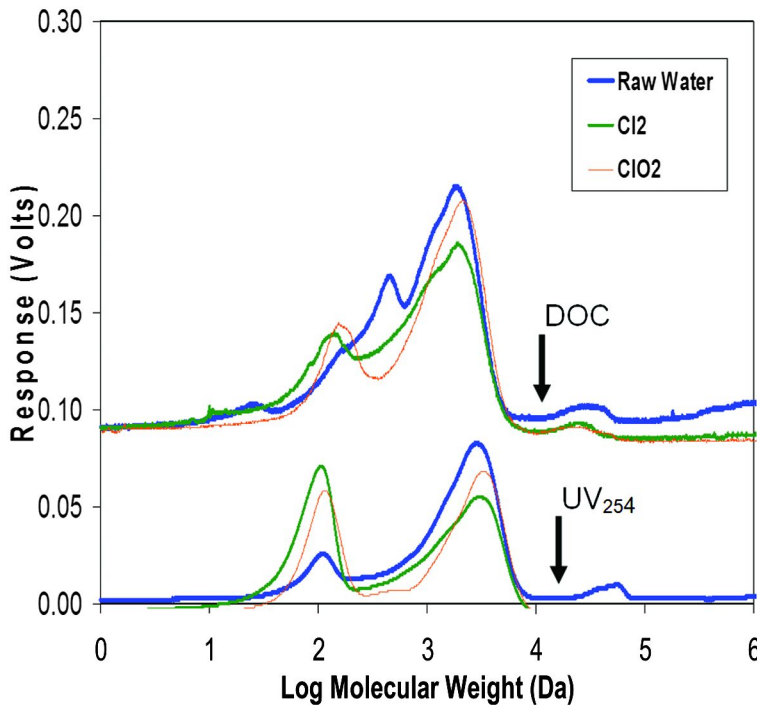


Figure 2. HPSEC DOC and UVA Response – OH Water.

These results, however, do not clarify the reaction pathway, where under low chlorination conditions, two mechanisms maybe occurring: 1) chlorine does not directly react via substitution with the large molecular weight, hydrophobic fraction to form large molecular weight, hydrophobic HOM or 2) once halogenated, the properties of this HOM are transformed into a fraction less amenable to coagulation removal.

Chlorine Dioxide Application

Experiments similar to the chlorination experiments were conducted with chlorine dioxide as the pre-oxidant with the OH, FL and KY waters. Post chlorine dioxide application, formed TTHM concentrations were below detection limit,

while that for HAA9 were less than 10 $\mu\text{g/L}$ for all waters, which accounted for less than 7% of the AOX concentration. The raw water AOX-U values were much lower than chlorinated waters; 57, 92 and 40 $\mu\text{g Cl}/\text{L}$ for the OH, FL and KY waters, respectively. This resulted in AOX-U yields (Table 4) that were on average 70% lower than chlorine dosed water (Table 3). Coagulation yielded 37, 49, and 63% AOX-U removal for the OH, FL and KY waters, respectively. The difference between the calculated AOX-U removal and that measured on the floc was less than 3 $\mu\text{g Cl}/\text{L}$ which represents a 5% error of the mass balance. These removals were on average 37% lower than the corresponding AOX-U removal by coagulation. This indicates that the AOX-U formed by reactions with chlorine dioxide is more difficult to remove by coagulation. The HPSEC-DOC profile of the OH water sample after chlorine dioxide exposure shows more reactions with the intermediate MW NOM, relative to the chlorinated sample (Figure 2).

Desorption of AOX from Floc

Desorption experiments were conducted in which settled floc with sorbed TOX was re-suspended in AOX free-water, to determine if TOX was released from the floc over a time frame close to the sedimentation tank residence time (2 hours) and over longer time frames similar to sludge residence times in a sedimentation basin (1 to 3 days). The results, Table 5, show that for all three waters tested no significant differences were found between the two-hour aqueous AOX value and the aqueous AOX value immediately after the flocs were re-suspended. The measured CO water floc TOX after two hours did not significantly differ from that of the initial solid phase TOX. The initial source of the AOX was from interstitial AOX which was not rinsed out so as not to disturb the floc structure. Any changes after initial fluidization were only considered.

The desorption from the OH and KY water flocs was monitored over longer times (24 and 72 hours) and the aqueous AOX values indicated a modest increase of 6 to 8 $\mu\text{g Cl}/\text{L}$. The TOX content of both floc samples were measured after 72 hours and a decrease of 25% was found for both waters resulting in a decrease of 19 $\mu\text{g Cl}/\text{L}$ for the KY water and 33 $\mu\text{g Cl}/\text{L}$ for the OH water. The difference between increasing aqueous AOX concentrations and the decrease in the solid phase TOX values represents a mass balance loss of 18%, which is similar to the 13% losses found for the sorption experiments. Previous studies have shown limited NOM desorption from mineral surfaces (27, 30), but studies on NOM desorption from metal hydroxide flocs were not found. Contributions to TTHM and HAA5 formation from precursors found on colloids were reported (31), where coagulation preferentially removed this colloidal material, incorporating it into the floc matrix. The AOX contribution by desorption was found not to be significant within the residence time of a sedimentation basin, 2 hours, however, if the desorption time increases to 3 days, modest AOX contributions, $\sim 10 \mu\text{g Cl}/\text{L}$, by desorption may occur.

Table 5. Desorption of AOX from Floc

Time (hours)	CO		OH		KY	
	Aqueous AOX ($\mu\text{g Cl/L}$)	Solid Phase TOX ($\mu\text{g Cl/L}$)	Aqueous AOX ($\mu\text{g Cl/L}$)	Solid Phase TOX ($\mu\text{g Cl/L}$)	Aqueous AOX ($\mu\text{g Cl/L}$)	Solid Phase TOX ($\mu\text{g Cl/L}$)
0	36	37	16	133	4	77
2	38	32	11	nm	1	nm
24	nm	nm	12	nm	1	nm
72	nm	nm	24	100	10	58

nm- not measured.

Impact of Flocs on HOM Formation

Chlorination

The role of flocs on HOM formation during coagulation was evaluated on four waters. Raw water, coagulated water with flocs and filtered coagulated water (no flocs) were chlorinated. The waters were dosed to yield a chlorine residual of 1.0 mg/L after 1 hour, and DBP samples taken after 2 hours. The chlorine doses of the coagulated waters, with and without flocs, were adjusted to yield a similar 1 hour residual, thus 2 hr-DBP formation comparisons could be made on an equal chlorine residual basis. Chlorination of the waters for this portion of the study yielded AOX-U, TTHM and HAA9 concentrations (Table 6) that were 20 to >90% lower than the raw waters contacting chlorine for 24 hours (Tables 1- 3).

Chlorination of the coagulated water containing flocs yielded a decrease in AOX-U, TTHM and HAA9 formation compared to that formed with chlorinating raw water. The decrease in AOX-U and TTHM formation reflected the TOC removal, while the decrease in HAA9 formation was about half the TTHM formation decrease. Reduction in DBP formation by coagulation of NOM fractions that serve as the DBP precursors is well established, correlating with researcher results that demonstrated removal of organic colloids led to decreased HOM yields averaging 32% for TTHM and 25% for HAA5 formation (30). Similar results have been demonstrated at the bench-, pilot- and full-scale and have led to utilities moving the chlorination point downstream of the raw water as a DBP control strategy (15, 16).

These coagulation results show that the HOM precursors in the presence of flocs are less available for substitution reactions with chlorine compared to the raw water, but they do not address the role of the OM sorbed by the flocs when chlorine is present during coagulation. The contribution of the HOM precursors sorbed by the flocs was assessed by comparing the DBP formation results when chlorine was dosed to the coagulated water without flocs to the results when flocs were

present. The results, Table 6, show that floc contribution to AOX-U formation ranged from less than detection to 20%, and 17 to 67 % for TTHM and HAA9 formation, respectively.

Table 6. Impact of Flocs on DBP Formation

Water Source	Water Characteristic	TOC (mg/L)	Chlorine Dose (mg/L)	Post Sedimentation HOM		
				AOX-U (µg Cl ⁻ /L)	TTHM (µg/L)	HAA9 (µg/L)
CO (Coag dose 35 mg/L)	Raw	3	1.9	115	34	27
	Coag	1.6	1.6	56	18	19
	Coag w/o flocs	1.6	1.4	45	10	7
	Flocs	1.4	--	11 (20%)	8 (44%)	12 (63%)
OH (Coag dose 90 mg/L)	Raw	5.8	3.8	190	66	40
	Coag	3.7	3.5	91	30	29
	Coag w/o flocs	3.6	3.1	98	25	22
	Flocs	2.1	--	< AE	5 (17%)	7 (24%)
FL (Coag dose 100 mg/L)	Raw	13.7	9.0	114	291	171
	Coag	5.65	8.0	< AE	106	132
	Coag w/o flocs	4.58	4.2	< AE	55	44
	Flocs	9.1	--	< AE	51 (48%)	88 (67%)
KY (Coag dose 10 mg/L)	Raw	2.6	2.1	58	25	17
	Coag	1.8	1.9	39	15	16
	Coag w/o flocs	1.9	1.6	43	14	11
	Flocs	0.7	--	< AE	< AE	5 (32%)

Values in parenthesis are the percent contribution of the floc to the coagulated HOM concentration. < AE – less than analytical error.

This implies that chlorine reacts with OM sorbed to the floc in a manner that yields only THMs and HAAs to the aqueous phase. Due to AOX analytical error, 8 µg Cl⁻/L, other halogenated compounds may be produced at levels below detection. Other halogenated compounds may be formed in the solid phase, but they are not released into solution, potentially due to availability of reactive sites that would oxidize and release while being shielded by the floc structure.

The FL water with the highest TOC and SUVA and lowest turbidity, had the greatest TTHM and HAA9 contributions from flocs (48 to 67%). The floc contained a large amount of TOC, as the mass TOC removal was greatest for this water. The mass TOC removed was normalized by the coagulant dose, which yielded 0.09 mg TOC/mg aluminum sulfate, which was the highest for the four waters examined. The order of floc contributions decreased with decreasing TOC to coagulant ratios: 0.090, 0.040 and 0.023 mg TOC/mg aluminum sulfate, for the FL, CO and OH waters, respectively. The KY water with the lowest TOC and SUVA and highest turbidity, had the least amount of DBP contributions from flocs (<AE to 32%). The TOC to coagulant ratio, 0.070 mg TOC /mg aluminum sulfate, was large for this water, however, this parameter does not account for the high turbidity, which acts as a coagulant aid and incorporates into the floc structure. Only a small dose of coagulant, 10 mg/L, was required to form settleable flocs, which yielded the highest mass of inorganic solids after sedimentation (231 mg) of all waters tested. Coagulation of the FL water at a coagulant dose of 100 mg/L yielded 90% less inorganic solids at 24 mg.

Chlorine Dioxide Application

The role of flocs on HOM formation was repeated using chlorine dioxide as the preoxidant, with the OH, FL and KY waters. No measureable THMs were formed and the HAA9 formation was less than 5 $\mu\text{g}/\text{L}$ for all waters (Table 7). The AOX-U values of the raw water after chlorine dioxide application were 20, 40 and 15 $\mu\text{g Cl}/\text{L}$ for the OH, FL and KY waters, respectively (Table 7). Chlorine dioxide addition to the coagulated water with floc waters yielded AOX-U values that were 20% lower for all waters. The calculated AOX-U contribution from the flocs was less than 7 $\mu\text{g Cl}/\text{L}$ for all waters, which is lower than the analytical error associated with AOX measurement. This indicates that flocs do not contribute AOX-U or HAA9 to aqueous solution for waters dosed with chlorine dioxide.

Sorption of AOX onto Preformed Flocs

To assess if preformed flocs sorb AOX from solution, an aliquot of preformed DBPs, from a high concentration stock solution, was spiked into jars that had proceeded to the 1/3-flocculation point of the treatment process. Based on visual inspection, mature flocs had already been formed and the OM had been incorporated into the floc structure at this point (15). Therefore OM sorption to the formed floc, not co-precipitation, would be the removal mechanism. Aqueous AOX samples were taken after 2 additional minutes of floc mixing and after sedimentation, where 18 minutes until the flocculation process finished were still available for sorption. Floc samples taken after sedimentation were measure for solid-phase AOX content. Waters with a range of turbidities were chosen for this experiment: OH, CO and KY waters. In all three cases, the spiked DBPs did not significantly sorb to the flocs during the course of the experiment (Table 8).

Table 7. Impact of Flocs on HOM Formation (Chlorine Dioxide)

Water Source	Water Characteristic	TOC (mg/L)	Chlorine Dioxide Dose (mg/L)	Post Sedimentation HOM		
				AOX-U ($\mu\text{g Cl/L}$)	TTHM ($\mu\text{g/L}$)	HAA9 ($\mu\text{g/L}$)
OH (Coag dose 90 mg/L)	Raw	5.8	1.4	18	BDL	3
	Coag	3.4	1.4	14	BDL	2
	Coag w/o flocs	3.6	1.1	11	BDL	3
	Flocs	2.2	--	< AE	--	< AE
FL (Coag dose 100 mg/L)	Raw	13.7	1.4	39	BDL	2
	Coag	5.8	1.4	31	BDL	2
	Coag w/o flocs	5.0	1.3	23	BDL	3
	Flocs	8.7	--	< AE	--	< AE
KY (Coag dose 10 mg/L)	Raw	2.6	1.0	14	BDL	2
	Coag	2.0	0.9	11	BDL	2
	Coag w/o flocs	1.9	0.9	10	BDL	2
	Flocs	0.7	--	< AE	--	< AE

BDL – below detection limit. < AE – less than analytical error.

Table 8. Sorption of AOX onto Preformed Flocs

Location	Time (min)	CO (coag dose = 35 mg/L)		OH (coag dose = 90 mg/L)		KY (coag dose = 10 mg/L)	
		Aqueous AOX ($\mu\text{g Cl/L}$)	Solid Phase TOX ($\mu\text{g Cl/L}$)	Aqueous AOX ($\mu\text{g Cl/L}$)	Solid Phase TOX ($\mu\text{g Cl/L}$)	Aqueous AOX ($\mu\text{g Cl/L}$)	Solid Phase TOX ($\mu\text{g Cl/L}$)
1/3 Floc*	10	270	--	1515	--	784	--
Post-Sed	120	259	10	1431	< AE	756	< AE

* Point of DBP spike.

The aqueous AOX values decreased by less 5% and the solid phase AOX values did not exceed 10 $\mu\text{g Cl/L}$ over the 2-hour process. The flocs from the KY water contained large amount of inorganic solids, which did not enhance the AOX sorption. These results demonstrated that the removal of AOX-U by coagulation

(Table 3) is not sorption onto mature metal hydroxide, turbidity (organic and inorganic) and OM precipitate making the ‘floc’ particle conglomerate, which has been postulated as the dominant coagulation mechanism for NOM removal (9, 11). The AOX removal occurs co-currently with the formation of the floc. This may involve the sorption and coating of colloidal microcrystals as they form from the reaction of the metal hydrolysis and particles, or from the reaction of the metal hydrolysis products and sites on the AOX compounds (9).

Conclusions

Chlorine and chlorine dioxide react with source water organic matter to form HOM, some of which is characterized, THMs and HAAs, and others that can be assessed with an AOX measurement. For five natural waters coagulated with alum preformed THMs and HAAs were not removed by coagulation. AOX-U, was removed by 55% on average over all coagulant doses and 75% at highest doses, with near complete AOX-U removal for three waters. This result indicates that optimized coagulation, even with in-plant chlorination, can greatly mitigate the formation of AOX-U through incorporation into the floc structure, where desorption in a water treatment plant residence time will be minimal. Turbidity influenced the removal of AOX-U, where the most turbid waters; both those spiked with kaolin and those with naturally occurring turbidity demonstrated near 100% removal of AOX-U. Overall it is worth noting that water treatment utilities that operate with poor DOC removal; at less than 20%, will likely exhibit poor AOX-U removal since there appears to be a lower threshold of DOC that must be removed prior to AOX-U removal. When the threshold of 20% DOC removal has been reached, AOX-U removal increases with coagulation removal of DOC, where a correlation was found within the data.

Acknowledgments

This research was funded in part by a cooperative agreement between the USEPA Technical Support Center, Office of Ground Water and Drinking Water, and the Center of Drinking Water Optimization at the University of Colorado at Boulder (CR-826722).

References

1. Rook, J. J. Haloforms in Drinking Water. *J. - Am. Water Works Assoc.* **1976**, *68*, 168–172.
2. Larson, R. A.; Weber, E. J. *Reaction Mechanisms in Environmental Organic Chemistry*, 1st ed.; Taylor & Francis: New York, 1994; pp 275–341.
3. Brezonick, P. L. *Chemical Kinetics and Process Dynamics in Aquatic Systems*, 1st ed.; Taylor & Francis: New York, 1994; pp 227–245.
4. Reckhow, D. A.; Singer, P. C. *Formation and Control of Disinfection By-products. Water Quality and Treatment*, 6th ed.; Edzwald, J., Ed.; Water

Resources and Environmental Engineering Series; McGraw-Hill: New York, 2011; pp 7.1–7.48.

5. Kopfler, F. C.; Ringhand, H. P.; Coleman, W. E.; Meier, J. R. *EPA 600 D-84* 196, 1984.
6. Khiari, D.; Krasner, S. W.; Hwang, C. J.; Chinn, R.; Barrett, J. Effects of chlorination and chloramination on the molecular weight distribution of natural organic matter and the production of high-molecular-weight disinfection byproducts. *AWWA Water Qual. Technol. Conf., S.E. Proc.* **1997**.
7. Swietlik, J.; Sikorska, E. Application of fluorescence spectroscopy in the studies of natural organic matter fractions reactivity with chlorine dioxide and ozone. *Water Res.* **2004**, *38*, 3791–3799.
8. O'Melia, C. R. Coagulation and sedimentation in lakes, reservoirs and water treatment plants. *Water Sci. Technol.* **1998**, *37*, 129–135.
9. Letterman, R. D.; Yiakoumi, S. *Coagulation and Flocculation. Water Quality and Treatment*, 6th ed.; Edzwald, J. Ed.; Water Resources and Environmental Engineering Series; McGraw-Hill: New York, 2011; pp 8.1–8.42.
10. O'Melia, C. R.; Becker, W. C.; Au, K. K. Removal of Humic Substances by Coagulation. *Water Sci. Technol.* **1999**, *40*, 47–54.
11. Edwards, M. Predicting DOC Removal during Enhanced Coagulation. *J. - Am. Water Works Assoc.* **1997**, *89*, 78–88.
12. Amirtharajah, A.; O'Melia, C. R. *Coagulation Processes: Destabilization, Mixing and Flocculation. Water Quality and Treatment, A Handbook of Community Water Supplies*, 4th ed.; Pontius, F. W., Ed.; McGraw-Hill: New York, 1990; pp 6.1–6.61.
13. Dotson, A.; Westerhoff, P. Character and Treatment of Organic Colloids in Impacted Drinking Water Sources. *J. Environ. Eng.* **2012**, *138*, 393–401.
14. Solarik, G.; Hatcher, V. A.; Isabel, R. S.; Stile, J. F.; Summers, R. S. Prechlorination and DBP formation: the impact of chlorination point and enhanced coagulation. *AWWA Water Qual. Technol. Conf., Proc.* **1997**.
15. Arias, M. S.; Summers, R. S. Understanding and optimizing chlorine interactions during coagulation. *Proc. - Annu. Conf., Am. Water Works Assoc.* **2003**.
16. Arias, M. S.; Summers, R. S. Preoxidation Optimization for DBP Control: A Scale-up Study. *AWWA Water Qual. Technol. Conf., Proc.* **2003**.
17. Reckhow, D. A.; Singer, P. C.; Malcolm, R. L. Chlorination of Humic Materials: byproduct formation and chemical interpretations. *Environ. Sci. Technol.* **1990**, *24*, 1655–1664.
18. Owen, D. M.; Chowdhury, Z. K.; Krasner, S. W. Impact of treatment on disinfection byproduct speciation. *Proc. - Annu. Conf., Am. Water Works Assoc.* **1993**.
19. Cook, R. L.; Langford, C. H. Structural characterization of a fulvic acid and a humic acid using Solid State Ramp-CP-MAS ^{13}C Nuclear Magnetic Resonance. *Environ. Sci. Technol.* **1998**, *32*, 719–725.
20. Eikebrokk, B. *Removal of Humic Substances by Coagulation. Chemical Water and Wastewater Treatment IV*. Hahn, H. H., Erhard Hoffmann, E.,

Ødegaard, H., Ed.; Springer Berlin Heidelberg: Heidelberg, Germany, 1996; pp 174–176.

21. BoltoDixon, B., D.; Eldridge, R.; King, S. Cationic polymer and clay or metal oxide combinations for natural organic carbon removal. *Wat. Res.* **2001**, *35*, 2669–2676.
22. Tsai, C. T.; Kuo, C. T.; Lin, S. T. Analysis of organic halides in hospital waste sludge disinfected using sodium hypochlorite. *Water Res.* **1999**, *33*, 778–784.
23. Zhang, X.; Minear, R. A. Characterization of high molecular weight disinfection byproduct resulting from chlorination of aqueous humic substances. *Environ. Sci. Technol.* **2002**, *36*, 4033–4038.
24. Au, K.- K.; Penisson, A. C.; Yang, S.; O'Melia, C. R. Natural organic matter at oxide/water interfaces: Complexation and conformation. *Geochim. Cosmochim. Acta* **1999**, *63*, 2903–2917.
25. Schwartzenbach, R. P.; Gschwend, P. M.; Imboden, D. M. *Sorption: Solid-Aqueous Solution Exchange*, 1st ed.; John Wiley & Sons: Hoboken, NJ, 1993; pp 277–279.
26. Stumm, W.; Morgan, J. J. *Aquatic Chemistry*, 3rd ed.; Schnoor, J. L., Zehnder, A. Ed.; John Wiley & Sons: Hoboken, NJ, 1995; pp 516–575.
27. Chi, F. H.; Amy, G. L. Kinetic study on the sorption of dissolved natural organic matter onto different aquifer materials: The effects of hydrophobicity and functional groups. *J. Colloid Interface Sci.* **2004**, *274*, 380–391.
28. McKnight, D. M.; Bencala, K. E.; Zellweger, G. W.; Aiken, G. R.; Feder, G. L.; Thorn, K. A. Sorption of dissolved organic carbon by hydrous aluminum and iron oxides occurring at the confluence of Deer Creek with the Snake River, Summit County, Colorado. *Environ. Sci. Technol.* **1992**, *26*, 1388–1396.
29. Specht, C. H.; Kumke, M. U.; Frimmel, F. H. Characterization of NOM adsorption to clay minerals by size exclusion chromatography. *Water Res.* **2000**, *34*, 4063–4069.
30. Gu, B.; Schmitt, J.; Chen, Z.; Liang, L.; McCarthy, J. F. Adsorption and desorption of natural organic matter on iron oxide: Mechanisms and models. *Environ. Sci. Technol.* **1994**, *28*, 38–46.
31. Clesceri, L.; Greenberg, A.; Eaton, A. *Standard Methods in the Examination of Water and Wastewater*, 20th ed.; John Wiley & Sons: New York, 1998; pp 4-55, 4-77.
32. *Methods for the Determination of Organic Compounds in Drinking Water- Supplement III*, EPA/600/R-95/131. Cincinnati, OH, 1995.
33. Her, N.; Amy, G; McKnight, D.; Sohn, J.; Yoon, Y. Characterization of DOM as a function of MW by fluorescence EEM and HPLC-SEC using UVA, DOC, and fluorescence detection. *Wat. Res.* **2003**, *37*, 4295–4303.
34. Summers, R. S.; Hooper, S. M.; Shukairy, H. M.; Solarik, G.; Owen, D. Assessing DBP Yield: Uniform Formation Conditions. *J. - Am. Water Works Assoc.* **1996**, *88*, 80–93.
35. Cho, H. M.S. Thesis, University of Colorado, Boulder, CO, 2007.

Chapter 13

DBP Reactivity of Organic Matter Fractions Collected During Extreme Weather Events

Aaron D. Dotson,^{*,1} Paul Westerhoff,² and Amlan Ghosh³

¹Civil Engineering, University of Alaska Anchorage, 3211 Providence Drive, Anchorage, Alaska 99515

²School of Sustainable Engineering and the Built Environment, Arizona State University, P.O. Box 5306, Tempe, Arizona 85287

³Corona Environmental Consulting, 1600 Shadywood Lane, Flower Mound, Texas 75028

*E-mail: addotson@uaa.alaska.edu.

A systematic study of disinfection byproduct (DBP) formation from dissolved organic matter (DOM) of six southwestern water samples, three of which were collected during climatic events was performed. DOM was evaluated in its natural state in whole water samples and in a fractionated state where the DOM was isolated through concentration and resin fractionation. Study included evaluation of DBP formation at 1 hour and 7 days during a DBP formation potential test to elucidate the rate of DOM reactivity. Additionally, fractionated DOM was isolated in a manner such that mathematical reconstruction of whole water DBP formation was possible using the results of individual DOM fraction DBP formation potential tests.

Introduction

Dissolved organic matter (DOM) is a material in freshwater that can be transported and transformed through natural biogeochemical processes (biodegradation, photolysis, hydrolysis, adsorption, precipitation, sedimentation) (1, 2). Dissolved organic carbon (DOC) is one of the most common ways to measure the concentration of DOM but does not account for all of the mass, DOC is about 50% of DOM. Aquatic DOM concentration and structural composition in many surface water ecosystems depends on characteristics of the watershed

(3). Organic matter is produced by soils and plants of the terrestrial water shed (allochthonous DOM) or from biological growth and decomposition of algae and macrophytes within lakes or reservoirs (autochthonous DOM) (4, 5). Terrestrial plant and soil sources contribute allochthonous organic matter to a stream mainly during runoff from overland water flow during rainfall events (6, 7). Algae and bacteria (autochthonous sources) produce and consume or alter the concentration and composition of organic matter (8, 9). Hydrologic flow paths and quantities of runoff water impact the relative importance of these DOM flux processes to impact DOM concentrations in drinking water supplies.

DOM is a precursor in the formation of carcinogenic by-products during drinking-water treatment when chemical disinfectants (e.g., chlorine) react with DOM to form disinfection by products (DBPs) (10, 11). The amount and chemical nature of DOM are important to influence DBP formation. Previous studies have shown that humic substances with high aromatic content and molecular weight yield more DBPs upon chlorination (10). The parameter of ultraviolet absorbance (UVA) was a good predictor of DBP formation potential (11). Specific UVA ($SUVA = UVA[m^{-1}]/DOC[mg/L]$) correlates with aromatic content and is also a good surrogate of DBP precursors (12, 13). Allochthonous sources of DOM have higher SUVA than autochthonous sources.

The relative influence of allochthonous and autochthonous DOM sources are strongly impacted by climate, through controlling vegetation, soil development and runoff patterns (e.g., rain, snowmelt, floods). Temperate weather conditions prevail through most of the U.S.A. and Western Europe and contribute to maintaining a constant source of terrestrial organic material for surface waters and soils. These allochthonous carbon inputs contribute significantly to the global carbon cycle (14). The transportation of DOC originating in temperate climates has been intensively studied and the processes involved are reasonably well understood. Arid regions throughout the world are experiencing rapid population growth and areal expansion, necessitating development of large urban areas requiring extensive water infrastructure systems (e.g., reservoirs, water treatment plants, distribution systems). In these regions, higher air and water temperatures, greater seasonal hydrologic variations, different vegetation and soils, and widespread impoundment of rivers suggest that DOC sources and transportation could be different from that found in temperate climates. Water storage reservoirs in arid and semi-arid regions, like Arizona, are implemented with longer hydraulic residence times (HRT) and most likely alter the DOC characteristics in these freshwater systems (15–17). Therefore, this paper focuses on the less documented trends present in Arizona, as a potential surrogate for other arid regions around the globe.

Whereas autochthonous DOM and other algal extracellular by-products (e.g. methylisoborneol (MIB) and geosmin) originating in U.S. Southwestern reservoirs has been discussed in literature (18, 19), little is known about the impact of extreme meteorological events (e.g. forest fires, floods, droughts, etc.) on the DOM responses in downstream reservoirs and utility water sources. In arid and semi-arid regions of the southwestern USA, a typical annual hydrologic sequence for major rivers includes a major hydrologic pulse associated with upland snowmelt, followed by a prolonged dry period with low stream flow. DOM

loading characteristics in Southwestern U.S. reservoirs reflect the hydrologic inputs, dominated by early spring snowmelt, with low DOM loading during the dry season. A small but significant DOM pulse during the first monsoon events in the early summer months was reported (15–17). The Intergovernmental Panel on Climate Change projects the likely to virtually certain changes in different extreme events globally (e.g., heavy precipitations, droughts, and heat waves) between now to 2100. According to The Flood Control District of Maricopa County, extreme weather events (relative to recorded history) such as winter storms and summer droughts were observed in Arizona over the last ten years. Consequently, these events would result in variability of DOM concentration and cause challenges for utilities to meet regulation compliance. A limiting factor to assessing variability of DOC in southwestern U.S.A. watersheds has been consistency of collected water quality data at key locations, superimposed by major changes on water infrastructure operations. Over the past decade our group has developed a comprehensive database spanning drought, flood and “normal” climate periods.

Differing hydrology and water management practices of three surface water sources serving the metropolitan Phoenix area in Arizona of 3.5 million people offers the opportunity to study climate variability on a key water quality parameter for drinking water sources, namely DOM. Changes in DOM associated with climatic variations will influence DBP formation. Here we focus on two aspects of DBP formation. First, we examine the total yields of two regulated DBP classes (trihalomethanes (THMs) and haloacetic acids (HAA)) from different DOM fractions obtained from surface waters influenced by different climatic events. Second, we examine the relative rates of DBP formation by comparing shorter- versus longer-term DBP formation as an indicator of changes in DOM chemical properties influencing substitution of halogens (Cl, Br) into the DOM.

Comparison of DBP formation kinetics and yields upon chlorination of the DOM fraction were compared to levels in the bulk, non-fractionated water. Finally, using DBP yields of each DOM fraction and reactive contribution of each DOM fraction on a DOC and dissolved organic nitrogen (DON) basis to the bulk water, we attempt to reconstruct DBP formation in a simulated bulk water.

Materials and Methods

As part of the City of Phoenix Water Quality Master Plan Update project in 2007-2008, water samples were collected from three drinking water reservoirs and two rivers that fed those reservoirs, or a canal from the Colorado River (for Lake Pleasant). The reservoirs included Saguaro Lake, Bartlett Lake and Lake Pleasant. The rivers included the Salt River and the Verde River, both of which were only sampled within 48 hours of a meteorologically relevant event (e.g. significant rain or storm event that affected DOM levels in the rivers due to the contributions from runoff water). Large quantity samples (76.2 – 77.7 liters) were collected in 20 liter high density polyethylene carboys. Most often the samples filtered through a 1 micron filter prior to being stored at 4 °C prior to processing (~3 days).

DOC was analyzed by a Shimadzu TOC V_{CSH} (high-temperature combustion/non-disperse infrared) according to the instrument manufacturers method. UVA₂₅₄ was analyzed using a Shimadzu UV/VIS spectrophotometer in a 1 centimeter path length quartz cuvette. All bulk water samples and reconstituted DOM isolate samples were analyzed for DOC prior to DBPFP testing.

DOM isolates were prepared by adapting a variety of published methods (20–22). The method is presented graphically in Figure 1. Utilizing this method resulted in the collection of six DOM isolate; colloids, hydrophobic acids (HPO-A), hydrophobic neutrals (HPO-N), amphiphilic acids (AMP-A), amphiphilic neutrals (AMP-N), and a hydrophilic acid/neutral salt (HPI-A+N). Isolation was performed quantitatively. DOC and mass was recorded throughout the procedure. Evaporation steps were carried out using a rotary evaporator operated at 60 °C or less bath temperatures.

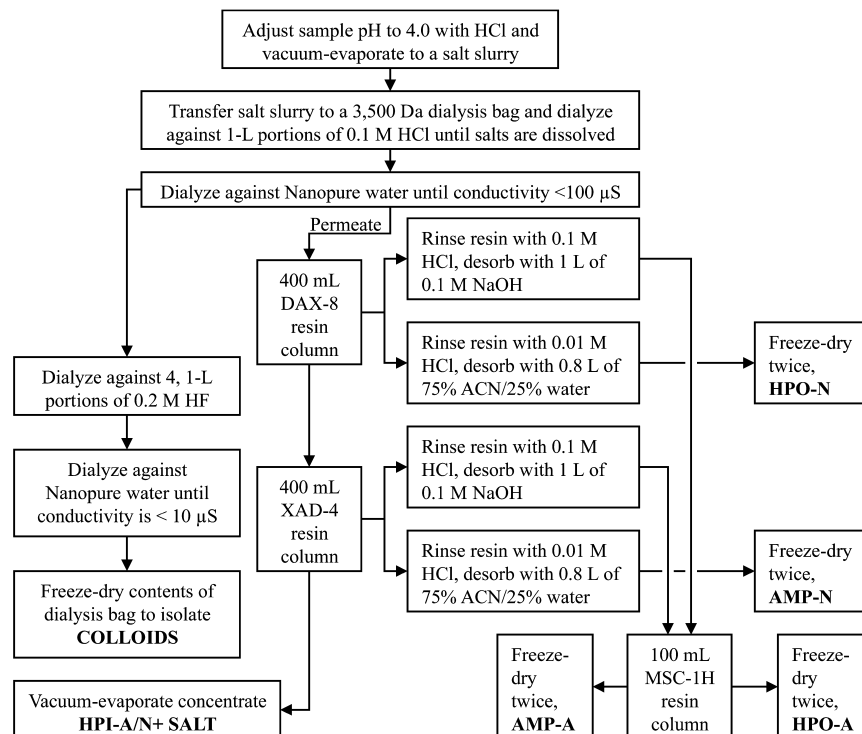


Figure 1. DOM Isolation Method.

DBPFP was determined by chlorinating the bulk sample or a solution containing a known concentration of a single DOM isolate. DOM isolates were dissolved in 1-L of laboratory grade water (Nanopure Infinity by Barnstead

International, MA) to a DOC concentration between 2 – 4 mg/L and buffered to a pH of 7.0 with 5 mM sodium phosphate buffer. The solution was filtered through a pre-muffled 0.7 μm glass fiber filter (Whatman GF/F) to remove any particulate DOM. Bulk water samples were similarly filtered but sample ionic strength was not adjusted. DOC present during chlorination was as sampled. The chlorine dose (mg-Cl₂/L) for each solution was calculated as five times the DOC concentration plus eight times the ammonia concentration (as N). The solutions were chlorinated using a stock solution of sodium hypochlorite of sufficient concentration to ensure no more than 1% change in solution volume. Upon chlorination, the solution was immediately transferred into two headspace free 500 mL bottles and placed in the dark at 20 °C. The first bottle was removed from the dark at 1 hour and decanted into bottles provided by the City of Phoenix for THM and HAA analysis. The provided bottles contained sufficient amount of preservative to preserve the sample and quench the residual chlorine. The second bottle was removed from the dark after 7 days and decanted into additional bottles provided by the city for THM and HAA analysis. THMs were analyzed using USEPA Method 551.1. The preservative used for this method is a mixture of phosphate buffer (sodium phosphate and potassium phosphate) and ammonium chloride (dechlorinating agent). Sodium azide was not used, but samples were refrigerated upon collection prior to analysis to prevent microbial growth. HAA5 were analyzed using USEPA Method 552.2. The preservative used for this method is ammonium chloride (dechlorinating agent). Sodium azide was not used, but samples were refrigerated upon collection prior to analysis to prevent microbial growth. The small amount of sample remaining in the 500 mL bottles after decanting into the THM and HAA bottles was analyzed for free chlorine residual using the Hach DPD method.

Mathematical reconstruction of whole water DBP contribution derived from DOM isolates was performed using equations 1 and 2.

$$DOC_{contributed} \left(\frac{\text{mg-C}}{\text{L}} \right) = DOC_{bulk} \times \frac{Mass_{isolate}}{Mass_{total\ isolated}} \quad (1)$$

$$DBP_{contributed} \left(\frac{\text{nmol}}{\text{L}} \right) = DOC_{contributed} \left(\frac{\text{mg-C}}{\text{L}} \right) \times DBP_{yield} \left(\frac{\text{nmol}}{\text{mg-C}} \right) \quad (2)$$

This mathematical representation assumes errors in DOM recovery are equally distributed among all isolated fractions. It must be clearly noted that a notable pitfall of this method is derived from the unequal distribution of bromide in the isolated fractions. Bromide is concentrated to the HPI-A+N fraction and not present in other fractions. As such it is expected that brominated DBPs will occur as a disproportionate contributor for HPI-A+N and be nearly non-existent in other isolates. The authors utilize molar masses of DBPs to limit the apparent discrepancy when comparing fractions.

Results

Bulk Water Quality

Water samples were determined to have DOC concentrations from 3.64 – 6.02 mg-C/L. The lake samples had higher DOC concentrations than their corresponding river, where the Verde River feeds Bartlett Lake and the Salt River feeds Saguaro Lake. The concentration of DON had a positive correlation with DOC in the Salt River, Verde River, and Lake Pleasant samples. Bartlett Lake and Saguaro Lake were depleted in DON in comparison to the other waters. While not measured in this study it should be noted that low concentrations of bromide are present in these waters and are typically 0.11 mg/L for the Salt River and Saguaro Lake, 0.08 mg/L for Lake Pleasant: 0.06 mg/L for the Verde River and Bartlett Lake. A compilation of basic water quality is provided in Table 1. Sampling on the upper Salt and Verde Rivers were made during climatic events (e.g. significant rainfall or flooding). For comparison, longer term trends in the terminal reservoirs are shown in Figure 2. Saguaro Lake is the fifth lake in series on the Salt River, which has a cumulative residence time of over 4 years – resulting in significant attenuation of “pulse” climatic inputs from the upper Salt River. Bartlett Lake is the second lake in series on the Verde River, which has a cumulative residence time of less than 1 year. Lake Pleasant is filled during the winter from the Central Arizona Project canal which pumps Colorado River water into the reservoir and then releases water during the summer to meet municipal and industrial demands; above the diversion on the Colorado River are reservoirs with greater than 15 years of hydraulic residence time. The Aqua Fria River flows into Lake Pleasant, but typically represents less than 4% of the total volume – except during extreme localized flow events. As a consequence of these reservoir hydraulics, Figure 2 shows that the DOC levels either experience annual rise/falls associated with high flows (attributed to snowmelt for Bartlett Lake), long-term gradual changes (Saguaro Lake), or repetitive small changes (Lake Pleasant).

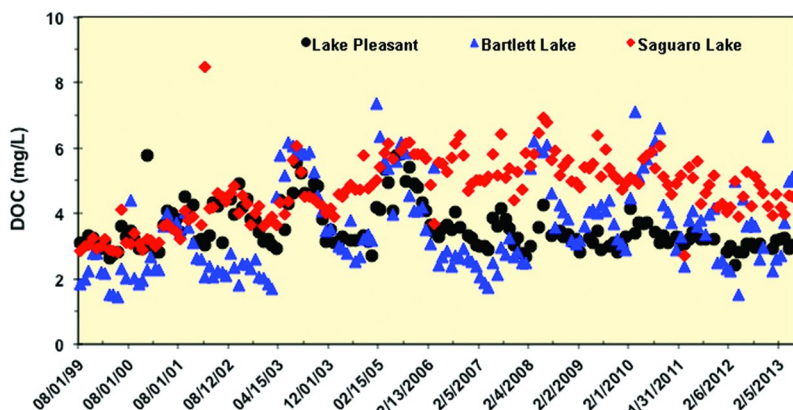


Figure 2. Longer Term Trends in the Terminal Reservoirs.

Table 1. Bulk Water Quality

<i>Location</i>	<i>Climatic Event Sample</i>	<i>Date</i>	<i>DOC</i>	<i>TDN</i>	<i>DON</i>
			<i>mg-C/L</i>	<i>mg-N/L</i>	<i>mg-N/L</i>
Upper Salt River	Yes	12/07	3.64	0.672	0.476
Saguaro Lake	No	3/08	5.85	1.08	0.426
Upper Verde River 1	Yes	12/07	5.49	1.98	0.720
Upper Verde River 2	Yes	1/08	4.82	1.22	0.640
Bartlett Lake	No	3/08	6.02	0.614	0.388
Lake Pleasant	No	3/08	4.56	1.07	0.593

Table 2. DOM Fractionation Recovery

<i>Location</i>	<i>Climatic Event Sample</i>	<i>DOM Recovery</i>	
		<i>DOC</i>	<i>DON</i>
		<i>%</i>	<i>%</i>
Upper Salt River	Yes	149	167
Saguaro Lake	No	91	126
Upper Verde River 1	Yes	77	77
Upper Verde River 2	Yes	92	73
Bartlett Lake	No	102	105
Lake Pleasant	No	100	102

DOM Fractionation

Fractionation of DOM in the collected samples was highly successful (i.e. the majority of the DOC and DON was able to be accounted for ($100\% \pm 10\%$)). Mass accounted for was determined by the volume of water from which DOM was isolated multiplied by the associated concentration of DOC or DON. River samples had lower/higher recoveries than their corresponding reservoirs likely due to elevated concentrations of organic and inorganic colloids that passed through the $0.45\text{ }\mu\text{m}$ filter that were subjected to subsequent acid/base/solvent processing. DOC and DON recovery for each sample is presented in Table 2.

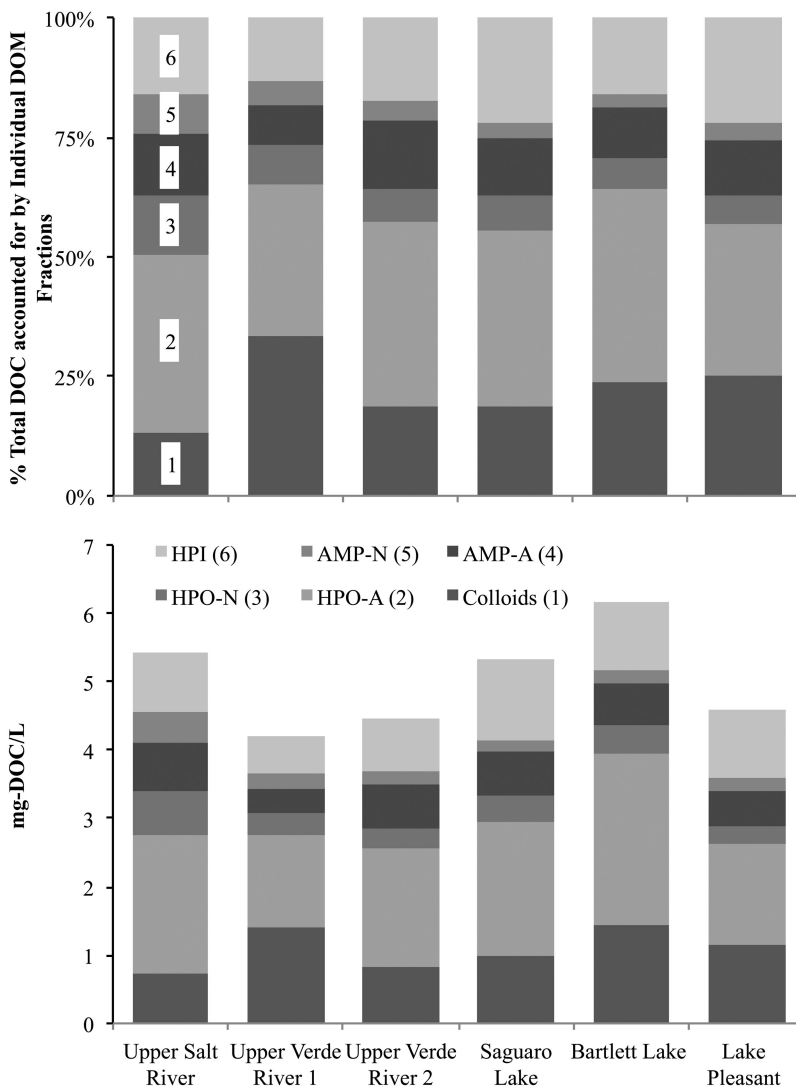


Figure 3. DOM Fractionation and Reconstruction of Whole Water.

Figure 3 illustrates the distribution of DOM isolates as fractionated (bottom) and normalized to 100% (top). HPO-A was the most dominant DOM fraction of all waters sampled accounting for between 20 – 40% of the DOC. As all of these samples are known to be impacted by seasonal algal blooms it was not surprising to identify that between 15 – 30% of the DOC was associated with organic colloids as observed previously (23). The relative distribution of remaining DOM fractions does not significantly vary by sample. The most notable difference, which was expected, is the variation in DOM fraction distribution in the two Verde River samples due to the associated varied associated event intensity. Comparing these

samples, the contribution of colloids, and amphiphilics vary notably and are likely associated with the status of the surrounding environment that was subject to the climatic event that was occurring during sampling.

Disinfection Byproduct Formation

Fraction Specific Formation Rates

While formation potential testing is usually a single data point, this effort shows evaluation of a short-term (1-hr) and long-term (7-day) formation potential can provide additional information regarding DOM reactivity. Tables 3 and 4 present these results as percentages of the 7-day formation potential using the following equation:

$$\% \text{ of 7-day formation} = \frac{1 \text{ hour yield } \left(\frac{nM \text{ DBP}}{mg-C} \right)}{7 \text{ day yield } \left(\frac{nM \text{ DBP}}{mg-C} \right)} \quad (3)$$

Generally, hydrophobic and amphiphilic acid fractions produced more DBPs, THMs or HAAs, at 1-hr than corresponding hydrophobic and amphiphilic neutral fractions. Hydrophilic fractions tended to form more DBPs at 1-hr than any other fractions as bromide more rapidly incorporates than chloride. This tendency of the hydrophilic fractions were exacerbated by the fact that bromide was concentrated in these fractions and typically removed from others. This was also illustrated by the higher percentage formation of brominated DBP species. For example 1-hr CHBrCl₂ formation was 38% to 63% for HPO, AMP and Colloid fractions whereas CHCl₃ formation was 9% to 26%. A similar trend was also observed for bromochloroacetic acid (BCAA).

Not all river samples formed reportable concentrations of monochloroacetic acid (MCAA) or BCAA at 1-hr whereas the reservoir samples did (Table 4). River samples did form MCAA and BCAA at the 7-day hold time at concentrations similar to that of the reservoir samples. It should be noted that while this trend seems to separate the river and reservoir samples, the reported concentrations of MCAA and BCAA are near the reporting limits of 1 µg/L.

Bulk Water Formation Rate

Similar to the formation rate of the DOM fractions, brominated DBPs formed more rapidly although at much lower concentrations than their chlorinated analogs. From 24% - 26% of 7-day TTHM formed in the first hour (Table 5). This percentage of 7-day TTHM formation was similar ($\pm 10\%$) to the most reactive isolates (hydrophobic acids and colloids) but was nearly always greater than the non-hydrophilic DOM fractions. Considering only chloroform (CHCl₃), the percentage of 7-day formation were closer to the formation rates of hydrophobic and amphiphilic acid fractions ($\pm 5\%$), the dominant fraction of DOC of the DOM pool. For reference and comparison, total THM yield is also presented in Table 5.

Table 3. Shorter-Term Reactivity of DOM Fractions. Percent of 7 Day TTHM Yield at 1 hour and 7-day TTHM Yield

	<i>Sample</i>	<i>CHCl₃</i>	<i>CHBrCl₂</i>	<i>CHBr₂Cl</i>	<i>CHBr₃</i>	<i>TTHM</i>	<i>7-day TTHM</i>
							<i>nM/mgC</i>
Saguaro Lake	Colloids	11%	40%			12%	242
	HPO-A	15%	45%			16%	547
	HPO-N	9%	44%			9%	411
	AMP-A	17%	46%			18%	517
	AMP-N	13%	55%			14%	410
	HPI	22%	27%	28%	29%	25%	353
Bartlett Lake	Colloids	21%	61%		38%	22%	421
	HPO-A	26%	63%		50%	26%	567
	HPO-N	12%	46%			13%	408
	AMP-A	17%	60%			18%	542
	AMP-N	14%	50%			14%	452
	HPI	24%	41%	49%		30%	369

	<i>Sample</i>	<i>CHCl₃</i>	<i>CHBrCl₂</i>	<i>CHBr₂Cl</i>	<i>CHBr₃</i>	<i>TTHM</i>	<i>7-day TTHM</i>
							<i>nM/mgC</i>
Lake Pleasant	Colloids	12%	BDL			11%	172
	HPO-A	15%	41%			15%	468
	HPO-N	8%	46%			8%	386
	AMP-A	17%	53%			17%	395
	AMP-N	10%	44%			10%	413
	HPI	26%	17%	23%	21%	21%	255
'Salt River	Colloids	22%	72%			23%	353
	HPO-A	21%	58%			21%	492
	HPO-N	14%	63%			15%	342
	AMP-A	22%	52%			22%	408
	AMP-N	18%	63%			19%	310
	HPI	24%	30%	42%	28%	33%	281

Continued on next page.

Table 3. (Continued). Shorter-Term Reactivity of DOM Fractions. Percent of 7 Day TTHM Yield at 1 hour and 7-day TTHM Yield

	<i>Sample</i>	<i>CHCl₃</i>	<i>CHBrCl₂</i>	<i>CHBr₂Cl</i>	<i>CHBr₃</i>	<i>TTHM</i>	<i>7-day TTHM</i>
							<i>nM/mgC</i>
Verde River 1	Colloids	25%	50%		150%	26%	544
	HPO-A	21%	41%		89%	22%	471
	HPO-N	12%	39%		133%	13%	389
	AMP-A	14%	58%		86%	14%	693
	AMP-N	7%	42%		100%	7%	558
	HPI	25%	34%	41%	54%	37%	263
Verde River 2	Colloids	21%	53%		300%	22%	643
	HPO-A	24%	45%			24%	436
	HPO-N	14%	38%		367%	14%	329
	AMP-A	19%	40%			20%	471
	AMP-N	15%	48%		140%	15%	322
	HPI	21%	35%	51%	75%	33%	316

Table 4. Shorter-Term Reactivity of DOM Fractions. Percent of 7 Day HAA Yield at 1 hour and 7-day HAA5 Yield

	<i>Sample</i>	<i>MCAA</i>	<i>DCAA</i>	<i>DBAA</i>	<i>BCAA</i>	<i>TCAA</i>	<i>HAA5</i>	<i>7 day HAA5</i>
								<i>nM/mgC</i>
Saguaro Lake	Colloids	33%	12%		93%	20%	16%	393
	HPO-A	36%	23%		93%	24%	24%	492
	HPO-N	35%	14%		100%	21%	18%	279
	AMP-A	38%	19%		115%	38%	28%	549
	AMP-N	32%	15%		92%	20%	18%	384
	HPI	56%	20%	38%	25%	48%	33%	363
Bartlett Lake	Colloids	35%	23%		100%	27%	22%	745
	HPO-A	38%	31%		117%	36%	26%	591
	HPO-N	44%	21%		100%	22%	13%	265
	AMP-A	37%	28%		120%	37%	18%	605
	AMP-N	40%	19%		73%	33%	14%	339
	HPI	73%	23%	67%	32%	49%	30%	514

Continued on next page.

Table 4. (Continued). Shorter-Term Reactivity of DOM Fractions. Percent of 7 Day HAA Yield at 1 hour and 7-day HAA5 Yield

	<i>Sample</i>	<i>MCAA</i>	<i>DCAA</i>	<i>DBAA</i>	<i>BCAA</i>	<i>TCAA</i>	<i>HAA5</i>	<i>7 day HAA5</i>
								<i>nM/mgC</i>
Lake Pleasant	Colloids	38%	14%		100%	20%	18%	320
	HPO-A	35%	25%		108%	24%	25%	546
	HPO-N	36%	19%			37%	28%	307
	AMP-A	41%	22%		63%	25%	24%	427
	AMP-N	34%	13%		110%	20%	17%	357
	HPI	48%	18%	28%	20%	62%	33%	308
Salt River	Colloids		22%			21%	20%	630
	HPO-A		19%			22%	20%	661
	HPO-N		16%			29%	20%	264
	AMP-A	15%	14%			23%	18%	674
	AMP-N		18%			30%	22%	291
	HPI		22%	50%	72%	45%	22%	276

	<i>Sample</i>	<i>MCAA</i>	<i>DCAA</i>	<i>DBAA</i>	<i>BCAA</i>	<i>TCAA</i>	<i>HAA5</i>	<i>7 day HAA5</i>
								<i>nM/mgC</i>
Verde River 1	Colloids		25%			23%	23%	1183
	HPO-A		17%			22%	20%	821
	HPO-N		17%			28%	21%	319
	AMP-A	18%	15%		24%	24%	19%	756
	AMP-N		18%			30%	21%	305
	HPI	25%	17%	49%	49%	43%	25%	475
Verde River 2	Colloids		30%			22%	24%	1327
	HPO-A		20%			22%	21%	801
	HPO-N		24%			29%	25%	228
	AMP-A		17%			23%	19%	742
	AMP-N		15%			20%	16%	408
	HPI	83%	14%	35%	43%	31%	24%	481

Table 5. Percent of 7 Day THM Formation at 1 hour and 7-day Yield for Bulk Waters

<i>Sample</i>	<i>CHCl₃</i>	<i>CHBrCl₂</i>	<i>CHBr₂Cl</i>	<i>CHBr₃</i>	<i>Total THM</i>	<i>Yield</i> <i>nM/mg-C</i>
Upper Salt River	20%	49%	72%	150%	25%	465
Saguaro Lake	20%	51%	87%	133%	25%	448
Upper Verde River 1	26%	45%	64%	200%	26%	356
Upper Verde River 2	23%	47%	80%	11%	25%	488
Bartlett Lake	23%	54%	111%	67%	25%	615
Lake Pleasant	17%	39%	62%	64%	24%	374

Table 6. Shorter-Term Reactivity of DOM Fractions. Percent of 7 Day HAA Yield at 1 hour and 7-day HAA Yield

<i>Sample</i>	<i>MCAA</i>	<i>DCAA</i>	<i>DBBA</i>	<i>BCAA</i>	<i>TCAA</i>	<i>HAA5</i>	<i>Yield nM/mg-C</i>
Upper Salt River	29%	15%	31%	52%	26%	29%	420
Saguaro Lake	31%	15%	29%	30%	29%	29%	380
Upper Verde River 1	34%	28%	26%	0%	22%	25%	369
Upper Verde River 2	34%	14%	32%	49%	38%	35%	429
Bartlett Lake	29%	19%	30%	200%	21%	25%	662
Lake Pleasant	29%	16%	23%	50%	23%	26%	268

Incorporation rate of bromide into bulk water formed HAAs deviated from the convention observed for DOM formed HAAs. DBAA generally was produced rapidly, high percentage of 7-day formation at 1-hr, while BCAA formed at a rate similar to other chlorinated HAAs. The two Verde River samples showed very different reactivities, where Verde River 2 produced HAA5 faster than Verde River 1. Furthermore, the Salt River and Verde River 2 samples produced HAA5 faster than their corresponding reservoirs, Bartlett Lake and Saguaro Lake, respectively. These results are presented numerically in Table 6.

Reconstruction of Disinfection Byproduct Formation

Reconstructed Formation Potential

When whole water DBP formation was reconstructed from isolate DBP yield and quantity of specific DOM fractions, the estimated DBP formation contribution of individual DBPs were reasonably close to that measured in the whole water. When the total DBP concentration calculated by the mathematical reconstruction was compared with what was measured in the bulk, DBPs containing only chlorine were more comparable with ratios from about 0.6 – 1.4. Brominated DBPs had much larger differences between reconstructed amount and bulk with ratios of up to 35. These percentages and ratios were calculated using equations 3 and 4 and the results of this analysis are presented in Tables 7 and 8.

$$\Delta \% \text{ Contribution} = \left(\frac{DBP_i}{\text{Total } DBP_{THM \text{ or HAA}}} \right)_{\text{Bulk}} - \left(\frac{DBP_i}{\text{Total } DBP_{THM \text{ or HAA}}} \right)_{\text{Reconstructed}} \quad (3)$$

$$\text{Ratio of DBP Formation} = \frac{DBP_i(t)_{\text{Reconstructed}}}{DBP_i(t)_{\text{Bulk}}} \quad (4)$$

Reconstructed Formation Potential

The observed similarity between the bulk water sample and reconstructed whole water DBP formation suggested that it would be acceptable to utilize the intermediate mathematical steps to present DOM origin of whole water DBPs. While this reconstruction method is not without pitfall and limited accuracy, this was performed in the interest connecting DOM fraction DBP yield and occurrence of a DOM fraction to determine the contribution of specific DBP fractions to the overall DBP formation. Here we present a representative figure (Figure 4) from our experiments illustrating mathematical reconstruction whole waters for the 7-day DBP formation derived from individual DOM fraction chlorination experiments.

Table 7. Bulk versus Reconstructed for THM Yield

<i>Sample</i>	<i>CHCl₃</i>	<i>CHBrCl₂</i>	<i>CHBr₂Cl</i>	<i>CHBr₃</i>
1 hour - Difference in % Contribution				
Saguaro Lake	-8%	9%	0%	-1%
Bartlett Lake	-7%	8%	-1%	0%
Lake Pleasant	-35%	25%	10%	0%
Salt River	-27%	25%	2%	0%
Verde River 1	-31%	27%	5%	-2%
Verde River 2	-14%	17%	-2%	-1%
1 hour - Ratio of DBP Production (isolate/bulk)				
Saguaro Lake	0.59	0.29	0.56	2.45
Bartlett Lake	1.41	0.79	3.30	6.61
Lake Pleasant	0.93	0.26	0.34	1.45
Salt River	1.11	0.25	0.74	2.34
Verde River 1	1.04	0.14	0.40	13.23
Verde River 2	0.68	0.23	1.14	15.40
7 day - Difference in % Contribution				
Saguaro Lake	0%	3%	-3%	-1%
Bartlett Lake	-2%	3%	-1%	0%
Lake Pleasant	-15%	14%	2%	-1%
Salt River	-13%	13%	0%	0%
Verde River 1	-19%	17%	2%	-1%
Verde River 2	-8%	9%	-1%	0%
7 day - Ratio of DBP Production (isolate/bulk)				
Saguaro Lake	0.78	0.51	1.69	11.30
Bartlett Lake	1.35	0.92	7.49	10.74
Lake Pleasant	1.04	0.56	0.95	5.87
Salt River	1.10	0.31	1.16	13.10
Verde River 1	1.03	0.16	0.44	30.17
Verde River 2	0.69	0.29	1.43	1.15

Table 8. Bulk versus Reconstructed for HAA Yield

<i>Sample</i>	<i>MCAA</i>	<i>MBAA</i>	<i>DCAA</i>	<i>DBAA</i>	<i>BCAA</i>	<i>TCAA</i>
1 hour - Difference in % Contribution						
Saguaro Lake	-1%	-1%	15%	-2%	2%	-13%
Bartlett Lake	1%	2%	31%	0%	-1%	-34%
Lake Pleasant	-3%	0%	2%	7%	14%	-21%
Salt River	3%	1%	3%	3%	6%	-17%
Verde River 1	3%	2%	2%	-1%	8%	-14%
Verde River 2	2%	1%	-2%	1%	2%	-4%
1 hour - Ratio of DBP Production (isolate/bulk)						
Saguaro Lake	0.91	1.15	0.53	1.81	0.62	1.06
Bartlett Lake	1.54	1.67	1.41	1.15	1.81	2.43
Lake Pleasant	1.35	1.20	1.08	0.79	0.45	2.51
Salt River	0.05	--	0.82	0.38	0.50	1.61
Verde River 1	0.23	--	1.20	--	0.35	2.05
Verde River 2	0.23	--	0.78	0.48	0.55	1.00
7 day - Difference in % Contribution						
Saguaro Lake	1%	0%	5%	-1%	2%	-8%
Bartlett Lake	-1%	0%	-5%	0%	0%	6%
Lake Pleasant	0%	1%	1%	3%	9%	-14%
Salt River	-1%	1%	-2%	2%	7%	-7%
Verde River 1	0%	2%	-3%	2%	6%	-7%
Verde River 2	1%	2%	0%	1%	4%	-7%
7 day - Ratio of DBP Production (isolate/bulk)						
Saguaro Lake	0.71	0.89	0.81	1.46	0.65	1.10
Bartlett Lake	1.12	1.42	1.51	2.98	1.84	1.49
Lake Pleasant	1.03	1.12	1.21	1.14	0.60	2.24
Salt River	1.09	0.57	1.33	0.40	0.32	1.84
Verde River 1	1.06	0.08	1.49	0.30	0.34	1.99
Verde River 2	0.75	0.08	1.19	0.67	0.53	1.69

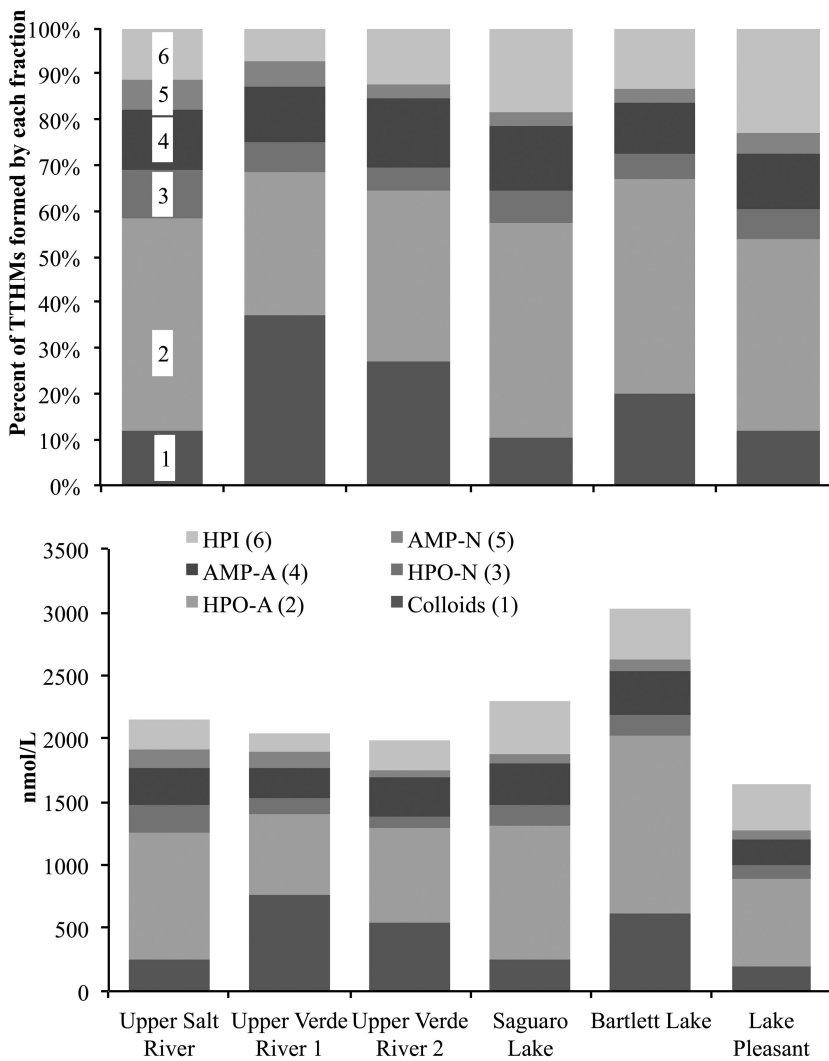


Figure 4. Distribution and Formation of TTHMs of 7-day Reconstructed DOM.

For all samples studied herein, colloids and hydrophobic acids accounted for 50 – 80% of the total TTHMs or HAAs formed at 1-hr or 7-day reaction times (Figure 3). While not shown, hydrophilics accounted for greater percentage of the DBPs formed at 1-hr than 7-day reaction times. This was associated the rapid rate of incorporation of bromide into DBPs and the hydrophilic fraction was the only DOM fraction that contained bromide.

The contribution of specific DOM isolates to the reconstructed whole water varied from source to source and during climatic events. Reviewing the two Verde River samples further illustrates that difference between climatic events. In Verde River 1 the dominant DOM fractions forming DBPs were colloids and hydrophobic acids. While these fractions also were the dominant DOM fractions associated with DBP formation in Verde River 2, lower percentage contributions were associated with these fractions and greater contributions were associated with amphiphilic and hydrophilic fractions. This finding supports the known dynamic nature of river systems where the status of watershed during a climatic event may produce variations in water quality.

Conclusions

Based on the study of these six whole water samples, three of which were sampled during climatic events, and their associated DOM fractions the following conclusions can be drawn:

- DOM isolated during “normal” and “climatic” influenced higher flows associated with snowmelt or heavy rains in the arid southwestern U.S.A. exhibited differences in the distribution of DOM fractions suggesting the event changes the source and/or quantity of contribution of specific DOM fractions.
- Through this realization that DOM quantity and distribution of DOM fractions change during climatic events, further consideration on developing operational procedures to mitigate potential impacts on treatment process can be evaluated (e.g. adapting to increased concentrations of amphiphilic and hydrophilic DOM).
- The formation rate (e.g. short versus long) did not appear to vary between water samples or climatic events. Differences in formation rates were associated with DOM fraction. Thus during climatic events, it isn’t the character of the DOM fractions at a local scale that are changing but the fractional distribution of the DOM pool that results in changes in DBP formation.
- DOM acid fractions produce DBPs at a more rapid rate than neutral DOM fractions. This could have a role on water treatment facilities as while acids are easily removed, increased concentrations of neutrals in derived from riverine systems could result in increased formation of DBPs at extended times as this fractions is not easily removed by conventional processes.
- Mathematical reconstruction of whole water DBP formation from DOM fraction DBP yields provided results that were 1) reasonably similar to the actual bulk water DBP formation and 2) allowed the opportunity identify significant DOM fraction contributions to the DBPs formed and 3) study the changes in DBP formation during climatic events.

Acknowledgments

This project was funded by the City of Phoenix as part of its Water Quality Master Plan Update. Collaborators on this project include the City of Phoenix, Salt River Project, Central Arizona Project, Malcolm Pirnie, Inc. (now ARCADIS), and Carollo Engineers, Inc. Contributions from Zaid Chowdhury, Laurel Passantino, Vance Lee, Mark Urban, Chao-An Chiu, Seong Nam Nam, Yu-Chu Hsu and Brian Fayle are greatly appreciated.

References

1. Hertkorn, N.; Claus, H.; Schmitt-Kopplin, P. H.; Perdue, E. M.; Filip, Z. Utilization and transformation of aquatic humic substances by autochthonous microorganisms. *Environ. Sci. Technol.* **2002**, *36*, 4334–4345.
2. Barber, L. B.; Leenheer, J. A.; Noyes, T. I.; Stiles, E. A. Nature and transformation of dissolved organic matter in treatment wetlands. *Environ. Sci. Technol.* **2001**, *35*, 4805–4816.
3. Aiken, G.; Cotsaris, E. Soil and Hydrology – Their Effect on NOM. *J. - Am. Water Works Assoc.* **1995**, *87*, 36–45(1995).
4. Baron, J.; McKnight, D.; Denning, A. S. Sources of Dissolved and Particulate Organic Material in Loch Vale Watershed Rocky Mountain National Park Colorado, U.S.A. *Biogeochemistry* **1991**, *15*, 89–110.
5. Tate, C. M.; Meyer, J. L. The Influence of Hydrologic Conditions and Successional State on Dissolved Organic Carbon Export from Forested Watersheds. *Ecology* **1983**, *64*, 25–32.
6. McKnight, D. M.; Andrews, E. D.; Spaulding, S. A.; Aiken, G. R. Aquatic Fulvic-Acids in Algal-rich Antarctic Ponds. *Limnol. Oceanogr.* **1994**, *39*, 1972–1979.
7. Onstad, G. D.; Canfield, D. E.; Quay, P. D.; Hedges, J. I. Sources of particulate organic matter in rivers from the continental U.S.A.: Lignin phenol and stable carbon isotope compositions. *Geochim. Cosmochim. Acta* **2000**, *64*, 3539–3546.
8. McDowell, W. H.; Likens, G. E. Origin, Composition, and Flux of Dissolved Organic Carbon in the Hubbard Brook Valley. *Ecol. Monogr.* **1988**, *58*, 177–195.
9. Leff, L. G.; Meyer, J. L. Biological Availability of Dissolved Organic-Carbon Along the Ogeechee River. *Limnol. Oceanogr.* **1991**, *36*, 315–323.
10. Reckhow, D. A.; Singer, P. C.; Malcolm, R. L. Chlorination of Humic Materials - By-product Formation and Chemical Interpretations. *Environ. Sci. Technol.* **1990**, *24*, 1655–1664.
11. Amy, G. L.; Chadik, P. A.; Chowdhury, Z. K. Developing Models for Predicting Trihalomethan Formation Potential and Kinetics. *J. - Am. Water Works Assoc.* **1987**, *79*, 89–97.
12. Weishaar, J. L.; Aiken, G. R.; Bergamaschi, B. A.; Fram, M. S.; Fujii, R.; Mopper, K. Evaluation of specific ultraviolet absorbance as an indicator of the chemical composition and reactivity of dissolved organic carbon. *Environ. Sci. Technol.* **2003**, *37*, 4702–4708.

13. Traina, S. J.; Novak, J.; Smeck, N. E. An Ultraviolet Absorbance Method for Estimating the Percent Aromatic Carbon Content of Humic Acids. *J. Environ. Qual.* **1990**, *19*, 151–153.
14. Malcolm, R. L. The Uniqueness of Humic Substances in each of Soil, Stream and Marine Environments. *Anal. Chim. Acta* **1990**, *232*, 19–30.
15. Nguyen, M.-L.; Baker, L. A.; Westerhoff, P. DOC and DBP precursors in western U.S. watersheds and reservoirs. *J. - Am. Water Works Assoc.* **2002**, *94*, 98–112.
16. Parks, S. J.; Baker, L. A. Sources and transport of organic carbon in an Arizona river-reservoir system. *Water Res.* **1997**, *31*, 1751–1759.
17. Westerhoff, P.; Anning, D. Concentrations and characteristics of organic carbon in surface water in Arizona: influence of urbanization. *J Hydrol.* **2000**, *236*, 202–222.
18. Mash, H.; Westerhoff, P. K.; Baker, L. A.; Nieman, R. A.; Nguyen, M. L. Dissolved organic matter in Arizona reservoirs: assessment of carbonaceous sources. *Org. Geochem.* **2004**, *35*, 831–843.
19. Westerhoff, P.; Rodriguez-Hernandez, M.; Baker, L.; Sommerfeld, M. Seasonal occurrence and degradation of 2-methylisoborneol in water supply reservoirs. *Water Res.* **2005**, *39*, 4899–4912.
20. Aiken, G. R.; McKnight, D. M.; Thorn, K. A.; Thurman, E. M. Isolation of Hydrophilic Organic-acids from Water using Nonionic Macroporous Resins. *Org. Geochem.* **1992**, *18*, 567.
21. Hwang, C.; Krasner, S.; Amy, G. L.; Dickenson, E.; Bruchet, A.; Prompsy, C.; Croue, J.-P.; Violette, D.; Leenheer, J. A. Polar NOM: Characterization, DBPs, Treatment. *Water Research Foundation Report*; Denver, CO, 2001.
22. Leenheer, J. A.; Dotson, A.; Westerhoff, P. Dissolved organic nitrogen fractionation. *Ann. Environ. Sci.* **2007**, *1*, 45.
23. Dotson, A. D.; Westerhoff, P. Character and Treatment of Organic Colloids in Challenging and Impacted Drinking Water Sources. *J. Environ. Eng.* **2012**, *138*, 4.

Chapter 14

Fluorescence Characterization of Humic Substance Coagulation: Application of New Tools to an Old Process

Julie A. Korak,* Fernando L. Rosario-Ortiz, and R. Scott Summers

Department of Civil, Environmental and Architectural Engineering,
University of Colorado Boulder, Boulder, Colorado 80309, U.S.A.

*E-mail: Julie.Korak@colorado.edu.

A classic process, the coagulation of humic and fulvic acids, is revisited in this chapter using contemporary fluorescence methods to characterize dissolved organic matter (DOM) removal. Different fluorescence metrics are explored and their insights into DOM behavior highlighted. Peak picking and fluorescence regional integration methods are compared and suggest that integrated data does not provide additional insight beyond simple peak picking approaches. The limitations of analyzing only fluorescence intensities are highlighted, because it is difficult to separate changes in DOM quantity, quality, and other interactions. While all methods captured the interactions between DOM and aluminum species before physical removal, quantum yields and fluorescence index (FI) offer more information regarding compositional changes. Finally, this study also provides evidence that ascribing the chemical significance of humic acid-like and fulvic acid-like is flawed and unsupported for aquatic DOM.

Background

The coagulation of humic substances has been an area of active research since the early 1960s. The earliest endeavors were motivated by the removal of color from drinking water sources. With the discovery of haloforms in drinking water (1) and the eventual link between disinfection byproducts and humic materials established (2), the motivation for dissolved organic matter (DOM)

removal shifted from aesthetic purposes to public health protection. Research ensued investigating the removal of humic and fulvic acids by coagulation. Two comprehensive research reviews with identification of knowledge gaps were published in 1979 and 1988 (3, 4).

When this process was initially investigated, the analytical methods for characterizing the processes were limited compared to today's capabilities. The main surrogate parameters for water quality analyses were turbidity, color, total organic carbon, total trihalomethane formation potential and UV absorbance at 254 nm (UV₂₅₄) (5). The quantification of DOM often relied on absorption measurements coupled with calibration curves rather than direct organic carbon measurements (6, 7).

Analytical methods have improved dramatically since then providing new tools for DOM characterization. Fluorescence spectroscopy started to gain popularity in the late 1980s/early 1990s to characterize soil derived organic matter (8, 9). The use of excitation-emission matrices (EEMs) to characterize DOM was introduced in 1990 and demonstrated that these heterogeneous mixtures show general similarities in their fluorescent material (10). Methods for analyzing fluorescence EEMs have developed over the past 30 years yielding techniques such as peak picking (11), calculation of quantum yields (12), fluorescence regional integration (FRI) (13), and DOM-specific indices, such as fluorescence index (FI) (14) and humification index (HIX) (15).

What Are Humic and Fulvic Acids?

Since DOM is a heterogeneous mixture, its fractionation based on chemical characteristics has been widely used to better understand the complex behaviors of whole waters by attributing certain behaviors to distinct fractions. Thus, humic and fulvic acids have been at the center of DOM research for decades. Whether the process of interest is a water treatment unit operation or the fate and transport of contaminants in the environment, DOM research has a pattern of investigating specific topics using well-characterized fractions and then extrapolating analyses to whole water samples in the environment. This chapter will only discuss aquatic DOM, humic acids and fulvic acids. It should be noted that soil organic matter and aquatic organic matter, while still containing humic and fulvic acids, exhibit different characteristics. The interpretation and discussions herein should not be extrapolated to soil-derived humic and fulvic acids.

Aquatic humic and fulvic acids have been defined using a variety of criteria. One of the simplest definitions is that a humic acid is soluble in basic conditions but insoluble in mineral acid, whereas a fulvic acid is soluble in both (3, 7). Other methods define humic substances (humic and fulvic acids combined) as organic matter that adsorbs onto an XAD-8 resin and desorbs with sodium hydroxide. Once eluted, the humic acid fraction precipitates at pH 1 while the fulvic acid fraction remains soluble (16). The International Humic Substances Society (IHSS) has adopted an XAD-8 method with cation exchange, but explicitly states that they do not endorse their own method as "the best" in the hope that research will continue.

In any case, it is important to note that these operationally defined DOM fractions are based on differences in chemical characteristics. Humic and fulvic acids, which elute together as hydrophobic acids before precipitation, account for about 60% of the DOC in a freshwater sample, but the mass ratio of fulvic acids to humic acids is about 3:1 (17). The average molecular weight of humic acids is larger than that of fulvic acids and unfractionated DOM (17). While the range of aromatic carbon content can vary greatly across waters (17), within one water the humic acid fraction typically has a higher percentage of aromatic carbon compared to fulvic acids and unfractionated DOM (18). The increased aromaticity in humic acids is manifested as a higher specific UV_{254} compared to fulvic acids and unfractionated waters (19). While humic acids absorb more light per unit carbon, fulvic acids fluoresce more light per unit carbon (20, 21). The fluorescence quantum yield, fraction of light emitted relative to the light absorbed, of fulvic acids is greater than the quantum yield of humic acids (22). Therefore, these fractions have different chemical characteristics and would be expected to behave differently.

In this chapter, we revisit a classic drinking water treatment process, the coagulation of humic and fulvic acids, but characterize DOM removal using contemporary fluorescence spectroscopy methods. We investigate three questions: What insight do fluorescence techniques give to the DOM coagulation process? How do these methods of analyzing fluorescence data reveal different aspects of the process? And what light does this classic process shed on prevailing interpretations of fluorescence data?

Materials and Methods

Materials

Three IHSS standards were used in the study: Suwannee River Natural Organic Matter (SRNOM, 2R101N), Suwannee River Fulvic Acid (SRFA, 1S101F) and Suwannee River Humic Acid (SRHA, 2S101H). Each isolate was dissolved in de-chlorinated tap water. Divalent cations and other inorganics can affect coagulation (4); so de-chlorinated tap was used in order to have a naturally occurring balance of inorganic ions and alkalinity. The water was prepared by passing Boulder, CO municipal drinking water through a 200 L barrel of granulated activated carbon (Norit 1240, 12×40 US standard mesh size, bituminous) with an empty bed contact time of 10 minutes followed by a 25 μ m cartridge filter (Pentek DGD-7525-20) to remove particles. The finished water has a dissolved organic carbon (DOC) concentration less than 0.1 mgC/L, UV_{254} absorbance less than 0.001, and no detectable fluorescence. Absorbance values are reported as unitless numbers. The water had an alkalinity of 29 mg/L as $CaCO_3$ and conductivity of 136 μ S. The water quality values after the isolates were dissolved in the de-chlorinated tap water are shown in Table I. The initial UV_{254} absorbance values of the dissolved isolates were below 0.2 to minimize non-ideal, concentration-dependent fluorescence behaviors (21).

Coagulation Methods

Coagulation studies were performed using a programmable jar tester (Phipps & Bird) in 1L volumes with alum (aluminum sulfate, $Al_2SO_4 \cdot 16H_2O$) at doses of 5, 10, 14, 18 and 20 mg/L as alum. Mixing conditions included a rapid mix period (1 minute at 290 rpm), two flocculation phases (10 minutes at 55 rpm and 10 minutes at 20 rpm) and a sedimentation period (30-minutes with no mixing). The supernatant was filtered through pre-combusted (500°C for 4 hours in a muffle furnace) and rinsed 0.7 μm GF/F filters (Whatman) prior to DOC, UV and fluorescence analyses. All samples were stored in pre-combusted amber bottles, refrigerated until use and analyzed within 7 days.

Table I. Summary of Initial Water Quality Characteristics for Each Isolate in Solution

DOM	pH	Alkalinity mg/L as $CaCO_3$	DOC mgC/L	UV ₂₅₄
SRNOM	7.6	27	3.4	0.133
SRHA	7.6	26	3.0	0.197
SRFA	7.5	28	3.7	0.157

Analytical Methods

Alkalinity was measured using a Hach digital titrator (Model 16900-01) with manufacturer specified methods. pH was measured on a Fisher Scientific Accumet AB15 meter. DOC was analyzed on a Shimadzu TOC-VCSH using a high temperature combustion non-purgeable organic carbon method. Duplicates were measured on 7 of the 19 samples (37%). For samples with a DOC greater than 1 mgC/L, the differences in concentration were less than 0.2 mgC/L. For samples with a DOC less than 1 mgC/L, the difference in duplicates was less than 0.1 mgC/L. UV absorbance was measured on a Cary Bio 100 (Agilent Technologies, CA) from 200 to 600 nm in a 1 cm path length quartz cuvette and baseline corrected to deionized water. Replicate UV₂₅₄ measurements had coefficient of variance values less than 1%.

Fluorescence excitation-emission matrices (EEMs) were collected on a spectrofluorometer (Fluoromax-4, John Yvon Horiba, NJ). Excitation wavelengths were incremented from 240 to 450 nm in 10 nm steps. Emission scans were collected from 300 to 560 nm in 2 nm increments. Both excitation and emission bandpass settings were set to 5 nm, and the integration time was 0.25 s. Intensities were collected in ratio mode (signal divided by reference), and instrument-specific correction factors were applied. All EEMs were blank subtracted, corrected for primary and secondary inner filter effects and normalized to the Raman area of deionized water at 370 nm. Lamp scans, cuvette contamination checks and Raman scans were performed daily to ensure proper operation. The average relative percent difference (RPD) between duplicate peak intensities (A and C)

and normalized integrated fluorescence volumes (V_{III} and V_V) were 3.3% and 2.7%, respectively. The average RPD between FI values and maximum quantum yields were 0.3% and 4.6%, respectively.

Results and Discussion

DOC and UV₂₅₄ Removal

Using the classic assessment with DOC and UV measures, the coagulation of the SRHA, SRFA and SRNOM as a function of coagulant dose is shown in Figure 1. At low coagulant doses (alum \leq 14 mg/L), there is little change in both DOC and absorbance. At a dose of 18 mg/L, there is a large and abrupt removal of both UV and DOC from solution, which is similar to that previously observed with other humic substances (7, 23–25). In general, UV absorbance is removed to a greater extent with 55 to 90% removal compared to DOC with 40 to 70% removal (26). At the same dose, SRHA is more amenable to removal compared to SRFA or SRNOM (6).

The pattern of removal depicted in Figure 1 has been referred to as Type I coagulation as opposed to Type II, which elicits a more regular dose response behavior (4). The mechanisms for removal are complex and depend on not only the DOM present but also if it behaves as a truly dissolved species or more like a colloid. Other factors that affect removal mechanisms include turbidity, pH and background water constituents (4). If it is assumed that the material is predominantly dissolved, then removal was likely a combination of aluminum-humate/fulvate precipitation and adsorption, where humic substances adsorb onto aluminum hydroxide particles, based on the study pH range of 7.3-7.6 (4).

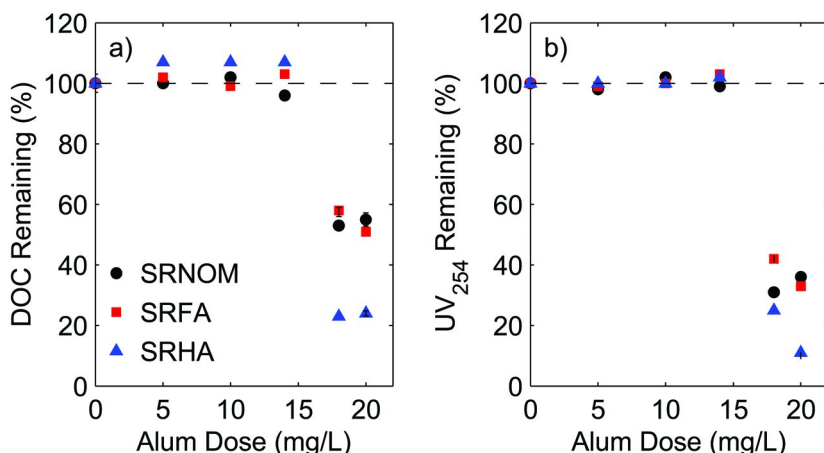


Figure 1. Relative remaining amount of a) DOC and b) UV₂₅₄ as a function of alum dose. Error bars represent the standard deviation between duplicates but most are smaller than the marker size.

DOC and UV measurements only provide a narrow glimpse into this process. They provide little insight into the interactions between DOM and aluminum species at low coagulant doses where there is no apparent change in either measurement.

Fluorescence Analysis

Many different methods have been developed for analyzing fluorescence data for DOM characterization. Table II presents initial water quality fluorescence measures using several different methods. In the following sections, we will explore these methods for analyzing fluorescence data with respect to this process and identify how each method provides different insight into the process.

Table II. Summary of Initial Fluorescence Metrics for the Isolates in Solution Including Peak Intensities (A and C) in Raman Units (RU), Regional Integration Areas (III and V), FI and Maximum Quantum Yields

DOM	Intensity (RU)		FRI Volume (RU nm ²)		
	A	C	V _{III}	V _V	FI
SRNOM	1.47	0.46	44780	14353	1.34
SRHA	0.97	0.34	30010	10606	1.14
SRFA	1.71	0.57	52842	17154	1.35

Fluorescence Intensities

One of the most common ways to analyze fluorescence data is to track how the fluorescence intensity changes. There are two prevailing methods. The first includes peak picking approaches where regions of interest are identified and then a single intensity from each region is extracted. Most peak picking methods follow the peak regions identified by Coble, because each region has been associated with a particular chemical significance (11). Peaks A and C, outlined in Figure 2a, have been associated with humic-like fluorescence. Coble states, “The overall similarity between the humic substance XAD extract and the other samples is the basis for referring to both peaks as humic-like” (11). The authors interpret this to refer to humic substances in general and not the humic acid fraction because no further distinction is made in that study. Peaks B and T (not shown) have been associated with the phenolic and indolic functional groups in the amino acids tyrosine and tryptophan, respectively (11). In this study, the reported peak intensities are the maximum from each region, many of which fall on a region boundary due to the shape of the EEM contours.

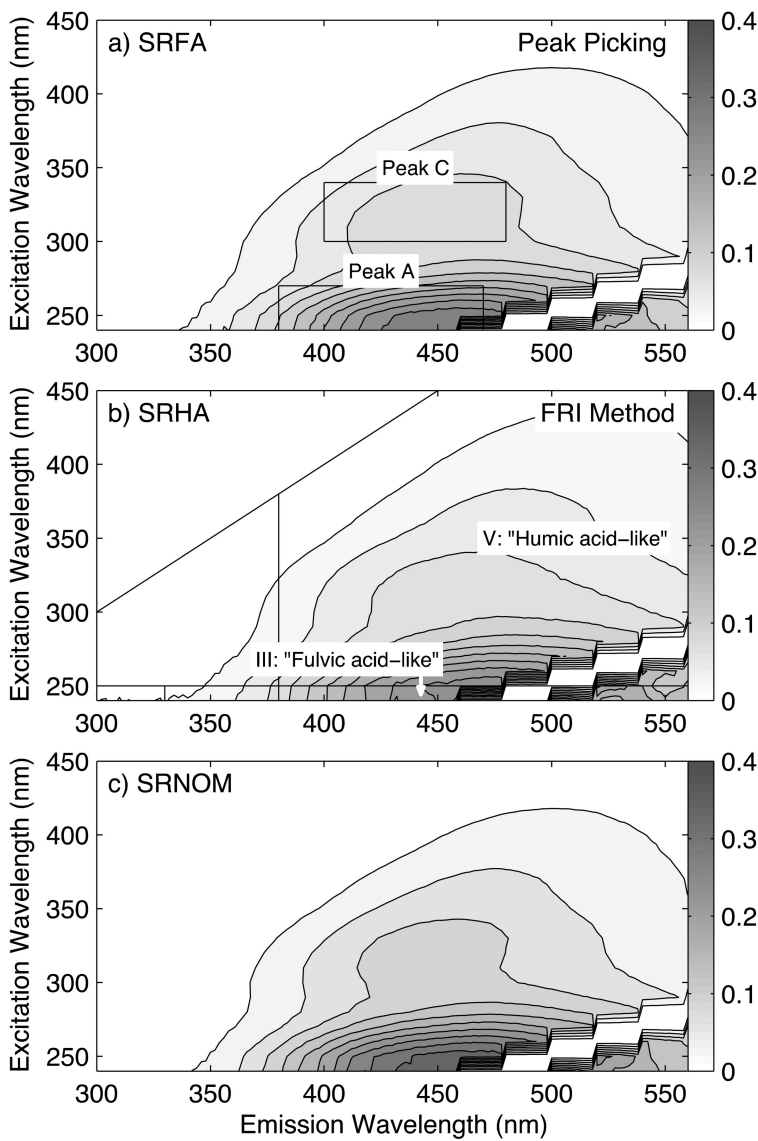


Figure 2. EEMs for a) SRFA, b) SRHA and c) SRNOM. Intensities are normalized to DOC concentration in units of RU L/mg_c. Peak picking regions A and C are outlined in a). The FRI regions are outlined in b) with the commonly ascribed chemical significance of humic acid-like and fulvic-acid like.

Chen et al realized that extracting a couple intensities from an entire EEM only provides a limited view, because it cannot capture how the contours are changing, and developed the fluorescence regional integration (FRI) method (13). This method slices the EEM into five regions (Figure 2b) and integrates each region yielding fluorescence volumes. To account for differences in region

size and wavelength increments, the data is normalized based on the fractional projected areas. The results can either be presented on a magnitude basis ($V_{i,n}$) or on a percent basis compared to the total integrated volume ($P_{i,n}$). The Greek capital letter phi is normally used to indicate the integrated volume (13). The letter V is used here as to not confuse this notation with quantum yield notation that also uses the same letter.

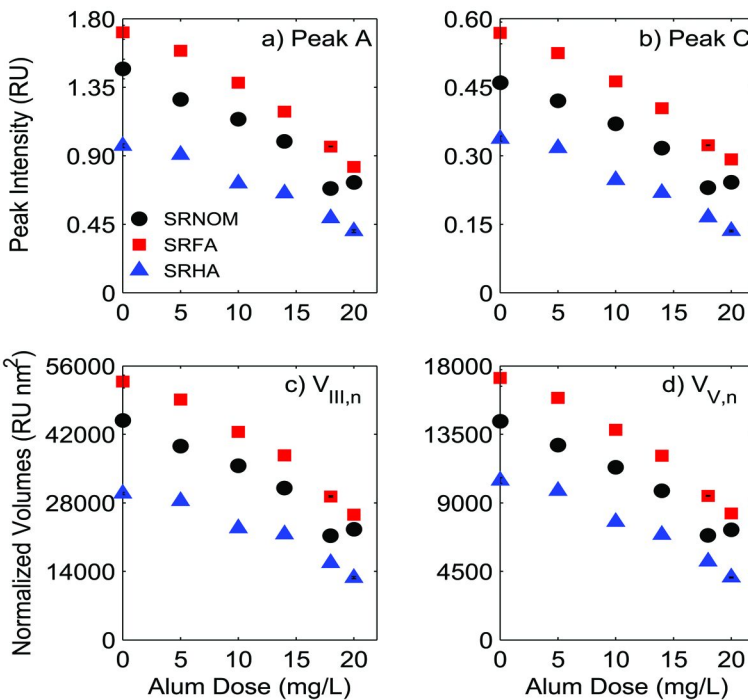


Figure 3. Fluorescence intensities (Peak A (a) and Peak C (b)) and normalized fluorescence volumes ($V_{III,n}$ (c) and $V_{V,n}$ (d)) as a function of alum dose.

If both approaches are applied to this example, fluorescence reveals a more complex behavior compared to DOC or UV₂₅₄ absorbance alone. Figures 3a and 3b depict Peaks A and C intensities as a function of alum dose and show that there is a monotonic decrease in fluorescence intensity across the entire dose range. Figures 3c and 3d present the same behavior in terms of the normalized integrated volumes ($V_{III,n}$ and $V_{V,n}$). At low alum doses, where DOC and UV showed little change, fluorescence decreases indicating that the interactions between DOM and aluminum species cause a quenching of fluorescence intensity. This phenomenon has been well documented elsewhere (27–29). One notable difference is the pH. Most studies investigating the interactions between aluminum species and humic substances hold the pH in the 4 to 5 range to limit the analysis to free aluminum in

solution (28–31). At pH values between 7.3 and 7.6 measured during this study, the aluminum equilibrium is dominated by aluminum hydroxide species (Al(OH)_3) (29). Cabaniss (1992) demonstrated similar quenching of fulvic acid fluorescence at pH 7.5 and concluded that the quenching is due to static interactions between the aluminum species and fulvic acid.

Had fluorescence been used in isolation without other complimentary analytical methods, it would be tempting to interpret the data as a removal of fluorescent material across the entire dose range, but the DOC and UV data prove otherwise. From these data alone, it is also very difficult to determine the alum dose at which DOM removal occurs as the relationship between fluorescence and alum dose appears continuous. This observation highlights that peak intensity or FRI volumes may not be the most informative tools for characterizing this process.

Table III. Percent Removals of DOC, Peak Intensities and Normalized Fluorescence Volumes for Select Alum Doses

	Alum Dose (mg/L)	pH	DOC	Percent Removals (%)			
				Peak		FRI Volume	
				A	C	$V_{III,n}$	$V_{V,n}$
SRNOM	14	7.4	<10	34	33	32	33
	18	7.4	47	55	51	53	53
	20	7.5	45	52	48	51	51
SRFA	14	7.3	<10	29	27	27	28
	18	7.4	42	43	42	43	44
	20	7.3	49	51	47	51	50
SRHA	14	7.3	<10	33	36	28	34
	18	7.4	77	50	52	48	51
	20	7.4	76	58	60	57	61

Comparing the peak picking and FRI methods, the data do not suggest that one method offers obvious advantages over the other for this dataset. The magnitudes differ, but in each case the relative relationships between the isolates and coagulant doses are similar. For example, at an alum dose of 20 mg/L, Peak A and Region $V_{III,n}$ for SRFA decrease by 51% compared to both starting values (Table III). Peak C and Region $V_{V,n}$ decrease by 47% and 50%, respectively. While FRI has the potential to better capture region heterogeneity and fluorescence behaviors that occur away from peak intensities, it does not appear to capture any differences in this system that peak picking cannot capture.

Quantum Yields

While peak intensities and integrated volumes are straightforward calculations, they are difficult to interpret directly. In an application such as coagulation, both DOM quantity and quality change. With intensities alone, it is hard to determine whether the observed decrease in intensity is due to a reduction in organic matter concentration or a change in the organic matter composition. Analyzing quantum yields provides a perspective that helps separate differences in quality and quantity.

Quantum yields (Φ) quantify the fluorescence efficiency relative to non-radiative decay mechanisms. By comparing the fluorescence intensity to the amount of light absorbed, quantum yields offer a compositional parameter to compare differences in DOM before and after coagulation. Quantum yields for DOM have been determined by comparing DOM behavior against a known standard like quinine sulfate (QS) in dilute (0.1 N) sulfuric acid using Equation 1 (12, 22, 32, 33). Quantum yields are calculated at specific excitation wavelengths (λ_{ex}) by integrating the fluorescence intensity (F) across all emission wavelengths (λ_{em}) and dividing it by the absorption coefficient (a) at the same excitation wavelength. By comparing the DOM values to the known standard QS, which has a well-characterized Φ_{QS} of 0.51 (32), the Φ of DOM is calculated. It is normally assumed that the refractive indexes of DOM and quinine sulfate are equal (terms not shown in Equation 1).

$$\frac{\Phi_{DOM}(\lambda_{ex})}{\Phi_{QS}(\lambda_{ex})} = \frac{\int F_{DOM}(\lambda_{ex}, \lambda_{em}) \delta \lambda_{em}}{a_{DOM}(\lambda_{ex})} \times \frac{a_{QS}(\lambda_{ex})}{\int F_{QS}(\lambda_{ex}, \lambda_{em}) \delta \lambda_{em}} \quad (1)$$

DOM Φ_s are dependent on excitation wavelength as shown in Figure 4. This trend of increasing Φ to 350 nm excitation followed by a decrease in Φ with increasing excitation wavelengths has been attributed to the different mechanisms for long wavelength fluorescence emissions, such as charge transfer interactions (22, 34). Figure 4 shows that the quantum yields of SRFA and SRNOM are similar to each other and are about a factor of three greater than SRHA. Even though humic acids typically absorb more light per unit carbon, they have a higher molecular weight, which has been shown to lead to a decrease in fluorescence in favor of internal conversion, a non-radiative decay pathway (34–37).

To characterize the changes in DOM optical properties during coagulation, the maximum quantum yield, which consistently occurs around 350 nm, was compared between coagulant doses as shown in Figure 5. During coagulation, the quantum yield decreases up to an alum dose of 14 mg/L and then increases dramatically. At 14 mg/L, the quantum yields of all three isolates has decreased by 33–35% compared to the initial value, but the difference appears larger for SRFA and SRNOM because of the higher initial values. Between these doses, the maximum observed increase in absorbance was only 6% at 350 nm (SRFA), so absorbance alone cannot explain the decrease in fluorescence efficiency. However, fluorescence intensity, as quantified by Peak C intensity, decreases 27–36% compared to the controls (Figure 3b) and accounts for the decrease observed in the quantum yield. Presenting the fluorescence results in this manner also confirms the quenching behavior observed in Figure 3.

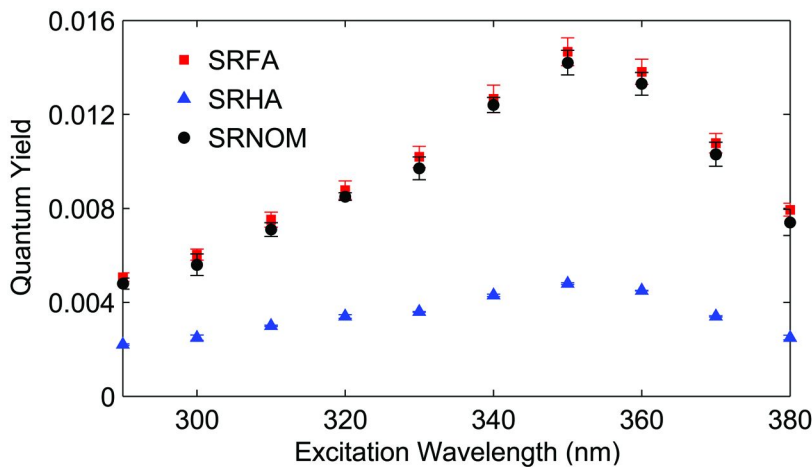


Figure 4. Fluorescence quantum yield as a function of excitation wavelength for SRNOM, SRFA and SRHA. Error bars represent the standard deviation between duplicates.

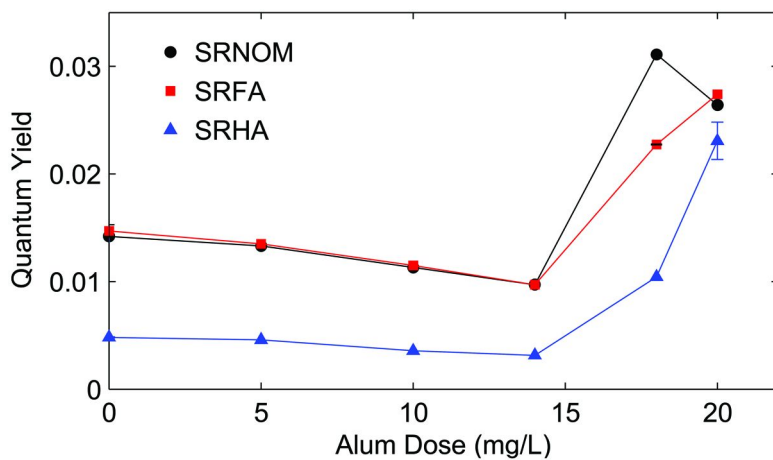


Figure 5. Maximum fluorescence quantum yields for each isolate as a function of alum dose. The maximum consistently occurred between 350 and 360 nm excitation wavelengths.

At alum doses of 18 and 20 mg/L, where there is a large removal of both UV₂₅₄ and DOC, the quantum yield increases significantly relative to that at 14 mg/L alum where little UV₂₅₄ and DOC removal occurred. Even though the fluorescence intensity decreases after coagulation, the fluorescence efficiency

increases in the remaining organic matter. It is well established that coagulation preferentially removes the hydrophobic and large molecular weight fractions of DOM (4) leaving organic matter that is more hydrophilic and lower in molecular weight. Quantum yields and fluorescence per unit absorbance have also been shown to be greater in lower molecular weight fractions (34–37). At 18 mg/L of alum, the quantum yields of both SRFA and SRHA increase by a factor of 2 (relative to the 14 mg/L dose), and the quantum yield of SRNOM increases by a factor of 3. SRFA and SRNOM exhibit similar quantum yields in the uncoagulated control samples and at the lower coagulant doses, but they have different quantum yields after a fraction of the DOM is removed by coagulation. These differences indicate that the organic matter has different affinities for removal (Figure 1) and the remaining DOM has compositional differences that result in different fluorescence efficiencies. Finally, at 20 mg/L alum, the quantum yields of all three fractions converge at similar values. This behavior suggests that the fraction of each DOM pool that is least amenable to coagulation shares similar chemical characteristics. However, it must be noted that it is unknown whether or not residual aluminum in the system is still interacting with the remaining DOM and affecting its fluorescence signature. At the experimental pH values, it is unlikely that there is free aluminum (Al^{3+}), but the dominant aluminum speciation would include $\text{Al}(\text{OH})_3(\text{s})$ and negatively charged hydrolysis products, such as $\text{Al}(\text{OH})_4^-$ (29). Interactions between negatively charged NOM and $\text{Al}(\text{OH})_4^-$ are unlikely, but there may be stable aluminum-fulvate/humate complexes in solution. Complexed aluminum will likely result in a static quenching of the associated DOM (27). Revisiting this classic process demonstrates the utility of moving past fluorescence intensities and analyzing fluorescence data from the perspective of quantum yields.

Fluorescence Index

Fluorescence index (FI) is another metric that provides insight into compositional differences between organic matter samples. This ratio has been correlated to aromatic carbon content, which is also associated with differences in DOM origin (allochthonous vs. autochthonous). Typical values range from 1.2 for allochthonous, higher aromaticity DOM to over 2 for autochthonous, lower aromaticity sources (14). Originally developed in 2001 and then modified in 2010, FI is the ratio of emission intensities (470 nm divided by 520 nm) collected at an excitation wavelength of 370 nm (14, 38).

FI provides an additional level of insight to the coagulation behavior and a message of caution. Comparing the bulk isolates, the FI values for SRFA and SRNOM are greater than that of SRHA (Figure 6). These differences suggest that SRHA is composed of organic matter that is more enriched in aromatic moieties, which can be confirmed with IHSS published aromaticity data (18). From a fluorescence perspective, these differences are manifested as a red-shift (to longer wavelengths) of the emission peak and (to a lesser degree) a broadening of the emission spectra (21). As alum is added to the system, the fluorescence index increases. At doses less than or equal to 14 mg/L, there was no change in DOC or UV_{254} yet FI increased for all isolates. Since there was no change in the mass of

organic matter in solution, this increase cannot be interpreted as a change in DOM composition but rather a change in how the DOM is interacting. The increase in FI is an indication that interactions with the coagulant are not quenching all intensities uniformly but preferentially targeting longer wavelength fluorescence. Non-uniform quenching was previously demonstrated at a lower pH (28). If long wavelength fluorescence is due to charge transfer interactions (22), it suggests that interactions with aluminum species preferentially disrupt the population and/or radiative decay of lower energy states. The FI for SRHA increased more in magnitude compared to SRFA and SRNOM suggesting the degree to which the DOM is interacting with the aluminum species is different between isolates.

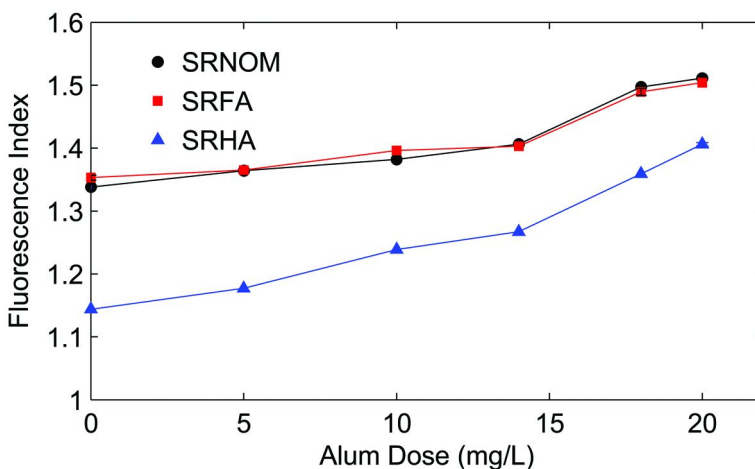


Figure 6. Fluorescence index (FI) as a function of alum dose.

At the highest alum doses (18 and 20 mg/L) where DOM is removed through coagulation processes, Figure 6 shows that the FI exhibited a discontinuous increase that is greater than what would have been predicted by the trends at lower coagulant doses. By preferentially removing the larger molecular weight, more hydrophobic and presumably more aromatic material, the remaining DOM is less aromatic and has a higher FI.

This work demonstrates that FI, which is almost exclusively discussed in the context of DOM composition, is affected by the presence of other inorganic species (e.g., metal hydroxides). These complex effects need to be explored and understood, if FI is used to determine compositional differences across systems with varying background constituents that impact the DOM fluorescence.

Interpretations of Fluorescence Chemical Significance

Fluorescence is an appealing analytical method because of its ease of use, small sample volumes, and limited preparation required. Difficulties arise in trying to relate fluorescence data to DOM chemical characteristics. Both peak

picking and FRI methods have been prescribed chemical characteristics at some point in their application. While Coble defined Peaks A and C as related to humic substances in general, some have assigned more specific designations to the different peak regions. Some fluorescence, such as Peak C, has sporadically been referred to as fulvic-like fluorescence (39, 40), but it is more common for interpretations of the FRI method to include chemical characteristics. When the method was introduced, Region III was associated with fulvic acids and Region V with humic acids (13). This interpretation has become very popular and is commonly applied, especially in water treatment applications (41–43).

By visual inspection alone, Figure 2 shows that both aquatic humic acids and fulvic acids fluoresce in both regions (A vs C and III vs V). Even though humic acid fluorescence occurs at longer wavelengths, both peak picking and the FRI methods would still capture the signal within the same prescribed area as the fulvic acids. In all three Suwannee River samples, the Peak A/Region III area has a higher fluorescence intensity compared to Peak C/Region V. Soil derived humic acids show a distinctly different fluorescence signature compared to aquatic humic acids, and this discussion is only limited to aquatic organic matter (20).

If both operationally defined DOM fractions fluoresce in the same regions, is there evidence to suggest that one region is associated with one fraction over another? Comparing the ratio of intensities or regional integration volumes provides insight into how the fluorescence in one region is changing relative to another. Table IV summarizes the ratio of three different quantitative methods: ratio of Peak A to Peak C intensities, ratio of fluorescence volumes ($V_{III,n} : V_{V,n}$) and ratio of volumetric percentages ($P_{III,n} : P_{V,n}$). Regardless of which ratio method is used, all three isolates (before coagulation) have ratios near 3. The ratio for SRHA is slightly lower near 2.85, whereas the ratios for SRNOM and SRFA are greater near 3.10. These values are still within 8% of each other. In the FRI method, Region V is attributed to the humic-like fraction, but the ratio of regions shows only a 10% enrichment of Region V fluorescence in SRHA compared to SRFA. These results suggest that there is not much difference in the distribution of fluorescence signals between humic and fulvic acids.

If fluorescence regions were associated with chemically distinct fractions of DOM, then it would be expected that the ratio between regions would change after coagulation. If coagulation is more efficient at removing humic acid-like material relative to fulvic acid-like material, then the region associated with humic acids should be removed with greater efficiency than fulvic acid fluorescence. Table III summarizes the relative removal of each peak and integrated region for the 18 and 20 mg/L alum doses compared to the controls. Each type of fluorescence was removed in roughly equal amounts, and there is no region that showed more than 5% additional removal relative to the other. For example, at 18 mg/L of alum, Peaks A and C were both removed by 42% and 43%, respectively, for SRFA. If the regions are compared on a relative basis to each other, the ratio of intensities or integrated volumes stays relatively constant around 3 as shown in Table IV. The range of ratios for each isolate is within 10% of the average, indicating that there is little change in one region relative to the other after coagulation. In other words, coagulation removes fluorescing material in each region in equal proportion and does not preferentially remove fluorescing material in one region over another.

Table IV. Summary of Fluorescence Ratios for Peak Picking (A:C), Normalized Fluorescence Volumes ($V_{III,n}$: $V_{V,n}$) and Normalized Region Percentages ($P_{III,n}$: $P_{V,n}$)

Alum Dose (mg/L)	Peaks A:C			$V_{III,n}$: $V_{V,n}$			$P_{III,n}$: $P_{V,n}$		
	SRNOM	SRFA	SRHA	SRNOM	SRFA	SRHA	SRNOM	SRFA	SRHA
0	3.21	3.04	2.85	3.12	3.10	2.83	3.12	3.10	2.83
5	3.02	3.04	2.86	3.09	3.09	2.90	3.09	3.09	2.90
10	3.09	2.99	2.91	3.14	3.08	2.95	3.14	3.08	2.95
14	3.14	2.94	2.97	3.17	3.12	3.13	3.17	3.12	3.13
18	2.97	2.97	2.98	3.10	3.11	3.05	3.10	3.11	3.05
20	2.99	2.84	3.01	3.13	3.08	3.13	3.13	3.08	3.13
Range/Mean	8%	7%	5%	2%	1%	10%	2%	1%	10%

Based on these observations, it seems like there is little basis to associate one fluorescing region with either humic or fulvic acids exclusively. Both regions behave similarly to each other during coagulation. For these isolates, which were all collected from the same location, the fluorescence is distributed between regions in constant proportion. Other work has also demonstrated that the A and C regions are likely related to each other. Many parallel factor analysis (PARAFAC) models identify dominant components that have dual excitation maxima with one occurring in each region (44–46), providing evidence that the fluorescence in both regions vary together in a set proportion to each other. Another study found that increasing DOM concentrations affect the apparent quantum yield in both regions simultaneously (21). Li et al also provided evidence for dual excitation fluorophores using size exclusion chromatography (47). These results suggest that each region is not associated with one operationally defined DOM fraction over another but are related to each other.

If any descriptor were to be used beyond general ‘humic substances’, the only reasonable interpretation would be that both regions (A/Region III and C/Region V) are most representative of the fulvic acid fraction compared to humic acids. Fulvic acids have higher quantum yields and higher fluorescence per unit carbon (20, 21). In a typical aquatic DOM sample, fulvic acids contribute three times as much mass as humic acids (17). More likely, fluorescence analysis of natural DOM samples would be more representative of fulvic acids compared to humic acids due to their greater abundance and higher fluorescence efficiency.

If fluorescence were to be used to differentiate the differences in humic and fulvic acid fractions, methods that can quantify subtle differences in EEMs would be more powerful. Both methods, peak picking and FRI, lump a wide range of fluorescence wavelengths into one number. Although humic acids have peak emissions shifted to longer wavelengths compared to fulvic acids, the fluorescence contribution of fulvic acids will overlap and likely out fluoresce the humic acids. Neither peak picking nor FRI can effectively capture this heterogeneity if fulvic acids dominate the local fluorescence at lower emission wavelengths. Statistical methods, like PARAFAC, that can simultaneously capture differences in fluorescence intensity and position would be more powerful in discerning differences between DOM fractions.

Conclusions

Fluorescence spectroscopy is a powerful analytical tool but data interpretation is difficult due to the complexity of the fluorescence phenomena. In this study, we revisited a classic process to compare the behavior of humic and fulvic acid fractions. Fluorescence offered insight into the complexity of the coagulation process that DOC concentration and UV₂₅₄ absorbance could not. At low coagulant doses (less than or equal to 14 mg/L), there was no change in either parameter. Changes in fluorescence revealed the complex interactions between DOM and aluminum species before any physical removal occurs. Fluorescence intensity is quenched and quantum yields decreased. Increases in FI demonstrate that fluorescence is not quenched uniformly, but preferentially quenched at the

longer emission wavelengths. The preferential change in the longer wavelength fluorescence compared to shorter wavelengths could not be captured following peak intensities, integrated regions or quantum yields alone. This work also illustrates that not all fluorescence indicators are equal, and it is important to explore multiple ones to gain a wider perspective of system behaviors.

The appealing aspects of fluorescence do not come without disadvantages. Fluorescence is impacted by a number of experimental factors, because intensity is a measure of not only the fluorescent material but also how that material interacts with its surroundings. This point was illustrated by analyzing the changes in fluorescence without any change in DOC concentration or UV₂₅₄ absorbance.

Finally, revisiting the fundamentals of humic and fulvic fluorescence suggest that the practice of relating fluorescing regions to either humic acids or fulvic acids is flawed. There is little evidence to suggest that regional DOM fluorescence is specific to different operationally defined fractions. For DOM analysis, specification beyond general humic substances should be approached cautiously and would likely require more complex data analysis than peak picking or FRI.

Acknowledgments

JAK would like to thank the National Science Foundation Graduate Research Fellowship Program for their financial support (DGE 1144083).

References

1. Rook, J. J. Haloforms in drinking water. *J. – Am. Water Works Assoc.* **1976**, *68*, 168–172.
2. Rook, J. J. Chlorination Reactions of Fulvic Acids in Natural-Waters. *Environ. Sci. Technol.* **1977**, *11*, 478–482.
3. AWWA Research Committee on Coagulation. Organics Removal by Coagulation: A Review and Research Needs. *J. – Am. Water Works Assoc.* **1979**, *71*, 588–603.
4. Randtke, S. J. Organic Contaminant Removal by Coagulation and Related Process Combinations. *J. – Am. Water Works Assoc.* **1988**, *80*, 40–56.
5. Edzwald, J. K.; Becker, W. C.; Wattier, K. L. Surrogate parameters for monitoring organic matter and THM precursors. *J. – Am. Water Works Assoc.* **1985**, *77*, 122–132.
6. Hall, E. S.; Packham, R. F. Coagulation of Organic Color With Hydrolyzing Coagulants. *J. – Am. Water Works Assoc.* **1965**, *57*, 1149–1166.
7. Edzwald, J. K. Coagulation of Humic Substances. *Water-1978 (AIChE Symp. Ser.)* **1978**, *75*, 54–62.
8. Senesi, N.; Miano, T. M.; Provenzano, M. R.; Brunetti, G. *Sci. Total Environ.* **1989**, *81*, 143–156.
9. Senesi, N.; Miano, T. M.; Provenzano, M. R.; Brunetti, G. Characterization, differentiation, and classification of humic substances by fluorescence spectroscopy. *Soil Sci.* **1991**, *152*, 259–271.

10. Coble, P.; Green, S. A.; Blough, N. V.; Gagosian, R. B. Characterization of Dissolved Organic-Matter in the Black-Sea by Fluorescence Spectroscopy. *Nature (London)* **1990**, *348*, 432–435.
11. Coble, P. Characterization of marine and terrestrial DOM in seawater using excitation emission matrix spectroscopy. *Mar. Chem.* **1996**, *51*, 325–346.
12. Green, S. A.; Blough, N. V. Optical-Absorption and Fluorescence Properties of Chromophoric Dissolved Organic-Matter in Natural-Waters. *Limnol. Oceanogr.* **1994**, *39*, 1903–1916.
13. Chen, W.; Westerhoff, P.; Leenheer, J. A.; Booksh, K. Fluorescence excitation - emission matrix regional integration to quantify spectra for dissolved organic matter. *Environ. Sci. Technol.* **2003**, *37*, 5701–5710.
14. McKnight, D. M.; Boyer, E. W.; Westerhoff, P.; Doran, P.; Kulbe, T.; Andersen, D. Spectrofluorometric characterization of dissolved organic matter for indication of precursor organic material and aromaticity. *Limnol. Oceanogr.* **2001**, *46*, 38–48.
15. Zsolnay, A.; Baigar, E.; Jimenez, M.; Steinweg, B.; Saccomandi, F. Differentiating with fluorescence spectroscopy the sources of dissolved organic matter in soils subjected to drying. *Chemosphere* **1999**, *38*, 45–50.
16. Leenheer, J. A. Systematic Approaches to Comprehensive Analyses of Natural Organic Matter. *Ann. Environ. Sci.* **2009**, *3*, 1–130.
17. Perdue, E. M.; Ritchie, J. D. In *Surface and Ground Water, Weathering and Soils*; Holland, H. D., Turekian, K. K., Eds.; Treatise on Geochemistry; Elsevier: Oxford, 2003; Vol. 5, pp 273–318.
18. Thorn, K. A.; Folan, D. W.; MacCarthy, P. *Characterization of the International Humic Substances Society Standard and Reference Fulvic and Humic Acids by Solution State Carbon-13 (¹³C) and Hydrogen-1 (¹H) Nuclear Magnetic Resonance Spectrometry*; Technical Report for U.S. Geological Survey: Denver, CO, 1989.
19. Weishaar, J. L.; Aiken, G. R.; Bergamaschi, B. A.; Fram, M. S.; Fujii, R.; Mopper, K. Evaluation of Specific Ultraviolet Absorbance as an Indicator of the Chemical Composition and Reactivity of Dissolved Organic Carbon. *Environ. Sci. Technol.* **2003**, *37*, 4702–4708.
20. Alberts, J. J.; Takács, M. Total luminescence spectra of IHSS standard and reference fulvic acids, humic acids and natural organic matter: comparison of aquatic and terrestrial source terms. *Org. Geochem.* **2004**, *35*, 243–256.
21. Korak, J. A.; Dotson, A. D.; Summers, R. S.; Rosario-Ortiz, F. L. Critical Analysis of Commonly Used Fluorescence Metrics to Characterize Dissolved Organic Matter. *Water Res.* **2014**, *49*, 327–338.
22. Del Vecchio, R.; Blough, N. V. On the origin of the optical properties of humic substances. *Environ. Sci. Technol.* **2004**, *38*, 3885–3891.
23. Dempsey, B. A.; Ganho, R. M.; O'Melia, C. R. The Coagulation of Humic Substances by Means of Aluminum Salts. *J. – Am. Water Works Assoc.* **1984**, *76*, 141–150.
24. Narkis, N.; Rebhun, M. Stoichiometric Relationship between Humic and Fulvic Acids and Flocculants. *J. – Am. Water Works Assoc.* **1977**, *69*, 325–328.

25. Randtke, S. J.; Jepsen, C. P. Chemical pretreatment for activated-carbon adsorption. *J. – Am. Water Works Assoc.* **1981**, *73*, 411–419.
26. Babcock, D. B.; Singer, P. C. Chlorination and Coagulation of Humic and Fulvic Acids. *J. – Am. Water Works Assoc.* **1979**, *71*, 149–152.
27. Cabaniss, S. E. Synchronous Fluorescence-Spectra of Metal-Fulvic Acid Complexes. *Environ. Sci. Technol.* **1992**, *26*, 1133–1139.
28. Sharpless, C.; McGown, L. Effects of aluminum-induced aggregation on the fluorescence of humic substances. *Environ. Sci. Technol.* **1999**, *33*, 3264–3270.
29. Elkins, K. M.; Nelson, D. J. Spectroscopic approaches to the study of the interaction of aluminum with humic substances. *Coordin. Chem. Rev.* **2002**, *228*, 205–225.
30. Luster, J.; Lloyd, T.; Sposito, G.; Fry, I. V. Multi-Wavelength Molecular Fluorescence Spectrometry for Quantitative Characterization of Copper(II) and Aluminum(III) Complexation by Dissolved Organic Matter. *Environ. Sci. Technol.* **1996**, *30*, 1565–1574.
31. Ohno, T.; Amirbahman, A.; Bro, R. Parallel factor analysis of excitation–emission matrix fluorescence spectra of water soluble soil organic matter as basis for the determination of conditional metal binding parameters. *Environ. Sci. Technol.* **2008**, *42*, 186–192.
32. Birks, J. B. *Photophysics of Aromatic Molecules*; Wiley Interscience: London, 1970; pp 84–141.
33. Lakowicz, J. R. *Principles of fluorescence spectroscopy*; Springer: New York, 2006; pp 27–62.
34. Boyle, E. S.; Guerriero, N.; Thiallet, A.; Vecchio, R. D.; Blough, N. V. Optical Properties of Humic Substances and CDOM: Relation to Structure. *Environ. Sci. Technol.* **2009**, *43*, 2262–2268.
35. Wang, Z. D.; C Pant, B.; H Langford, C. Spectroscopic and structural characterization of a Laurentian fulvic acid: notes on the origin of the color. *Anal. Chim. Acta* **1990**, *232*, 43–49.
36. Stewart, A. J.; Wetzel, R. G. Asymmetrical Relationships between Absorbance, fluorescence and dissolved organic carbon. *Limnol. Oceanogr.* **1981**, *26*, 590–597.
37. Richard, C.; Trubetskaya, O.; Trubetskoy, O.; Reznikova, O.; Afanas'eva, G.; Aguer, J. P.; Guyot, G. Key Role of the Low Molecular Size Fraction of Soil Humic Acids for Fluorescence and Photoinductive Activity. *Environ. Sci. Technol.* **2004**, *38*, 2052–2057.
38. Cory, R. M.; Miller, M. P.; McKnight, D. M.; Guerard, J. J.; Miller, P. L. Effect of instrument-specific response on the analysis of fulvic acid fluorescence spectra. *Limnol. Oceanogr. Methods* **2010**, *8*, 67–78.
39. Bieroza, M.; Baker, A.; Bridgeman, J. Relating freshwater organic matter fluorescence to organic carbon removal efficiency in drinking water treatment. *Sci. Total Environ.* **2009**, *407*, 1765–1774.
40. Hudson, N.; Baker, A.; Reynolds, D. Fluorescence analysis of dissolved organic matter in natural, waste and polluted waters—a review. *River Res. Appl.* **2007**, *23*, 631–649.

41. Ayache, C.; Pidou, M.; Croue, J.-P.; Labanowski, J.; Poussade, Y.; Tazi-Pain, A.; Keller, J.; Gernjak, W. Impact of effluent organic matter on low-pressure membrane fouling in tertiary treatment. *Water Res.* **2013**, *47*, 2633–2642.

42. Jiang, W.; Xia, S.; Liang, J.; Zhang, Z.; Hermanowicz, S. W. Effect of quorum quenching on the reactor performance, biofouling and biomass characteristics in membrane bioreactors. *Water Res.* **2013**, *47*, 187–196.

43. Zhang, W.; Li, Y.; Wang, C.; Wang, P.; Wang, Q. Energy recovery during advanced wastewater treatment: Simultaneous estrogenic activity removal and hydrogen production through solar photocatalysis. *Water Res.* **2013**, *47*, 1480–1490.

44. Ishii, S. K.; Boyer, T. H. Behavior of reoccurring PARAFAC components in fluorescent dissolved organic matter in natural and engineered systems: A critical review. *Environ. Sci. Technol.* **2012**, *46*, 2006–2017.

45. Cory, R. M.; McKnight, D. M. Fluorescence spectroscopy reveals ubiquitous presence of oxidized and reduced quinones in dissolved organic matter. *Environ. Sci. Technol.* **2005**, *39*, 8142–8149.

46. Pifer, A. D.; Fairey, J. L. Improving on SUVA₂₅₄ using fluorescence-PARAFAC analysis and asymmetric flow-field flow fractionation for assessing disinfection byproduct formation and control. *Water Res.* **2012**, *46*, 2927–2936.

47. Li, W. T.; Xu, Z. X.; Li, A. M.; Zhou, Q.; Wang, J. N. HPLC/HPSEC-FLD with Multi-Excitation/Emission Scan for EEM Interpretation and DOM Analysis. *Water Res.* **2013**, *47*, 1246–1256.

Subject Index

A

Adsorbable organic halogen (AOX), 209
Aerosol-derived humic-like substances (HULIS), 87
Dark Fenton oxidation, 103
distribution in aerosol and in atmosphere, 98
ecological and epidemiological impacts, 102
hygroscopic, cloud nucleating, and light-absorbing properties, 99
metals and organic pollutant, complexation, 103
Allochthonous versus autochthonous, relative importance, 37
AOX. *See* Adsorbable organic halogen (AOX)
Aquatic humic acids and fulvic acids fluoresce, 294
Aquatic humic substances
1980, classic papers, 20
citation classics, 15
classic books, 20
classic papers
defining, 12
dissolved organic matter 1960s, 17
environmental science, 14
1970s, 17
1990s, 22
decade of 1960s, 16
decade of 1970s, 17
decade of 1980s, 18
decade of 1990s, 22
decade of 2000s, 23
environmental journals, 9*t*
 h_j -index over time, 13
Journal Hirsch Index (h_j), 8, 11*f*
Aquatic organic matter (OM), photophysics and photochemistry, 159
BWW samples characteristics and quantum efficiencies, 167*t*
fluorescence EEMs for BWW and each size fraction, 169*f*
fluorescence EEMs for SRNOM and each size fraction, 168*f*
fluorescence quantum yields, 170*f*
formation of reactive intermediates, 170
materials and methods
characterization and optical measurements, 162
reactive species measurements, 163

sample collection and preparation, 161
 UV_{254} detection, 164*f*
measured properties, relation, 172
observed results
factor contributing, 175
interpretation, 174
optical properties, 166
quantum yields, 171*f*
quantum yields as function of fluorescence index, 173*f*
quantum yields as function of sample spectral slope, 172*f*
quantum yields as function of SEC retention time weighted average, 174*f*
SRNOM samples characteristics and quantum efficiencies, 166*t*
water quality and molecular size, 165

C

Coagulation of natural waters with chlorine or chlorine dioxide application, 235
adsorptive and desorptive interactions, 238
AOX-U and TOC behavior during coagulation chlorination, 244
chlorine dioxide application, 248
AOX-U removal versus sorbable TOC removal, 247*f*
AOX-U sorption/incorporation (chlorine dioxide), 246*t*
DBP formation, impact of flocs, 251*t*
desorption of AOX from floc, 249, 250*t*
HOM formation, impact of flocs chlorination, 250
chlorine dioxide application, 252
HPSEC DOC and UVA response – OH water, 248*f*
impact of flocs on HOM formation (chlorine dioxide), 253*t*
materials, 239
maximum contaminant level (MCL), 236
methods
coagulation testing, 239
desorption of halogenated organic matter from flocs, 240

halogenated organic matter analysis, 239
 halogenated organic matter formation from flocs, 241
 halogenated organic matter sorption by flocs, 240
 halogenated organic matter sorption onto existing flocs, 241
 high-performance size exclusion chromatography (HPSEC), 241
 NOM sorption, 238
 organic DBPs, removal, 237
 raw water characteristics and HOM formation, 241
 sorption of AOX onto preformed flocs, 252, 253^t
 source water OM, 237
 TTHM and HAA9 sorption to flocs, 243^t

D

DBP. *See* Disinfection byproduct (DBP)
 DBP reactivity of organic matter fractions
 allochthonous DOM, 28
 autochthonous DOM, 258
 bulk water quality, 262, 263^t
 bulk waters, THM formation, 272^t
 carcinogenic by-products, 258
 DOC concentration, 260
 DOM fractionation, 263
 DOM fractionation recovery, 263^t
 DOM fractions, shorter-term reactivity
 7 day HAA yield, 269^t, 273^t
 7 day TTHM yield, 266^t
 DOM isolation method, 260^f
 materials and methods, 259
 terminal reservoirs, longer term trends, 262^f
 THM and HAA analysis, 260
 whole water, DOM fractionation and reconstruction, 264^f
 Disinfection byproduct (DBP), 40
 Disinfection byproduct formation
 bulk water formation rate, 265
 fraction specific formation rates, 265
 Dissolved organic carbon (DOC), 28, 116, 162, 194
 Dissolved organic matter (DOM), 1
 Dissolved organic matter association with hydrophobic organic pollutants
 characterization methods for NOM, 196
 fluorescence quenching, 198

free fraction of perylene and calculated fraction of Benzo(a)pyrene (BaP), 202^t
 HOP probe, characteristics, 195
 polarity rapid assessment method (PRAM), 197
 pollution levels and form of HOPs, 195
 PRAM analysis, 199
 sample collection, 196
 sample preparation, 196
 size characterization by ultrafiltration, 200
 stormwater runoff samples, water quality parameters, 200^t
 ultrafiltration (UF) analysis of stormwater runoff samples, 201^f
 ultrafiltration to measure size fraction of DOM, 197
 use of perylene as probe, 193
 water quality, 197
 water quality data, 199
 Dissolved organic matter-HO[•] reaction, temperature dependence, 181
 Arrhenius parameters, summary, 188^t
 comparison of PEG and DOM kinetics
 molecular weight, 187
 temperature dependence, 189
 experimental, 183
 $k_{\text{PEG-HO}^{\bullet}}$ versus PEG molecular weight, 188^f
 PEG-HO[•] experiments, kinetic data, 185^f
 PEG-HO[•] kinetics, 184
 temperature-dependent $k_{\text{PEG-HO}^{\bullet}}$ Values, 186^t
 DOC. *See* Dissolved organic carbon (DOC)
 DOM fractions fluoresce, 294

E

EEM-PARAFAC. *See* Excitation emission matrix fluorescence combined with parallel factor analysis (EEM-PARAFAC)
 Effect of NOM against harmful phototrophs, 122
 Estuarine and coastal DOM character other factors influencing, 49
 distributional patterns, 50
 heterotrophic bacterial, 50
 particulate organic matter (POM), 50
 phytoplankton, microbial degradation, 50
 seasonal changes, 48

Excitation emission matrix fluorescence combined with parallel factor analysis (EEM-PARAFAC), 27

F

FDOM. *See* Fluorescent DOM (FDOM)
 Fluorescence characterization of humic substance coagulation
 analytical methods, 284
 coagulation, 294
 coagulation methods, 284
 DOC and UV₂₅₄ removal, 285
 DOC concentration, 287/*f*
 fluorescence analysis, 286
 fluorescence chemical significance, interpretations, 293
 fluorescence index, 292
 fluorescence index (FI) as function of alum dose, 293/*f*
 fluorescence intensities, 286
 fluorescence intensities and normalized fluorescence volumes, 288/*f*
 fluorescence quantum yield as function of excitation wavelength, 291/*f*
 fluorescence ratios, summary, 295/*t*
 humic and fulvic acids, 282
 intensities or regional integration volumes, 294
 materials, 283
 maximum fluorescence quantum yields as function of alum dose, 291/*f*
 quantum yields, 290
 removals of DOC, peak intensities and normalized fluorescence volumes, 289/*t*
 water quality characteristics, 284/*t*
 Fluorescent DOM (FDOM), 50

H

HSs. *See* Humic substances (HSs)
 HULIS. *See* Aerosol-derived humic-like substances (HULIS)
 Humic substances (HSs), 116
 antiviral activity, 118
 effects on plant growth and yield, 123
 reactive oxygen species, 118

M

Marine humic-like PARAFAC components, 37

N

Natural dissolved organic matter (DOM), assessing environmental dynamics, 27
 allochthonous and autochthonous DOM dynamics in lakes, 36
 alteration of DOM quality in wetlands, 43
 DOM quality, 42
 DOM sources in wetlands, 40
 estuaries and coasts
 DOM character, spatial changes, 46
 humic-like and protein-like components, fluorescence intensity, 47/*f*
 PARAFAC components, list of behavior classifications, 48/*t*
 estuarine PARAFAC component dynamics, 45/*f*
 FDOM distributions, 53
 fluorescent components in sea ice, characteristics, 58
 headwater streams and rivers
 effects of land-use and pollution, 32
 environmental heterogeneity and spatial connectivity in fluvial systems, 29
 environmental processing of DOM in streams, 31
 humic- and fulvic-like PARAFAC components, 34/*f*
 hydrological flow paths and DOM quality, 30
 landscape factors, 33
 PARAFAC components, relative abundance, 32
 relative abundance of EEM-PARAFAC components, 35/*f*
 lake stratification and spatial variation in DOM source within lakes, 39
 open ocean, 52
 AOU and humic-like PARAFAC components, relationships, 53
 apparent oxygen utilization (AOU), 53
 Atlantic surface layer, meridional transects, 56

EEM-PARAFAC component, quantitative evaluation, 55
 humic-like components and trace metals, interactions evaluation, 55
 humic-like fluorescence components, distribution, 56^f
 PARAFAC components, distribution, 54
 photo-chemical history, 57
 protein-like components, 57
 quantitative estimates based on EEM-PARAFAC, 51
 redox processes in wetlands, 44
 spatial distribution of PARAFAC components, 41^f
 spatial variation in DOM sources among lakes, 38
 surface water DOM, 42
 tracing allochthonous DOM components, 52
 Natural organic matter (NOM), 75
 NOM. *See* Natural organic matter (NOM)
 NOM as modulator of redox regimes, 117
 NOM as natural xenobiotics, 115
 allelochemicals, 120
 cyanobacteria, 121
 cylindrospermopsin, photosensitized degradation, 120^f
 growth of *Anabaena circinalis*, 121^f
 human viruses and bacteriophages, 119^f
 internal redox homeostasis, 121
 oxidative stress mechanism, 119
 survival of ayu fish, 118^f
 NOM interaction with animals, 126
Caenorhabditis elegans
 cep-1 gene, 129^f
 vit-6 gene, 130^f
 cytosine-methylation, 132^f
 fluctuating osmotic conditions, stress tolerance, 130^f
 health-promoting activity, 127
 life trait variables, hormetic modulation, 127
 multiple stress resistance or cross-tolerance, 128
 sex ratio, female-bias, 127
 stress resistance, transgenerational heritage, 129
 stress resistance to filial generations, 132^f
 survive acidic conditions
Caridina sp., 131^f
Gammarus pulex, 131^f
 NOM interactions with higher plants, 123
Arabidopsis, 124^f
 surface roots of wheat, 124^f

transcriptional expression, 125^f
 NOM origin and quality, 132

O

Organic aerosol, 87
 analysis of HULIS and LV/HMWOA, mass spectrometric approach, 91
 ambient surface ionization techniques, 92
 atmospheric pressure chemical ionization (APCI), 92
 atmospheric pressure photoionization (APPI), 92
 electrospray ionization (ESI), 92
 high resolution mass spectrometry (HRMS), 93
 matrix-assisted laser desorption ionization (MALDI), 92
 soft ionization techniques, 92
 aromatic and aliphatic content of HULIS, 96
 chemical and physical properties of HULIS, 89
 pondering conclusions, problems, 90
 techniques, 90
 chemical structure of HULIS, 91
 EEMs obtained from WSOC extracts, 100^f
 formation of LV/HMWOA and HULIS, 96
 HULIS composition, sources, and formation pathways, 94
 biogenic and anthropogenic VOC, 95
 biogenic VOC oxidation, 95
 fulvic acids, 96
 ultra-high resolution FT-ICR mass spectrometry, 95
 time series of aerosol-derived bulk WSOC and bulk base-extracted OC fluorescence, 97^f

P

Protein-like PARAFAC components, 37

Q

Quality of NOM matters
C. elegans, survival rate and lifespan, 135^f

reduction in photosynthetic oxygen, 135*f*
Saprolegnia parasitica growth modulation, 134*f*
 Quinone-like PARAFAC components, 37

R

Raw water quality and HOM formation, 242*t*
 Reconstruction of disinfection byproduct formation
 bulk versus reconstructed
 HAA yield, 276*t*
 THM yield, 275*t*
 distribution and formation of TTHMs, 277*f*
 reconstructed formation potential, 274

S

Secondary organic aerosol (SOA), 94
SOA. See Secondary organic aerosol (SOA)
SRNOM. See Suwannee River natural organic matter (SRNOM)
 Surface waters natural organic matter, 209
 analysis of haloacetonitriles (HANs), 216
 analysis of halogen-specific AOX, 214
 analysis of halonitromethanes (HNMs)
 and haloacetamides (HAMs), 216
 analysis of N-DBPs, 214
 analysis of N-nitrosamines, 216
 analytical HPSEC chromatograms, 217*f*
 analytical scale HPSEC, 213
 chemicals and standards, 212
 concentrations of N-DBPs and SUVA₂₅₄, 229*t*
 disinfectant consumption and incorporation of halogens, 224*t*
 disinfection experiments, 214
 elution volumes and calculated molecular weight cutoffs, 220*t*
 formation of halogenated DBPs during chlorination and chloramination, 221
 formation of N-DBPs during chlorination and chloramination, 223
 fractionation of NOM concentrates by preparative scale HPSEC, 219
 halogenated N-DBPs, 228
 hydrophobic and hydrophilic fractions, characteristics and reactivity, 211
 list of N-DBPs species analysed, 215*t*

molar concentrations, 225*f*, 226*f*, 227*f*
 molar concentrations of halogen-specific AOX, 222*f*
 NOM concentrate, fractionation, 213
 raw surface waters, water quality characteristics, 218*t*
 sample collection and preparation, 212
 size exclusion chromatography (SEC), 211
 water quality analysis, 213
 water quality and molecular weight characteristics, 218

Suwannee river, acidic functional groups carboxyl and phenolic contents, 80*t*
 comparison with IHSS fitting parameters, 84
 experimental, 76
 binding sites, 78
 cations and anions, concentrations, 77
 Gaussian distribution model, 78
 ionic strength, 77
 organic charge, 77
 pH 8 and 10 method, 78
 titrations, 76
 Henderson-Hasselbalch model, results, 83*t*
 model fitting parameters, 80
 reverse osmosis, 77
 titrations and inorganic contributions, 79

Suwannee River natural organic matter (SRNOM), 161

W

Water conservation areas (WCAs), 147
 Water soluble organic carbon (WSOC), 89
WCAs. See Water conservation areas (WCAs)
 Wetland soils, phosphorus speciation and carbon humification, 145
¹³C NMR spectrum of soil from WCA, 155*f*
 distribution of major organic carbon species, 153*f*
 distributions of phosphorus species, 152*f*
 methods
¹³C NMR spectroscopy, 149
 elemental analysis, 148
³¹P NMR spectroscopy, 148
 phosphorus extraction, 148
 O-alkyl groups, 151
 organic phosphate monoesters (O-mono), 151

³¹P NMR spectrum of NaOH extract, 154
phosphorus speciation along gradient in WCA 2A, 154
phosphorus speciation in WCA 2A soils, 155
phosphorus stability as function of soil organic matter composition, 150
sample descriptions, Everglades water conservation area 2, 150

sampling sites, 149
WSOC. *See* Water soluble organic carbon (WSOC)
WSOC-derived HULIS, 103

X

Xenobiotics, 115